Role of metabolic pathways and sensors in regulation of dendritic cell-driven T cell responses

Pelgrom, L.R.

Citation

Pelgrom, L. R. (2022, February 23). *Role of metabolic pathways and sensors in regulation of dendritic cell-driven T cell responses*. Retrieved from https://hdl.handle.net/1887/3275848

Version:	Publisher's Version
License:	Licence agreement concerning inclusion of doctoral thesis in the Institutional Repository of the University of Leiden
Downloaded from:	https://hdl.handle.net/1887/3275848

Note: To cite this publication please use the final published version (if applicable).

ROLE OF METABOLIC PATHWAYS AND SENSORS IN REGULATION OF DENDRITIC CELL-DRIVEN T CELL RESPONSES

LEONARD R. PELGROM

Role of metabolic pathways and sensors in regulation of dendritic cell-driven T cell responses

LEONARD R. PELGROM

Colofon

Role of metabolic pathways and sensors in regulation of dendritic cell-driven T cell responses, Leonard R. Pelgrom

Provided by thesis specialist Ridderprint, ridderprint.nl
Printing: Ridderprint
Layout and design: Mila Slappendel, persoonlijkproefschrift.nl
Cover design: Elise Metekohy

ISBN: 978-94-6458-023-5

Copyright 2022 © Leonard Pelgrom

The Netherlands. All rights reserved. No parts of this thesis may be reproduced, stored in a retrieval system or transmitted in any form or by any means without permission of the author.

Role of metabolic pathways and sensors in regulation of dendritic cell-driven T cell responses

Proefschrift

ter verkrijging van de graad van doctor aan de Universiteit Leiden op gezag van rector magnificus Prof. dr. ir. H. Bijl, volgens besluit van het college voor promoties te verdedigen op woensdag 23 februari 2022 klokke 11:15 uur

door

Leonard Reinier Pelgrom

geboren te Haarlem in 1988

Promotor

Prof.dr. M. Yazdanbakhsh

Co-promotor

Dr. B. Everts

Leden promotiecommissie

Prof. dr. C. van Kooten

Prof. dr. I.J.M. de Vries, Radboud Universitair Medisch Centrum, Nijmegen, Nederland

Prof. dr. J.G. Borst

Dr. J. Van den Bossche, Amsterdam Universitair Medisch Centrum, locatie VUmc, Amsterdam, Nederland

Dr. B. Guigas

Table of contents

	List of abbreviations	6
Chapter 1	General introduction	9
Chapter 2	Dendritic cells are what they eat: how their metabolism shapes T helper cell polarization	17
Chapter 3	Analysis of TLR-Induced Metabolic Changes in Dendritic Cells Using the Seahorse XFe96 Extracellular Flux Analyzer	33
Chapter 4	Cell-Intrinsic Glycogen Metabolism Supports Early Glycolytic Reprogramming Required for Dendritic Cell Immune Responses	49
Chapter 5	Butyrate Conditions Human Dendritic Cells to Prime Type 1 Regulatory T cells via both Histone Deacetylase Inhibition and G Protein-Coupled Receptor 109A Signaling	79
Chapter 6	Metabolic control of type 2 immunity	111
Chapter 7	Protein O-GlcNAcylation and low glycolysis underpin Th2 polarization by dendritic cells	135
Chapter 8	LKB1 expressed in dendritic cells governs the development and expansion of thymus-derived regulatory T cells	175
Chapter 9	mTORC1 signalling in antigen-presenting cells of the skin restrains CD8+ T cell priming	225
Chapter 10	General discussion	273
	Nederlandse samenvatting	300
	Curriculum vitae	305
	List of publications	306
	Acknowledgements	308

List of abbreviations

2-DG	2-deoxyglucose
AMP	Adenosine monophosphate
AMPK	AMP-activated protein kinase
ATP	Adenosine triphosphate
CTLs	Cytotoxic T cells
DCs	Dendritic cells
BDMCs	Bone marrow-derived DCs
GMDCs	BMDCs generated using GM-CSF
cDC1s	Type 1 conventional DCs
cDC2s	Type 2 conventional DCs
moDCs	Monocyte-derived DCs
pDCs	Plasmacytoid DCs
ECAR	Extracellular acidification rate
FAO	Fatty acid oxidation
GPRs	G protein-coupled receptors
HBP	Hexosamine biosynthesis pathway
HDACs	Histone deacetylases
HDM	House dust mite
IFN	Interferon
IL	Interleukin
LCs	Langerhans cells
LKB1	Liver kinase B1
mTOR	Mechanistic target of rapamycin
mTORC1	mTOR complex 1
OCR	Oxygen consumption rate
OGT	O-GlcNAc transferase
OGA	O-GlcNAcase
OXPHOS	Oxidative phosphorylation
PLC-β1	Phospholipase C beta-1
PYG	Glycogen phosphorylase
RA	Retinoic acid
RALDH	Retinaldehyde dehydrogenase
SCFAs	Short-chain fatty acids
SEA	Soluble egg antigens
ST	ST045849

TG	Thiamet G
TGFβ1	Transforming growth factor beta-1
Th cells	T helper cells
Th2 cells	T helper 2 cells
TNF	Tumor necrosis factor
Tregs	Regulatory T cells
Tr1	IL-10-producing type 1 Tregs
iTregs	Induced/in vitro Tregs
pTregs	Tregs generated in the periphery
tTregs	Tregs generated in the thymus
UDP-GlcNAc	Uridine diphosphate N-acetylglucosamine
XF	Extracellular flux

1

General introduction

Introduction

We are constantly exposed to microorganisms and parasites that can invade our body (i.e. infect) and have the capacity to cause disease (i.e. pathogenic). Yet we rarely become ill. This is because we have developed specialized molecules, cells and tissues that together are involved in our ability to resist infection (i.e. immunity) and collectively are known as the immune system. Immunology is the science that studies the immune system and Edward Jenner is generally recognized to have performed the first immunological experiment. He demonstrated in the late 18th century that inoculation with cowpox could confer protection against its more fatal cousin smallpox. As cowpox is caused by the vaccinia virus ('vacca' is Latin for cow), this procedure was called vaccination, a term now used for any form of immunization with a weakened microorganism or substitute thereof.

It is now well described that immune cells make drastic changes to their biology to transition between different life stages and efficiently deal with the threat of infection. These changes can include activation, growth, multiplication (i.e. proliferation), movement (i.e. migration), specialization (i.e. differentiation), gain of effector/regulatory functions and finally, the generation and maintenance of immunological memory. Over the past 10 years or so, immunologists have come to realize that these processes are underpinned by unique metabolic states, which ignited the field of immunometabolism.

Metabolism is the total sum of life sustaining chemical reactions in organisms and their cells. This can be broadly divided into on the one hand the breakdown of molecules to generate energy (i.e. catabolism) and on the other hand the synthesis of complex molecules from simple molecules (i.e. anabolism). The latter provides fundamental building blocks for the cell. Seminal work by Chawla and colleagues in 2006 [1] and Rathmell and colleagues in 2011 [2] showed that immune cells on opposite sides of the immunological spectrum – that is to say immune cells which are associated with the initiation and maintenance of inflammation (i.e. effector cells) versus immune cells which are associated with resolution or suppression of inflammation (i.e. regulatory cells) - can be distinguished based on their metabolic profiles. More importantly, they showed that gain of effector functions was dependent on breakdown of glucose into lactate when oxygen is abundant (i.e. aerobic glycolysis) followed by the synthesis of complex molecules, while the gain of regulatory functions was dependent on the breakdown of fatty acids to generate energy through oxidative phosphorylation (i.e. fatty acid oxidation or beta oxidation). This sparked the idea that immunity could be boosted by enhancing aerobic glycolysis in immune cells or diminishing their beta-oxidation, while immune responses could be dampened by promoting beta-oxidation in immune cells or decreasing their aerobic glycolysis.

Dendritic cells (DCs) play a crucial role in the initiation and maintenance of effector T cell responses and regulatory T cell responses. They do so by providing antigen (signal 1), co-stimulation (signal 2) and cytokines (signal 3) to T cells. The strength of these combined signals determines whether the T cell becomes activated or unresponsive (i.e. anergic) and in the case of CD4+ T cells, the nature of these combined signals also determines whether the T cells becomes anti-bacterial/viral IFN producing T helper 1 (Th1) cells, anti-parasitic IL-4-producing T helper 2 (Th2) cells, anti-fungal/yeast IL-17 producing T helper 17 (Th17) cells or immune-suppressive regulatory T cells (Tregs). Effector CD8+ T cells are also known as cytotoxic T lymphocytes (CTLs) because they are specialized in secreting molecules that are toxic to cells (cyto = prefix meaning cell) which have become infected or cancerous.

Pioneering work by Pearce and colleagues in the early 2010s [3, 4] showed that the activation of inflammatory DCs is dependent on aerobic glycolysis. However, little was known about the metabolic properties of different DC subsets. Another unanswered question was if DCs with different T cell polarizing properties - that is to say they preferentially skew T cells towards a specific specialization (e.g. Th1 over Th2) - rely on distinct metabolic characteristics for their T cell polarizing ability. Moreover, while there has been a long-standing interest in understanding how the mechanistic target of rapamycin (mTOR) - a master regulator of anabolic metabolism [5] - controls DC biology and function, its role in shaping DC-mediated T cell responses is far from unambiguous [6]. In addition, there have been very few studies interrogating the role of AMP-activated protein kinase (AMPK) - a master regulator of catabolic metabolism and a negative controller of mTOR [7] - or its upstream activator liver kinase B1 (LKB1) in DC biology [8]. This is in part because no pharmacological inhibitors of AMPK and LKB1 were available.

Although it has been six years since the first major review on DC metabolism was published [9], its conclusion is as relevant as ever: “It will be important to more fully characterize how metabolism controls the immune priming function of DCs and whether metabolic manipulation of DCs can be used to alter their immune polarizing properties.”

Thesis outline

This thesis aims to characterize the metabolic programs that DCs rely on for activation and polarization of different T cell responses, as well as elucidate the roles of mTOR and AMPK therein. As DCs play a central role in the establishment of protective immune response to infection and after vaccination and are critical regulators of tolerance to host self-antigens, manipulation of DC function through manipulation of DC metabolism may be an attractive therapeutic strategy.

Chapters 2 and 3 serve as extended introduction to this thesis, as they lay the theoretical and practical groundwork for the subsequent chapters. In **Chapter 2**, an updated overview is provided on publications that investigate the link between DC metabolism and their T cell-polarizing capacities. In **Chapter 3**, the workings of extracellular flux (XF) analysis, the method that revolutionized the field of immunometabolism a decade ago, are explained, and recommendations for XF analysis of DCs are given.

Chapters 4 to 7 explore and compare the metabolic profiles of *in vitro*-cultured DCs that preferentially prime either Th1 cells, Th2 cells, Th17 cells or Tregs after stimulation with known antigens or immunomodulatory compounds. In **Chapter 4**, the contribution of intracellular glycogen stores to early metabolic reprogramming of activated murine DCs is evaluated. In **Chapter 5**, metabolism is both the beginning and the end, as metabolic and other changes in human DCs are assessed after stimulation with tolerogenic/regulatory short-chain fatty acids. **Chapter 6**, summarizes and discusses the studies that have interrogated the role of cellular metabolism in controlling the function of various type 2 immune cells, including that of Th2-priming DCs. In **Chapter 7**, transcriptomic and metabolomic data are integrated to provide new insights in the poorly understood metabolic reprogramming of human DCs for Th2 priming. Together, these chapters paint a picture of how DCs with different T cell-polarizing properties can have unique metabolic profiles that might selectively be targeted to alter the nature of the ensuing T cell response.

In Chapters 8 and 9 the *in vivo* role of the LKB1/AMPK pathway and mTOR complex 1 (mTORC1) signalling in DC driven T cell responses is interrogated. Advantage was taken of murine models with DC-specific deletions of these master regulators of metabolism, which allowed the characterization of how DC metabolism shapes the adaptive immune response *in situ*. In **Chapter 8**, mice are studied with DCs that are deficient in LKB1 and are therefore expected to display defects in catabolic metabolism. In **Chapter 9**, mice are examined with DCs that are deficient in raptor, a component of mTORC1, and are therefore expected to display defects in anabolic metabolism. Together these two chapters reveal that the general dogma of anabolic metabolism = pro-inflammatory versus catabolic metabolism = anti-inflammatory may not be generally applicable to DCs *in vivo*. Instead, the immunological outcome of metabolic editing of DCs seems to be greatly influenced by DC subset and tissue localization.

Finally, **Chapter 10** serves as a conclusion to this thesis, as it relates and integrates the work presented herein to studies on DC-driven T cell responses and other works on immunometabolism. It is moreover a representation of the topics the defendant wants to explore in the future and which he thinks may have potential to further mature the field of DC metabolism.

References

1. Vats, D., et al., *Oxidative metabolism and PGC-1beta attenuate macrophage-mediated inflammation*. Cell Metab, 2006. **4**(1): p. 13-24.
2. Michalek, R.D., et al., *Cutting edge: distinct glycolytic and lipid oxidative metabolic programs are essential for effector and regulatory CD4+ T cell subsets.* J Immunol, 2011. **186**(6): p. 3299-303.
3. Everts, B., et al., *TLR-driven early glycolytic reprogramming via the kinases TBK1-IKKvarepsilon supports the anabolic demands of dendritic cell activation.* Nat Immunol, 2014. **15**(4): p. 323-32.
4. Krawczyk, C.M., et al., *Toll-like receptor-induced changes in glycolytic metabolism regulate dendritic cell activation.* Blood, 2010. **115**(23): p. 4742-9.
5. Saxton, R.A. and D.M. Sabatini, *mTOR Signaling in Growth, Metabolism, and Disease*. Cell, 2017. **168**(6): p. 960-976.
6. Weichhart, T., M. Hengstschlager, and M. Linke, *Regulation of innate immune cell function by mTOR.* Nat Rev Immunol, 2015. **15**(10): p. 599-614.
7. Herzig, S. and R.J. Shaw, *AMPK: guardian of metabolism and mitochondrial homeostasis.* Nat Rev Mol Cell Biol, 2018. **19**(2): p. 121-135.
8. Patente, T.A., L.R. Pelgrom, and B. Everts, *Dendritic cells are what they eat: how their metabolism shapes T helper cell polarization.* Curr Opin Immunol, 2019. **58**: p. 16-23.
9. Pearce, E.J. and B. Everts, *Dendritic cell metabolism*. Nat Rev Immunol, 2015. **15**(1): p. 18-29.

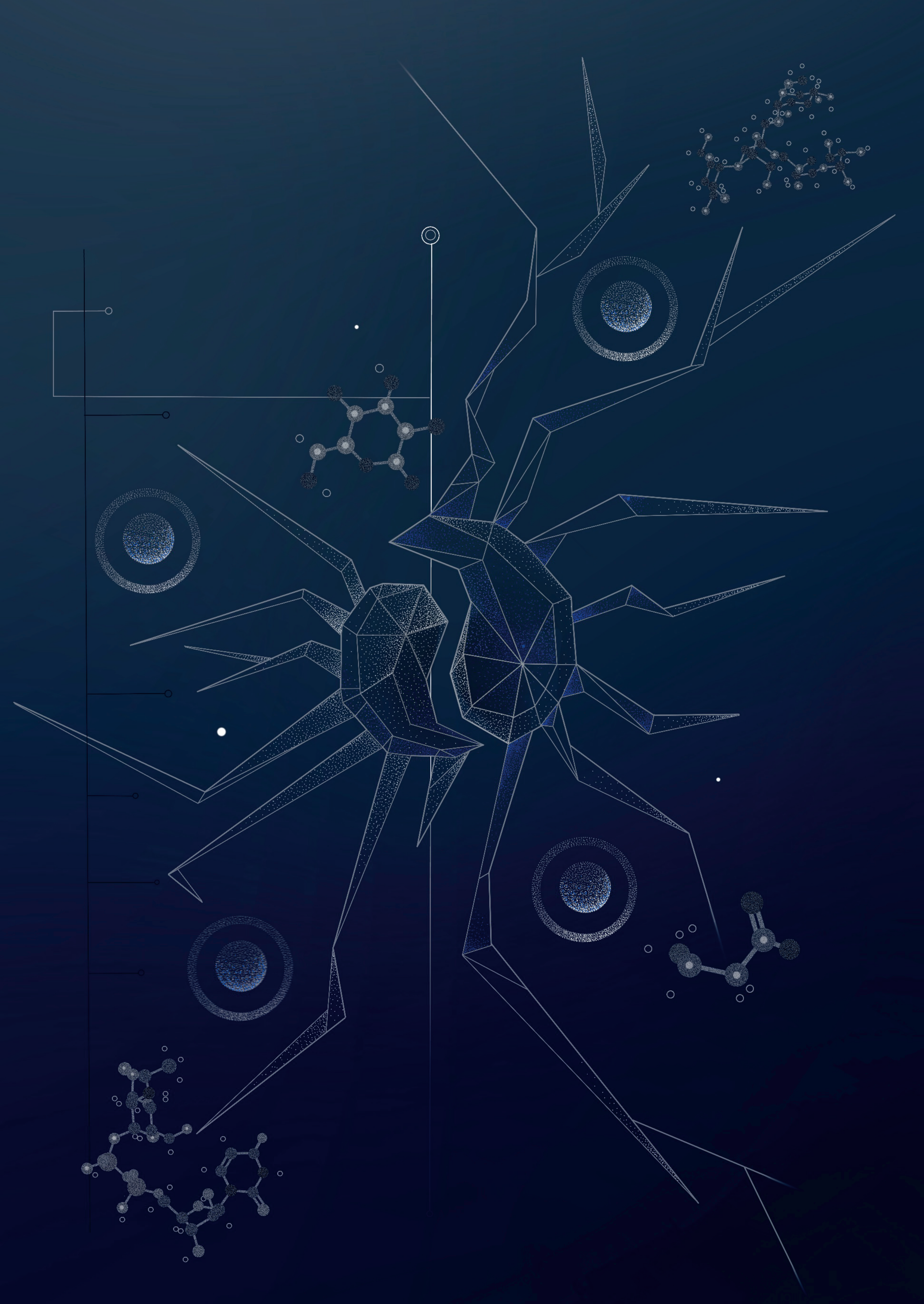

2

Dendritic cells are what they eat: how their metabolism shapes T helper cell polarization

Thiago A. Patente, Leonard R. Pelgrom, Bart Everts

Review
Curr Opin Immunol. 2019 Jun;58:16-23
PMID: 30875606
DOI: 10.1016/j.coi.2019.02.003

Abstract

Dendritic cells (DCs) are professional antigen-presenting cells that play a crucial role in the priming and differentiation of CD4+ T cells into several distinct subsets including effector T helper (Th) 1, Th17 and Th2 cells, as well as regulatory T cells (Tregs). It is becoming increasingly clear that cellular metabolism shapes the functional properties of DCs. Specifically, the ability of DCs to drive polarization of different Th cell subsets may be orchestrated by the engagement of distinct metabolic pathways. In this review, we will discuss the recent advances in the DC metabolism field, by focusing on how cellular metabolism of DCs shapes their priming and polarization of distinct Th cell responses.

Introduction

Dendritic cells (DCs) are professional antigen-presenting cells that play a crucial role in the development of adaptive immune responses by governing the priming and maintenance of CD4+ and CD8+ T cell responses. Classically, DCs reside in a quiescent state in peripheral tissues acting as sentinels of the immune system. Upon capturing pathogen-derived antigens or detecting tissue- derived danger signals, DCs become activated and migrate to draining lymph nodes (LNs). Herein, processed antigens are presented to T cells to initiate an adaptive immune response. Depending on the DC subset involved and the nature of the activation signal received, DCs control the priming and differentiation of CD4+ T cells into several distinct subsets including effector T helper (Th) 1, Th17, and Th2 cells, as well as regulatory T cells (Tregs) [1].

It is becoming increasingly clear that immune cell activation and function, including that of DCs, are coupled to, and underpinned by, profound changes in cellular metabolism [2, 3]. There is a growing body of literature showing that acquisition of an immunogenic phenotype by DCs, characterized by enhanced migratory-capacity and overall T cell priming-capacity, is accompanied by, and dependent on a switch from oxidative phosphorylation (OXPHOS) to glycolysis [4-13]. In addition, more recent studies show that the ability of DCs to drive polarization of different Th cell subsets may be underpinned by engagement of distinct metabolic pathways. In this review, we will discuss these recent advances in the DCs metabolism field, by specifically focusing on how DC metabolism shapes the priming and polarization of distinct CD4+ T cell responses. For a discussion of the metabolic requirements of DCs to shape CD8+ T cell responses please refer to the following recent studies/ reviews [14-18].

Metabolic regulation of MHC II-mediated antigen presentation and costimulation

A prerequisite for priming of CD4+ T cell responses is antigen presentation in the context of MHC II. TLR-driven upregulation of surface expression of MHC II by murine DCs has been shown to depend on glycolysis [5, 9, 19]. DC activation involves acidification of the lysosomal compartment, which is required for efficient generation of peptides for loading into MHC II and that is dependent on activity of ATP-driven proton pumps [20]. In addition, TLR-driven surface expression of MHC II by DCs is primarily thought to arise from redistribution of molecules from endocytic compartments through an energy-dependent process called lysosome tubulation [21, 22]. Therefore, it is conceivable that glycolysis is required for efficient upregulation of surface expression of MHC II because it serves as a key source of ATP to support these two steps in antigen presentation (Figure 1). Mammalian target of rapamycin complex 1 (mTORC1) is an important nutrient sensor that promotes glycolysis, anabolic metabolism and translation [23]. Consistent with a role for glycolysis in regulation of MHC II expression, mTORC1 is activated in DCs upon TLR stimulation [16] and is implicated in TLR-induced MHC II surface expression by DCs [19, 24], through its ability to promote lysosome acidification and tubulation [24, 25]. However, constitutive activation of mTORC1 in murine DCs has been shown to result in impaired MHC II expression, via mTORC1-driven suppression expression of complex transactivator (CIITA), a protein that directly drives the expression of MHC II [26]. In this scenario, as a consequence of constitutive mTORC1 activation, low CIITA expression already in immature DCs leads to reduced synthesis of MHC II molecules and thereby lower levels of the molecules on the surface on DCs following TLR stimulation, despite the promotion of lysosome acidification and tubulation [25]. Finally, mTORC1 may be involved in shaping the antigen repertoire loaded into MHC II. In immature DCs, autophagy – a process classically activated under bioenergetic stress that degrades cellular components to restore cellular energy levels – is thought to allow for cytosolic proteins to enter endosomes and thereby the MHC II-restricted presentation pathway [27]. Upon TLR stimulation, mTORC1 activity is increased and is likely to reduce basal levels of autophagy in activated DCs to limit endogenous but favor exogenous antigen presentation [28]. Together, this implicates glycolysis and mTOR signaling in the regulation of peptide-loading into, and surface expression of MHC II (Figure 1), although to what extent mTOR regulates these processes through control of glycolysis or other metabolic pathways is currently unclear.

In addition to antigen presentation in the context of MHC II, the upregulation of co-stimulatory molecules is also essential for efficient priming of Th cell responses by DCs. TLR-induced CD40 and CD86 expression has been shown to critically depend on glycolysis [5, 9]. In line with this observation, blocking glycolysis in TLR-activated DCs reduced their overall CD4+ T cell-priming capacity [5]. Mechanistically, it was found that increased glycolysis, by fueling the TCA cycle, supports *de novo* synthesis of fatty acids for the expansion of the endoplasmic reticulum (ER) and Golgi allowing for effective translation of those molecules [5]. This highlights the importance of anabolic metabolism fueled by glycolysis to support expression of costimulatory molecules by DCs that is required for effective priming of effector CD4+ T cell responses. Yet to what extent Th polarization by DCs is controlled by metabolism through regulation of expression of MHC II and costimulatory molecules is unclear at this point.

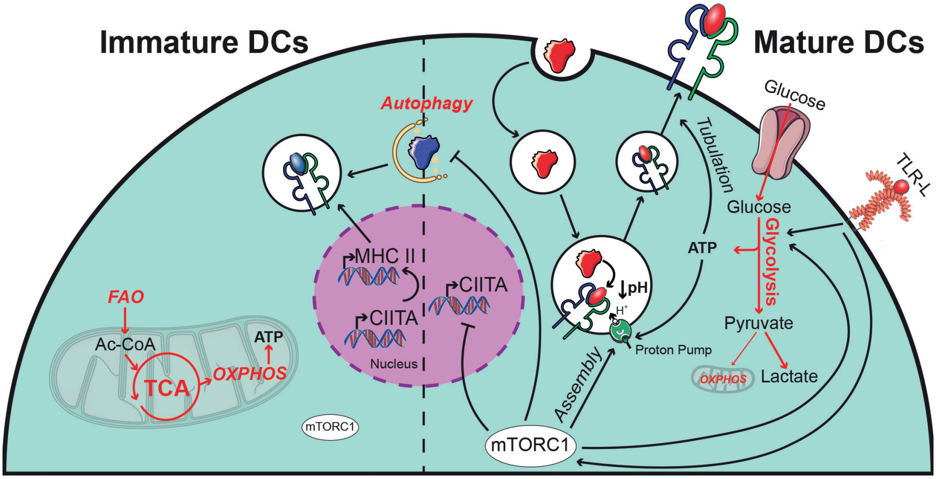

Figure 1. Role of mTOR and cellular metabolism in the regulation of MHC II-dependent antigen presentation by DCs.

Metabolic pathways and upstream signaling pathways regulating these are indicated in red and black, respectively. The left and the right sides of the figure depict how MHC II-dependent antigen presentation is metabolically regulated in unactivated (immature) and TLR-stimulated (mature) DCs, respectively.

Metabolic regulation of DC-driven Th1 polarization

A key Th1-polarizing cytokine produced by DCs is IL-12 [29]. IL-12 expression by DCs has been shown to critically depend on glycolysis by supporting the *de novo* synthesis of fatty acids for the expansion of the endoplasmic reticulum (ER) and Golgi required for effective translation [5]. Concordantly, inhibition of glycolysis in murine LPS-activated DCs impaired their ability to promote IFN-γ secretion by CD4+ T cells. Moreover, type 1 conventional DCs (cDC1s), the primary DC subset that produces IL-12 and drives Th1 responses *in vivo* [30, 31], are more glycolytic than cDC2s [15]. Despite the importance of mTORC1 in driving glycolytic metabolism and translation, interfering with mTORC1 signaling has been shown to augment IL-12 secretion [32-34]. In line with this, hyperactivation of mTORC1 in CD11c+ cells, by ablation of its negative regulator tuberous sclerosis 1 (TSC1), resulted in downregulation of *il12a* and consequently in impaired Th1 priming by BMDCs generated with FLT3L [35]. Presumably this suppressive effect of mTORC1 signaling on IL-12 production is mediated by a an mTORC1-driven negative feedback loop involving IL-10 [33, 36]. Nonetheless, favoring anabolic metabolism, by inactivation of AMP-activated kinase (AMPK), which normally promotes OXPHOS and catabolic metabolism in part by suppressing mTOR activity, increases IL-12 production by DCs [9, 37]. This points toward an important role for anabolic metabolism supported by glycolysis in supporting the ability of DCs to promote Th1 differentiation (Figure 2a).

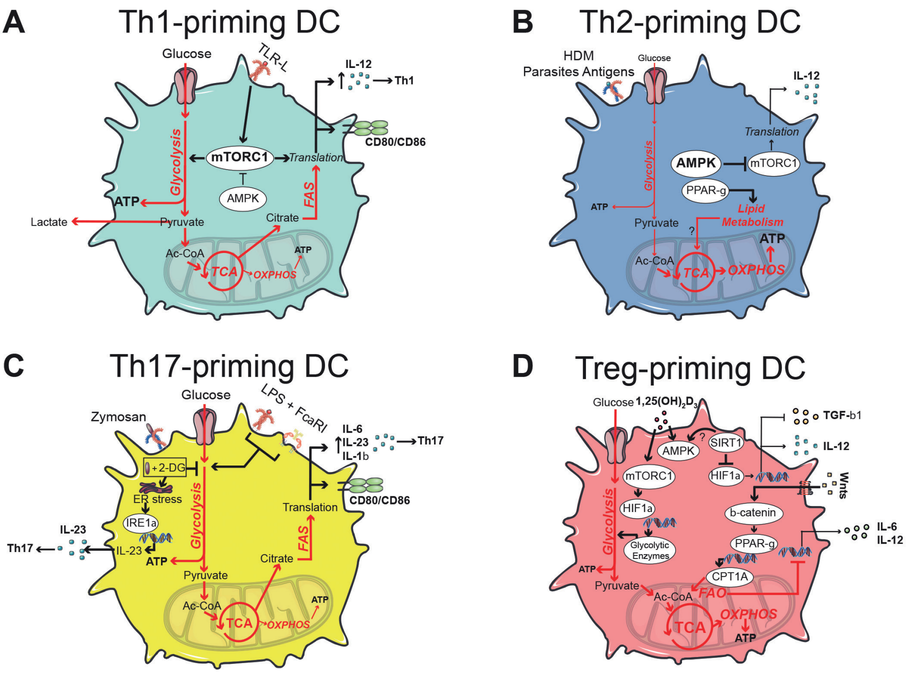
A
Th1-priming DC
Glucose
TLR-L
IL-12
Th1
CD80/CD86
Glycolysis
mTORC1
Translation
AMPK
FAS
ATP
Lactate
Pyruvate
Citrate
Ac-CoA
TCA
OXPHOS
ATP
B
Th2-priming DC
HDM
Parasites Antigens
Glucose
IL-12
Translation
Glycolysis
AMPK
mTORC1
PPAR-g
Lipid Metabolism
ATP
Pyruvate
?
ATP
Ac-CoA
TCA
OXPHOS
C
Th17-priming DC
Glucose
LPS + FcaRI
Zymosan
+2-DG
ER stress
IRE1a
IL-6
IL-23
IL-1b
Th17
CD80/CD86
Translation
Glycolysis
IL-23
Th17
IL-23
ATP
FAS
Citrate
Pyruvate
Ac-CoA
TCA
OXPHOS
ATP
D
Treg-priming DC
Glucose
1,25(OH)2D3
?
AMPK
SIRT1
TGF-b1
IL-12
mTORC1
HIF1a
Wnts
HIF1a
Glycolysis
b-catenin
Glycolytic Enzymes
PPAR-g
IL-6
IL-12
ATP
CPT1A
Pyruvate
Ac-CoA
FAO
OXPHOS
TCA
ATP

Figure 2. Metabolic characteristics of DCs that prime different Th cells.

Metabolic pathways and upstream signaling pathways regulating these in DCs that prime Th1 (a), Th2 (b), Th17 (c) and Treg (d) responses are indicated in red and black, respectively.

Metabolic regulation of DC-driven Th2 polarization

Despite the evidence that DCs are crucially important for induction of Th2 responses, the nature of the polarizing signals derived from DCs to drive these responses are not fully understood, although reduced TCR signal strength, absence of IL-12 and secretion of type 2 cytokines by other innate type 2 immune cells have been suggested [38, 39]. Likewise, the metabolic properties of Th2-priming DCs are not well defined.

In contrast to activation with LPS, stimulation of DCs with house dust mite extract (HDM), an antigen mixture known to promote DC-dependent Th2 responses in the lung resulting in allergic asthma, was recently found to induce only a mild increase in glycolysis with no loss of OXPHOS over time [19]. This suggests a more catabolic metabolic state of Th2-priming DCs, similar to what has been implied for other cells involved in type 2 immune responses [40]. Consistent with this, increased phosphorylation of AMPK was found in CD11b+ lung cDC2s of mice infected with hookworm that promotes strong Type 2 immune responses in the lung [37]. Moreover, mice with a specific deletion of AMPKα1 in CD11c-expressing cells fail to mount protective Th2 responses against this parasitic worm infection, suggesting AMPK-driven catabolic metabolism in DCs may be functionally relevant for Th2 priming. This would be supported by the observations that acute mTOR inhibition potentiates Th2 priming by human DCs *in vitro* [41] and that mice with a DC-specific deletion of mTOR have higher circulating titers of type 2 cytokine-dependent antibodies IgE and antigen-specific IgG1, in a model of allergic asthma, although this is not mirrored by an enhanced Th2 response in the lungs [42].

Lipid metabolism, regulated by PPAR-γ, may also play an important role in Th2 priming by DCs. Mice with a deletion of PPAR-γ in CD11c-expressing cells are resistant to induction of allergic asthma [43]. In contrast, stimulation of DCs with PPAR-γ activator rosiglitazone, ameliorates airway inflammation in a mouse model of asthma [44]. In agreement with this, deletion of Sirtuin-1 (SIRT1) in DCs restricts an allergen-induced Th2 response in the lung by activating PPAR-γ [45]. This may indicate that a certain level of PPAR-γ activity is required for Th2 priming by DCs, but strong activation may interfere with this, possibly by rendering DCs tolerogenic [46, 47]. Taken together, these studies provide a first indication that Th2-priming DCs, have a more oxidative metabolic profile dependent on AMPK and low PPAR-γ signaling (Figure 2b). One could hypothesize that this oxidative/catabolic metabolic profile limits high expression of IL-12 and MHC II, thereby favoring Th2 polarization by DCs. However, this link remains to be experimentally addressed.

Metabolic regulation of DC-driven Th17 polarization

The polarization of naïve CD4+ T cells into Th17 cells is driven by TGF-β and IL-6, while IL-23 and IL-1β play a prominent role in the expansion and survival of Th17 cells [48, 49]. Little is known about the metabolic regulation of TGF-β production by DCs. However, both the secretion of IL-6 by murine DCs in response to TLR stimulation [6, 50] and the secretion of IL-23 and IL-1β by human DCs following the combined engagement of TLRs and FCαR [51, 52] seem to be dependent on anabolic metabolism characterized by *de novo* fatty acid synthesis fueled by glycolysis. However, another study found that blocking glycolysis during TLR stimulation increased IL-23 expression by human DCs due to enhanced expression of the ER stress sensor IRE1α [53]. Consistent with this latter observation, treatment of murine DCs with glycolysis inhibitor 2-deoxyglucose (2-DG) can enhance their Th17-priming potential [5] (Figure 2c). These opposing may suggest that the metabolic requirements for cytokine production can be context specific and depend on the DC subset and type of stimulus involved, as has been demonstrated for different TLR ligands in monocytes [54].

The metabolic pathways involved in Th17 differentiation by DCs *in vivo* are not well defined. Mice with a defect in mTORC1 in CD11c-expressing cells, show a switch toward Th17 instead of Th2 polarization in response to HDM-induced asthma, that is accompanied by changes in the frequency and metabolic profile of lung DCs [42]. This was found to be mediated by inflammatory DCs, that expressed higher levels of IL-23, IL-6, and IL-1β, which the authors postulated to be due to enhanced fatty acid oxidation in these cells. However, it is conceivable that loss of mTORC1-driven IL-10 secretion, that could otherwise suppress expression of these pro-inflammatory cytokines, also contributes to this phenotype [33, 36]. Of note, susceptibility to develop Th17-driven experimental autoimmune encephalomyelitis (EAE), a murine model for multiple sclerosis, was not increased, implying that mTOR in DCs restricts Th17 responses in a tissue-specific manner [42]. Furthermore, DCs in which cholesterol accumulated as a consequence of deletion of ATP binding cassette transporters A1 and G1 (ABCA1 and ABCG1), two transporters responsible for cholesterol efflux, displayed increased secretion of IL-23, IL-6, and IL-1β and a potentiated ability to drive Th17 polarization [55]. The known stimulating effect of cholesterol on pro-inflammatory TLR signaling and inflammasome activation is likely to explain these effects [56]. However, whether cholesterol synthesis and/or regulation of its efflux is a metabolic process general employed by DCs to prime Th17 responses such as following exposure to Th17-priming pathogens is unknown and warrants further investigation.

Metabolic regulation of DC-driven Treg polarization

DCs are also key regulators of maintenance of immune tolerance by governing the development of regulatory T cells (Tregs). Tregs can be induced in the thymus, referred to as thymic-derived Tregs (tTregs), as well as in the periphery (pTregs) or *in vitro* (iTregs) from naïve T cells [57]. A diverse set of mechanisms has been identified through which pTreg and iTreg differentiation from naïve T cells can be induced by DCs, including low costimulatory signal strength, increased expression of IL-10 and TGF-β and enhanced activity of retinaldehyde dehydrogenase (RALDH) and indoleamine 2,3-dioxygenase (IDO) [58, 59]. Now, the metabolic characteristics of tolerogenic DCs and requirements for their tolerogenic phenotype leading to pTreg and iTreg differentiation are also starting to be elucidated.

It has long been appreciated that differentiation of human monocytes toward DCs in the presence of mTORC1 inhibitor rapamycin, generates tolerogenic DCs [60], providing a first indication that inhibition of anabolic metabolism could favor acquisition of a tolerogenic DC phenotype. Consistent with this notion, two recent studies characterizing the metabolic properties of human moDCs rendered tolerogenic with $1,25(OH)_2D_3$ (VitD3) alone [61] or together with dexamethasone [62], reported increased mitochondrial activity evidenced by heightened OXPHOS. In the latter study, acquisition of tolerogenic phenotype by the DCs was partly dependent on increased FAO [62]. Interestingly, VitD3–DCs additionally displayed increased mTOR/hypoxia induced factor (HIF)-1α-dependent glycolytic rates [61]. This increased glycolysis was functionally relevant as several markers of a tolerogenic phenotype (i.e. reduced expression of costimulatory molecules CD86 and CD80 and increased production of IL-10) was lost by VitD3–DCs in which glycolysis was inhibited [61]. Concordantly, glycolysis inhibition limited their ability to suppress CD4+ T cell proliferation. Interestingly, the observations that these cells show an increased AMPK activation [61] and elevated glucose carbon tracing into the TCA cycle [63], suggest that this increased glycolytic flux, in contrast to immunogenic DCs, may primarily serve a catabolic role by fueling mitochondrial OXPHOS.

Largely consistent with these human DC data, a recent *in vivo* study focusing on the metabolic properties of DCs in tumors [64], a microenvironment that is a well-known to render DCs tolerogenic [65], revealed that these cells displayed increased FAO-dependent OXPHOS. This metabolic shift as well as IDO activity was driven by tumor cell-derived Wnt5a and dependent on β-catenin and PPAR-γ signaling. Importantly, when FAO was blocked in DCs, Wnt5a failed to enhance IDO activity in these cells as well as to instruct them to promote FoxP3+ pTreg differentiation and as a consequence enhanced anti-tumor immunity *in vivo*. Interestingly, a similar β-catenin-PPAR-γ-dependent pathway is required for the maintenance tolerogenic DCs in visceral adipose tissue [66]. This, together with the findings that tolerogenic DCs in mucosal tissues depend on PPAR-γ signaling for RALDH expression and activity [46, 47], points toward a crucial role for PPAR-γ in supporting tolerogenic properties of DCs in various settings (Figure 2d). However, to what extent these PPAR-γ-driven effects are mediated by controlling lipid metabolism remains to be determined.

Conversely, a switch from OXPHOS toward aerobic glycolysis by stabilization of hypoxia induced factor (HIF)-1α, as seen in SIRT1-deficient DCs, redirects pTreg toward Th1 priming by enhancing IL-12 production and reducing TGF-βeta expression [67], providing further support for a key role in catabolic/oxidative metabolism in pTreg induction by DCs. Given the key role for AMPK signaling in promoting this type of metabolism it is tempting to speculate that this kinase is important in DC-driven iTreg and pTreg polarization. The fact that SIRT1 can promote the activation of AMPK, through deacetylation of LKB1 [68], and that VitD3-treated human DCs showed increased AMPK activation [61], would be consistent with this idea and warrants a more direct assessment of the role of AMPK signaling in regulating the tolerogenic properties in DCs. The aforementioned studies have focused on the metabolic requirements for DCs to promote iTreg or pTreg differentiation. To what extent these observations, can be extrapolated to DC-driven tTreg differentiation in the thymus remains an open question.

Concluding remarks

Ever since the appearance of the first studies focusing on the role of cellular metabolism in DC function about a decade ago, this field has rapidly grown and has provided key novel insights into the metabolic pathways that shape the functional properties of DCs. As reviewed here, a picture is emerging that the metabolic requirements for DCs to drive Th1 and Th17 polarization share similarities in which glycolysis and mTOR-driven anabolic metabolism play a central role. In contrast, Th2 and Treg induction by DCs seem to rely on more oxidative lipid metabolism driven by AMPK and PPAR-γ signaling (Figure 2). This shared dependency on anabolic metabolism by Th1-priming and Th17-priming DCs, and on catabolism by DC-driven Th2 and Treg priming, largely correspond with the respective strong and more muted activation profiles of these DCs. Yet, whether there are specific additional metabolic cues that underpin or instruct DCs to either prime a Th1 versus Th17 response or a Th2 versus Treg response is still poorly understood. It is conceivable that this polarizing instruction is primarily provided by external cues such as cytokines, pathogen or danger signals that through classical signaling cascades drive expression of certain combination of polarizing cytokines by DCs. In this scenario, metabolic sensors, such AMPK and mTOR, integrate signals from these external stimuli with nutrient availability to engage a metabolic program tailored to the bioenergetic and bio-synthetic requirements for DC activation that is needed to prime a specific Th cell response. In this context, certain changes in cellular metabolism would have an essential supportive function, yet not in itself be sufficient for providing instructive signals that shape Th cell polarization by DCs. However, primarily based on studies with T cells and macrophages, the growing realization that certain external stimuli can coopt specific metabolic pathways, enzymes or promote production of particular metabolites in order to dominantly regulate expression of certain cytokines, makes it tempting to speculate that such metabolic regulatory mechanisms are also operational in DCs to actively promote or repress expression of proteins that shape Th cell polarization. More in-depth functional comparison of the upstream metabolic regulators and metabolic pathways in different Th cell-priming DCs will be needed, to determine whether there are unique metabolic programs that underpin and truly drive the ability of DCs to prime distinct Th cell responses both *in vitro* and *in vivo*. In addition, such studies will help to better understand the relative contribution of, and interplay between, intracellular metabolic and signaling pathways in shaping Th cell polarization by DCs. Finally, to what extent the metabolic characteristics and thereby Th cell-polarizing properties of DC subsets are determined by their ontogeny versus the micro-environment they reside is an intriguing question that remains to be answered. Addressing these issues, will contribute to a more complete understanding of the multifaceted role of cellular metabolism in Th cell priming by DCs, and will reveal whether directed targeting of metabolic pathways in DCs could hold promise as novel approach to direct Th cell polarization that can be exploited in DC-based immunotherapy for the treatment of various types of immune-mediated disease.

Conflicts of interest statement

Nothing declared.

Acknowledgements

This work was supported by an LUMC fellowship to BE and by FAPESP (#2014/26437 and #2108/00719-9) to TAP.

References

1. Kapsenberg, M.L., *Dendritic-cell control of pathogen-driven T-cell polarization.* Nat Rev Immunol, 2003. **3**(12): p. 984-93.
2. Buck, M.D., et al., *Metabolic Instruction of Immunity.* Cell, 2017. **169**(4): p. 570-586.
3. O'Neill, L.A., R.J. Kishton, and J. Rathmell, *A guide to immunometabolism for immunologists.* Nat Rev Immunol, 2016. **16**(9): p. 553-65.
4. Basit, F., et al., *Human Dendritic Cell Subsets Undergo Distinct Metabolic Reprogramming for Immune Response.* Front Immunol, 2018. **9**: p. 2489.
5. Everts, B., et al., *TLR-driven early glycolytic reprogramming via the kinases TBK1-IKKvarepsilon supports the anabolic demands of dendritic cell activation.* Nat Immunol, 2014. **15**(4): p. 323-32.
6. Everts, B., et al., *Commitment to glycolysis sustains survival of NO-producing inflammatory dendritic cells.* Blood, 2012. **120**(7): p. 1422-31.
7. Fliesser, M., et al., *Hypoxia-inducible factor 1alpha modulates metabolic activity and cytokine release in anti-Aspergillus fumigatus immune responses initiated by human dendritic cells.* Int J Med Microbiol, 2015. **305**(8): p. 865-73.
8. Jantsch, J., et al., *Hypoxia and hypoxia-inducible factor-1 alpha modulate lipopolysaccharide-induced dendritic cell activation and function.* J Immunol, 2008. **180**(7): p. 4697-705.
9. Krawczyk, C.M., et al., *Toll-like receptor-induced changes in glycolytic metabolism regulate dendritic cell activation.* Blood, 2010. **115**(23): p. 4742-9.
10. McKeithen, D.N., et al., *The emerging role of ASC in dendritic cell metabolism during Chlamydia infection.* PLoS One, 2017. **12**(12): p. e0188643.
11. Pantel, A., et al., *Direct type I IFN but not MDA5/TLR3 activation of dendritic cells is required for maturation and metabolic shift to glycolysis after poly IC stimulation.* PLoS Biol, 2014. **12**(1): p. e1001759.
12. Ryans, K., et al., *The immunoregulatory role of alpha enolase in dendritic cell function during Chlamydia infection.* BMC Immunol, 2017. **18**(1): p. 27.
13. Thwe, P.M., et al., *Cell-Intrinsic Glycogen Metabolism Supports Early Glycolytic Reprogramming Required for Dendritic Cell Immune Responses.* Cell Metab, 2017. **26**(3): p. 558-567.e5.
14. Amiel, E., et al., *Inhibition of mechanistic target of rapamycin promotes dendritic cell activation and enhances therapeutic autologous vaccination in mice.* J Immunol, 2012. **189**(5): p. 2151-8.
15. Du, X., et al., *Hippo/Mst signalling couples metabolic state and immune function of CD8alpha(+) dendritic cells.* Nature, 2018.
16. Lawless, S.J., et al., *Glucose represses dendritic cell-induced T cell responses.* Nat Commun, 2017. **8**: p. 15620.
17. Nicoli, F., S. Paul, and V. Appay, *Harnessing the Induction of CD8(+) T-Cell Responses Through Metabolic Regulation by Pathogen-Recognition-Receptor Triggering in Antigen Presenting Cells.* Front Immunol, 2018. **9**: p. 2372.
18. Schouppe, E., et al., *Modulation of CD8(+) T-cell activation events by monocytic and granulocytic myeloid-derived suppressor cells.* Immunobiology, 2013. **218**(11): p. 1385-91.

19. Guak, H., et al., *Glycolytic metabolism is essential for CCR7 oligomerization and dendritic cell migration*. Nat Commun, 2018. **9**(1): p. 2463.
20. Trombetta, E.S., et al., *Activation of lysosomal function during dendritic cell maturation*. Science, 2003. **299**(5611): p. 1400-3.
21. Villadangos, J.A., et al., *MHC class II expression is regulated in dendritic cells independently of invariant chain degradation*. Immunity, 2001. **14**(6): p. 739-49.
22. Vyas, J.M., et al., *Tubulation of class II MHC compartments is microtubule dependent and involves multiple endolysosomal membrane proteins in primary dendritic cells*. J Immunol, 2007. **178**(11): p. 7199-210.
23. Powell, J.D., et al., *Regulation of immune responses by mTOR*. Annu Rev Immunol, 2012. **30**: p. 39-68.
24. Saric, A., et al., *mTOR controls lysosome tubulation and antigen presentation in macrophages and dendritic cells*. Mol Biol Cell, 2016. **27**(2): p. 321-33.
25. Liberman, R., et al., *Regulated assembly of vacuolar ATPase is increased during cluster disruption-induced maturation of dendritic cells through a phosphatidylinositol 3-kinase/mTOR-dependent pathway*. J Biol Chem, 2014. **289**(3): p. 1355-63.
26. Pan, H., et al., *Critical role of the tumor suppressor tuberous sclerosis complex 1 in dendritic cell activation of CD4 T cells by promoting MHC class II expression via IRF4 and CIITA*. J Immunol, 2013. **191**(2): p. 699-707.
27. Dengjel, J., et al., *Autophagy promotes MHC class II presentation of peptides from intracellular source proteins*. Proc Natl Acad Sci U S A, 2005. **102**(22): p. 7922-7.
28. Schmid, D., M. Pypaert, and C. Münz, *Antigen-loading compartments for major histocompatibility complex class II molecules continuously receive input from autophagosomes*. Immunity, 2007. **26**(1): p. 79-92.
29. Hamza, T., J.B. Barnett, and B. Li, *Interleukin 12 a key immunoregulatory cytokine in infection applications*. Int J Mol Sci, 2010. **11**(3): p. 789-806.
30. Everts, B., et al., *Migratory CD103+ dendritic cells suppress helminth-driven type 2 immunity through constitutive expression of IL-12*. J Exp Med, 2016. **213**(1): p. 35-51.
31. Mashayekhi, M., et al., *CD8α(+) dendritic cells are the critical source of interleukin-12 that controls acute infection by Toxoplasma gondii tachyzoites*. Immunity, 2011. **35**(2): p. 249-59.
32. Macedo, C., et al., *Rapamycin augments human DC IL-12p70 and IL-27 secretion to promote allogeneic Type 1 polarization modulated by NK cells*. Am J Transplant, 2013. **13**(9): p. 2322-33.
33. Ohtani, M., et al., *Mammalian target of rapamycin and glycogen synthase kinase 3 differentially regulate lipopolysaccharide-induced interleukin-12 production in dendritic cells*. Blood, 2008. **112**(3): p. 635-43.
34. Stenger, E.O., et al., *IL-12hi rapamycin-conditioned dendritic cells mediate IFN-gamma-dependent apoptosis of alloreactive CD4+ T cells in vitro and reduce lethal graft-versus-host disease*. Biol Blood Marrow Transplant, 2014. **20**(2): p. 192-201.
35. Wang, Y., et al., *Tuberous sclerosis 1 (Tsc1)-dependent metabolic checkpoint controls development of dendritic cells*. Proc Natl Acad Sci U S A, 2013. **110**(50): p. E4894-903.

36. Ohtani, M., et al., *Cutting edge: mTORC1 in intestinal CD11c+ CD11b+ dendritic cells regulates intestinal homeostasis by promoting IL-10 production*. J Immunol, 2012. **188**(10): p. 4736-40.
37. Nieves, W., et al., *Myeloid-Restricted AMPKalpha1 Promotes Host Immunity and Protects against IL-12/23p40-Dependent Lung Injury during Hookworm Infection*. J Immunol, 2016. **196**(11): p. 4632-40.
38. Lloyd, C.M. and R.J. Snelgrove, *Type 2 immunity: Expanding our view*. Sci Immunol, 2018. **3**(25).
39. Paul, W.E. and J. Zhu, *How are T(H)2-type immune responses initiated and amplified?* Nat Rev Immunol, 2010. **10**(4): p. 225-35.
40. Pelgrom, L.R. and B. Everts, *Metabolic control of type 2 immunity*. Eur J Immunol, 2017. **47**(8): p. 1266-1275.
41. Hussaarts, L., et al., *Rapamycin and omega-1: mTOR-dependent and -independent Th2 skewing by human dendritic cells*. Immunol Cell Biol, 2013. **91**(7): p. 486-9.
42. Sinclair, C., et al., *mTOR regulates metabolic adaptation of APCs in the lung and controls the outcome of allergic inflammation*. Science, 2017.
43. Nobs, S.P., et al., *PPARgamma in dendritic cells and T cells drives pathogenic type-2 effector responses in lung inflammation*. J Exp Med, 2017. **214**(10): p. 3015-3035.
44. Hammad, H., et al., *Activation of peroxisome proliferator-activated receptor-gamma in dendritic cells inhibits the development of eosinophilic airway inflammation in a mouse model of asthma*. Am J Pathol, 2004. **164**(1): p. 263-71.
45. Legutko, A., et al., *Sirtuin 1 promotes Th2 responses and airway allergy by repressing peroxisome proliferator-activated receptor-gamma activity in dendritic cells*. J Immunol, 2011. **187**(9): p. 4517-29.
46. Housley, W.J., et al., *PPARgamma regulates retinoic acid-mediated DC induction of Tregs*. J Leukoc Biol, 2009. **86**(2): p. 293-301.
47. Khare, A., et al., *Cutting Edge: Dual Function of PPARgamma in CD11c+ Cells Ensures Immune Tolerance in the Airways*. J Immunol, 2015. **195**(2): p. 431-5.
48. Harrington, L.E., et al., *Interleukin 17-producing CD4+ effector T cells develop via a lineage distinct from the T helper type 1 and 2 lineages*. Nat Immunol, 2005. **6**(11): p. 1123-32.
49. Patel, D.D. and V.K. Kuchroo, *Th17 Cell Pathway in Human Immunity: Lessons from Genetics and Therapeutic Interventions*. Immunity, 2015. **43**(6): p. 1040-51.
50. Carroll, K.C., B. Viollet, and J. Suttles, *AMPKalpha1 deficiency amplifies proinflammatory myeloid APC activity and CD40 signaling*. J Leukoc Biol, 2013. **94**(6): p. 1113-21.
51. Hansen, I.S., et al., *FcαRI co-stimulation converts human intestinal CD103(+) dendritic cells into pro-inflammatory cells through glycolytic reprogramming*. Nat Commun, 2018. **9**(1): p. 863.
52. Moon, J.S., et al., *mTORC1-Induced HK1-Dependent Glycolysis Regulates NLRP3 Inflammasome Activation*. Cell Rep, 2015. **12**(1): p. 102-115.
53. Marquez, S., et al., *Endoplasmic Reticulum Stress Sensor IRE1alpha Enhances IL-23 Expression by Human Dendritic Cells*. Front Immunol, 2017. **8**: p. 639.

54. Lachmandas, E., et al., *Microbial stimulation of different Toll-like receptor signalling pathways induces diverse metabolic programmes in human monocytes*. Nat Microbiol, 2016. **2**: p. 16246.
55. Westerterp, M., et al., *Cholesterol Accumulation in Dendritic Cells Links the Inflammasome to Acquired Immunity*. Cell Metab, 2017.
56. Tall, A.R. and L. Yvan-Charvet, *Cholesterol, inflammation and innate immunity*. Nat Rev Immunol, 2015. **15**(2): p. 104-16.
57. Shevach, E.M. and A.M. Thornton, *tTregs, pTregs, and iTregs: similarities and differences*. Immunol Rev, 2014. **259**(1): p. 88-102.
58. Domogalla, M.P., et al., *Tolerance through Education: How Tolerogenic Dendritic Cells Shape Immunity*. Front Immunol, 2017. **8**: p. 1764.
59. Rodrigues, C.P., et al., *Tolerogenic IDO(+) Dendritic Cells Are Induced by PD-1-Expressing Mast Cells*. Front Immunol, 2016. **7**: p. 9.
60. Fischer, R., et al., *Use of rapamycin in the induction of tolerogenic dendritic cells*. Handb Exp Pharmacol, 2009(188): p. 215-32.
61. Ferreira, G.B., et al., *Vitamin D3 Induces Tolerance in Human Dendritic Cells by Activation of Intracellular Metabolic Pathways*. Cell Rep, 2015. **10**(5): p. 711-725.
62. Malinarich, F., et al., *High mitochondrial respiration and glycolytic capacity represent a metabolic phenotype of human tolerogenic dendritic cells*. J Immunol, 2015. **194**(11): p. 5174-86.
63. Vanherwegen, A.S., et al., *Vitamin D controls the capacity of human dendritic cells to induce functional regulatory T cells by regulation of glucose metabolism*. J Steroid Biochem Mol Biol, 2018.
64. Zhao, F., et al., *Paracrine Wnt5a-beta-Catenin Signaling Triggers a Metabolic Program that Drives Dendritic Cell Tolerization*. Immunity, 2018. **48**(1): p. 147-160.e7.
65. Ramos, R.N., et al., *Monocyte-derived dendritic cells from breast cancer patients are biased to induce CD4+CD25+Foxp3+ regulatory T cells*. J Leukoc Biol, 2012. **92**(3): p. 673-82.
66. Macdougall, C.E., et al., *Visceral Adipose Tissue Immune Homeostasis Is Regulated by the Crosstalk between Adipocytes and Dendritic Cell Subsets*. Cell Metab, 2018. **27**(3): p. 588-601.e4.
67. Liu, G., et al., *Dendritic cell SIRT1-HIF1α axis programs the differentiation of CD4+ T cells through IL-12 and TGF-β1*. Proc Natl Acad Sci U S A, 2015. **112**(9): p. E957-65.
68. Chen, X., et al., *Intercellular interplay between Sirt1 signalling and cell metabolism in immune cell biology*. Immunology, 2015. **145**(4): p. 455-67.

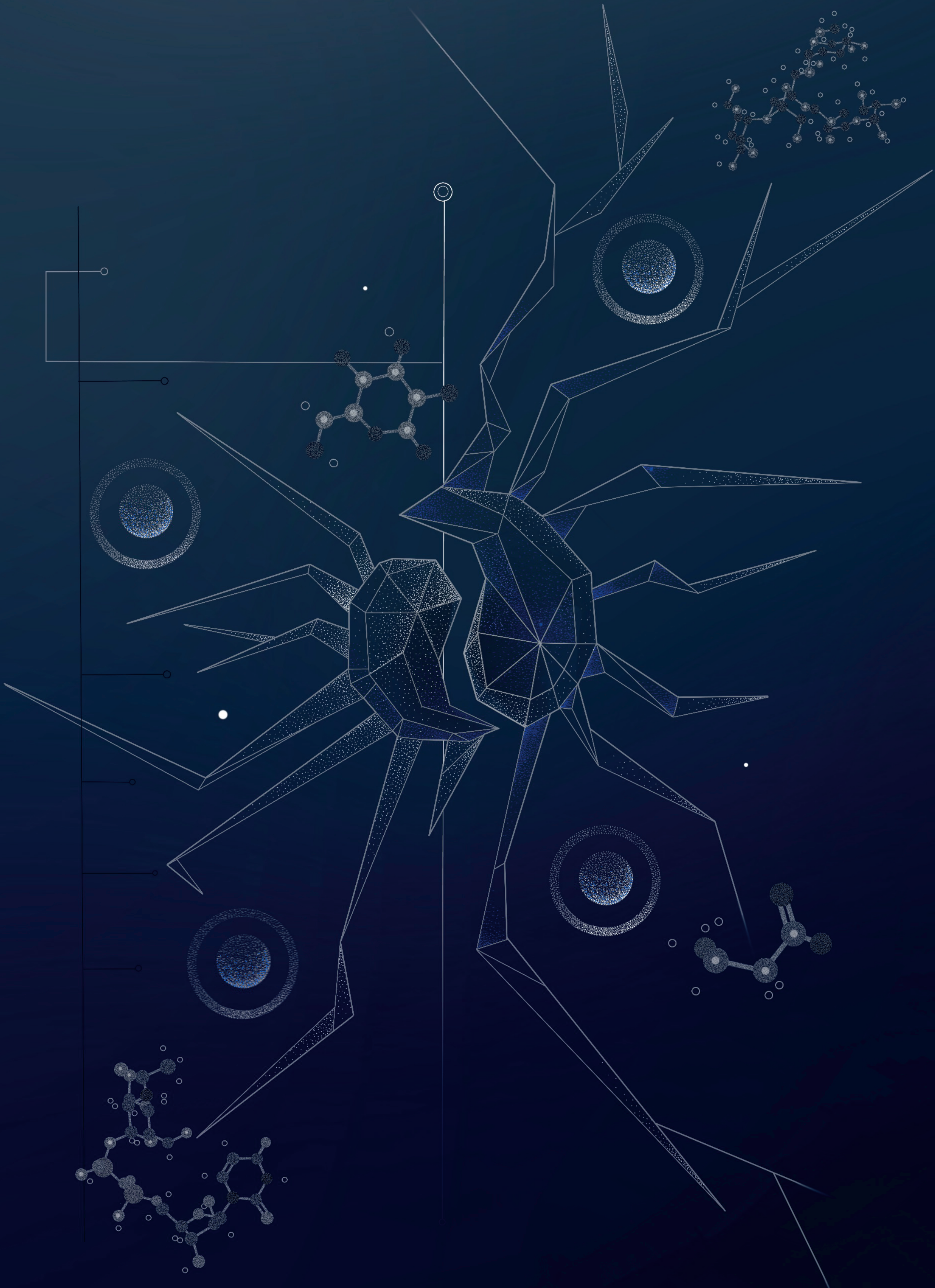

3

Analysis of TLR-Induced Metabolic Changes in Dendritic Cells Using the Seahorse XF^{e}96 Extracellular Flux Analyzer

Leonard R. Pelgrom
Alwin J. van der Ham
Bart Everts

Methods Mol Biol. 2016;1390:273-85
PMID: 26803635
DOI: 10.1007/978-1-4939-3335-8_17

Abstract

Engagement of Toll-like receptors (TLRs) on dendritic cells (DCs) triggers the expression of a large set of genes involved in DC activation and maturation, which allow them to act efficiently as antigen-presenting cells. Recently, it has become clear that TLR signalling in DCs also results in dramatic metabolic changes that are integral to their changed biology. Here, we describe a detailed protocol on how DC metabolism can be studied after TLR stimulation using the 96-well format Extracellular Flux (XF^{e}96) Analyzer from Seahorse Bioscience, a machine that allows one to simultaneously assess rates of oxidative phosphorylation and glycolysis in real-time, in live cells and in a high-throughput manner.

Introduction

Signalling via Toll-like receptors (TLRs) on dendritic cells (DCs) drives a program of activation that includes the enhanced capturing and processing of antigens for loading and presentation on major histocompatibility complex (MHC) class I and II, and the increased expression of chemokine receptors, cytokines and co-stimulatory molecules. It is not surprising that this dramatic change in the biology of DCs requires a metabolic adaptation to meet the bioenergetic and anabolic demands of this activation process. We and others have recently found that in murine DCs, triggering of TLRs is accompanied by a metabolic switch characterized by an increase in glycolysis and a complementary decrease in oxidative phosphorylation [3, 4, 14, 16, 18]. Specifically, loss of mitochondrial oxidative function was found to be a direct consequence of TLR-induced production of nitric oxide (NO) by inducible nitric oxide synthase (iNOS) that poisons the mitochondrial respiratory chain in an autocrine fashion. This forces the cells to increase glycolytic flux to maintain sufficient ATP levels [14, 76]. In addition to this bioenergetic adaption, we have recently observed that TLR engagement also triggers a rapid increase in glycolysis, preceding iNOS expression, that primarily appears to serve an anabolic role allowing DCs to express activation markers and cytokines and therefore, to acquire their full T-cell-priming potential [3].

Some of these observations regarding TLR-driven metabolic changes in DCs have been performed using traditional cellular metabolic assays that typically involve radioactivity, cell destruction and large numbers of cells [77]. Recently, Extracellular Flux (XF) Analyzers from Seahorse Bioscience have been developed that perform highly accurate real-time measurements of cellular metabolism of living cells and tissues by simultaneously quantifying rates of extracellular acidification (ECAR) and oxygen consumption (OCR) as measures of glycolysis and mitochondrial respiration, respectively. This apparatus has allowed us to gain exciting new insights in immune cell metabolism and has been shown to be instrumental in moving the field of DC metabolism forward [9]. This state-of-the-art technology offers a robust and simple high-throughput method for studying substrate utilization, mitochondrial function, and energy expenditure in a 24- or 96-well plate format, without the use of large number of cells, electrodes, dyes, radioactive materials or lysis of cells that is typical of other more laborious metabolic assays. During measurements, the XF assay cartridge is lowered, creating a temporary 7 μL microchamber with limited diffusion. In this small volume of medium, oxygen consumption and lactic acid excretion by the cells will rapidly result in significant changes in oxygen and proton concentration, which is registered by proton and oxygen-quenchable fluorophores that are embedded in the sensor (*see* Fig. 1).

In addition, as the assay is running, compounds can be injected through the four injection ports surrounding the sensor. This allows evaluation of the acute effects that compounds such as TLR ligands, metabolic substrates, activators/ inhibitors of signalling pathways and other compounds of interest have on cellular metabolism and energetics. In conclusion, XF Analyzers from Seahorse Bioscience are easy to use and allow for the measurement and manipulation of metabolic pathways in real-time, helping the researcher to elucidate the involvement of metabolic processes in TLR-driven changes in DC biology. We here describe a detailed protocol of how cellular metabolism of DCs can be studied following TLR stimulation, using the 96-well format Extracellular Flux (XF^{e}96) Analyzer (*see* **Note 1**). We will provide one example of how changes in metabolism can be followed in real-time in response to acute TLR stimulation and one example of how mitochondrial function can be assessed in TLR-activated DCs.

Materials

1. Poly-D-lysine hydrobromide (PDL; Sigma).
2. RPMI-1640 medium powder with L-glutamine, without glucose and sodium bicarbonate (Sigma) (*see* **Note 2**).
3. 37 % HCl solution.
4. 500 mL vacuum filter/storage bottle system, 0.22 μM pore 40 cm^2 PES membrane (Corning).
5. Oligomycin (Cayman Chemical).
6. Carbonyl cyanide 4-(trifluoromethoxy)phenylhydrazone (FCCP; Sigma).
7. Rotenone (Sigma).
8. Antimycin A (Sigma).
9. DMSO.
10. XF^{e}96 FluxPak (Seahorse Bioscience) (*see* **Note 3**).
11. XF Calibrant (Seahorse Bioscience).
12. 10 % D-glucose (Sigma).
13. Fetal calf serum, heat-inactivated at 56 °C for 30 min (HI-FCS; Bodinco).
14. 200 μL Flextop ultra-fine point tips (VWR).
15. XF^{e}96 Extracellular Flux Analyzer (Seahorse Bioscience).

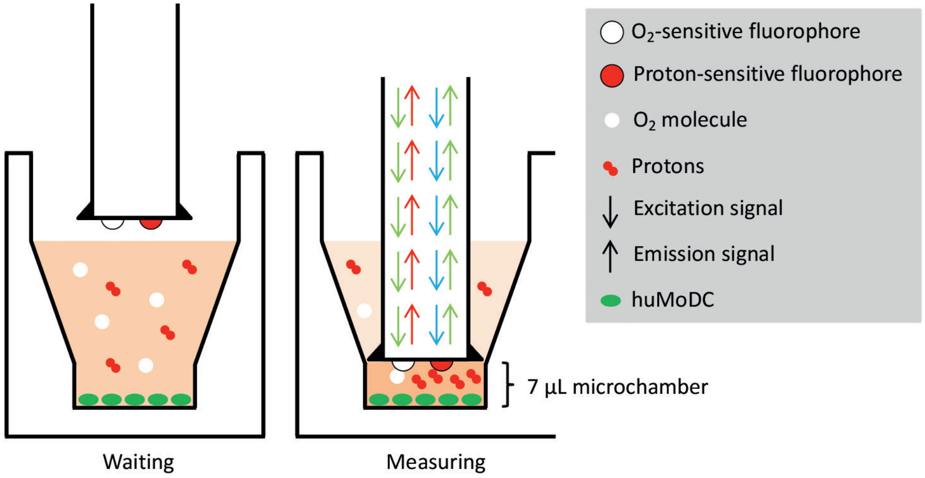
O₂-sensitive fluorophore
Proton-sensitive fluorophore
O₂ molecule
Protons
Excitation signal
Emission signal
huMoDC
7 µL microchamber
Waiting
Measuring

Figure 1. Schematic representation of the XF Analyzers from Seahorse Bioscience.

Methods

3.1 Preparation of the Reagents

3.1.1 Poly-D-Lysine Hydrobromide

1. Dissolve 5 mg poly-D-lysine hydrobromide (PDL) in 100 mL MilliQ H_2O to reach a concentration of 50 µg/mL.
2. Sterilize by filtration (0.2 µM) and store at −20 °C. Thawed aliquots can be stored at 4 °C.

3.1.2 Assay Media

1. Dissolve 8.4 mg RPMI-1640 medium powder with L-glutamine in 500 mL MilliQ H_2O by gentle swirling.
2. Once the powder is dissolved, add MilliQ H_2O to a total of approximately 1000 mL.
3. Adjust the pH with 37 % HCl solution to pH 7.4.
4. Sterilize the medium using a filter system.
5. To prepare 0 % FCS/XF media containing 10 mM D-glucose for use in the injection ports (*see* **Note 4**), add 0.91 mL of 10 % D-glucose to 49.09 mL of RPMI-1640 medium with L-glutamine. To prepare 5 % FCS/XF media containing 10 mM D-glucose for the cells (*see* **Notes 5 and 6**), add 0.91 mL of 10 % D-glucose and 2.5 mL of HI-FCS to 46.59 mL of RPMI-1640 medium with L-glutamine.

3.1.3 Oligomycin

1. To prepare a 1 mM stock solution, dissolve 1 mg of oligomycin in 1.26 mL DMSO. This stock needs to be diluted to 1 µM (1000×) for use in an XF assay run (*see* Table 2).
2. Prepare aliquots of 27 µL/vial and store at −20 °C.

3.1.4 FCCP

1. To prepare a 30 mM superstock, dissolve 10 mg of FCCP in 1.3 mL DMSO.
2. Subsequently, dilute 30 mM FCCP 1:10 with DMSO to generate a 3 mM stock solution. This stock needs to be diluted to 3 µM (1000×) for use in an XF assay run (*see* Table 2).
3. Prepare aliquots of 29 µL/vial and store at −20 °C.

3.1.5 Rotenone

1. To prepare a 10 mM superstock, dissolve 10 mg of rotenone in 2.5 mL DMSO.
2. Subsequently, dilute 10 mM rotenone 1:10 with DMSO to generate a 1 mM stock solution. This stock needs to be diluted to 1 µM (1000×) for use in an XF assay run (*see* Table 2).
3. Prepare aliquots of 35 µL/vial and store at −20 °C.

3.1.6 Antimycin A

1. To prepare a 10 mM superstock, dissolve 25 mg of antimycin A in 4.5 mL DMSO.
2. Subsequently, dilute 10 mM antimycin A 1:10 with DMSO to generate a 1 mM stock solution. This stock needs to be diluted to 1 µM 1000× for use in an XF assay run (*see* Table 2).
3. Prepare aliquots of 35 µL/vial and store at −20 °C.

3.2 Preparation of the XFe96 Assay Run

In brief, the general procedure for an XF assay run consists of the following steps:

1. Hydrate the XF assay cartridge.
2. Seed the cells in the cell culture plate.
3. Replace the culture medium with the assay medium.
4. Load the injection ports of the assay cartridge with the drugs/ stimuli of interest.
5. Create an assay template using XF Wave.
6. Start the calibration of the sensors in the cartridge.
7. Load the cell culture plate that contains the cells.
8. Optional: recover the cells for future cell count normalization (*see* **Note 7**).

3.2.1 Hydration of the XF Assay Cartridge

1. Place the assay cartridge upside down next to the utility plate.
2. Fill each well of the utility plate with 200 µL of calibration solution and put the cartridge back onto the utility plate, submerging the sensors in the solution.
3. Incubate for 4-24 h at 37 °C in a dry incubator without CO_2.

3.2.2 Seeding and Adherence of DCs

1. If using murine bone marrow-derived dendritic cells (BMDCs) that are cultured with GM-CSF, proceed to **Step 5**. If using any other type of DCs, coat the wells of the XF cell culture 96-well microplate with 25 µL 50 µg/mL PDL (*see* **Note 8**). Gently tap the plate to make sure that the liquid completely covers the bottom of the well.
2. Incubate with PDL for at least 1 h at 37 °C. The type of incubator does not matter at this specific step.
3. Add 175 µL sterile MilliQ H_2O to the wells, resuspend and pipet off as much liquid as possible (*see* **Note 9**).
4. Let the cell culture plate dry in a sterile flow hood for 30–60 min.
5. Culture or isolate your preferred type of DC for use in the XF assay run according to protocols described elsewhere for human monocyte-derived DCs (moDCs) [78], murine BMDCs [79] or DCs isolated from human or murine tissues [3, 80].
6. Seed the number of DCs needed to obtain a confluent mono- layer in 50 µL of the same type of culture medium in which the DCs were grown. Different DC types have different sizes and therefore, their seeding density differ (*see* Table 1).
7. Quick-spin the plate to bring all DCs to the bottom of the well.
8. Check under the microscope for a confluent monolayer.
9. Incubate the cells for 1 h at 37 °C, 5 % CO_2, 95 % humidity to allow the cells to adhere.
10. Check under the microscope for adherence.
11. Proceed to Subheading 3.2.3 to perform a mitochondrial stress test or Subheading 3.2.4 to assess in real-time metabolic changes in response to acute TLR stimulation. Of note, the assays described here are only examples of assays that can be performed using XF Analyzers (*see* **Note 10**).

Table 1. Proposed seeding densities for different DC types to reach a confluent monolayer in a XF cell culture 96-well microplate.

Source	Cells/well
Mouse bone marrow-derived, cultured with GM-CSF	70,000
Mouse bone marrow-derived, cultured with Flt3L	150,000
Mouse spleen	150,000
Human skin	200,000
Human blood	200,000
Human monocyte-derived	50,000

3.2.3 Mitochondrial Stress Test

The mitochondrial stress test allows one to interrogate the functional properties of the electric transport chain. It consists of the sequential injection of oligomycin (inhibitor of mitochondrial ATP synthase), FCCP (ionophore) and rotenone + antimycin A (inhibitors of complex one and three of the respiratory chain respectively). This allows one to assess baseline respiration (BR), oxygen consumption used for ATP production (ATP) following oligomycin injection, the maximum rate of mitochondrial respiration (MR) following FCCP injection, and non-mitochondrial respiration (NMR) following rotenone + antimycin A injection. The difference in oxygen consumption rate (OCR) between BR and MR is known as the spare respiratory capacity (SRC) and the difference in OCR after oligomycin treatment versus rotenone + antimycin A is the amount of respiration used to compensate for proton leak (PL), which is also known as uncoupling. An example of a mitochondrial stress test performed on LPS-stimulated murine BMDCs is shown in Fig. 2. The concentrations of oligomycin, FCCP and rotenone + antimycin A used in this assay can be found in Table 2.

1. Slowly add 150 μL more culture medium with or without your Toll-like receptor (TLR) ligand(s) of interest.
2. Incubate the TLR-stimulated DCs for 2 up to 48 h at 37 °C, 5 % CO_2 and 95 % humidity.
3. An hour before the XF assay run, prepare 10× working concentrations of oligomycin, FCCP and rotenone + antimycin A by diluting the drugs 1:100 in 0 % FCS/XF assay medium. For example, dilute 25 μL oligomycin in 2475 μL 0 % FCS/XF assay medium. Do not use 5 % FCS/XF assay medium for injection of compounds (*see* **Note 4**) and dilute rotenone and antimycin A together.
4. Carefully pipette off all the culture medium (*see* **Note 8**).
5. Slowly add 180 μL 5 % FCS/XF assay medium to the cells. Be especially careful with the first 50 μL (*see* **Note 8**). If the cells detach, spin-down the plate again.
6. Incubate the cells for 1 h at 37 °C in a dry incubator without CO_2 in order to remove any CO_2 dissolved in the assay medium (*see* **Note 11**).

7. Add 20 µL oligomycin to port A, 22 µL of FCCP to port B and 25 µL of rotenone + antimycin A to port C (*see* Fig. 3). Use a multichannel, special narrow tips (*see* **Item 14**, Subheading 2) and the provided loading guides to pipet the compounds of interest into the injection ports of the XF assay cartridge via a single stream (*see* **Note 12**).
8. Fill any empty injection ports of series A, B and C with 20, 22 and 25 µL of 0 % FCS/XF assay medium respectively (*see* **Note 12**).
9. Put the assay cartridge back into a 37 °C incubator without CO_2 until the start of the run (*see* Subheading 3.3).

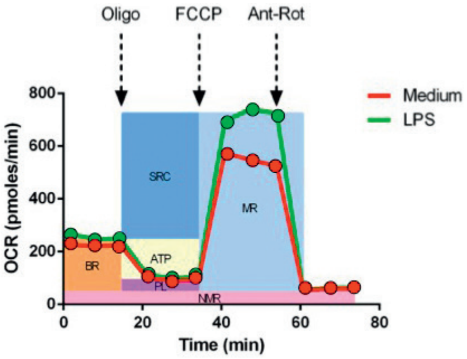

Figure 2. Murine BMDCs are stimulated with medium or LPS for 2 h and then subjected to the mitochondrial stress test. This graph suggests that short-term LPS stimulation promotes maximal respiration and spare respiratory capacity in these DCs.

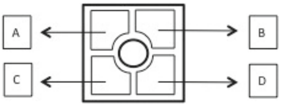

Figure 3. Schematic drawing of the four injection ports per well.

Table 2. Proposed final concentrations of the mitochondrial stress test compounds.

Oligomycin	1 µM
FCCP	3 µM
Rotenone	1 µM
Antimycin A	1 µM

3.2.4 Tracking Real-Time Metabolic Changes

DCs can also be stimulated with TLR ligands during a run in the XF Analyzer. This enables one to follow in real-time the immediate metabolic changes that are induced by TLR engagement. This can easily be combined with pre-incubations of stimulatory/inhibitory compounds to interrogate the involvement of specific signalling pathways in TLR-induced metabolic changes. An example is given in Fig. 4.

1. Slowly add an additional 150 µL culture medium.
2. Allow the cells to fully adhere and rest overnight at 37 °C, 5 % CO_2 and 95 % humidity.
3. The next day, prepare 10× working concentrations of your TLR ligand(s) and stimulatory/inhibitory compound(s) of interest in 0 % FCS/XF assay medium. Do not use 5 % FCS/ XF assay medium for injection (*see* **Note 3**).
4. Carefully pipette off all the culture medium (*see* **Note 7**).

5. Slowly add 180 µL 5 % FCS/XF assay medium to the cells. Be especially careful with the first 50 µL (*see* **Note 7**).
6. Incubate the cells for 1 h at 37 °C in a dry incubator without CO_2 in order to remove the CO_2, which was dissolved in the culture medium (*see* **Note 11**).
7. Add 20 µL of your stimulatory/inhibitory compound(s) of interest to port A and 22 µL of your TLR ligand(s) to port B (*see* Fig. 3). Use a multichannel, special narrow tips (*see* **Item 14**, Subheading 2) and the provided loading guides to pipet the compounds of interest into the injection ports via a single stream (*see* **Note 12**).
8. Fill any empty injection ports of series A and B with 20 and 22 µL of 0 % FCS/XF assay medium respectively (*see* **Note 12**).
9. Put the assay cartridge back at 37 °C in a dry incubator without CO_2 until the start of the run (*see* Subheading 3.3).

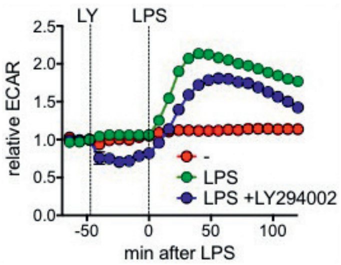

Figure 4. Murine BMDCs are stimulated with medium or LPS during a XF Assay run and the effects on extracellular acidification rate (ECAR) are assessed in real-time. Moreover, in one condition, an inhibitor of PI3K signalling (LY204002) is injected into the wells prior to LPS stimulation. This suggests that baseline glycolysis rates are partially dependent on PI3K signalling, whereas LPS-induced glycolysis is not.

3.3 Starting a XF Assay Run

A Seahorse XF Analyzer comes with a desktop computer and software (XF Wave) that is used to set up the assay template (i.e. plate layout, number and timing of injection(s), and measurement frequency and duration) and to start or cancel the XF assay run.

1. Select the 'Blank' template and click the 'Design' button.
2. Click on the vertical bar of the 'Group Definitions' tab. Define your assay conditions and then, click the 'Generate Groups' button. XF Wave will automatically generate groups based on every possible combination of assay conditions you define.

3. Click on the vertical bar of the 'Plate Map' tab. Determine the groups in the plate layout by first selecting a specific group and then, clicking on or dragging across the corresponding well(s).
4. Click on the 'Instrumental Protocol' tab. Then, click on the 'Injection Button' three times when performing the mitochondrial stress test (*see* Subheading 3.2.3) or two times when performing the real-time tracking of metabolic changes (*see* Subheading 3.2.4). For each new injection, the software will automatically select the next available port, i.e. injection 1 = port A, 2 = B, 3 = C and 4 = D.
5. A measurement typically consists of 3 min of 'mixing' and 3 min of 'measuring', repeated for 3 times (i.e. 3 cycles). Correspondingly, with one basal measurement and 3 measurements after injection, the mitochondrial stress test as described here is 72 min long (*see* Fig. 2), excluding calibration and equilibration. Longer measurement times, for example after stimulation with TLR ligands (*see* Fig. 3), can easily be achieved by increasing the number of cycles (*see* **Notes 10 and 13**). Do not forget to set the 'waiting' time at 0 min and 0 s.
6. Go to the 'Review and Run' tab to find the 'Run' button. Click 'Run'.
7. The machine will first ask to load the XF assay cartridge and the utility plate in which the sensors of the assay cartridge were hydrated (*see* Subheading 3.2.1). It is important to remove the lid from the assay cartridge and orient the cartridge and plate in a way that the blue-marked corner faces you. In this orientation, the barcode on the cartridge should not be visible.
8. Press 'Continue'.
9. The sensors in the cartridge will now be calibrated to assure the accuracy of your instrument. Equilibration occurs after calibration and ensures temperature stability before beginning your assay. Together this will take approximately 20–25 min.
10. After the calibration and equilibration, the XF Analyzer will eject the utility plate. Replace this plate with the cell culture plate containing the DCs as prepared in Subheading 3.2.3. Again, it is important to remove the lid from the plate and to orient the plate in a way that the blue marked corner faces you.
11. Press 'Continue' to start the XF assay run. Data will be displayed in real-time during the measurement.

A full tutorial on how to set up an assay template using the XF Wave software can be found on the website of Seahorse Bioscience: http://www.seahorsebio.com/resources/pdfs/user-guide-xfe- wave.pdf.

3.4 Data Analysis

Data that are obtained include ECAR and OCR as well as the raw pH and O_2 tension values. XF Wave software allows one to visualize all these parameters by creating and exporting various graphs. Moreover, this software allows one to directly export the raw data tables to programs such as Excel or GraphPad Prism, which you can use to make your own graphs. An extensive guide on how to analysis your data using Wave can be found on the website of Seahorse Bioscience: http://www.seahorsebio.com/resources/ pdfs/user-guide-xfe-wave.pdf.

4 Notes

1. The same assays can be performed using a 24-well format. The number of cells per well in the XF^{e}24 Extracellular Flux Analyzer needs to be increased by 2.5-fold compared to the 96-well format described here (*see* Table 1). In addition, the volumes of assay media in the wells and the injection ports need to be increased by 2.5-fold.
2. The assay medium should not contain any buffering reagents, because glycolysis is determined by changes in extracellular pH.
3. An XF^{e}96 FluxPak contains equal amounts of XF assay cartridges and XF cell culture 96-well microplates. Each assay cartridge comes with its own 96-well microplate, which is referred to as the XF utility plate and is used to hydrate the cartridge sensors. Moreover, each cartridge comes with its own loading guides. The XF cell culture 96-well microplate is used for loading the cells.
4. Large proteins such as bovine serum albumin (BSA) may block the injection port.
5. FCS has some buffering capacity. The more FCS is added to the XF assay medium, the lower your ECAR readings will be.
6. FCCP concentration is dependent on the amount of protein in the XF assay medium. The higher the protein concentration, the more the effect of FCCP is quenched. In our hands, 3 μM FCCP works well with the amount of proteins present in 5 % FCS/assay medium to induce maximum respiration and glycolysis (*see* Table 2).
7. Generally, DCs are fully differentiated, non-dividing cells. However, in the case observed differences in metabolism are suspected to be due to differences in cell density rather than inherent differences in metabolism, one can do a normalization after the XF Assay run. For example, one can normalize the obtained metabolic readouts based on protein quantification methods such as the bicinchoninic acid (BCA) assay. The XF Wave software has a feature to enter such data and automatically perform normalization.
8. During measurement, the XF assay cartridge sensors only measure the bottom 7 μL of the XF cell culture 96-well microplates. Therefore, your cells need to be at the bottom of the well and immobilized. XF cell culture microplates are made of polystyrene and are tissue culture-treated, but in our experience, all DCs, except murine bone marrow-derived DCs cultured with GM-CSF, require an additional plate bound substrate such as PDL for proper adherence. Note that adherence by PDL may cause some activation of DCs.
9. It is preferable to wash with unbuffered solutions.

10. Other regularly performed assays include the beta-oxidation assay and the glycolysis stress test. Reagents for these assays are available through Seahorse Bioscience. Moreover, the flexibility of XF Analyzers allows one to easily deviate from standard protocols in order to address specific metabolic questions. For example, the presence of certain nutrients in the medium, the nature of the compounds, the timing of injections and the duration of measurements can be adjusted.
11. CO_2 reacts with H_2O to form $HCO_3^- + H^+$, which acidifies the medium and results in incorrect ECAR readings.
12. XF Analyzers use compressed air to inject compounds from the ports into the wells. Moreover, series of injection ports are linked (i.e. all A ports, all B ports, etc.). Therefore, each series of injection ports must contain the same amount of volume for the injections to work.
    a. The combination of these tips (*see* **Item 14**, Subheading 2) and the loading guides allows on to insert the tip into the injection port at a specific depth. Too high and droplets may stick at the top of the well. Too low and the solution may be pipetted through the injection port.
    b. Dispense the solution via a single stream. Otherwise, droplets may stick at the end of the tip.
    c. Do not tap the XF assay cartridge in order to get the solution at the bottom of the injection port. The XF assay cartridge is fragile and tapping may cause leaking of the injection ports.
13. We experienced that reliable ECAR and OCR reads can be obtained up to 6 h into a run. After 6 h, XF assay medium becomes too acidified.

References

1. Everts, B., et al., *TLR-driven early glycolytic reprogramming via the kinases TBK1-IKKvarepsilon supports the anabolic demands of dendritic cell activation.* Nat Immunol, 2014. **15**(4): p. 323-32.
2. Everts, B., et al., *Commitment to glycolysis sustains survival of NO-producing inflammatory dendritic cells.* Blood, 2012. **120**(7): p. 1422-31.
3. Jantsch, J., et al., *Hypoxia and hypoxia-inducible factor-1 alpha modulate lipopolysaccharide-induced dendritic cell activation and function.* J Immunol, 2008. **180**(7): p. 4697-705.
4. Krawczyk, C.M., et al., *Toll-like receptor-induced changes in glycolytic metabolism regulate dendritic cell activation.* Blood, 2010. **115**(23): p. 4742-9.
5. Pantel, A., et al., *Direct type I IFN but not MDA5/TLR3 activation of dendritic cells is required for maturation and metabolic shift to glycolysis after poly IC stimulation.* PLoS Biol, 2014. **12**(1): p. e1001759.
6. Amiel, E., et al., *Mechanistic target of rapamycin inhibition extends cellular lifespan in dendritic cells by preserving mitochondrial function.* J Immunol, 2014. **193**(6): p. 2821-30.
7. Ferrick, D.A., A. Neilson, and C. Beeson, *Advances in measuring cellular bioenergetics using extracellular flux.* Drug Discov Today, 2008. **13**(5-6): p. 268-74.
8. Pearce, E.J. and B. Everts, *Dendritic cell metabolism.* Nat Rev Immunol, 2015. **15**(1): p. 18-29.
9. Sallusto, F. and A. Lanzavecchia, *Efficient presentation of soluble antigen by cultured human dendritic cells is maintained by granulocyte/macrophage colony-stimulating factor plus interleukin 4 and downregulated by tumor necrosis factor alpha.* J Exp Med, 1994. **179**(4): p. 1109-18.
10. Lutz, M.B., et al., *An advanced culture method for generating large quantities of highly pure dendritic cells from mouse bone marrow.* J Immunol Methods, 1999. **223**(1): p. 77-92.
11. Stoitzner, P., et al., *Isolation of skin dendritic cells from mouse and man.* Methods Mol Biol, 2010. **595**: p. 235-48.

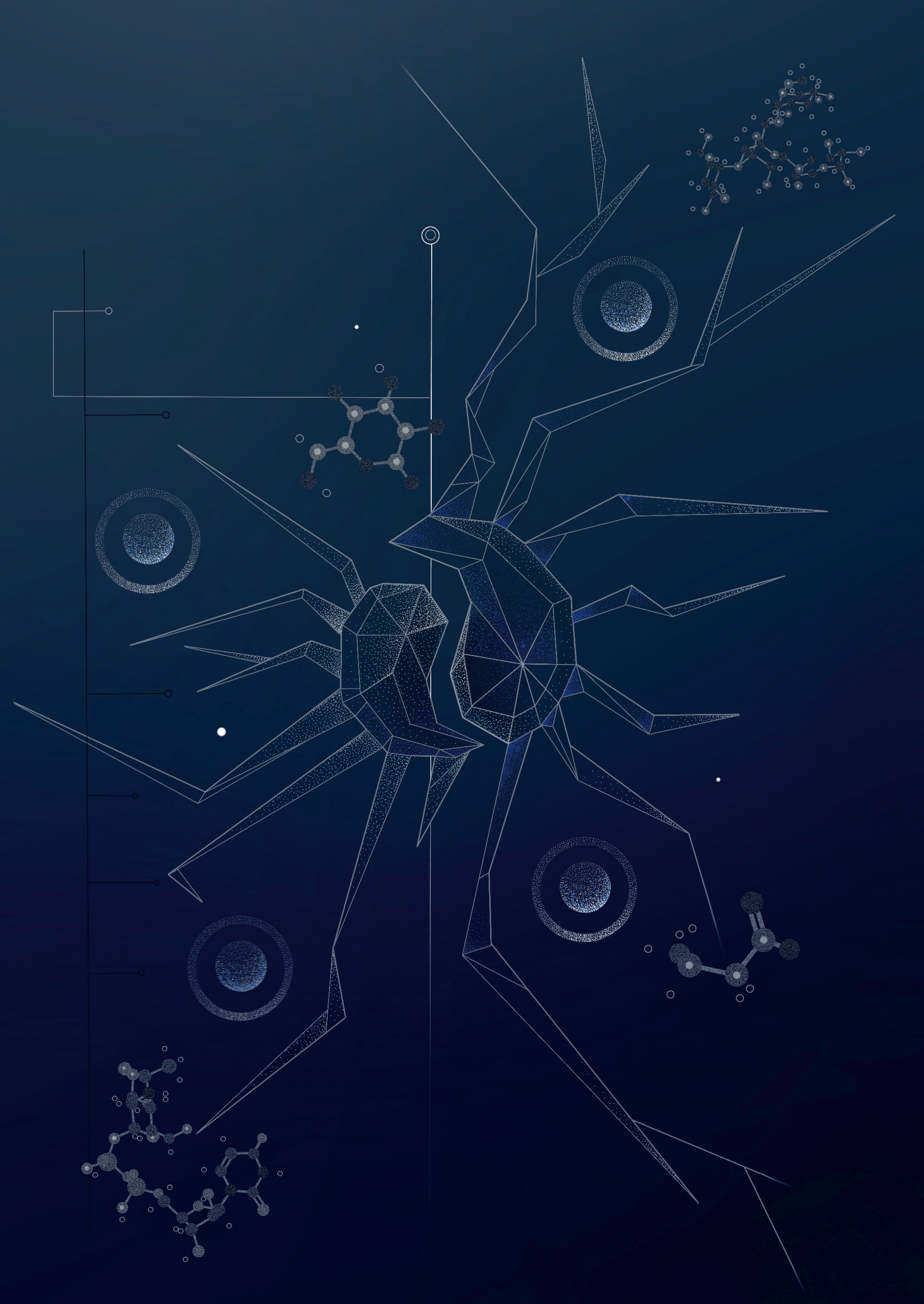

4

Cell-Intrinsic Glycogen Metabolism Supports Early Glycolytic Reprogramming Required for Dendritic Cell Immune Responses

Phyu M. Thwe
Leonard R. Pelgrom
Rachel Cooper
Saritha Beauchamp
Julie A. Reisz
Angelo D’Alessandro
Bart Everts
Eyal Amiel

Cell Metab. 2019 Jul 2;30(1):225
PMID: 31269426
DOI: 10.1016/j.cmet.2019.05.017

Summary

Dendritic cell (DC) activation by Toll-like receptor (TLR) agonists causes rapid glycolytic reprogramming that is required to meet the metabolic demands of their immune activation. Recent efforts in the field have identified an important role for extracellular glucose sourcing to support DC activation. However, the contributions of intracellular glucose stores to these processes have not been well characterized. We demonstrate that DCs possess intracellular glycogen stores and that cell-intrinsic glycogen metabolism supports the early effector functions of TLR-activated DCs. Inhibition of glycogenolysis significantly attenuates TLR-mediated DC maturation and impairs their ability to initiate lymphocyte activation. We further report that DCs exhibit functional compartmentalization of glucose- and glycogen-derived carbons, where these substrates preferentially contribute to distinct metabolic pathways. This work provides novel insights into nutrient homeostasis in DCs, demonstrating that differential utilization of glycogen and glucose metabolism regulates their optimal immune function.

Introduction

Dendritic cells (DCs) are canonical ‘‘professional antigen presenting cells’’ of the immune system and play a central role in coordinating both innate and adaptive immune responses [1-3]. DCs recognize microbial pathogens and other inflammatory stimuli through the expression of innate immune receptors including the Toll-like receptor (TLR) family [4-6]. DC activation by TLR signaling initiates a complex set of transcriptional and translational events that are characterized by the upregulation of surface co-stimulatory molecule expression, inflammatory cytokine secretion, and the ability to stimulate T lymphocytes via antigen presentation by major histocompatibility (MHC) molecules.

TLR stimulation initiates a shift in DC metabolism characterized by upregulation of aerobic glycolysis, which plays a vital role in supporting the immune effector function and survival of both human and mouse DCs [7-10]. Rapid glycolysis induction supports the metabolic requirements associated with the high levels of protein synthesis that contribute to DC immune activity. The TLR-mediated ‘‘glycolytic burst’’ drives *de novo* fatty acid synthesis via glucose-dependent citrate metabolism, which supports the synthesis and secretion of inflammatory cytokines [8, 11]. Interrupting the glucose-to-citrate pathway significantly impairs DC maturation, cytokine secretion, and T cell stimulatory capacity [8-10].

Immune cells are thought to primarily support activation-associated glycolysis via increased expression of glucose transporters [12-15]. Consistent with this, the role of the inducible glucose transporter, GLUT1, in regulating activation-associated glucose flux in both myeloid and lymphoid immune cells has been a major focus in the field [16, 17]. In DCs, however, GLUT1 upregulation occurs several hours after TLR stimulation, while TLR-mediated glycolytic reprogramming happens within minutes of activation. Thus, the source of glucose supporting the earliest events in DC activation, namely whether glucose is sourced from the extracellular environment or from intracellular pools, has not been fully defined. We propose that the DCs utilize intracellular glycogen reserves to fuel their metabolic needs during early immune activation and that glycogen metabolism is required by these cells to initiate proper immune effector responses.

Glycogen, a large branch-chained glucose polymer, has been extensively characterized in hepatocytes, muscle cells, and neuronal tissue where it serves as an intracellular carbon reservoir [18-20]. Cells in the liver, muscle, and brain express tissue-specific enzymes for glycogen synthase (GYS) and glycogen phosphorylase (PYG), the rate-limiting enzymes of glycogen synthesis and breakdown, respectively. Cells in these tissues store glucose in the form of glycogen to be utilized according to their specific metabolic demands [18-20]. During glycogenolysis, PYG isozymes break down glycogen into glucose-1-phosphate (G1P), which is subsequently converted into glucose-6-phosphate (G6P) and can serve as a direct substrate for further catabolism via glycolysis. In this manner, glycogen-storing cells, such as those in muscle and brain tissue, can maintain intracellular glycogen reserves for cell-intrinsic metabolic requirements [18, 20]. The significance of cell-intrinsic glycogen metabolism in immune cells has not been well characterized.

We demonstrate that DCs express specific isoforms of enzymes essential for glycogen synthesis and breakdown and that these cells require glycogen metabolism to support their immune function. Although the presence of glycogen in DCs has been previously implicated [21], the direct role for glycogen in DC metabolism and immune function has not been described. We propose that DCs use intracellular glycogen reserves to support early glycolytic metabolism that accompanies their activation. We show that disruption of glycogen metabolism significantly impairs DC maturation and immune effector function, particularly at early stages of activation and in glucose-restricted conditions. We further show that glycogen-derived carbons preferentially contribute to the TCA- dependent citrate pool compared to glucose catabolized directly by the cell. These findings elucidate a novel metabolic regulatory pathway in DCs and provide new insights into energy and nutrient homeostasis in these cells in support of their immune activation.

Results and discussion

DCs Express Glycogen Metabolic Machinery and Utilize Cell-Intrinsic Glycogen Metabolism upon Activation

TLR stimulation drives DCs to undergo glycolytic reprogramming in order to meet cellular anabolic demands associated with activation [8, 10]. We performed a nutrient screening assay using single-carbon-source defined media and found that DCs can catabolize both short- and long-chain glucose polymers (Figure 1A). The ability of DCs to generate NADH from glycogen (Figure 1A) is of particular interest given its role as the predominant form of glucose macromolecule storage in normal physiology. While cells are unlikely to encounter extracellular glycogen *in vivo*, these assays demonstrate that DCs exhibit the capability to catabolize glycogen and are likely to express the key enzymes of glycogen metabolism.

We analyzed mRNA levels of glycogen phosphorylase (PYG) and glycogen synthase (GYS), the rate-limiting enzymes of glycogen breakdown and synthesis pathways, respectively in DCs. Glycogenolysis is executed by three different tissue-specific PYG isozymes in mice and humans: PYGL in the liver, PYGM in muscle, and PYGB in brain tissue. Glycogen synthesis is controlled by two different tissue-specific GYS isozymes: GYS1 in muscles and other peripheral tissue, and GYS2 in the liver. Both mRNA and protein analysis in mouse bone marrow-derived DCs (BMDCs) (Figures 1B and 1C) and human monocyte-derived DCs (moDCs) (Figure 1D) showed that DCs express PYGL and GYS1 isozymes. These enzymes were not appreciably regulated following 6 hr stimulation with LPS (Figures 1C and 1D). Detection of intracellular glycogen in freshly isolated human CD14$^+$ monocytes and CD1a$^+$ dendritic cells (Figure 1E) indicates a physiological role for glycogen in these cells. Unactivated DCs contain intracellular glycogen pools that are fully depleted when cells are cultured in glucose-free media (Figure 1F) and partially depleted by LPS stimulation in BMDCs (Figure 1G) and moDCs (Figure 1H). TEM images of BMDCs show distinct glycogen deposits by tannic acid stain that are absent in cells grown without glucose (Figure 1I) [22].

To validate the efficacy and specificity of the PYG inhibitor, CP91149 (CP), we incubated BMDCs with CP in the nutrient screening assay (as in Figure 1A) and assessed inhibition of glucose or glycogen catabolism. Glycogen-dependent NADH levels were fully attenuated in the presence of CP, while glucose-dependent NADH levels were unaffected (Figure 1J), demonstrating the specificity of this inhibitor. PYG inhibition caused a reduction in basal glycolysis rates in unactivated BMDCs (Figure 1K), indicating that DCs utilize intracellular glycogen to support basal glycolytic demands. Importantly, the effect of glycolysis inhibitor 2-deoxyglucose (2DG) was non-redundant with CP, showing that free glucose and intracellular glycogen stores make distinct contributions to DC metabolism (Figure 1K).

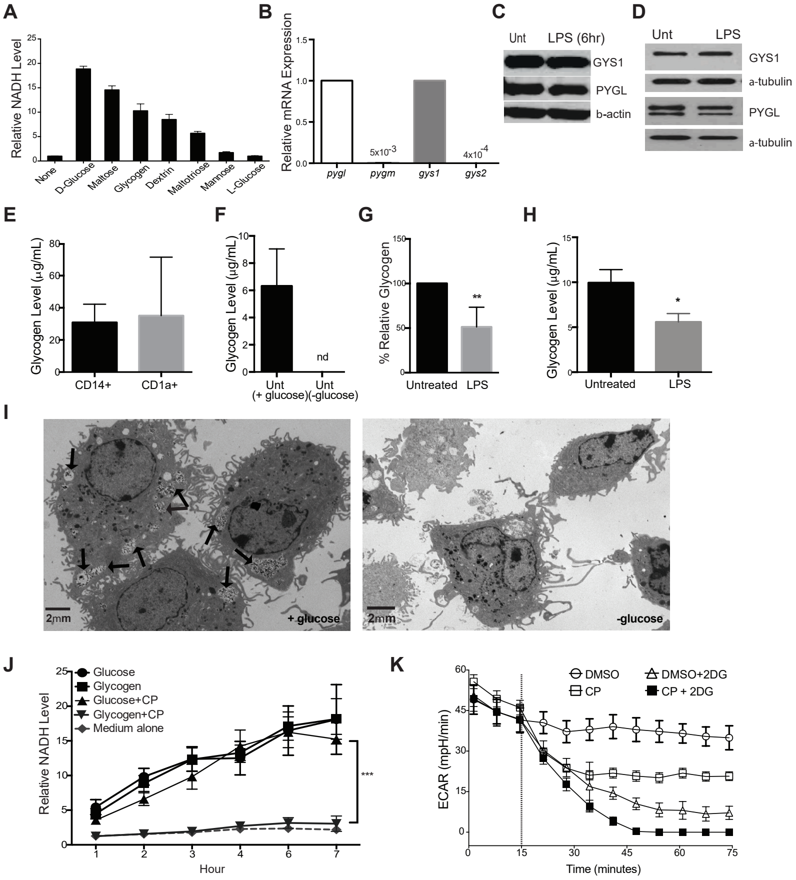
A
Relative NADH Level
25
20
15
10
5
0
None
D-Glucose
Maltose
Glycogen
Dextrin
Maltotriose
Mannose
L-Glucose
B
Relative mRNA Expression
1.5
1.0
0.5
0.0
5x10^-3
4x10^-4
pygl
pygm
gys1
gys2
C
Unt
LPS (6hr)
GYS1
PYGL
b-actin
D
Unt
LPS
GYS1
a-tubulin
PYGL
a-tubulin
E
Glycogen Level (μg/mL)
80
60
40
20
0
CD14+
CD1a+
F
Glycogen Level (μg/mL)
10
8
6
4
2
0
nd
Unt (+ glucose)
Unt (-glucose)
G
% Relative Glycogen
150
100
50
0
**
Untreated
LPS
H
Glycogen Level (μg/mL)
15
10
5
0
*
Untreated
LPS
I
2mm
+ glucose
2mm
-glucose
J
Relative NADH Level
25
20
15
10
5
0
Glucose
Glycogen
Glucose+CP
Glycogen+CP
Medium alone
***
1
2
3
4
6
7
Hour
K
ECAR (mpH/min)
60
45
30
15
0
DMSO
CP
DMSO+2DG
CP + 2DG
0
15
30
45
60
75
Time (minutes)

Figure 1. DCs Utilize Intracellular Glycogen Metabolism upon LPS Stimulation.

(A) BMDCs were cultured in the indicated substrates as the sole nutrient sources and measured for ability to produce NADH as described in STAR Methods. Data indicate relative NADH production at 6 hr normalized to no carbon source controls, n = 3.
(B) Relative mRNA expression of PYG and GYS isoforms in naive BMDCs.
(C and D) PYGL, GYS1, and β-actin protein expression in unactivated and 6 hr LPS-stimulated BMDCs (C) and 24 hr LPS-stimulated moDCs (D).
(E–H) Intracellular glycogen levels of human peripheral blood $CD14^+$ monocytes and $CD1a^+$ DCs (E), untreated BMDCs cultured overnight ± glucose (F), and BMDCs (G) and moDCs (H) stimulated ± LPS in 5 mM glucose (n = 3-6, mean ± SD, Student's t test, $*p < 0.05$, $**p = 0.0021$, nd = not detected). Glycogen levels were normalized to 10^5 cells.
(I) TEM images of unactivated BMDCs in 5 mM glucose (left) and 0 mM glucose (right), with arrows indicating intracellular glycogen deposits identified by tannic acid staining.
(J) NADH levels over time in BMDCs cultured in glucose or glycogen containing media (as in A) ± CP (n = 4, mean ± SD, $***p < 0.0001$).
(K) Basal ECAR of resting BMDCs treated with CP, 2DG, or both (treatment introduced at dotted line); representative of at least three replicates.

PYG Inhibition Impacts DC Survival in Hypoglycemic Conditions

Glycogen metabolism supports cancer cell growth, proliferation, and cellular lifespan [23]. We tested the effect of PYG inhibition on the survival of BMDCs at early (6 hr) and late (24 hr) time points after LPS activation. PYG inhibition resulted in modest increases in cell death at early time points under low-glucose conditions (Figure 2A). This phenotype was increased after 24 hr of inhibition (Figure 2B). In contrast, the viability of human moDCs was not impacted at all glucose concentrations tested (Figure 2C).

Glycogen Metabolism Preferentially Supports Early DC Maturation

TLR-driven early glycolytic burst is a metabolic hallmark of activated DCs [24], and both lymphoid and myeloid cells depend heavily on extracellular glucose for glycolysis-dependent effector responses [9, 10, 15, 25]. This may pose a limitation on the abundance of glucose in highly inflamed tissues and secondary lymphoid organs where DCs likely experience nutrient competition with proliferating lymphocytes [26]. We hypothesized that glycogen metabolism supports early TLR-mediated glycolysis and activation in DCs by providing an intracellular source of glucose carbons. We examined the surface expression of CD40 and CD86 in BMDCs stimulated with LPS for 6 and 24 hr in the presence or absence of PYG inhibitor over a range of glucose concentrations representing both hyper- and hypoglycemic states. CD40 and CD86 expression was attenuated by CP treatment (Figures 2D and S1A), with a more pronounced effect at 6 hr and in hypoglycemic conditions (Figures 2D and S1A). PYG inhibition with an alternative inhibitor, DAB, at 6 hr after stimulation gave similar outcomes (Figure S1B). Reduced CD40 and CD86 expression was observed both in BMDCs starved of intracellular sugar (Figure 2E) and in moDCs inhibited by CP (Figure 2F), further suggesting a role for glycogen pools in sustaining DC maturation. In addition, PYG-targeted siRNA was used to silence PYG expression in moDCs. As mRNA expression data indicated that both PYGB and PYGL isoenzymes are expressed in human moDCs (Figure S1C), both isoforms were silenced simultaneously in moDCs using targeted siRNA (Figure S1D). Genetic silencing of PYG in moDCs resulted in attenuation of LPS- induced expression of maturation markers (Figure 2G).

While the importance of GLUT1 has been conclusively delineated in both myeloid and lymphoid immune cells [8, 16, 17, 27], the kinetics of GLUT1 regulation do not account for the acute glycolytic reprogramming that occurs in activated DCs. GLUT1 upregulation in activated DCs is not detected before 6 hr of LPS stimulation (Figure S1E), which correlates with the finding that extracellular glucose is depleted only after 6 hr of stimulation (Figure 2H). To confirm that the cells are less dependent on imported glucose for early activation, we assessed DC maturation at 6 and 24 hr after LPS stimulation while blocking GLUT1 activity with inhibitor STF31 (Figures 2I and S1F). In contrast to PYG inhibition, GLUT1 inhibition had a significant impact on the maturation at 24 hr but not 6hrs after activation. These data provide strong evidence that cell-intrinsic glycogen metabolism plays a central role in driving DC maturation, particularly during early time points and in glucose-restricting conditions.

PYG Inhibition Impacts DC Immune Effector Function

Blocking glycolysis in TLR-activated DCs impairs their ability to produce inflammatory cytokines and stimulate T cells [8, 10]. We tested whether these responses are also affected by PYG inhibition. Intracellular cytokine staining for TNF-α and IL-12 after 4 hr of LPS stimulation showed that PYG inhibition attenuates inflammatory cytokine production, with a larger effect in low-glucose conditions (Figures 3A, 3B, and S2A). Multiplex cytokine analysis of LPS-stimulated DCs showed reduced pro-inflammatory cytokines and chemokine production in PYG-inhibited cells compared to controls in both BMDCs (Figure 3C) and moDCs (Figure 3D). CP did not globally impact all LPS-mediated protein production as other cytokines were unaffected (Figures S2B and S2C). siRNA-mediated knockdown of PYG expression in moDCs recapitulated the inhibitor data, as LPS-driven IL-12 production was attenuated in PYG-silenced moDCs (Figure 3E).

To examine the ability of DCs to take up and process antigens, we stimulated BMDCs with LPS plus OVA-AF488 or OVA-DQ for 3 hr (Figure 3F). OVA-AF488 allows tracking of antigen uptake, while OVA-DQ only fluoresces upon antigen uptake and processing. PYG-inhibited DCs showed reduced antigen uptake regardless of LPS stimulation (Figure 3F), while antigen processing was unexpectedly enhanced by PYG inhibition. We next tested the effect of PYG inhibition or silencing on DC ability to stimulate CD4$^+$ T cells. PYG-inhibited BMDCs exhibited significantly reduced capacity to stimulate T cells (Figures 3G and 3H). PYG-silenced moDCs exhibited similar impairments in CD4$^+$ T cell stimulation (Figure 3I). These data demonstrate that cell-intrinsic glycogen metabolism contributes to the regulation of the multifaceted dimensions of DC immune effector function.

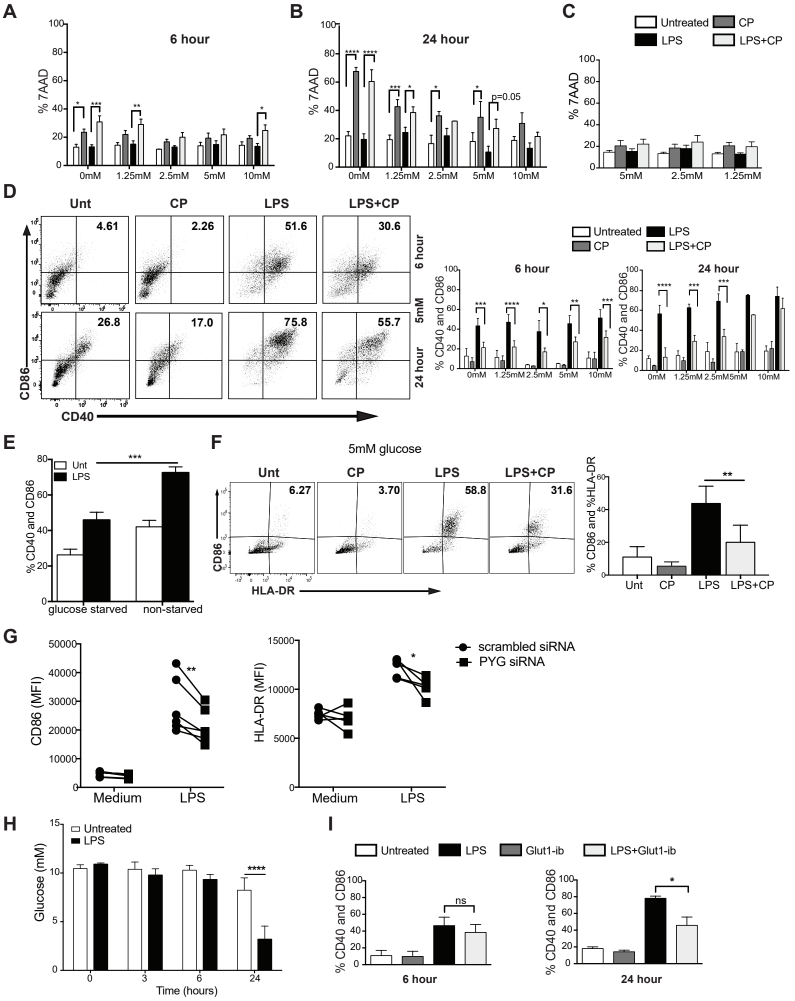
A
6 hour
% 7AAD
0mM
1.25mM
2.5mM
5mM
10mM
B
24 hour
p=0.05
C
Untreated
CP
LPS
LPS+CP
5mM
2.5mM
1.25mM
D
Unt
CP
LPS
LPS+CP
4.61
2.26
51.6
30.6
26.8
17.0
75.8
55.7
6 hour
5mM
24 hour
CD86
CD40
% CD40 and CD86
E
Unt
LPS
glucose starved
non-starved
F
5mM glucose
6.27
3.70
58.8
31.6
HLA-DR
% CD86 and %HLA-DR
G
CD86 (MFI)
HLA-DR (MFI)
Medium
LPS
scrambled siRNA
PYG siRNA
H
Glucose (mM)
Time (hours)
I
Glut1-ib
LPS+Glut1-ib
ns

Figure 2. Glycogen Metabolism Supports Survival and Early Maturation of TLR-Activated DCs.

(A and B) 7AAD viability staining of BMDCs stimulated with LPS ± CP for 6 hr (A) and 24 hr (B) at 5 mM glucose.
(C) 7AAD viability staining of moDCs stimulated with LPS ± CP for 24 hr.
(D) BMDCs were stimulated for 6 and 24 hr and analyzed for CD40 and CD86 surface expression.
(E) CD40 and CD86 expression of BMDCs stimulated for 6 hr in free glucose medium with and without glucose starvation.
(F) CD86 and HLA-DR expression of moDCs stimulated with LPS ± CP for 24 hr in 5 mM glucose.
(G) CD86 and HLA-DR surface expression of 24 hr LPS-stimulated moDCs silenced with control (scrambled) or PYG-targeted siRNA.
(H) Glucose measurements from supernatant of BMDCs stimulated with LPS for 3, 6, and 24 hr.
(I) CD40 and CD86 surface expression of BMDCs stimulated ± GLUT1-inhibitor in normal glucose for 6 and 24 hr. (A-F, H-I) n = 3-6, mean ± SD, two-way ANOVA with Tukey's post-test; *p % 0.05, ***p = 0.0006, ****p < 0.0001.
(G) n = 5, paired t test; *p = 0.04, **p = 0.0093.

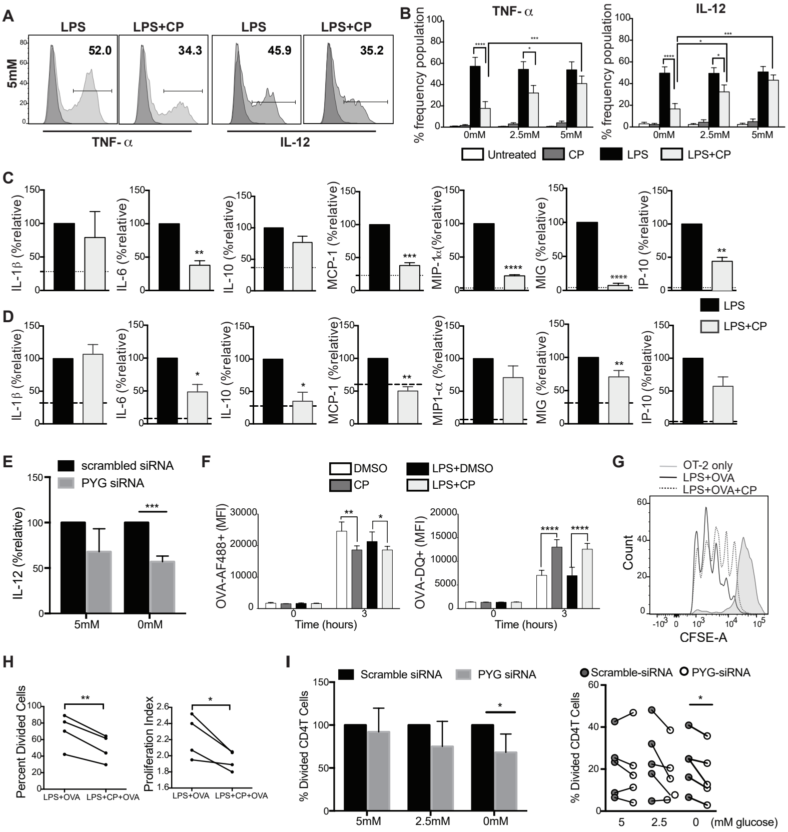

Figure 3. PYG Inhibition Attenuates Immune Effector Functions of DC.

(A) Intracellular staining of TNF-α and IL-12 of BMDCs stimulated with LPS for 4 hr in 5 mM glucose.
(B) Intracellular staining of TNF-α and IL-12 of BMDCs stimulated with LPS for 4 hr in 5, 2.5, and 0 mM glucose.
(C and D) Multiplex panels of cytokine and chemokine measurements from the supernatant of BMDCs (C) and moDCs (D) activated with LPS for 6 hr. Dotted lines represent unstimulated levels.
(E) Relative IL-12 production by moDCs LPS-stimulated for 24 hr transfected with control or PYG-targeted siRNA.
(F) BMDCs treated with LPS ± CP plus OVA-AF488 or OVA-DQ for 3 hr and analyzed by flow cytometry for antigen uptake and processing.
(G) BMDCs were pulsed for 6 hr with indicated treatments and subsequently co-cultured with CFSE-labeled OT-II T cells. CFSE dilution was measured on day 3 post co-culture.
(H) Measurements of proliferation of OT-II T cells (from G) stimulated by BMDCs pre-treated with indicated conditions.
(I) siRNA transfected moDCs were co-cultured with CellTrace Violet-labeled human naive CD4$^+$ T cells for 4 days. Data were normalized to scrambled siRNA. Proliferation was measured after 4 days.
(A-I) n = 3-5, mean ± SD. (B and F) Two-way ANOVA Tukey's post-test. (C–E, H, and I)

Student's t test; *p % 0.05, **p < 0.001, ***p = 0.0004, ****p < 0.0001.

Glycogen-Derived Carbons Fuel Both Glycolytic Reprogramming and Mitochondrial Respiration in Activated DCs

We proposed that glycogen-derived glucose drives early glycolytic flux in TLR-activated DCs prior to GLUT1 upregulation. To test this, we performed a real-time extracellular flux analysis on BMDCs and moDCs. LPS-driven glycolytic burst was significantly attenuated by PYG inhibition in both BMDCs (Figures 4A and S3A) and moDCs (Figure 4B). We further tested whether cell-intrinsic glycogen metabolism also contributes to mitochondrial respiration during early activation. Concomitant with glycolysis reduction, PYG inhibition attenuated the oxygen consumption rate (OCR) in BMDCs regardless of activation (Figure 4C). These data suggest that pre-existing glycogen pools contribute metabolic substrates for mitochondrial respiration. Consistent with this, PYG inhibition accelerates LPS-mediated ATP depletion during early activation in a time-dependent manner (Figure 4D). The synergistic effect of combined CP and ATP-synthase inhibitor oligomycin in reducing ATP production (Figure 4E) indicates that glycogen catabolism contributes to both cytosolic and mitochondrial ATP generation. These findings indicate the intriguing possibility that there may be distinct roles for glucose and glycogen-derived carbon molecules in DC metabolism.

Since PYG inhibition resulted in reduced intracellular ATP levels (Figures 4D and 4E), we assessed the effect of PYG inhibition on the activation of AMPK, a key metabolic sensor of intra-cellular nutrient and ATP levels [28]. PYG inhibition resulted in increased phosphorylation of AMPK (Figure S3B), which is reported to antagonize BMDC activation [10]. This is consistent with reports showing that inhibition of glycolysis induces compensatory activation of AMPK [29, 30]. However, PYG inhibition had no impact on LPS-mediated GLUT1 upregulation (Figure S3C), suggesting that AMPK regulation of glucose transport is not a significant mechanism at play in our model. Nevertheless, LKB1 deficient BMDCs, which are incapable of activating AMPK, show decreased sensitivity to PYG inhibition during maturation at normal glucose concentrations, suggesting that AMPK compensatory activation during PYG inhibition may be involved in regulating maturation in these conditions (Figure S3D).

Previous work has demonstrated that glucose consumed by activated DCs enters the TCA cycle to generate citrate, which is preferentially translocated from the mitochondria into the cytosol via the citrate shuttle to support *de novo* fatty acid synthesis. This process is linked to ER and Golgi membrane expansion, which is hypothesized to enhance the production of effector molecules central to DC activation [8, 11]. To examine the role of glycogenolysis in citrate metabolism explicitly, we performed metabolic tracing experiments in which BMDCs were differentiated in ^{13}C-labeled glucose to label all intracellular metabolites. Cells were subsequently switched to normal glucose at the time of LPS stimulation in the presence or absence of CP for 1 and 3 hr. As previously published, LPS stimulation induces substantial metabolic flux through glycolysis and TCA citrate production ([31] and data not shown). PYG inhibition significantly reduced ^{13}C-labeled citrate while no statistically significant impact on hexose phosphate, pyruvate, lactate, and post-citrate metabolites fumarate and malate was observed (Figures 4F and S3E). Hexose phosphate refers to any 6-carbon sugar since our metabolite tracing approach could not distinguish individual sugars among this group. These data indicate that intracellular glycogen reserves preferentially support the generation of citrate following LPS stimulation.

Glutamine can also serve as an important carbon source for the TCA cycle. However, the findings that nearly the entire glutamine pool is derived from ^{12}C-labeled sources (Figure S3F) and that CP has very little effect on glutamine levels (Figure S3F) suggest that glutamine metabolism is not directly impacted by PYG inhibition. This is further supported by observations that (1) CP attenuates the maturation of BMDCs stimulated in the presence or absence of glutamine (Figure S3G) and (2) glutaminolysis inhibitor DON has no significant impact on glycolytic burst or OCR (Figure S3H).

To identify the role of glycogen metabolism in regulating extra-cellular glucose flux, the reverse metabolomics experiment was performed in which BMDCs differentiated in normal glucose were switched to ^{13}C-glucose at the time of LPS activation and analyzed at 3 and 6 hr post stimulation (Figure 4G). PYG inhibition minimally affected the ^{13}C-glucose contribution to cytoplasmic hexose phosphate, lactate, and pyruvate, while it severely attenuated both ^{12}C- and ^{13}C-glucose contributions to citrate production (Figure 4G).

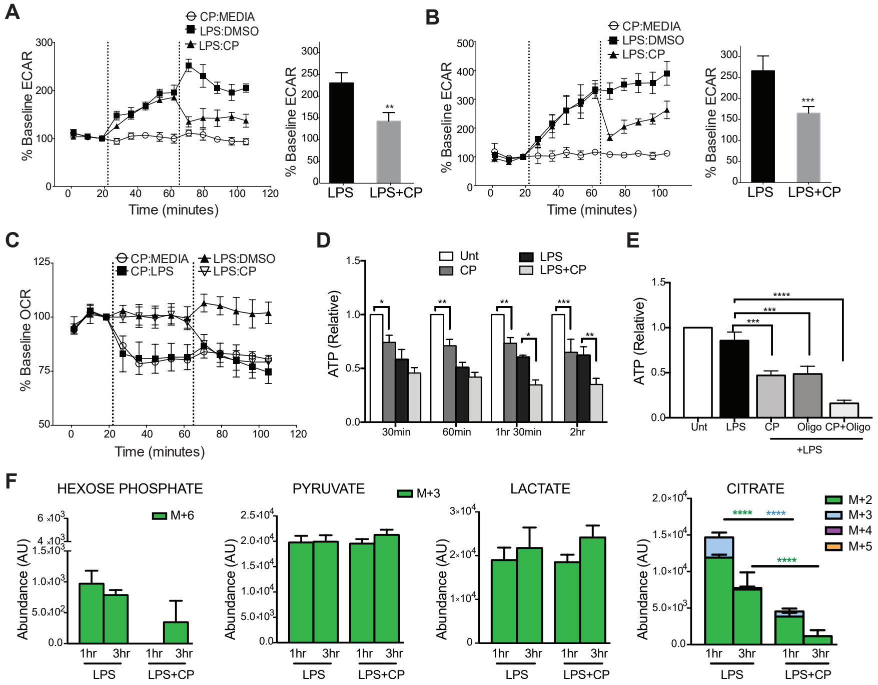

Figure 4. Glycogen-Derived Carbons Fuel Early Glycolytic Reprogramming and Mitochondrial Respiration in Activated DCs.

(A and B) Real-time changes in ECAR of BMDCs (A) and moDCs (B).
(C) Real-time changes in OCR of BMDCs.
For (A)–(C), treatments were introduced at dotted lines (first injection: second injection).
(D and E) ATP levels of BMDCs in 30 min intervals (D) and at 2 hr (E) after stimulation with indicated treatments.
(F) BMDCs cultured and differentiated in $^{13}C_6$-glucose were switched to normal glucose at the time of stimulation with LPS ± CP for 1 and 3 hr, and ^{13}C-labeled metabolites were detected by LC-MS spectrometry.
(G) Inverse metabolomics of (F), where BMDCs were differentiated in normal ^{12}C-glucose and switched to $^{13}C_6$-glucose at the time of stimulation with LPS ± CP for 3 and 6 hr.
Data represent n = 4, mean ± SD; (A and B) paired Student's t test; (D-G) n = 5, two-way ANOVA, Tukey's post-test. $*p < 0.05$, $**p < 0.005$, $***p < 0.0005$, $****p < 0.0001$.
(F and G) Statistical significance of each color * represents color-coded $^{13}C_6$ or black * for ^{12}C groups. White bars indicate l2C-glucose, and all color bars denote $^{13}C_6$-glucose.

The metabolite tracing data are consistent with previously published work [31] in which extracellular glucose contributes heavily to cytoplasmic glycolytic metabolites and citrate production from the TCA cycle (Figures 4F and 4G). However, these data also uncover two previously unappreciated aspects of glucose metabolism in DCs: (1) glycogen-derived carbons from basal glycogen stores (CP-sensitive ^{13}C metabolites in Figure 4F) preferentially support initial glycolytic intermediates and citrate synthesis; (2) a significant amount of glucose imported from the extracellular environment gets rapidly converted into glycogen (CP-sensitive ^{13}C metabolites in Figure 4G). The finding that extracellular ^{13}C-glucose incorporation into citrate (Figure 4G), succinate, fumarate, and malate (Figure S3I) is sensitive to PYG inhibition suggests that a significant portion of extracellular glucose destined for mitochondrial oxidation is metabolically routed via a glycogen-dependent pathway during DC activation. The routing of glucose carbons via a rapid sequence of glycogen synthesis and glycogenolysis is characteristic of a metabolic pathway described in astrocytes and muscle cells as the ‘‘glycogen shunt’’ [32, 33]. Our metabolic profiling studies support a model where glucose processing in TLR-stimulated DCs undergoes three functionally distinct pathways: (1) the catabolism of pre-activation intracellular glycogen stores; (2) the catabolism of imported glucose directly; (3) the incorporation of imported glucose into synthesis and breakdown of glycogen via the glycogen shunt (modeled in Figure S4).

While the glycogen shunt is clearly inefficient from an energetic perspective, others have argued that glycogen breakdown and synthesis may occur in separate spatial pools within brain and muscle cells to fuel rapid bursts of metabolic activity required in these cells that override the total energetic cost of this process [34-36]. DCs may employ a similar strategy of compartmentalized glycogen metabolism in order to fuel early immune activation. However, how this occurs and how it may be regulated in DCs remains an important question. Precedent for distinct and parallel sugar metabolism has been previously reported, whereby granulocyte phagocytic capability is driven by glycogen-derived carbons, while their chemotaxis is fueled by catabolism of free glucose carbons [37]. We propose that the source of carbons in activated DCs, namely whether it is glucose or glycogen derived, may dictate differential functional responses. We speculate that spatial compartmentalization of these processes in the cytoplasm may be an important component of how glycogen metabolism is regulated.

While glycogen metabolism has been previously implicated in myeloid cells of the immune system [21, 37-40], the role of glycogen metabolism in specific immune effector functions of DCs has not been previously defined. We show here a definitive role for glycogen metabolism in regulating immune effector functions of both human and mouse DCs. We further demonstrate that glucose- and glycogen-derived carbons exhibit distinct metabolic fates, a phenomenon that we suspect is not DC specific and likely occurs in other cells that utilize cell-intrinsic glycogen metabolism. Ongoing studies are focused on elaborating the mechanistic details of how glycogen-dependent compartmentalization of metabolic pathways occurs in response to different immune stimuli. With a growing interest in understanding how metabolic regulation controls the functional effector responses of immune cells, this work delineates an intricate and novel layer of complexity to how metabolic pathways operate at a subcellular level, which may be exploited in cell-based therapeutic applications in the future.

Author contributions

Conceptualization, P.T. and E.A.; Methodology, P.T., A.D., B.E., and E.A.; Formal Analysis, P.T., J.A.R., and A.D.; Investigation, P.T., L.R.P., R.C., B.E., S.B., J.A.R., A.D., and E.A.; Writing – Original Draft, P.T. and E.A.; Writing – Review & Editing, P.T., L.R.P., A.D., B.E., and E.A.; Funding Acquisition, E.A.; Resources, A.D., B.E., and E.A.; Supervision, A.D., B.E., and E.A.

Acknowledgements

The authors would like to acknowledge the UVM core facilities (Flow Cytometry, Animal Resource, Microscopy Imaging, and Advance Genome Technology Cores) for services provided in support of this work. Special acknowledgment to Dr. Ralph Budd, Dr. Paula Deming, and the VCIID COBRE for extensive support. Thank you to Dr. Matt Poynter for OVA-AF488 and OVA-DQ reagents. Funding sources: Boettcher Webb-Waring Biomedical Research - Early Career grant (2017) (A.D.), Veni Fellowship NWO (Grant# 91614087) (B.E.), LUMC fellowship (B.E.), 2016 AAI Careers in Immunology Fellowship (P.T. and E.A.), UVM College of Nursing and Health Sciences Incentive Grant (E.A.), UVM start-up Funds (E.A.), and P30GM118228 (E.A.).

References

1. Banchereau, J. and R.M. Steinman, *Dendritic cells and the control of immunity.* Nature, 1998. **392**(6673): p. 245-52.
2. Lee, H.K. and A. Iwasaki, *Innate control of adaptive immunity: dendritic cells and beyond.* Semin Immunol, 2007. **19**(1): p. 48-55.
3. Lipscomb, M.F. and B.J. Masten, *Dendritic cells: immune regulators in health and disease.* Physiol Rev, 2002. **82**(1): p. 97-130.
4. Akira, S. and K. Takeda, *Toll-like receptor signalling.* Nat Rev Immunol, 2004. **4**(7): p. 499-511.
5. Amati, L., et al., *Toll-like receptor signaling mechanisms involved in dendritic cell activation: potential therapeutic control of T cell polarization.* Curr Pharm Des, 2006. **12**(32): p. 4247-54.
6. Barton, G.M. and R. Medzhitov, *Control of adaptive immune responses by Toll-like receptors.* Curr Opin Immunol, 2002. **14**(3): p. 380-3.
7. Amiel, E., et al., *Inhibition of mechanistic target of rapamycin promotes dendritic cell activation and enhances therapeutic autologous vaccination in mice.* J Immunol, 2012. **189**(5): p. 2151-8.
8. Amiel, E., et al., *Mechanistic target of rapamycin inhibition extends cellular lifespan in dendritic cells by preserving mitochondrial function.* J Immunol, 2014. **193**(6): p. 2821-30.
9. Everts, B., et al., *Commitment to glycolysis sustains survival of NO-producing inflammatory dendritic cells.* Blood, 2012. **120**(7): p. 1422-31.
10. Krawczyk, C.M., et al., *Toll-like receptor-induced changes in glycolytic metabolism regulate dendritic cell activation.* Blood, 2010. **115**(23): p. 4742-9.
11. Rehman, A., et al., *Role of fatty-acid synthesis in dendritic cell generation and function.* J Immunol, 2013. **190**(9): p. 4640-9.
12. Everts, B. and E.J. Pearce, *Metabolic control of dendritic cell activation and function: recent advances and clinical implications.* Front Immunol, 2014. **5**: p. 203.
13. Fox, C.J., P.S. Hammerman, and C.B. Thompson, *Fuel feeds function: energy metabolism and the T-cell response.* Nat Rev Immunol, 2005. **5**(11): p. 844-52.
14. Pearce, E.J. and B. Everts, *Dendritic cell metabolism.* Nat Rev Immunol, 2015. **15**(1): p. 18-29.
15. Pearce, E.L. and E.J. Pearce, *Metabolic pathways in immune cell activation and quiescence.* Immunity, 2013. **38**(4): p. 633-43.
16. Freemerman, A.J., et al., *Metabolic reprogramming of macrophages: glucose transporter 1 (GLUT1)-mediated glucose metabolism drives a proinflammatory phenotype.* J Biol Chem, 2014. **289**(11): p. 7884-96.
17. Macintyre, A.N., et al., *The glucose transporter Glut1 is selectively essential for CD4 T cell activation and effector function.* Cell Metab, 2014. **20**(1): p. 61-72.
18. Adeva-Andany, M.M., et al., *Glycogen metabolism in humans.* BBA Clin, 2016. **5**: p. 85-100.
19. Roach, P.J., et al., *Glycogen and its metabolism: some new developments and old themes.* Biochem J, 2012. **441**(3): p. 763-87.

20. Voet, D., J.G. Voet, and C.W. Pratt, *Fundamentals of biochemistry: life at the molecular level*. 2016: John Wiley & Sons.
21. Maroof, A., et al., *Developing dendritic cells become 'lacy' cells packed with fat and glycogen*. Immunology, 2005. **115**(4): p. 473-83.
22. Afzelius, B.A., *Section staining for electron microscopy using tannic acid as a mordant: a simple method for visualization of glycogen and collagen*. Microsc Res Tech, 1992. **21**(1): p. 65-72.
23. Favaro, E., et al., *Glucose utilization via glycogen phosphorylase sustains proliferation and prevents premature senescence in cancer cells*. Cell Metab, 2012. **16**(6): p. 751-64.
24. O'Neill, L.A., *Glycolytic reprogramming by TLRs in dendritic cells*. Nat Immunol, 2014. **15**(4): p. 314-5.
25. Pearce, E.L., et al., *Enhancing CD8 T-cell memory by modulating fatty acid metabolism*. Nature, 2009. **460**(7251): p. 103-7.
26. Lawless, S.J., et al., *Glucose represses dendritic cell-induced T cell responses*. Nat Commun, 2017. **8**: p. 15620.
27. Wieman, H.L., J.A. Wofford, and J.C. Rathmell, *Cytokine stimulation promotes glucose uptake via phosphatidylinositol-3 kinase/Akt regulation of Glut1 activity and trafficking*. Mol Biol Cell, 2007. **18**(4): p. 1437-46.
28. Hardie, D.G., F.A. Ross, and S.A. Hawley, *AMPK: a nutrient and energy sensor that maintains energy homeostasis*. Nat Rev Mol Cell Biol, 2012. **13**(4): p. 251-62.
29. Wang, Q., et al., *2-Deoxy-D-glucose treatment of endothelial cells induces autophagy by reactive oxygen species-mediated activation of the AMP-activated protein kinase*. PLoS One, 2011. **6**(2): p. e17234.
30. Wu, Y., et al., *Combined inhibition of glycolysis and AMPK induces synergistic breast cancer cell killing*. Breast Cancer Res Treat, 2015. **151**(3): p. 529-39.
31. Everts, B., et al., *TLR-driven early glycolytic reprogramming via the kinases TBK1-IKKvarepsilon supports the anabolic demands of dendritic cell activation*. Nat Immunol, 2014. **15**(4): p. 323-32.
32. Shulman, R.G., F. Hyder, and D.L. Rothman, *Cerebral energetics and the glycogen shunt: neurochemical basis of functional imaging*. Proc Natl Acad Sci U S A, 2001. **98**(11): p. 6417-22.
33. Shulman, R.G. and D.L. Rothman, *The "glycogen shunt" in exercising muscle: A role for glycogen in muscle energetics and fatigue*. Proc Natl Acad Sci U S A, 2001. **98**(2): p. 457-61.
34. Calder, P.C. and R. Geddes, *Heterogeneity of glycogen synthesis upon refeeding following starvation*. Int J Biochem, 1992. **24**(1): p. 71-7.
35. Elsner, P., et al., *Partly ordered synthesis and degradation of glycogen in cultured rat myotubes*. J Biol Chem, 2002. **277**(7): p. 4831-8.
36. Obel, L.F., et al., *Brain glycogen-new perspectives on its metabolic function and regulation at the subcellular level*. Front Neuroenergetics, 2012. **4**: p. 3.
37. Weisdorf, D.J., P.R. Craddock, and H.S. Jacob, *Glycogenolysis versus glucose transport in human granulocytes: differential activation in phagocytosis and chemotaxis*. Blood, 1982. **60**(4): p. 888-93.
38. Scott, R.B., *Glycogen in human peripheral blood leukocytes. I. Characteristics of the synthesis and turnover of glycogen in vitro*. J Clin Invest, 1968. **47**(2): p. 344-52.

39. Yunis, A.A. and G.K. Arimura, *ENZYMES OF GLYCOGEN METABOLISM IN WHITE BLOOD CELLS. I. GLYCOGEN PHOSPHORYLASE IN NORMAL AND LEUKEMIC HUMAN LEUKOCYTES*. Cancer Res, 1964. **24**: p. 489-92.
40. Yunis, A.A. and G.K. Arimura, *Enzymes of glycogen metabolism in white blood cells. II. Activation and inactivation of glycogen phosphorylase of rat chloroma*. Biochim Biophys Acta, 1966. **118**(2): p. 325-34.

Methods

Mouse Models

The University of Vermont's Animal Facility is a barrier facility housing only mice. All animals are housed in autoclaved Lab Products microisolator cages on ventilated racks and handled using aseptic technique in laminar flow work stations and are provided with sterile water and irradiated rodent chow (Lab Diets Isopro RMH 3000). Mice are maintained in a pathogen free environment at a constant temperature and humidity, with 12-hour light and 12-hour dark cycle. Personnel wear shoe covers, isolation gowns, masks, bouffant and exam gloves. In addition, animal husbandry personnel wear dedicated scrubs and footwear. Health monitoring of colony and sentinel animals is performed quarterly. The University's program of animal care has been fully-accredited by AAALAC, International for over 25 years. OT-II (B6.Cg-Tg (TcraTcrb)425Cbn/J and C57/Bl6J mice mice were purchased from Jackson Laboratory and were maintained at the University of Vermont animals care facility under protocols approved by Institutional Animal Care and Use Committee. For most experiments, adult mice (2-6 months of age) were used. Mouse experiments include data from both male and female mice, however the specific sex distribution for each individual experiment was not explicitly tracked. Itgax^{cre} LKB1$^{fl/fl}$ mice PubMed: 21124450 were housed and bred at the LUMC, Leiden, Netherlands, under SPF conditions. All animal experiments were performed in accordance with local government regulations, and the EU Directive 2010/63EU and Recommendation 2007/526/EC regarding the protection of animals used for experimental and other scientific purposes and approved by the CCD, animal license number AVD116002015253.

Mouse DC Culture and Activation

Bone marrow-derived DCs (BMDCs) were generated as follows: BM cells were flushed from femurs of 9-18-week-old mice and the cells were differentiated in GM-CSF (20 ng/mL; Peprotech) in complete DC medium (CDCM), comprised of RPMI1640, 10% FCS, 2mM L-glutamine, 1 IU/mL Pen-Strep, 1 mM beta-mercaptoethanol, for 7 days, with a medium change every 2 days. On day 7, DCs were washed in CDCM and cultured at 2x10^5 cells per 200 mL of media alone, STF31 (12.5 μM), CP91149 (75-100 μM), DAB (1 mM), LPS (100 ng/mL), LPS plus STF31 or CP91149, or DAB, or OVA (from whole egg white) at indicated time points. Where appropriate, DCs were stimulated in CDCM containing 0 mM, 1.25 mM, 2.5 mM, or 5 mM glucose.

Glucose Starvation Experiment

BMDCs were starved for glucose overnight, with a non-starved group as a control. On the next day, DCs from both groups were washed with sugar free

RPMI and stimulated with LPS in glucose free medium ± CP for 6 hours. CD40 and CD86 expression was analyzed by Flow cytometry.

Human DC Culture and Activation

Human monocyte-derived DCs (moDCs) were differentiated from peripheral blood monocytes as follows: Blood filters from de-identified blood donors were provided by CVPH Medical Center Blood Bank in Plattsburgh, NY. Filters were reverse-flushed in sterile PBS, and PBMCs were prepared by Ficoll-Paque (density gradient of 1.0772) centrifugal separation using LSM media (MP biochemical; Fisher). Resulting monocytes were enriched using CD14 positive selection beads per manufacturer instructions (Miltenyi Bioscience) and cultured in complete DC medium (CDCM) supplemented with human recombinant GM-CSF (20 ng/mL) plus human recombinant IL-4 (20 ng/mL) (Peprotech) for 7 days. On day 7, moDC were harvested, stimulated as indicated, and analyzed by FACS for maturation and by multiplex panels (Life Technologies) for cytokine production.

Quantitative Real-time PCR of *pygl, pygm, gys1,* and *gys2* Expression

RNA was isolated with an RNAeasy Kit (QIAGEN) and cDNA was synthesized with an iScript cDNA Synthesis Kit (Biorad). *pygl*, *pygm*, *gys1*, *gys2*, and *slc2a1* Taqman primer probes (Applied Bioscience system) and AB7500 sequence detection system or QuantStudio 3.0 were used for relative mRNA expression. mRNA relative quantitative values were calculated based on 2(-ΔΔCT) and normalized to untreated samples.

Glycogen Phosphorylase Knockdown by siRNA Transfection of moDC

For knockdown of glycogen phosphorylase isoforms, moDCs were generated as mentioned above. At day 4 of the culture, the cells were harvested, washed with PBS, brought to a concentration of 1x10^6 cells / 100 mL resuspension buffer, and finally, transfected by electroporation with either 10 nM anti-PGYL siRNA in combination with 10 nM anti-PYGB siRNA or 20 nM scrambled siRNA (Dhar- macon). Electroporation was performed using a Neon Transfection System (Invivogen) with the following settings: 1600 V, 20 ms and one pulse. Immediately after electroporation, 1x10^6 cells were taken up in 5 mL 10% HI-FCS basal media, containing no antibiotics, and plated at 200 cells / mL. The next morning, the media was re-supplemented with penicillin, streptomycin, rGM-CSF and rIL-4. At day 6, the cells were harvested, stimulated as indicated, and analyzed by FACS for maturation and by ELISA for cytokine production. Silencing efficiency was determined by qPCR on 6 day-old cells. The transfection efficiency was routinely greater than 80%.

Antigen Uptake, Processing, and In-Vitro T Cell Responses

BMDCs were stimulated ± LPS with OVA-AF488 (5 mg/mL) and OVA-DQ (5 mg/mL) for antigen uptake and processing, respectively. For *in vitro* T cell responses, T cells were generated using mouse CD4 positive selection beads from spleens of 6-10-week-old transgenic OT-II mice and age-matched wild-type B6 mice. BMDCs were pulsed with whole ovalbumin protein (OVA), extracted from egg white, and LPS in the presence or absence of CP for 6 hours, washed 3 times, and co-cultured with CFSE-labeled OT-II T cells at a 1:5 ratio for 72 hours. T cell proliferation (CFSE dilution) was analyzed by flow cytometry.

For alloreaction studies of siRNA transfected moDC, the cells were washed 2 times, and co-cultured with CellTrace Violet-labeled human naive CD4$^+$ T cells, which were isolated using a naive pan T cell isolation kit (Miltenyi) followed by negative selection using CD8 MicroBeads (Miltenyi), at a 1:4 ratio for 4 days. T cell proliferation was analyzed by flow cytometry.

Metabolism Assays

Extracellular glucose and intracellular glycogen levels were measured with a Glucose assay kit (Eton Biosciences) and a Glycogen assay kit (Biovision), respectively. For Biolog assays, (Metabolic phenotypic screening assays), IFM-1 reagent, Biolog MA redox dye, and Biolog plates were purchased from Biolog Inc. Fully differentiated BMDC were plated overnight at 50,000 cells per well in specified nutrient sources in basal MC-0 medium (IFM1 media with 5% FCS, 0.3 mM L-glutamine, 100 I/U Pen Strep). 20 mL of Biolog MA dye was added to each well the next morning. The assays were measured at 592 nm absorbance as indicated. Data were normalized to the readings at time 0. Extracellular acidification rate (ECAR) and oxygen consumption rate (OCR) were measured with Metabolic Flux Analyzer (Seahorse Bioscience, North Billerica, MA 24XP and/or 96XP). ATP concentrations were measured with an ATP Determination Kit (Invitrogen) according to the manufacturer's instructions.

BMDC Cultures and Activation for Metabolomics

For metabolomics tracing in Figure 4F, BMDCs were differentiated in $^{13}C_6$-glucose containing CDCM. On day 7, the cells were switched to $^{12}C_6$-glucose medium, with LPS and LPS+CP added at the time of media switch and stimulated for 1 and 3 hours. At each time point, cells were harvested, counted, pelleted, and frozen for the UHPLC-MLS metabolomics processing below. For inverse metabolomics in Figure 4G, BMDCs normally differentiated in regular CDCM were switched to $^{13}C_6$-glucose medium at the time of stimulation, with and without CP for 3 and 6 hours. Cells were harvested and processed as above. Supernatant from the 6 hour stimulation groups was collected for Multiplex Cytokine analysis.

UHPLC-MS Metabolomics

Frozen cell pellets were extracted at 2e6 cells/mL in ice cold lysis/extraction buffer (methanol:acetonitrile:water 5:3:2). Samples were agitated at 4°C for 30 min followed by centrifugation at 10,000 g for 10 min at 4°C. Protein and lipid pellets were discarded, and supernatants were stored at -80°C prior to metabolomic analysis. Ten mL of extracts were injected into an UHPLC system (Vanquish, Thermo, San Jose, CA, USA) and run on a Kinetex C18 column (150 x 2.1 mm, 1.7 µm – Phenomenex, Torrance, CA, USA) at 250 ml/min (phase A: Optima H_2O, 0.1% formic acid; phase B: acetonitrile, 0.1% formic acid). The autosampler was held at 7°C and the column compartment at 25°C. The UHPLC system was coupled online with a Q Exactive mass spectrometer (Thermo, Bremen, Germany), scanning in Full MS mode (2 mscans) at a 70,000 resolution in the 60-900 m/z range in negative and then positive ion mode (separate runs). Eluate was subjected to electrospray ionization (ESI) with 4 kV spray voltage, 15 sheath gas and 5 auxiliary gas. Metabolite assignments and isotopologue distributions were determined using the software Maven (Princeton, NJ, USA), upon conversion of .raw files into .mzXML format through MassMatrix (Cleveland, OH, USA). Chromatographic and MS technical stability were assessed by determining CVs for heavy and light isotopologues in a technical mixture of extract run every 10 injections. Relative quantitation was performed by exporting the values for integrated peak areas of light metabolites and their isotopologues into Excel (Microsoft, Redmond, CA, USA) for statistical analysis including t test and ANOVA (significance threshold for p values < 0.05).

Electron Microscopy

Samples were fixed in Karnovsky's Fixative for 1hr at 4°C, washed in 0.1 M Cacodylate Buffer, and post-fixed in 1% OsO4 for 1hr at 4°C followed by an extensive rinse with Cacodylate buffer. Samples were then dehydrated in a graded series of ethanol, and embedded in Spurr. Sections were cut with a Reichert Ultracut Microtome and stained with toluidine blue. For contrast, 1% tannic acid was added to the cut sections of the grids for 10 min, followed by 6 min of uranyl acetate and 4 min of lead citrate. Cells were examined with a JEM1400 transmission electron microscope (JEOL USA).

Immunoblot Analysis

Cell lysates were prepared using 2X NP-40 lysis buffer. 20 mg protein was loaded into each well of a 12.5% polyacrylamide gel, transferred onto activated nitrocellulose membrane (BioRad). Electrophoretic transfer was performed using Trans-Blot Turbo RTA mini Nitrocellulose transfer kit. Membranes were blocked in 2% milk in 1xTBST at RT for 1hr, and incubated in indicated antibody at 4°C overnight. Blots were washed 3x in 1xTBST at RT, probed with secondary antibodies at RT for 45-60 min, and washed 3-4x with 1xTBST. Proteins were visualized by SuperSignal West Pico Chemiluminescent substrate and exposed with GeneXpert System imager. Trans-Blot Turbo Transfer system and secondary antibodies for western blots were generously provided by Dr. Paula Deming, Medical Laboratory and Radiation Science Department, UVM.

Flow Cytometry and Cytokine Measurements

The following fluorescently labeled antibodies were used for flow cytometry: anti-CD11c (N418), anti-CD40 (3/23), anti-CD86 (GL1), IA-b (AF6-120.1), anti-CD1a (HI149), anti-CD40 (5C3), anti-CD86 (IT2.2), anti-TNF-α (MP6-XT22), anti-IL-12p40 (C15.6). Stimulated cells as indicated were harvested and washed in 1% FACS buffer (PBS plus 1% FBS), stained with specific antibodies, and incubated on ice for 30 min. All samples were acquired using a LSRII flow cytometer (BD Biosciences). For intracellular cytokine expression, cells were activated with indicated treatment groups for a total of 4 hours with an addition of Golgi plug (1:1000) (Biolegend) after the first hour of stimulation. For intracellular staining of TNF-α and IL-12 (Biolegend), cells were fixed in 4% paraformaldehyde, permeabilized in 0.2% saponin, and stained with antibodies in FACS buffer (1% FBS in PBS). Samples were analyzed on a BD LSRII flow cytometer. For cytokine levels of BMDCs and moDCs, supernatants were collected as indicated time points and measured with Mouse Cytokine Magentic 20-Plex and Human Cytokine Magnetic 30-Plex panels (Life Technologies) per manufacture instructions using Bio-Plex array suspension system.

Quantification and statistical analysis

Throughout the manuscript, ‘‘n’’ refers to independent cell cultures from individual mice or human samples. All the experiments reported in Figure 1 were repeated n = 3-6 mice per condition, with the following detailed n values: Figures 1A–1E and 1I, n = 3; Figures 1F and 1G, n = 6; Figure 1H, n = 4; and Figure 1J, n = 4. The survival and maturation experiments in Figures 2A–2F and S1 were repeated with n = 6. Intracellular cytokine experiments in Figures 3 and S2 were repeated with n = 4. Multiplex analyses in Figures 3 and S2 were repeated with n = 6. All metabolomics experiments in Figures 4 and S3 were repeated with n = 4, and the seahorse experiments in Figures 1, 4, and S3 were repeated with n = 3-5. All the siRNA experiments in Figure 2G, 3I, S1C, and S1D were repeated with n = 5. Data were analyzed with GraphPad Prism software (version 6.0). Samples were analyzed using Student's t test, One-way, and Two-way ANOVA where appropriate. ANOVA tests were post-calculated by Tukey's multiple comparison test or Sidak test. Results are means +/-SD as indicated, and statistical values are represented significant when p values were equal or below 0.05.

Supplementary figures

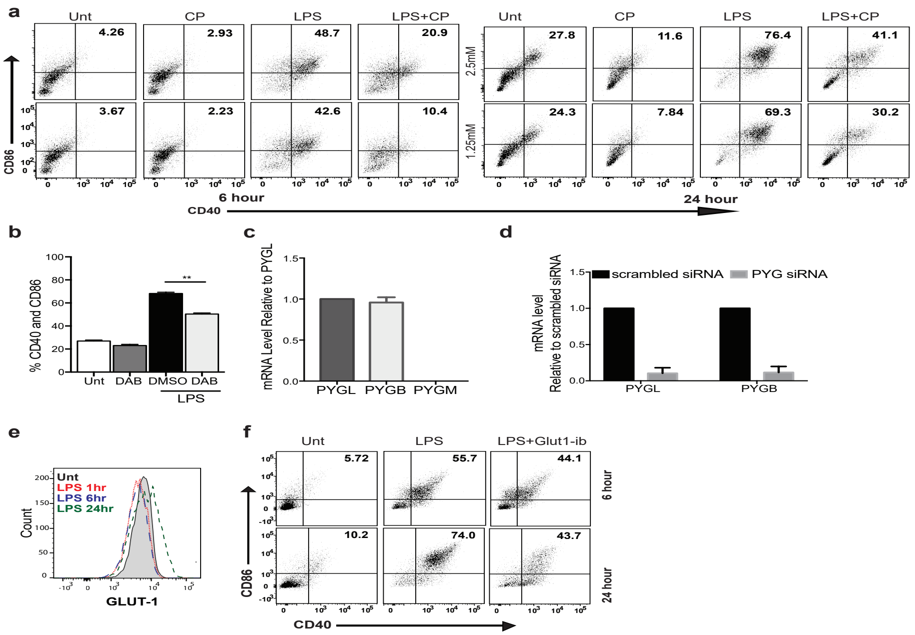

Figure S1. (related to Figure 1 and Figure 2).

(a) BMDCs stimulated with LPS+/-CP for 6 and 24 hours in indicated glucose concentrations were analyzed for CD40 and CD86 surface expression.
(b) CD40 and CD86 expression of BMDCs stimulated with LPS+/-DAB for 6 hours in normal glucose concentration.
(c) mRNA expression of 3 PYG isoforms in moDCs; data normalized to PYGL; n=6.
(d) Relative mRNA level for confirmation of knockdown of pygl and pygb by si-RNA transfection of moDCs.
(e) Intracellular stain of Glut-1 expression in BMDCs stimulated for 1, 6, and 24 hrs.
(f) CD40 and CD86 surface expression of BMDCs stimulated with LPSGlut1-ib for 6 and 24 hours in normal glucose concentration.
(a, e-f) representative of more than 3 experiments. (b) n=4, mean+/-SD, One-way ANOVA with Sidak Post-test,**P=0.0038.

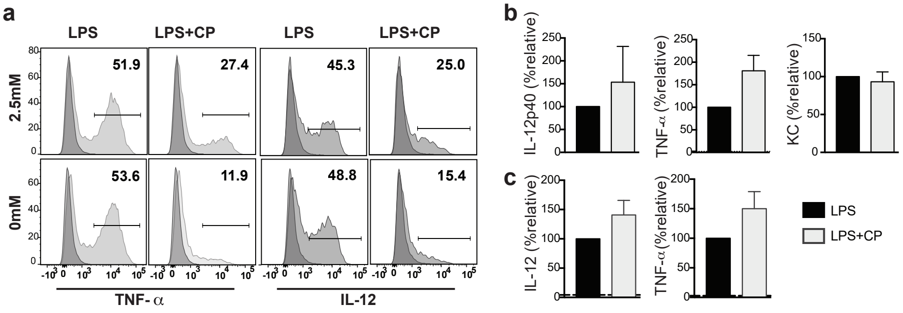

Figure S2. (related to Figure 3).

(a) Intracellular staining of TNF-α and IL-12 of BMDCs stimulated with LPS+/-CP for 4 hours in 2.5 and 0 mM glucose. Data are from one experiment representative of four. (b-c) Multiplex panel of cytokine and chemokine measurements from the supernatant of (b) BMDCs and (c) moDCs activated with LPS+/-CP for 6 hours. Dotted lines represent unstimulated levels. n=4, mean+/-SD, student's t-test.

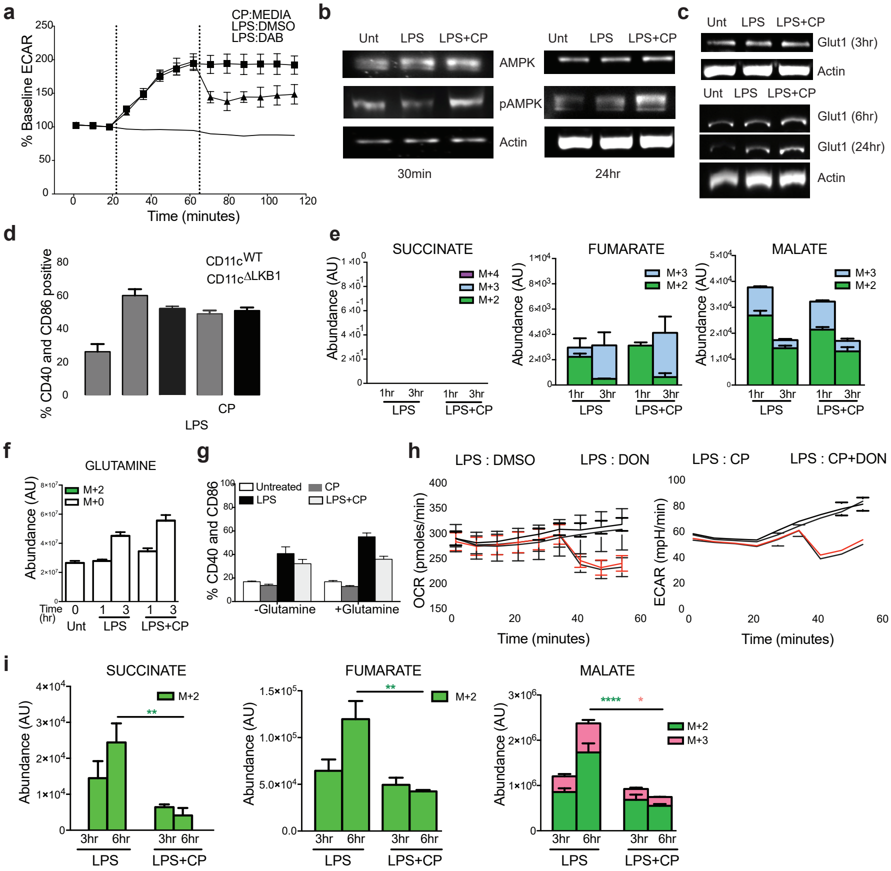

Figure S3. (related to Figure 4).

(a) Real-time changes in ECAR of BMDCs using an alternate PYGL inhibitor, DAB; treatments introduced at dotted lines (1st injection: 2nd injection). Representative of 3 experiments.
(b) Protein expression of AMPK and pAMPK in BMDCs stimulated with LPS+/-CP for 30 minutes and 24 hrs in normal glucose.
(c) Protein expression of Glut-1 in BMDCs stimulated with LPS+/-CP for 3, 6, and 24 hours in normal glucose.
(d) Surface expression of CD40 and CD86 of BMDCs from WT or LKB1-/- mice stimulated with LPS+/- CP for 6 hrs. Data represents replicates n=3. mean+/-SD.
(e,f) BMDCs differentiated in $^{13}C_6$ -glucose were switched to normal glucose at the time of stimulation with LPS+/-CP for 1 and 3 hrs and detected by LC-MS spectrometry. Color bars denote heavy ($^{13}C_6$glucose) whereas white bars represent light ^{12}C glucose.
(e)$^{13}C_6$ glucose not detected in succinate after stimulation.
(g) CD40 and CD86 expression was analyzed in BMDCs stimulated for 6 hours with LPS+/-CP in the presence or absence of glutamine in the medium. n=6
(h) Real-time OCR and ECAR with CP, glutaminolysis inhibitor (DON), or combination; treatment injected at dotted lines (1st injection: 2nd injection).
(i) Inverse metabolite tracing of b and c, where BMDCs differentiated in normal light

glucose were switched to $^{13}C_6$-glucose medium at the time of stimulation with LPS+/-CP for 3 and 6 hrs and selected TCA intermediates were shown. Data represents n=4, mean+/-SD, Two-way ANOVA with Tukey-Post-test. *P=0.019, **P<0.0039, and ****P<0.0001.

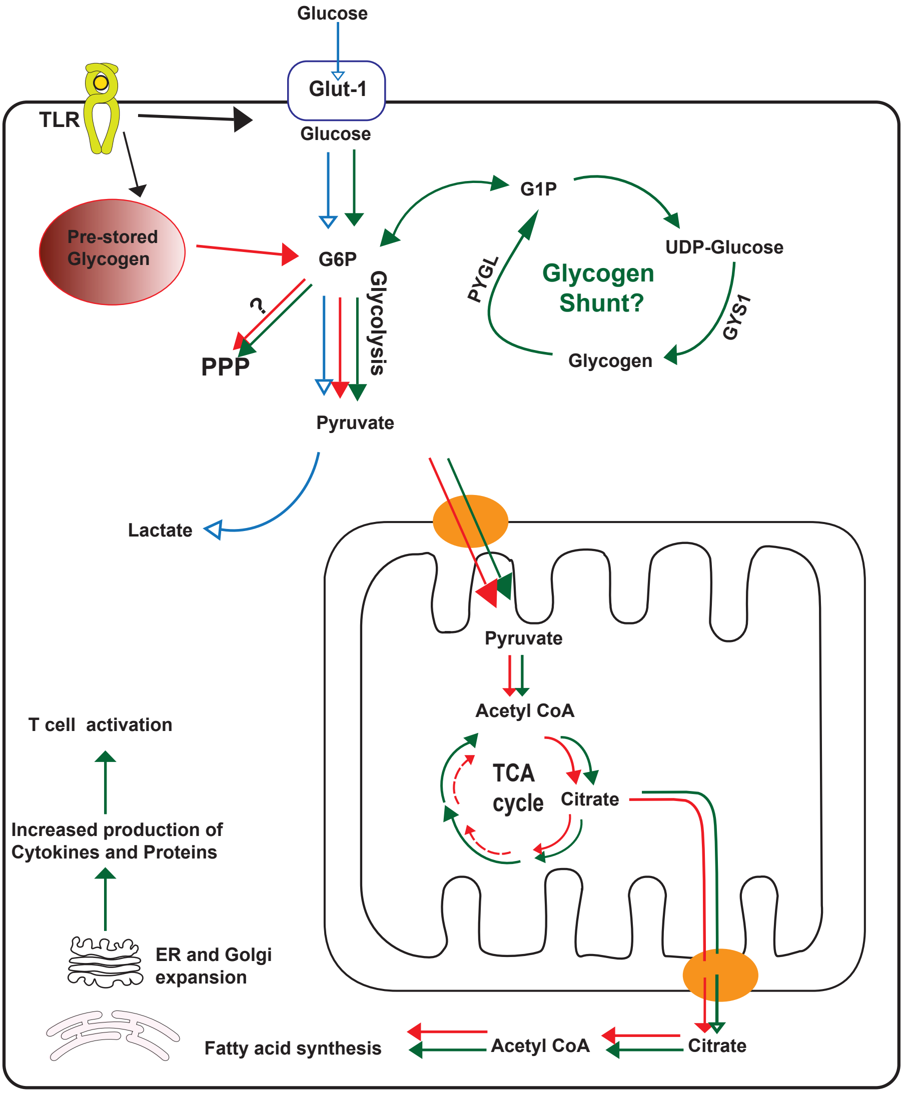
Glucose
Glut-1
TLR
Glucose
G1P
UDP-Glucose
Pre-stored Glycogen
G6P
Glycogen Shunt?
PYGL
GYS1
?
Glycolysis
PPP
Glycogen
Pyruvate
Lactate
Pyruvate
Acetyl CoA
T cell activation
TCA cycle
Citrate
Increased production of Cytokines and Proteins
ER and Golgi expansion
Fatty acid synthesis
Acetyl CoA
Citrate

Figure S4. (related to Figure 4).

Proposed Model: Pathway 1 (red) represents the catabolism of basal glycogen stores primarily driving citrate generation. Pathway 2 (blue) represent the catabolism of free glucose which primarily supports the formation of intracellular lactate. Pathway 3 (green) represents glycogen shunt activity, which primarily supports citrate production and a full TCA cycle. PPP=Pentose phosphate pathway

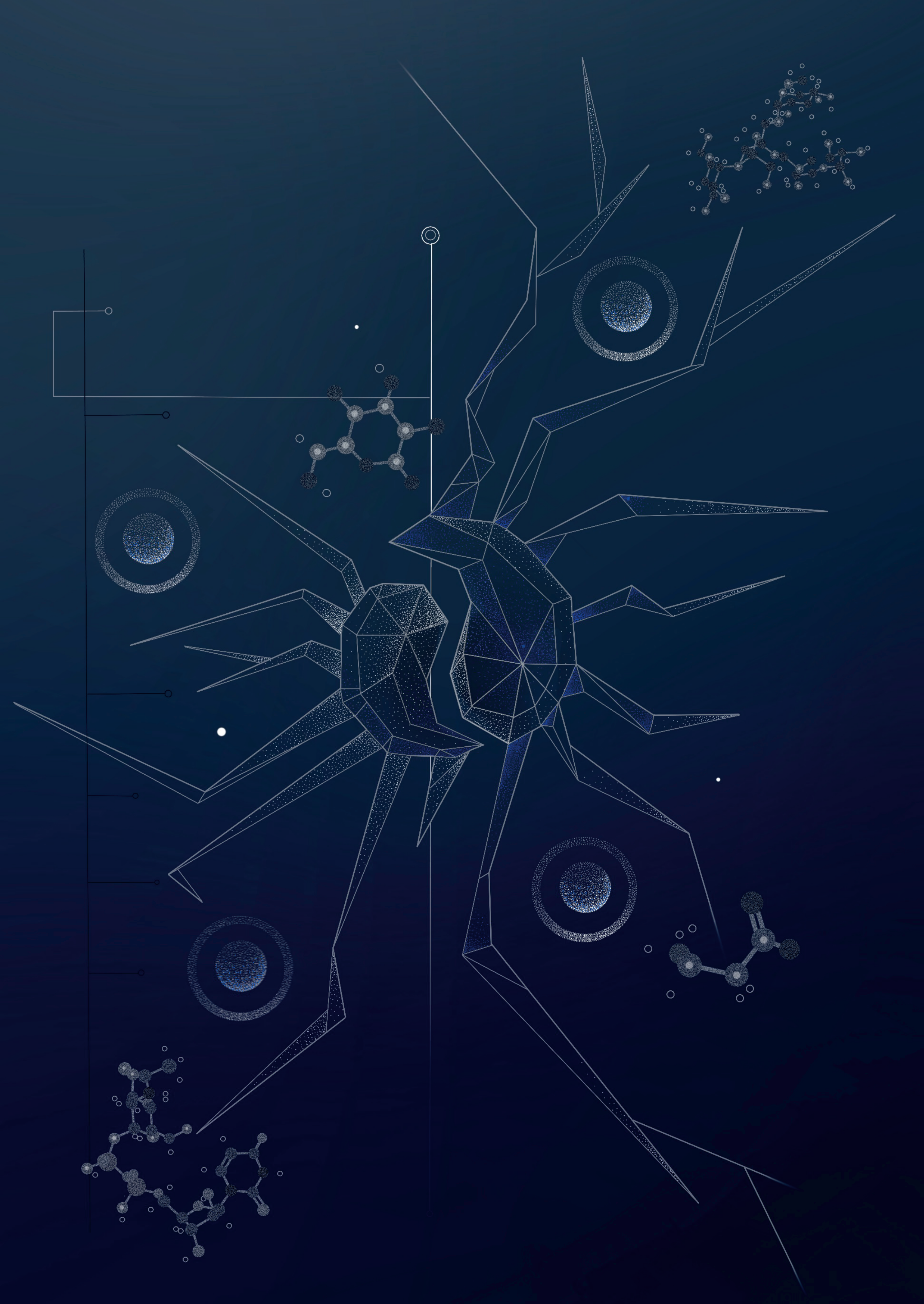

5

Butyrate Conditions Human Dendritic Cells to Prime Type 1 Regulatory T cells via both Histone Deacetylase Inhibition and G Protein-Coupled Receptor 109A Signaling

Maria M. M. Kaisar
Leonard R. Pelgrom
Alwin J. van der Ham
Maria Yazdanbakhsh
Bart Everts

Front Immunol. 2017 Oct 30;8:1429
PMID: 29163504
DOI: 10.3389/fimmu.2017.01429

Abstract

Recently, it has become clear that short-chain fatty acids (SCFAs), and in particular butyrate, have anti-inflammatory properties. Murine studies have shown that butyrate can promote regulatory T cells via the induction of tolerogenic dendritic cells (DCs). However, the effects of SCFAs on human DCs and how they affect their capacity to prime and polarize T-cell responses have not been addressed. Here, we report that butyrate suppresses LPS-induced maturation and metabolic reprogramming of human monocyte-derived DCs (moDCs) and conditions them to polarize naive CD4$^+$ T cells toward IL-10-producing type 1 regulatory T cells (Tr1). This effect was dependent on induction of the retinoic acid-producing enzyme retinaldehyde dehydrogenase 1 in DCs. The induction of retinaldehyde dehydrogenase activity and Tr1 cell differentiation by butyrate was dependent on simultaneous inhibition of histone deacetylases and signaling through G protein-coupled receptor 109A. Taken together, we reveal that butyrate is a potent inducer of tolerogenic human DCs, thereby shedding new light on the cellular and molecular mechanisms through which SCFAs can exert their immunomodulatory effects in humans.

Introduction

Dendritic cells (DCs) play a crucial role in the development of adaptive immune responses during infections and inflammatory diseases, as well as in the regulation of immune homeostasis during steady state, by governing the activation and maintenance of T-cell responses. In response to many viral and bacterial infections, DCs promote the generation of immune responses that are dominated by $CD4^+$ T helper 1 (Th1) cells and cytotoxic $CD8^+$ T cells. By contrast, fungal and parasitic worm infections are predominantly associated with Th17 and Th2 responses, respectively. In addition to these effector responses, DCs can be instructed to become tolerogenic and promote regulatory T cells (Tregs) responses, a process that is crucial for maintenance of immune homeostasis and control of autoimmune disorders and allergies [1-3].

Over the years, there has been a growing appreciation that microbiota are central players in the education and maintenance of a well-balanced immune system. Among the various mechanisms through which intestinal microbiota have been described to modulate the immune system, the production of short-chain fatty acids (SCFAs) is a major one [4]. SCFAs are organic fatty acids with acyl chains consisting of 1–6 carbon atoms (C1–C6) that are the fermentation products of non-digestible polysaccharides by gut microbiota. Acetate (C2), propionate (C3), and butyrate (C4) are among the most abundant species found in the intestine [5]. Given their ability to be transported into the circulation, SCFAs can exert functions in organs distal to the intestine [2, 4, 6, 7]. In line with this, SCFAs have beneficial effects on a broad range of inflammatory diseases in animal models of inflammatory bowel disease, colitis, asthma, obesity, and arthritis [2, 4, 8, 9].

Short-chain fatty acids have diverse functions depending on the tissue or cell type involved. For instance, SCFAs are crucial for the maintenance of intestinal epithelium physiology by regulating the cellular turnover and barrier functions. SCFAs can also regulate the activation, recruitment and differentiation of immune cells, including neutrophils, DCs, macrophages, and T lymphocytes. In general, SCFAs have anti-inflammatory effects on immune cells. For instance, SCFAs reduce expression of pro-inflammatory cytokines such as tumor necrosis factor (TNF)-α, IL-6 and IL-12 by macrophages, and DCs. In addition, SCFAs, in particular butyrate, can condition murine DCs to promote the differentiation and expansion of Tregs. SCFAs can additionally act on T cells directly, resulting in reduced proliferation and polarization toward a regulatory phenotype [10-12].

Two main mechanisms have been described thus far through which SCFAs can modulate immune cell function. SCFAs can affect immune cells via signaling through specific G protein-coupled receptors (GPRs). The most well-characterized SCFAs-sensing GPRs are GPR41, GPR43, and GPR109A [5, 13, 14]. In addition, following transport across the plasma membrane via monocarboxylate transporter Slc5a8 [15-17], propionate and butyrate can act as inhibitors of histone deacetylase (HDAC) 1 and 3. HDACs together with histone acetylase (HATs) control histone acetylation, which plays a key role in epigenetic regulation of gene expression by serving as a switch between permissive (via HAT-induced acetylation) and repressive chromatin (through HDAC-driven deacetylation). While inhibition of HDAC activity can have a wide range of effects including changes in gene expression, chemotaxis, differentiation, proliferation, and apoptosis [9, 10, 18], studies on immune cells have linked HDAC inhibition by SCFAs primarily to suppression of inflammatory responses [19-22]. Finally, SCFAs can also act as direct substrates for metabolic processes in cells. For instance, butyrate is known to be a major energy source for gut epithelium [23]. However, whether SCFAs also feed into core metabolic pathways of immune cells in a similar manner to regulate their bioenergetic status and whether this has an immunomodulatory effect still needs to be investigated.

Despite the advances in the field, there is still an incomplete understanding of the mechanisms through which SCFAs promote tolerogenic DCs and how these DCs drive Tregs. While one study found that butyrate-driven Treg cell induction by murine DCs is dependent on signaling through GPR109A [14], others have refuted this [16, 24]. These latter studies instead implicated the requirement for transport through Slc5a8 and subsequent inhibition of HDAC activity in promoting tolerogenic murine DCs. These butyrate-conditioned murine DCs were found to have increased expression of known immunosuppressive enzymes retinaldehyde dehydrogenase (RALDH) 2 and indoleamine-pyrrole 2,3-dioxygenase (IDO) [16]. However, whether RALDH and/or IDO were important in tolerance induction by these DCs was not assessed. Importantly, to date, there has only been a single study assessing the effects of SCFAs on human DCs, in which particularly butyrate was found to suppress LPS-induced maturation [13]. Yet, whether or how SCFAs can condition human DCs to prime Tregs remains to be addressed. Given these inconsistencies in murine literature and the paucity in our understanding of how SCFAs affect the functional properties of human DCs, we here set out to assess whether and through which molecular mechanisms SCFAs affect T-cell polarization by human DCs. We find that butyrate through a combination of signaling via GPR109A and HDAC inhibition drives retinaldehyde dehydrogenase 1 (RALDH1) expression in human DCs which licenses them to prime type 1 regulatory T cells (Tr1). This provides important new insights into the cellular and molecular mechanisms through which SCFAs can exert their immunomodulatory effects in humans.

Results

Butyrate suppresses LPS-induced activation and metabolic reprogramming in human DCs

Tolerogenic compounds are often able to interfere with DC activation induced by pro-inflammatory signals. Therefore, we examined how acetate, propionate and butyrate influenced several markers of activation of human moDCs during co-stimulation with LPS, a toll-like receptor-4 ligand. Initial dose response experiments revealed that stimulation of moDCs with 2 mM SCFAs had the strongest biological effects (Figure S1A in Supplementary Material) without becoming toxic (Figure S1B in Supplementary Material). This, together with the fact that several other studies, in which the effects of SCFAs on immune cells were investigated, used a similar concentration [19, 24-26], we decided to use SCFAs at 2 mM in these and further experiments. Treatment with butyrate, and to a lesser extent with acetate and propionate, antagonized the LPS-induced upregulation of costimulatory markers CD83, CD80, and CD40 (Figure 1A). In line with this, all SCFAs lowered production of both IL-10 and IL-12 induced by LPS, with the strongest suppression induced by butyrate (Figure 1B). Given the importance of metabolic rewiring for DC activation [27] and the fact that SCFAs can act as direct substrates for several core metabolic pathways in the intestinal epithelium [23], we also analyzed the effects of SCFAs on DC metabolism. As previously reported [28], LPS stimulation enhanced the ECAR, a measure of glycolysis, of human DCs. Interestingly, while acetate and propionate showed a trend to suppress LPS-induced ECAR, we found that only butyrate significantly antagonized this response (Figure 1C). Moreover, we found that butyrate significantly reduced baseline mitochondrial OCR (Figure 1D) as well as the spare respiratory capacity of LPS-stimulated DCs (Figure 1D), together suggesting that butyrate reduces the overall metabolic activity of DCs. These findings indicate that propionate and more strongly butyrate, have the capacity to suppress LPS-induced DC activation and that butyrate additionally renders DCs metabolically less active.

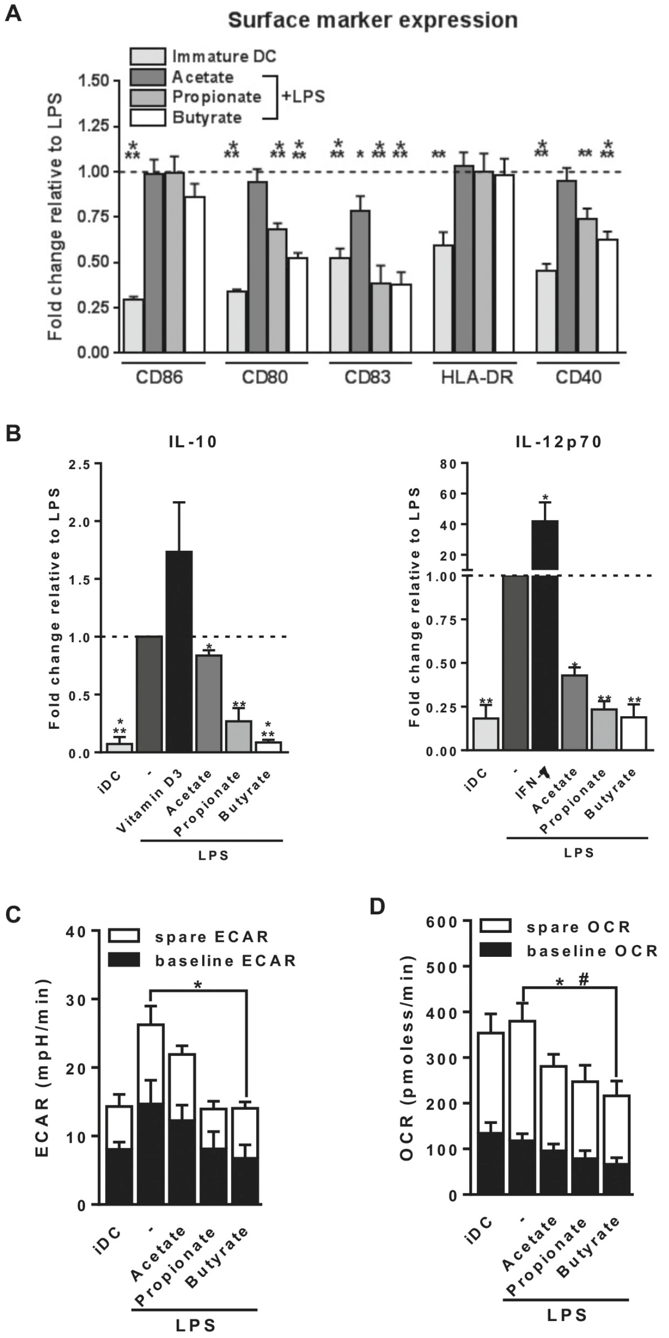
A
Surface marker expression
Immature DC
Acetate
Propionate
Butyrate
+LPS
Fold change relative to LPS
1.50
1.25
1.00
0.75
0.50
0.25
0.00
CD86
CD80
CD83
HLA-DR
CD40
B
IL-10
Fold change relative to LPS
2.5
2.0
1.5
1.0
0.5
0.0
iDC
-
Vitamin D3
Acetate
Propionate
Butyrate
LPS
IL-12p70
80
60
40
20
1.00
0.75
0.50
0.25
0.00
iDC
-
IFN-γ
Acetate
Propionate
Butyrate
LPS
C
spare ECAR
baseline ECAR
ECAR (mpH/min)
40
30
20
10
0
iDC
-
Acetate
Propionate
Butyrate
LPS
D
spare OCR
baseline OCR
OCR (pmoless/min)
600
500
400
300
200
100
0
*
#
iDC
-
Acetate
Propionate
Butyrate
LPS

FIGURE 1. Butyrate suppresses LPS-induced activation and metabolic changes in human dendritic cells (DCs).

(A,B) Monocyte-derived DCs were left untreated (iDC) or stimulated as indicated for 48 h after which (A) expression of maturation markers was analyzed by flow cytometry and (B) supernatants were collected and concentrations of indicated cytokines were determined by ELISA. (A) The expression levels of maturation markers are based on the geometric mean fluorescence and are shown relative to DCs stimulated with LPS, which was set to 1 for each marker (dashed line). (B) Vitamin D3 and IFN-γ-stimulated DCs were taken along as IL-10- and IL-12-inducing controls, respectively. (C,D) Metabolic phenotype of differently stimulated DCs was assed using a Seahorse extracellular flux analyzer. (C) Baseline and spare extracellular acidification rate (ECAR) were determined as described in Section "Materials and Methods," with significant differences in baseline ECAR indicated with *. (D) Baseline and spare mitochondrial oxygen consumption rate (OCR) were determined as described in Section "Materials and Methods," with significant differences in baseline or spare OCR indicated with * and #, respectively. (A-D) Bar graphs represent means ± SEM of at least five experiments. *,#p < 0.05, **p < 0.01, ***p < 0.001 based on paired Student's t-test.

Butyrate conditions human DCs to induce Tr1 cells

We next set out to address how these phenotypic and metabolic changes induced by SCFAs on DCs would translate into their ability to prime T helper (Th) cell responses. To assess this, we cocultured the SCFAs-pulsed DCs with naive CD4$^+$ T cells and measured the intracellular cytokine production by the T cells. We found that all three SCFAs did not condition DCs to drive Th1 or Th2 responses, since neither IFN-γ nor IL-4 production was altered (Figure 2A). Instead, we found that butyrate-stimulated DCs significantly promoted IL-10 production by T cells after restimulation with either PMA and ionomycin (Figure 2B) or anti-CD3/CD28 (Figure 2C) in a dose-dependent manner (Figure S2 in Supplementary Material). Because IL-10 is a well-known immunosuppressive cytokine released by Tregs, we next examined whether these IL-10-producing T cells were bona-fide Tregs, by determining their capacity to suppress the proliferation of other T cells. T cells that had been primed by butyrate-conditioned DCs strongly suppressed proliferation of target T cells. Propionate had a similar effect, although to a lesser extent (Figure 2D). To further characterize the phenotype of Tregs primed by butyrate-treated DCs, protein expression of three common Treg markers were measured, namely, glucocorticoid-induced TNF receptor (GITR), cytotoxic T-lymphocyte-associated protein 4 (CTLA4), and forkhead box P3 (FOXP3) [1, 29]. In contrast to Tregs that were primed by DCs rendered tolerogenic by vitamin D3, Tregs induced by butyrate-stimulated DCs did not display increased expression of these markers (Figure 2E). This phenotype of a Treg with high IL-10 production but low FOXP3 expression is typical for Tr1 cells, which are defined by their dependency on IL-10 production to suppress bystander T cell proliferation [29]. Indeed, when IL-10 (Figure 2F), but not transforming growth factor beta-1

(TGF-β1) (Figure S3 in Supplementary Material), was neutralized in the T cell suppressor assay, the suppressive capacity of these Tregs was significantly reduced. Together, these data demonstrate that butyrate conditions human DCs to prime IL-10-secreting Tr1 cells.

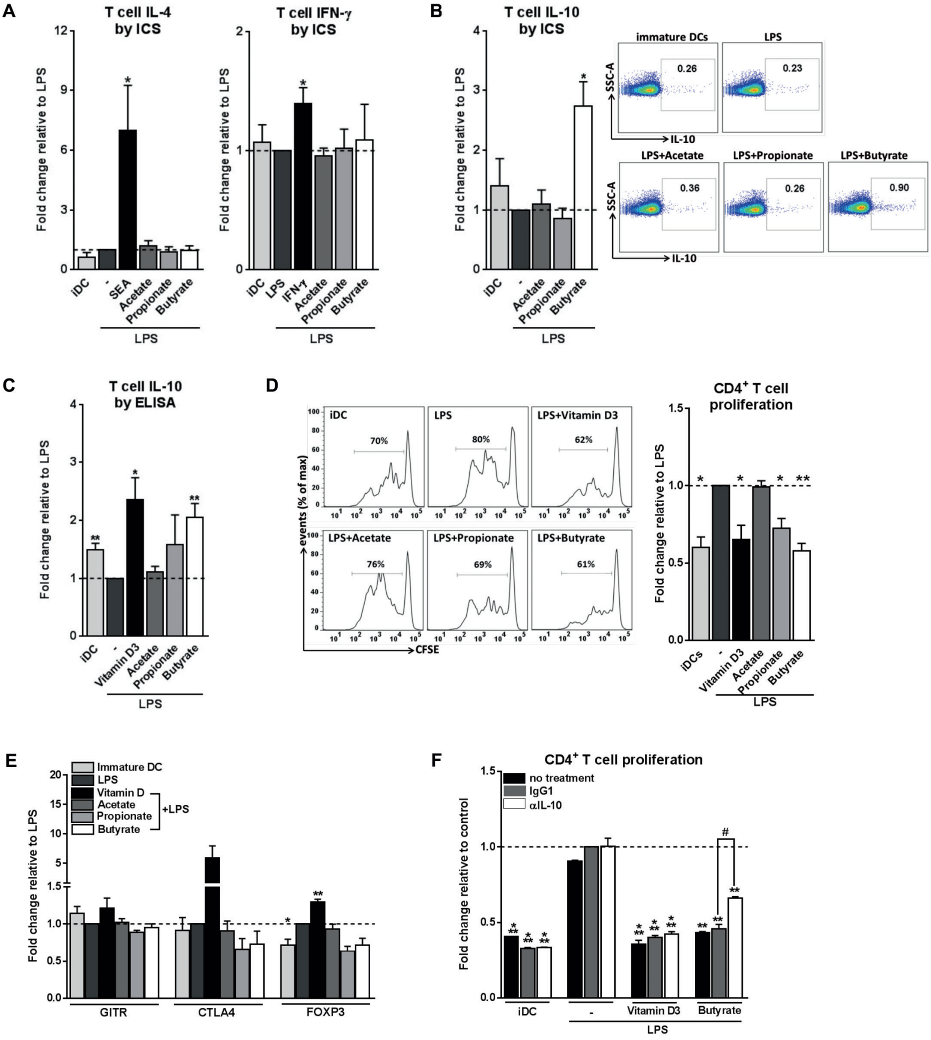

FIGURE 2. Butyrate conditions human dendritic cells (DCs) to induce type 1 regulatory T cells.

(A–C) Differently stimulated DCs were cocultured with allogenic naive CD4$^+$ T cells. After 11 days, cytokine production by T cells was analyzed (A,B) by intracellular cytokine staining by flow cytometry after 6 h of stimulation with PMA and ionomycin or (C) by ELISA after 24 h restimulation with anti-CD3/CD28. (A–C) Data represent fold change in panels (A,B) percentage of T cells that stain positive for indicated cytokines or in panel (C) IL-10 levels in culture supernatants, relative to data from LPS-stimulated DCs which was set to 1 for each cytokine (dashed line). (B) Representative flow cytometry plots are shown on the right. (D) T-cell suppression assay in which irradiated test T cells were cocultured with activated CFSE-labeled responder CD4$^+$ T cells. On day 6, CFSE dilution of the responder T cells was assessed by flow cytometry. The left panels are representative histograms of CFSE dilution by responder T cells. Quantification of these data is shown in the bar graph and is depicted as fold change relative to data from LPS-stimulated DCs, which was set to 1 (dashed line). (E) Expression of regulatory markers by T cells was analyzed by flow cytometry. Bar graphs represent relative differences based on geometric mean fluorescence for glucocorticoid induced TNF receptor (GITR) and cytotoxic T-lymphocyte-associated protein 4 (CTLA4) or frequency of T cells that express forkhead box P3 (FOXP3). (F) For the duration of the assay as described in panel (D) indicated antibodies were added. Data are from one experiment representative of two, shown as means ± SEM of triplicates. (A-E) Bar graphs represent means ± SEM of at least three experiments. *,#$p < 0.05$, **$p < 0.01$, ***$p < 0.001$ for significant differences with the control (*) or between test conditions (#) based on paired Student's t-test.

Tr1 cell induction by butyrate-conditioned DCs Depends on RALDH1 expression

We next aimed to determine through which mechanism(s) butyrate-conditioned DCs prime Tr1 cells. To address this, we analyzed gene expression of several immune-regulatory factors that are known to be expressed by tolerogenic DCs and have been shown to be induced by SCFAs in immune cells, namely, *IL-10*, *IDO1*, *TGFB1*, and *RALDH1* and *RALDH2* (also known as aldehyde dehydrogenase 1 family member A1 and A2, respectively) [30] (Figure 3A). We found that *TGFB1* mRNA was upregulated by both butyrate and propionate, while *RALDH1* was selectively induced by butyrate. This prompted us to further study the role of TGF-β and RALDH1 in Tr1 cell induction by butyrate-conditioned DCs. To this end, we quantified LAP expression, which is a protein derived from the N-terminal region of the *TGFB1* gene product and binds TGF-β on the cell surface to keep it in its inactive form. In line, with the mRNA expression data, we found that the level of LAP protein expression was significantly increased by both propionate- and butyrate-stimulated DCs (Figure 3B; Figure S4A in Supplementary Material). However, while blocking of TGF-β signaling using the SMAD2/3 inhibitor ALK5 did reverse Treg induction by exogenously added TGF-β, it did not affect the Tr1-priming capacity of butyrate-conditioned DCs (Figure 3C). This suggests that butyrate does not license DCs to prime Tr1 cells through induction of TGF-β.

We next assessed the role of RALDH1. RALDH1 converts vitamin A into retinoic acid, which through the activation of retinoic acid receptor has been shown to induce tolerogenic properties in DCs as well as to directly drive Treg differentiation of T cells [31]. We found that in line with the increased mRNA expression of *RALDH1*, DCs stimulated with butyrate, but not with acetate or propionate, increased the enzymatic activity of RALDH in a time-dependent manner both in the presence (Figure 3D) and absence of LPS (Figures S4B,C in Supplementary Material). To test the role of RALDH activity in Tr1 cell induction by butyrate-treated DCs, we used DEAB, a reversible inhibitor of RALDH [32] during the DC–T cell coculture. This treatment abolished IL-10 production and reduced the suppressive capacity of the T cells (Figures 3E,F), indicating that RALDH activity is a key factor expressed by DCs to promote Tr1 cells and that DC-derived RA acts on T cells to prime their regulatory properties. In addition, we wondered whether RA produced by DCs may also act in an autocrine fashion to enforce their tolerogenic potential. Blocking RA generation by DCs from the beginning of the stimulation with butyrate blunted the ability of butyrate to increase RALDH activity in these cells (Figure 3G) and, as a consequence, in the inability of these cells to promote Tr1 cells (Figures 3H,I). Together, these findings suggest that initial butyrate-driven RALDH activity by means of production of RA is required to maintain its own expression, which licenses these DCs to subsequently prime Tr1 cells.

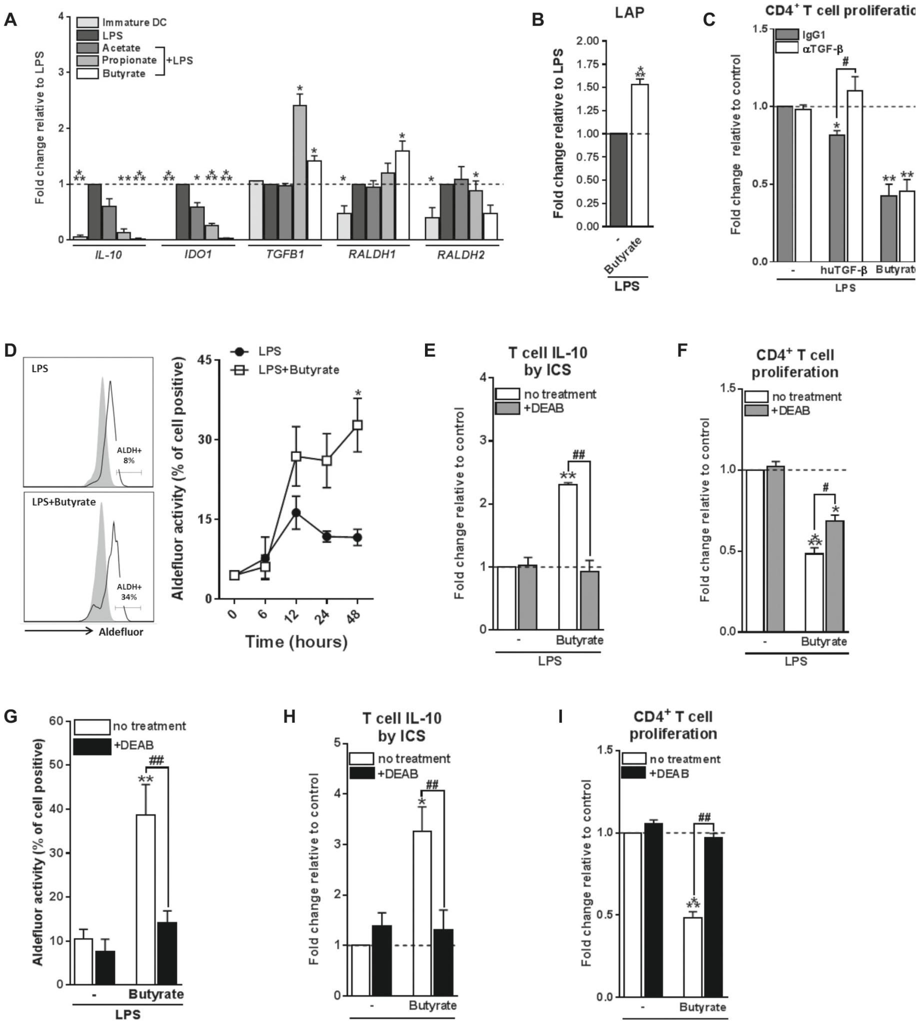

FIGURE 3. Type 1 regulatory T cell induction by butyrate-conditioned human dendritic cells (DCs) depends on retinaldehyde dehydrogenase 1 (RALDH1) expression.

(A) mRNA expression of indicated genes was quantified using real-time qPCR of monocyte-derived DCs stimulated for 16 h. (B) Relative membrane bound latency-associated peptide (LAP) expression on DCs stimulated with indicated reagents as determined by flow cytometry. (C) T-cell suppression assay as described in Figures 2D, (F) blocking antibody of human TGF-β was added during the co-culture of DCs with T cells. Human TGF-β was taken along as positive control. (D) Retinaldehyde dehydrogenase (RALDH) activity in DCs was assessed using an Aldefluor assay with a readout by flow cytometry. Representative histograms of RALDH activity 48 h after stimulation are shown on the left, with gray shaded histograms and black lines representing DCs in which RALDH activity was assessed in the presence or absence of reversible RALDH inhibitor diethylaminobenzaldehyde (DEAB), respectively. Right graph:

RALDH activity was measured at different times after stimulation and frequencies of DCs positive for RALDH activity are depicted. *$p < 0.005$ based on two-way ANOVA test. (E) IL-10 production by T cells as described in Figure 2B or (F) T-cell suppression assay as described in Figure 2D, but with the addition that DEAB or vehicle control was added during the DC–T cell coculture. (G) RALDH activity assay as described in Figure 3D, but during stimulation DEAB or vehicle control were added. (H,I) Same as (E,F), but now DEAB was added during stimulation of DCs with LPS ± butyrate. (A-I) Bar graphs represent means ± SEM of at least three experiments and (A-C,F,G,I) are shown as fold change relative to control conditions. *,#$p < 0.05$, **,##$p < 0.01$, ***$p < 0.001$ for significant differences with the control (*) or between test conditions (#) based on paired Student's t-test.

HDAC inhibition by butyrate is not sufficient for inducing tolDCs

We next set out to investigate the mechanisms through which butyrate drives RALDH1 expression in human DCs. Two mechanisms have been described in other immune cells, namely, HDAC inhibition and GPR signaling [5, 10, 12, 33, 34]. To first establish whether butyrate could affect HDAC activity in human DCs, we performed an HDAC activity assay on differently stimulated moDCs. As expected, TSA, a well-known HDAC inhibitor with broad specificity [20, 33], was effective in inhibiting HDAC activity in DCs (Figure 4A). Butyrate, and to a lesser extent propionate, also displayed the capacity to inhibit HDAC activity in human DCs. Importantly, this finding was corroborated by the observation that histone 4 acetylation was increased in DCs exposed to butyrate (Figure 4B). We did not see major changes in histone 3 acetylation as determined by flow cytometry (Figure S5 in Supplementary Material). We hypothesized that if HDAC inhibition would be underlying the ability of butyrate to induce tolDCs, then TSA would be able to recapitulate the effects of butyrate. Indeed, TSA suppressed LPS-induced expression of several DC activation markers (Figure 4C). However, TSA treatment only marginally promoted RALDH activity in DCs (Figure 4D) and concordantly, failed to significantly induce IL-10-producing (Figure 4E) functional Tr1 cells (Figure 4F). These data indicate that while HDAC inhibition alone is sufficient to recapitulate some of the modulatory effects of butyrate (e.g., suppression of LPS-induced maturation marker expression), it is insufficient in inducing Tr1 cells by DCs.

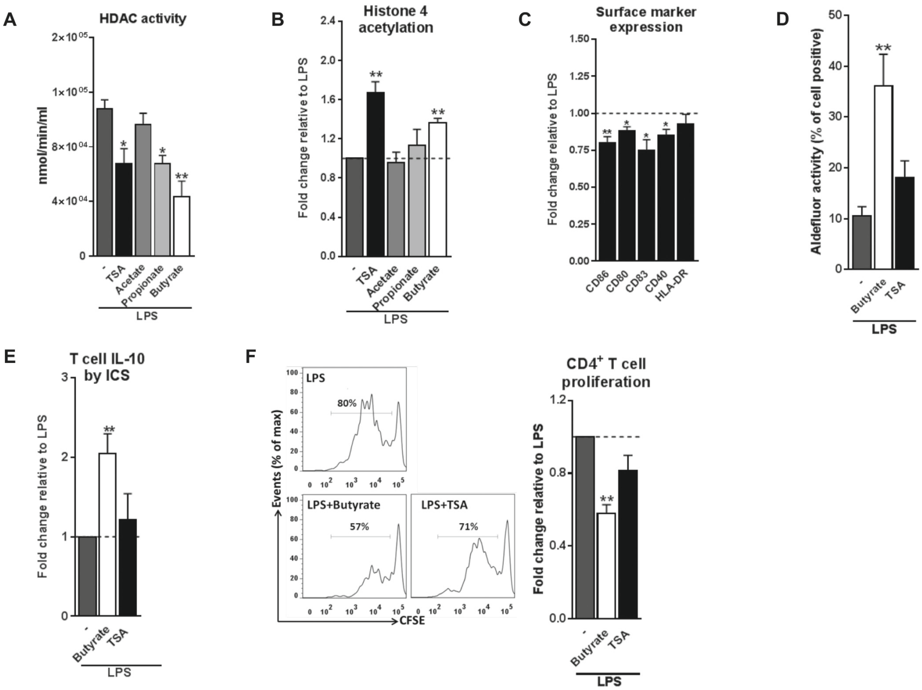

FIGURE 4. Histone deacetylases (HDAC) inhibition by butyrate is not sufficient for inducing type 1 regulatory T cells-promoting human tolDCs.

(A) Dendritic cells (DCs) were stimulated for 24 h with indicated reagents and then assayed for HDAC activity. (B) Analysis of histone 4 acetylation by flow cytometry of DCs stimulated with indicated reagents for 6 h. (C) The expression of maturation markers of DCs stimulated for 48 h with TSA was analyzed using flow cytometry. The expression of surface marker levels is based on the geometric mean fluorescence. (D) Retinaldehyde dehydrogenase activity assay as described in Figure 3D. (E) IL-10 production by T cells as described in Figure 2B. (F) T-cell suppression assay as described in Figure 2D. (A-F) Bar graphs represent means ± SEM of at least three experiments and (B,C,E,F) are shown as fold change relative to control conditions. *p < 0.05, **p < 0.01, ***p < 0.001 based on paired Student's t-test.

Signaling through GPR109A by butyrate is required but not sufficient for inducing Tr1 cell-promoting tolDCs

The inability of HDAC inhibition to induce Tr1 cell-priming tolDCs, led us to assess the role of GPRs in this process. The major GPRs activated by SCFAs are GPR41, GPR43, and GPR109A [4, 10, 11]. Acetate and propionate are the most potent activators of GPR41 and GPR43, while butyrate more effectively binds to GPR109A [4, 9]. Consistent with a recent report [13], we found that GPR109A but not GPR41 or GPR43 are expressed by moDCs (Figure 5A). To investigate the role of GPR109A in mediating the modulatory effects of butyrate on human DCs, *GPR109A* was silenced using siRNA, resulting in >85% silencing at the mRNA level (Figure 5B) and a corresponding loss of the ability of niacin, a natural ligand of GPR109A, to suppress LPS-induced TNF-α production [14] (Figure S6A in Supplementary Material). Silencing of *GPR109A* did not interfere with the capacity of butyrate to modulate LPS-induced DC maturation (Figure S6B in Supplementary Material). Importantly, however, we found that butyrate failed to induce RALDH activity in DCs in which *GPR109A* was silenced (Figure 5C). As a result, these DCs largely lost the ability to promote IL-10 production by T cells (Figure 5D) and functional Tr1 cells (Figure 5E). Interestingly, however, stimulation with niacin was not sufficient to promote RALDH activity in DCs nor did it enhance their ability to induce Tr1 cells. This suggests that GPR109A signaling is required yet not sufficient for human tolDC induction by butyrate.

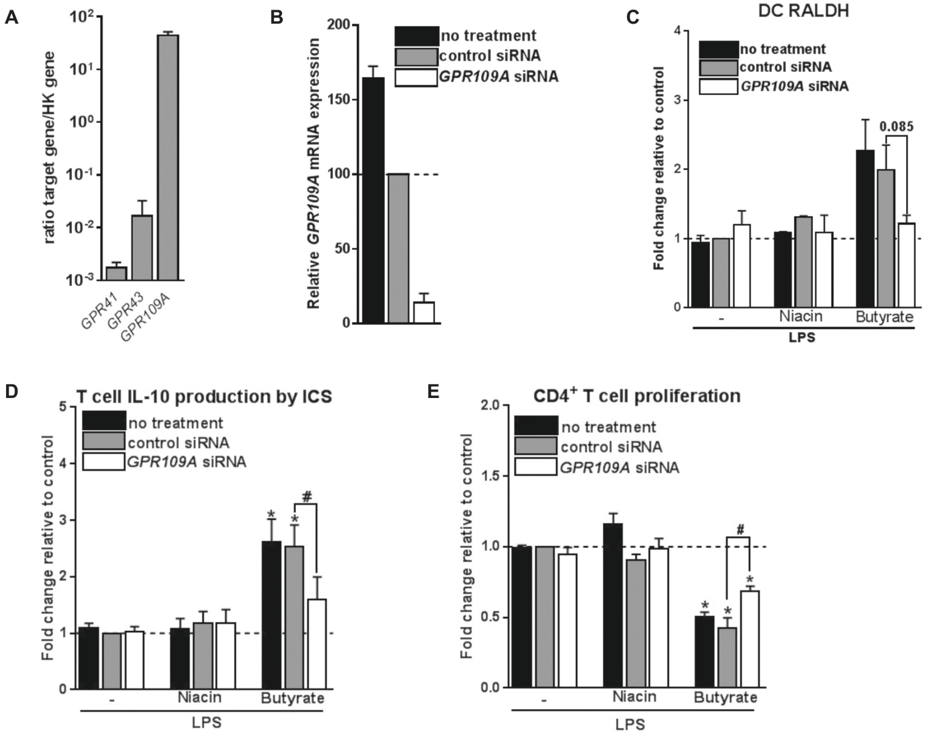

FIGURE 5. Signaling through G protein-coupled receptor (GPR) 109A by butyrate is required yet not sufficient for inducing type 1 regulatory T cells-promoting human tolDCs.

(A) mRNA expression of indicated genes was quantified using real-time qPCR of unstimulated dendritic cells (DCs). Expression is shown relative to housekeeping gene beta-actin. (B–E) *GPR109A* expression was silenced by small interfering RNA (siRNA) on day 4 of DC differentiation after which (B) silencing efficacy was determined by real-time qPCR on day 6. (C) Retinaldehyde dehydrogenase (RALDH) activity induced by butyrate and GPR109A ligand niacin was assessed as described in Figure 3D. (D) IL-10 production by T cells as described in Figure 2B was determined, and (E) T-cell suppression assay was performed as described in Figure 2D. (A) Bar graphs represent means ± SEM of at least three experiments and (B-E) are shown as fold change relative to control conditions. *,#$p < 0.05$, **$p < 0.01$, ***$p < 0.001$ for significant differences with the control (*) or between test conditions (#) based on paired Student's t-test.

Butyrate depends on the combination of HDAC inhibition and GPR109A signaling to prime Tr1 cell-inducing tolDCs

Given that butyrate inhibited HDAC activity in human DCs and that it depends on GPR109A signaling to promote tolDCs, but that neither stimulation of GPR109A signaling nor HDAC inhibition alone was sufficient for induction of tolDCs, we evaluated whether butyrate requires both HDAC inhibition and GPR109A activation for its optimal modulatory effect. To test this, we co-incubated human DCs with both HDAC inhibitor TSA and GPR109A ligand niacin. Strikingly, in contrast to the single treatments, the combinatorial treatment synergistically induced RALDH activity to a level similar to what was induced by butyrate (Figure 6A). Consistent with these findings, T cells that were primed by DCs that had been treated with the combination of TSA and niacin, displayed a stronger suppressive capacity compared to the single treatment conditions (Figure 6B). Finally, to get a better understanding of how HDAC inhibition in conjunction with GPR109A signaling would result in RALDH expression we performed an ATAC-seq analysis on the promoter region of RALDH1 to assess the level of chromatin accessibility following stimulation with butyrate, TSA, niacin or TSA in combination with niacin. We found that TSA treatment, relative to unstimulated cells, resulted in a stronger ATAC-seq signal in the promoter region of RALDH1, which was comparable to the profile induced by butyrate (Figure 6C). By contrast, niacin treatment alone did not lead to opening of the chromatin in this locus, nor did it significantly alter the ATAC-seq profile induced by TSA. These findings point to two distinct roles of HDAC inhibition and GPR109A signaling in driving RALDH1 expression. Together with the observation that only the combined treatment with TSA and niacin significantly induced RALDH activity in DCs, this suggests that HDAC activity is needed for opening of the chromatin of the locus encoding RALDH1, while GPR109 signaling is required for initiation of transcription once the locus is accessible for transcription factors. Taken together, our data suggest that butyrate depends on both HDAC inhibition as well as GPR109A signaling to efficiently drive RALDH1 expression and to promote an anti-inflammatory phenotype in human DCs.

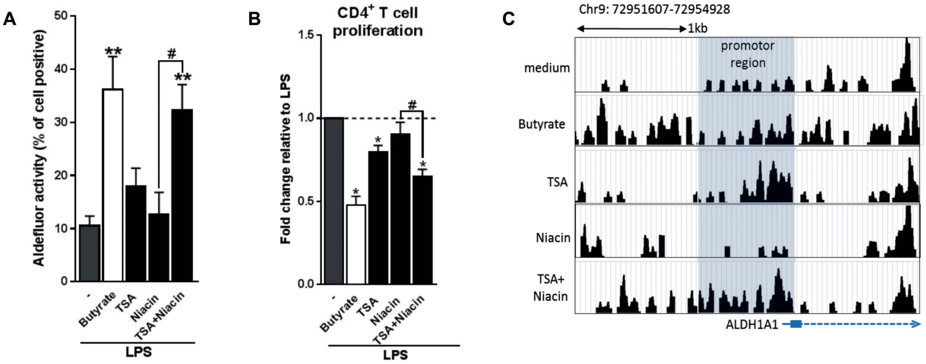

FIGURE 6. Butyrate depends on the combination of histone deacetylases inhibition and G protein-coupled receptor 109A signaling to prime type 1 regulatory T cell-inducing human tolDC.

(A) Retinaldehyde dehydrogenase (RALDH) activity assay as described in Figure 3D. (B) T-cell suppression assay as described in Figure 2D. (C) Assay for Transposase-Accessible Chromatin with high-throughput sequencing analysis of the promoter region (highlighted in gray) of RALDH1 gene locus 6 h after stimulation of dendritic cells (DCs) with indicated reagents. (A) Bar graphs represent means ± SEM of at least three experiments and (B) are shown as fold change relative to control conditions. (C) Data from one of three experiments are shown. *,#$p < 0.05$, **$p < 0.01$ for significant differences with the control (*) or between test condition (#) based on paired Student's t-test.

Discussion

Short-chain fatty acids produced by commensal bacteria, such as butyrate, have been well documented to promote anti-inflammatory responses through the modulation of various immune cells such as neutrophils, DCs, macrophages and T cells. This has been described to occur particularly in tissues that are in close contact with the lumen of the gut, where SCFAs concentrations are known to exceed 20 mM [35]. Since gut-associated DCs have been shown to probe for antigens in the lumen by extending dendrites into the intestinal lumen [36], particularly DCs are likely to be exposed to high concentrations of immunomodulatory SCFAs. However, the effects of SCFAs on human DC phenotype and function have not been studied in detail. Here we find that SCFAs, in particular butyrate, suppresses LPS-induced activation and licenses them to prime functional Tr1 cells. Mechanistically, we provide evidence that butyrate, through the concerted action of both GPR109A activation and HDAC inhibition, drives the induction of RALDH1 expression and activity in human

DCs. The resultant RA production on the one hand acts in autocrine manner to reinforce RALDH expression and maintain the tolerogenic properties of the DCs themselves, and on the other hand acts in a paracrine manner on T cells to differentiate them into regulatory IL-10-producing Tr1 cells (Figure 7).

FIGURE 7 **|** Proposed model of how butyrate conditions human dendritic cells (DCs) to prime type 1 regulatory T cells (Tr1). (1) Butyrate inhibits histone deacetylases (HDAC) activity in DCs to enhance net histone acetylation, resulting in opening of the gene locus of retinaldehyde dehydrogenase 1 (RALDH1) in human DCs. (2) The now open promoter region of RALDH1 enables butyrate through signaling via G protein-coupled receptor (GPR) 109A to promote transcription and expression of RALDH1. (3) This initial RALDH1 expression results in retinoic acid (RA) synthesis that further reinforces RALDH1 expression. Butyrate-induced RALDH1 expression endows human DCs with the capacity to prime IL-10-producing type 1 regulatory T cells.

Our observation that SCFAs, especially butyrate, downregulate LPS-induced expression of DC activation markers as well as cytokines released by DCs is consistent with earlier studies in murine DCs and more recently human DCs [13, 37, 38]. This effect is likely to be in part mediated by the ability of butyrate to interfere with LPS-induced translocation of NF-κB, which has been described in myeloid cells before [38, 39]. Here, we additionally find that this inhibitory effect of butyrate on LPS-driven changes in DC biology can be extended to cellular metabolism, by showing that butyrate lowers activity of core metabolic pathways, i.e., glycolysis and oxidative phosphorylation (OXPHOS), in human DCs. Since LPS-induced glycolysis, which occurs independently of NF-κB signaling is known to be crucial for DC activation [27], it is possible that one of the mechanisms through which butyrate interferes with LPS-driven DC activation is via modulation of DC metabolism. It remains to be determined how butyrate affects metabolism in DCs, but it is interesting to consider that SCFAs including butyrate can directly act as substrates for core metabolic pathways as has been well documented in intestinal epithelial cells [5, 10]. In addition, butyrate has been shown to affect hypoxia-induced factor, which is a transcription factor that among others is transcriptional regulator of glycolytic enzymes [23]. This low metabolic activity of butyrate-conditioned tolDCs appears to be different from what has been described for DCs that were rendered tolerogenic by vitamin D3, which were found to be metabolically characterized by increased glycolysis and OXPHOS [40, 41], suggesting that not all tolerogenic DCs share a common metabolic signature.

Several studies have demonstrated that SCFAs, in particular butyrate, are potent inducers of Tregs through the functional modulation of murine DCs [14, 24]. While butyrate was recently reported to suppress pro-inflammatory cytokine expression of human DCs, the consequence of this in terms of T-cell polarization or Treg induction remained unclear. We now show that butyrate-conditioned human DCs promote the *de novo* induction of Tregs from naive T cells. Specifically, we found that butyrate-exposed DCs prime IL-10 secreting Tr1 cells. However, it should be noted that IL-10 neutralization did no completely block their suppressive effect in our model, suggesting that additional mechanisms are involved. Our findings are in line with study of Jeon et al. who found that murine colonic DCs, when exposed to butyrate, also promote Tr1 cells differentiation [42]. Given that butyrate can also directly act on T cells to favor differentiation of Foxp3$^+$ Tregs [24], it is likely that Tregs induced by butyrate *in vivo* through both DC-dependent and independent pathways are comprised of different subsets that mediate their immune-regulatory effects through a number of different mechanisms.

Mechanistically, our data reveal that specifically induction of *RALDH1* expression and activity is the key mechanism through which butyrate-conditioned human DCs prime Tr1 cells. RALDH enzymes are necessary for RA production by DCs from retinol (vitamin A) [43]. The role of DC-derived RA in promoting Tregs responses has been well documented, especially in the gut in both mouse [44] and human DC models [31]. However, the link between butyrate and the induction of RALDH1 expression in DCs has only been recently made. In this respect, our observation is in line with a recent study showing that the expression of *RALDH1* gene is induced by butyrate in human moDCs [13]. However, its role in T-cell priming was not assessed. In addition, consistent with our *in vitro* findings with human DCs, high dietary fiber intake and butyrate synthesis have been linked to increased activity of RALDH in murine intestinal CD103$^+$ DCs, which was found to be important for protection against colitis [14] and food allergy [45]. A striking observation was that blocking of the enzymatic activity of RALDH in DCs during exposure to butyrate resulted in loss of butyrate-induced RALDH activity and Tr1-inducing ability, suggesting that RALDH-derived RA acts in an autocrine loop on DCs to reinforce their own RALDH activity required to maintain their tolerogenic potential. We additionally found that inhibition of RALDH activity during DC–T cell co-culture also reduced their Treg priming ability, implying that RALDH-derived RA subsequently acts as a key signal from DCs to differentiate naive T cells into Tregs. Independent support for this model comes from a recent study showing that treatment of moDCs with RA itself is indeed sufficient to induce RALDH expression and to endow these cells with the capacity to induce IL-10-producing Tregs in an RA-dependent manner [31].

Two of the most well-studied mechanisms through which butyrate has been shown to modulate immune cell function are inhibition of HDAC activity and signaling through GPRs [4, 5, 9, 11, 18]. Our data suggest that butyrate depends on both mechanisms together to efficiently induce RALDH expression and promote functional tolDCs. This is based on the following observations: (1) silencing of *GPR109A*, resulted in the inability of butyrate to drive RALDH activity in DCs and to license them to induce Tr1 cells; (2) yet signaling through this receptor induced by a GPR109A ligand, niacin, could not recapitulate the tolerogenic effects of butyrate; (3) likewise, TSA, a general HDAC inhibitor, failed to do so as well; and (4) only simultaneous treatment of DCs with niacin and TSA could functionally mimic the effects of butyrate. Other studies, using murine models, have either highlighted a role for signaling via GPR109A or a role for inhibition of HDAC activity in the ability of butyrate to promote tolDCs [14, 24]. However, to the best of our knowledge, we now for the first time show that both modes of action are equally important and act in concert to drive RALDH expression and a tolerogenic phenotype in human DCs. These findings, together with the ATAC-seq data, lead us to speculate that inhibition of HDAC activity drives the opening of the chromatin encoding RALDH1, while concurrent signaling via GPR109A promotes the activation of transcription factors that then can efficiently access the promoter region of this gene to drive transcription of RALDH1. The model of how we propose this epigenetic change precedes and underpins the phenotypic change in DCs is shown in Figure 7. Further studies are warranted to identify which transcription factors downstream of GPR109A would mediate *RALDH1* expression. In summary, we found that human DCs treated with butyrate acquire a tolerogenic phenotype, which is dependent on RALDH activity driven by the combined action of HDAC inhibition and GPR109A signaling. Our findings provide key new mechanistic insights into the immunomodulatory effects of SCFAs on human cells and highlight the importance of a well-balanced composition of our gut microbiota with sufficient SCFA-generating genera to ensure maintenance of an immune tolerant state. In addition, in line with the well documented therapeutic potential of SCFAs for a wide range of diseases [2, 4, 8-10], our work could spur the design of targetable drugs that exploit the synergetic effect of GPR109 signaling and HDAC activity in DCs to favor tolerogenic responses to treat inflammatory disorders.

References

1. Lutz, M.B., *Induction of CD4(+) Regulatory and Polarized Effector/helper T Cells by Dendritic Cells*. Immune Netw, 2016. **16**(1): p. 13-25.
2. Minarrieta, L., et al., *Metabolites: deciphering the molecular language between DCs and their environment*. Semin Immunopathol, 2017. **39**(2): p. 177-198.
3. Yoo, S. and S.J. Ha, *Generation of Tolerogenic Dendritic Cells and Their Therapeutic Applications*. Immune Netw, 2016. **16**(1): p. 52-60.
4. Tan, J., et al., *The role of short-chain fatty acids in health and disease*. Adv Immunol, 2014. **121**: p. 91-119.
5. den Besten, G., et al., *The role of short-chain fatty acids in the interplay between diet, gut microbiota, and host energy metabolism*. J Lipid Res, 2013. **54**(9): p. 2325-40.
6. Murase, M., Y. Kimura, and Y. Nagata, *Determination of portal short-chain fatty acids in rats fed various dietary fibers by capillary gas chromatography*. J Chromatogr B Biomed Appl, 1995. **664**(2): p. 415-20.
7. Topping, D.L. and P.M. Clifton, *Short-chain fatty acids and human colonic function: roles of resistant starch and nonstarch polysaccharides*. Physiol Rev, 2001. **81**(3): p. 1031-64.
8. Kamada, N., et al., *Role of the gut microbiota in immunity and inflammatory disease*. Nat Rev Immunol, 2013. **13**(5): p. 321-35.
9. Koh, A., et al., *From Dietary Fiber to Host Physiology: Short-Chain Fatty Acids as Key Bacterial Metabolites*. Cell, 2016. **165**(6): p. 1332-1345.
10. Corrêa-Oliveira, R., et al., *Regulation of immune cell function by short-chain fatty acids*. Clin Transl Immunology, 2016. **5**(4): p. e73.
11. Thorburn, A.N., L. Macia, and C.R. Mackay, *Diet, metabolites, and "western-lifestyle" inflammatory diseases*. Immunity, 2014. **40**(6): p. 833-42.
12. Trompette, A., et al., *Gut microbiota metabolism of dietary fiber influences allergic airway disease and hematopoiesis*. Nat Med, 2014. **20**(2): p. 159-66.
13. Nastasi, C., et al., *The effect of short-chain fatty acids on human monocyte-derived dendritic cells*. Sci Rep, 2015. **5**: p. 16148.
14. Singh, N., et al., *Activation of Gpr109a, receptor for niacin and the commensal metabolite butyrate, suppresses colonic inflammation and carcinogenesis*. Immunity, 2014. **40**(1): p. 128-39.
15. Donohoe, D.R., et al., *The Warburg effect dictates the mechanism of butyrate-mediated histone acetylation and cell proliferation*. Mol Cell, 2012. **48**(4): p. 612-26.
16. Gurav, A., et al., *Slc5a8, a Na+-coupled high-affinity transporter for short-chain fatty acids, is a conditional tumour suppressor in colon that protects against colitis and colon cancer under low-fibre dietary conditions*. Biochem J, 2015. **469**(2): p. 267-78.
17. Miyauchi, S., et al., *Functional identification of SLC5A8, a tumor suppressor down-regulated in colon cancer, as a Na(+)-coupled transporter for short-chain fatty acids*. J Biol Chem, 2004. **279**(14): p. 13293-6.
18. Rooks, M.G. and W.S. Garrett, *Gut microbiota, metabolites and host immunity*. Nat Rev Immunol, 2016. **16**(6): p. 341-52.

19. Chang, P.V., et al., *The microbial metabolite butyrate regulates intestinal macrophage function via histone deacetylase inhibition.* Proc Natl Acad Sci U S A, 2014. **111**(6): p. 2247-52.
20. Frikeche, J., et al., *Impact of HDAC inhibitors on dendritic cell functions.* Exp Hematol, 2012. **40**(10): p. 783-91.
21. Singh, N., et al., *Blockade of dendritic cell development by bacterial fermentation products butyrate and propionate through a transporter (Slc5a8)-dependent inhibition of histone deacetylases.* J Biol Chem, 2010. **285**(36): p. 27601-8.
22. Tao, R., et al., *Deacetylase inhibition promotes the generation and function of regulatory T cells.* Nat Med, 2007. **13**(11): p. 1299-307.
23. Kelly, C.J., et al., *Crosstalk between Microbiota-Derived Short-Chain Fatty Acids and Intestinal Epithelial HIF Augments Tissue Barrier Function.* Cell Host Microbe, 2015. **17**(5): p. 662-71.
24. Arpaia, N., et al., *Metabolites produced by commensal bacteria promote peripheral regulatory T-cell generation.* Nature, 2013. **504**(7480): p. 451-5.
25. Segain, J.P., et al., *Butyrate inhibits inflammatory responses through NFkappaB inhibition: implications for Crohn's disease.* Gut, 2000. **47**(3): p. 397-403.
26. Weber, T.E. and B.J. Kerr, *Butyrate differentially regulates cytokines and proliferation in porcine peripheral blood mononuclear cells.* Vet Immunol Immunopathol, 2006. **113**(1-2): p. 139-47.
27. Everts, B. and E.J. Pearce, *Metabolic control of dendritic cell activation and function: recent advances and clinical implications.* Front Immunol, 2014. **5**: p. 203.
28. Everts, B., et al., *Commitment to glycolysis sustains survival of NO-producing inflammatory dendritic cells.* Blood, 2012. **120**(7): p. 1422-31.
29. Hoeppli, R.E., et al., *The environment of regulatory T cell biology: cytokines, metabolites, and the microbiome.* Front Immunol, 2015. **6**: p. 61.
30. Li, H. and B. Shi, *Tolerogenic dendritic cells and their applications in transplantation.* Cell Mol Immunol, 2015. **12**(1): p. 24-30.
31. Bakdash, G., et al., *Retinoic acid primes human dendritic cells to induce gut-homing, IL-10-producing regulatory T cells.* Mucosal Immunol, 2015. **8**(2): p. 265-78.
32. Koppaka, V., et al., *Aldehyde dehydrogenase inhibitors: a comprehensive review of the pharmacology, mechanism of action, substrate specificity, and clinical application.* Pharmacol Rev, 2012. **64**(3): p. 520-39.
33. Park, J., et al., *Short-chain fatty acids induce both effector and regulatory T cells by suppression of histone deacetylases and regulation of the mTOR-S6K pathway.* Mucosal Immunol, 2015. **8**(1): p. 80-93.
34. Vinolo, M.A., et al., *Suppressive effect of short-chain fatty acids on production of proinflammatory mediators by neutrophils.* J Nutr Biochem, 2011. **22**(9): p. 849-55.
35. Cummings, J.H., et al., *Short chain fatty acids in human large intestine, portal, hepatic and venous blood.* Gut, 1987. **28**(10): p. 1221-7.
36. Niess, J.H., et al., *CX3CR1-mediated dendritic cell access to the intestinal lumen and bacterial clearance.* Science, 2005. **307**(5707): p. 254-8.
37. Berndt, B.E., et al., *Butyrate increases IL-23 production by stimulated dendritic cells.* Am J Physiol Gastrointest Liver Physiol, 2012. **303**(12): p. G1384-92.
38. Säemann, M.D., et al., *Bacterial metabolite interference with maturation of human monocyte-derived dendritic cells.* J Leukoc Biol, 2002. **71**(2): p. 238-46.

39. Maa, M.C., et al., *Butyrate reduced lipopolysaccharide-mediated macrophage migration by suppression of Src enhancement and focal adhesion kinase activity.* J Nutr Biochem, 2010. **21**(12): p. 1186-92.
40. Ferreira, G.B., et al., *Vitamin D3 Induces Tolerance in Human Dendritic Cells by Activation of Intracellular Metabolic Pathways.* Cell Rep, 2015. **10**(5): p. 711-725.
41. Malinarich, F., et al., *High mitochondrial respiration and glycolytic capacity represent a metabolic phenotype of human tolerogenic dendritic cells.* J Immunol, 2015. **194**(11): p. 5174-86.
42. Jeon, S.G., et al., *Probiotic Bifidobacterium breve induces IL-10-producing Tr1 cells in the colon.* PLoS Pathog, 2012. **8**(5): p. e1002714.
43. Schilderink, R., et al., *The SCFA butyrate stimulates the epithelial production of retinoic acid via inhibition of epithelial HDAC.* Am J Physiol Gastrointest Liver Physiol, 2016. **310**(11): p. G1138-46.
44. Vitali, C., et al., *Migratory, and not lymphoid-resident, dendritic cells maintain peripheral self-tolerance and prevent autoimmunity via induction of iTreg cells.* Blood, 2012. **120**(6): p. 1237-45.
45. Tan, J., et al., *Dietary Fiber and Bacterial SCFA Enhance Oral Tolerance and Protect against Food Allergy through Diverse Cellular Pathways.* Cell Rep, 2016. **15**(12): p. 2809-24.
46. Hussaarts, L., et al., *Rapamycin and omega-1: mTOR-dependent and -independent Th2 skewing by human dendritic cells.* Immunol Cell Biol, 2013. **91**(7): p. 486-9.
47. Sallusto, F. and A. Lanzavecchia, *Efficient presentation of soluble antigen by cultured human dendritic cells is maintained by granulocyte/macrophage colony-stimulating factor plus interleukin 4 and downregulated by tumor necrosis factor alpha.* J Exp Med, 1994. **179**(4): p. 1109-18.
48. Everts, B., et al., *Omega-1, a glycoprotein secreted by Schistosoma mansoni eggs, drives Th2 responses.* J Exp Med, 2009. **206**(8): p. 1673-80.
49. Rigby, L., et al., *Methods for the analysis of histone H3 and H4 acetylation in blood.* Epigenetics, 2012. **7**(8): p. 875-82.
50. Pelgrom, L.R., A.J. van der Ham, and B. Everts, *Analysis of TLR-Induced Metabolic Changes in Dendritic Cells Using the Seahorse XF(e)96 Extracellular Flux Analyzer.* Methods Mol Biol, 2016. **1390**: p. 273-85.
51. Buenrostro, J.D., et al., *ATAC-seq: A Method for Assaying Chromatin Accessibility Genome-Wide.* Curr Protoc Mol Biol, 2015. **109**: p. 21.29.1-21.29.9.

Materials and methods

Ethics statement

Human monocytes and T cells were obtained from blood that was donated to the Bloodbank (Sanquin, Amsterdam) by healthy volunteers. The donated material was processed and analyzed anonymously. As such, not ethical approval was required for these studies.

Human DC culture, stimulation, and analysis

Monocytes were isolated from venous blood and differentiated into moDCs as described previously [46]. In brief, monocytes were isolated using CD14 MACS beads (Miltenyi) according to the manufacturer's recommendations, routinely resulting in a monocyte purity of >95%. Monocytes were subsequently cultured in RPMI medium supplemented with 10% FCS, 50 ng/mL human rGM-CSF (Invitrogen), and 25 U/mL human rIL4 (R&D Systems) for 6 days to differentiate them into a homogeneous population of CD14 low, CD1a$^+$ monocyte-derived DCs (moDCs) [47]. On day 6, immature DCs were left untreated or were stimulated with 2 mM SCFAs, namely: acetate, butyrate (both Sigma-Aldrich, kind gift from Dr. Martin Giera) or propionate (Sigma-Aldrich); 2.5 µM vitamin D3 (Sigma-Aldrich), trichostatin A (TSA) (100 ng/mL), niacin (2 mM) (Sigma-Aldrich), soluble egg antigens (SEA) (50 µg/mL), and IFN-γ (1,000 U/mL). SEA was prepared as previously described [48]. All stimulations were done in the presence of 100 ng/mL ultrapure LPS (E. coli 0111 B4 strain, InvivoGen, San Diego, CA, USA), unless indicated otherwise. The DCs were incubated with 10 µM RALDH inhibitor diethylaminobenzaldehyde (DEAB) (Stem Cell Technologies) in the indicated conditions. After 48 h of stimulation, surface expression of costimulatory molecules was determined by flow cytometry (FACS-Canto, BD Biosciences, Breda, The Netherlands) using the following antibodies: CD14 HV450 (MΦP9), CD86 FITC (2331 FUN-1), CD40 APC (5C3), CD80 Horizon V450 (L307.4), CD274/PDL1 PE-Cy7 (MIH1) (all BD Biosciences), HLA-DR APC-eFluor 780 (BL6), CD273/PDL2 PE (MIH18) (eBioscience, San Diego, CA, USA), CD83 PE (HB15e), CD1a PE (BL6) (all Beckman Coulter, Fullerton, CA, USA), and latency-associated peptide (LAP) APC (TW4-2FB) (BioLegend). In addition, 1×10^4 matured moDCs were cocultured with 1×10^4 CD40L-expressing J558 cells. Supernatants were collected after 24 h, and the concentration of IL-10 (Sanquin) and IL-12p70 (using mouse anti-human IL-12, clone 20C2 and biotinylated mouse-anti-human IL-12 clone 8.6, both BD Bioscience) was determined by ELISA.

Aldefluor assay

Aldefluor kit (Stemcell Technologies) was used, according to the manufacture's protocol, to determine RALDH activity.

Histone 3 (H3) and H4 acetylation by flow cytometry

H3 and H4 acetylation was determined by flow cytometry according to the protocol described elsewhere [49].

HDAC activity assay

Histone deacetylases activity was determined using a commercial HDAC cell-based activity assay kit (Cayman Chemical, Ann Arbor, MI, USA) according to the manufacture's guidelines. The HDAC activity was measured with the Wallac 1420 (PerkinElmer Life and Analytical Sciences, Turku, Finland).

Functional metabolic analyses

The metabolic characteristics of moDCs were analyzed using a Seahorse XF^{e}96 Extracellular Flux Analyzer (Seahorse Bioscience) as described previously [28, 50]. In brief, after 48 h of pulsing, 4×10^4 DCs were plated in unbuffered, glucose-free RPMI supplemented with 5% dialyzed FCS and left to rest 1 h before the assay. Subsequently extracellular acidification rate (ECAR) and oxygen consumption rate (OCR) were analyzed in response to glucose (10 mM; port A), oligomycin (1 µM; port B), fluoro-carbonyl cyanide phenylhydrazone (3 µM; port C), and rotenone/antimycin A (1/1 µM; port D) (all Sigma-Aldrich). Baseline ECAR = increase in ECAR in response to injection A. Spare ECAR = increase in ECAR in response to injection B. Baseline OCR = difference in OCR between readings following port A injection and readings after port D injection. Spare OCR is difference between basal and maximum OCR, which is calculated based on the difference in OCR between readings following port C injection and readings after port A injection.

Human T-cell culture and analysis of T-cell Polarization

For analysis of T-cell polarization, 48 h-pulsed moDCs were cultured with allogenic naive CD4^{+} T cells for 11 days in the presence of staphylococcal enterotoxin B (10 pg/mL). On day 6 and 8, rhuIL-2 (10 U/mL, R&D System) was added to expand the T cells. Intracellular cytokine production was analyzed after restimulation with 100 ng/mL phorbol myristate acetate and 2 µg/mL ionomycin for a total 6 h; 10 µg/mL brefeldin A was added during the last 4 h. Subsequently the cells were fixed with 3.7% paraformaldehyde (all Sigma-Aldrich). The cells were permeabilized with 0.5% saponin (Sigma-Aldrich) and stained with PE-, FITC-, and APC-labeled antibodies against IL-4 (8D4-8), IFN-γ (25723.11) (both BD Biosciences), and IL-10 (JES3-19F1) (BioLegend), respectively. Alternatively, 1×10^5 T cells were restimulated using anti-CD3 and anti-CD28 (both BD Biosciences), 24 h after restimulation, supernatants were collected, and IL-10 production by T cells was measured by ELISA (Sanquin).

T-cell suppression assay

For analysis of suppression of proliferation of bystander T cells by test T cells, 5×10^4 SCFA-pulsed DCs were cocultured with 5×10^5 naive $CD4^+$ T cells for 6 days. These T cells (test T cells) were harvested, washed, counted, stained with the cell cycle tracking dye 1 µM Cell Trace Violet dye (Thermo Fisher Scientific) and irradiated (3,000 RAD) to prevent expansion. Bystander target T cells (responder T cells), which were allogeneic memory T cells from the same donor as the test T cells, were labeled with 0.5 µM cell tracking dye 5,6-carboxy fluorescein diacetate succinimidyl ester (CFSE). Subsequently, 5×10^4 test T cells, 2.5×10^4 responder T cells, and 1×10^3 LPS-stimulated DCs were cocultured for 6 days. Proliferation was determined by flow cytometry, by co-staining with CD4 PE-Cy7 (clone SK3) and CD25 APC (clone 2 A3) (both BD Bioscience). To some cultures, where indicated, 10 µg/mL anti-IL-10 anti-body (BioLegend), 10 µM ALK5 (Sigma-Aldrich), 10 µM DEAB, 20 ng/mL recombinant human TGF-β1 (BioLegend) (kind gift from Dr. L. Boon), or control antibody IgG1 (BioLegend) was added during the DC-T cell coculture or during the test-responder T cell coculture.

Quantitative real-time PCR

RNA was extracted from snap-frozen 16 h-stimulated DCs. The isolation of mRNA was performed according to the manufacturer's instruction using RNeasy plus micro kit (Qiagen). cDNA was synthesized with reverse transcriptase kit (Promega), and PCR amplification by the SYBER Green method was done using CFX (Biorad). Specific primers for detected genes are listed in supplemental experimental procedures. Relative expression was determined using the ΔΔCt method.

Small interfering RNA (siRNA) electroporation

On day 4 of the DC culture, the cells were harvested and transfected with either no siRNA (R buffer only, provided by Invitrogen), 20 nM control siRNA or 20 nM GPR109A siRNA (both Dharmacon) using Neon Transfection System (Invitrogen) with the following setting: 1,600 V, 20 ms width, one pulse. Following electroporation, 3.5×10^5 cells were seeded per well in to a 24-well plate containing RPMI media without antibiotics. After 24 h, culture medium (RPMI) supplemented with 10% HI-FCS, rIL4 (0.86 ng/mL. R&D system Minneapolis, MN, USA) and rGM-CSF (20 ng/mL, Invitrogen, Carlsbad, CA, USA) was added. The transfection efficiency was routinely greater than 80%. GPR109A silencing efficiency was determined by quantitative RT PCR.

Assay for Transposase-Accessible Chromatin with high-throughput sequencing (ATAC-seq) analysis

5×10^4 moDCs stimulated for 6 h with indicated reagents were subjected to ATAC-seq as described elsewhere [51]. In brief, the cells were spun down immediately at 500 × g for 10 min at 4°C. Subsequently, the pellet was resuspended in TD Buffer (Illumina Nextera kit), transposase enzyme (Illumina Nextera kit, 15028252), and nuclease-free water in a total of 50 μL reaction for 30 min at 37°C. The DNA was then purified using Ampure XP beads (Beckman Coulter) and eluted in a final volume of 10 μL. Libraries were constructed according to Illumina protocol using the DNA treated with transposase, Kapa HiFi master mix and library-specific Nextera index primers. The following PCR condition was used to generate the libraries: 72°C, 5 min; 95°C, 2 min; (98°C, 20 s; 63°C, 30 s; 72°C, 1 min) 11× cycles; hold at 4°C. Prepared libraries went through quality control analysis using an Agilent Bioanalyzer. Samples were then used for next generation sequencing using Illumina Hiseq 2500 platform. All ATAC-seq datasets were aligned to build version NCBI37/ HG19 of the human genome using Bowtie2 (version 2.2.1). For alignment and peak-calling of the ATAC-seq data the Biopet Carp pipeline was used (http://biopet-docs.readthedocs.io/en/ latest/pipelines/carp/).

Statistical analysis

Data were analyzed for statistical significance using GraphPad Prism 7.0 statistical software (GraphPad Software, La Jolla, CA, USA). Comparison between groups was performed using the Student's t-test or two-way ANOVA test. All data are shown as means ± SEM. Differences were considered significant if $p < 0.05$.

Author contributions

MK, LP, AH, and BE designed and performed experiments. MK, MY, and BE wrote the manuscript. MY and BE conceptualized and supervised the study.

Acknowledgments

The authors thank Dr. Martin Giera for providing them SCFAs used in this project and Dr. Stefan White for help with the ATAC-seq analysis.

Funding

This work was supported by the Indonesian Directorate General of Higher Education (DGHE/DIKTI) to MK and a Veni grant from Netherlands Organisation for Scientific Research to BE.

Supplementary figures

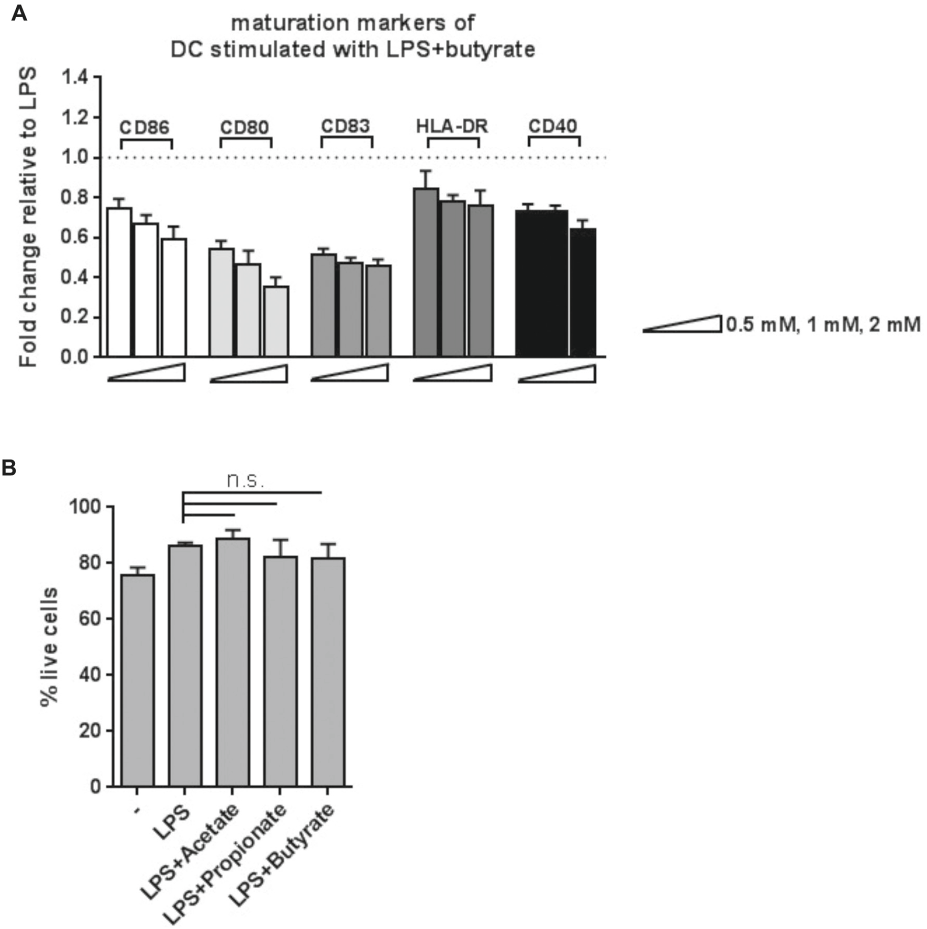

FIGURE S1. Butyrate suppresses LPS-induced maturation of human DCs in a dose-dependent manner.

(A) Monocyte-derived DCs were left untreated (iDC) or stimulated with butyarate as indicated for 48 h after which expression of maturation markers was analysed by flow cytometry. (B) MoDCs were left untreated or stimulated with different SCFAs at 2mM for 48 h after which cell death was determined by staining for 7AAD. Bar graphs represent means ± SEM of at least 3 experiments and (A) are shown as fold change relative to control condition.

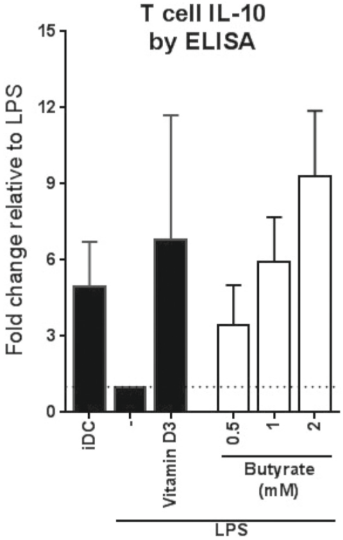

FIGURE S2. Butyrate conditions human DCs to prime IL-10 producing T cells in a dose-dependent manner.

DC-T cell co-culture assay as described in Fig. 2A. Bar graphs represent means ± SEM of 3 experiments and are shown as fold change relative to control condition.

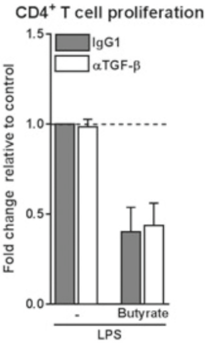

FIGURE S3. Suppression of proliferation by T cells that are differentiated by butyrate-conditioned DCs is independent from TGF-β signaling.

T cell suppression assay as described in Fig. 2D. Blocking antibody against TGF-β or IgG1 control antibody was added during the DC-T cell co-culture. Bar graphs represent means ± SEM of two experiments and are shown as fold change relative to control condition.

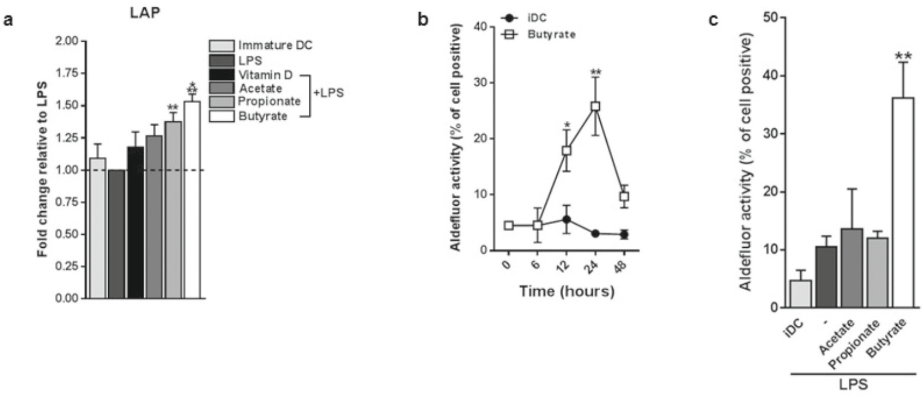

FIGURE S4. LAP expression and RALDH activity of differently stimulated DCs.

(A) Surface LAP expression on stimulated DCs was determined as described in Fig. 3B. (B and C) RALDH activity was assessed in stimulated DCs as described in Fig. 3D and 3E. In (B) the kinetic of RALDH activity was assessed on iDC and butyrate-stimulated DCs (in the absent of LPS) at 0, 6, 12, 24 and 48 h after stimulation and in (C) RALDH activity was measured on 6 h-differently stimulated DCs. (B) Bars represent means ± SEM, statistically significance of different time points per condition compared to 6 h time point. *$p<0.05$, **$p<0.01$ based on two-way ANOVA test. (A and C) Bar graphs represent means ± SEM of at least three experiments and (A) are shown as fold change relative to control conditions. **$p<0.01$, ***$p<0.001$ based on paired student's T-test.

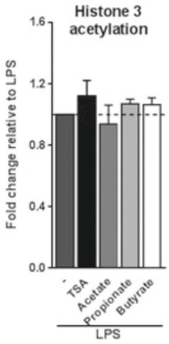

FIGURE S5. Histone 3 acetylation in differently stimulated DCs.

Analysis of histone 3 acetylation by flow cytometry of DCs stimulated with indicated reagents for 6 h. Bar graphs represent means ± SEM of at least three experiments and are shown as fold change relative to LPS control which is set to 1 (dashed line).

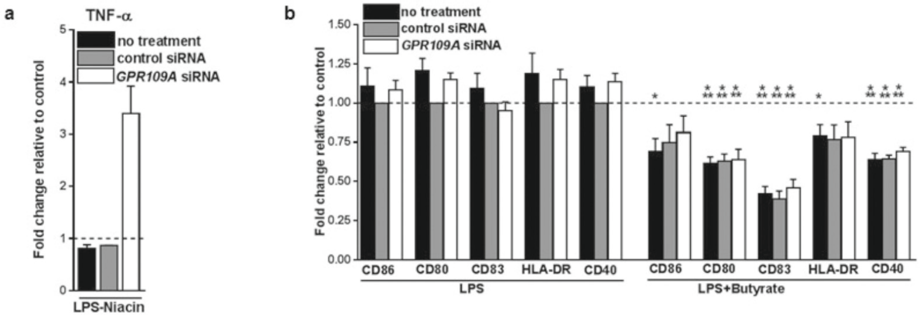

FIGURE S6. Effect of GPR109A silencing on niacin and butyrate conditioned-DCs.

GPR109A expression was silenced by small interfering RNA (siRNA) on day 4 of DC differentiation after which (A) the ability of niacin, as a natural ligand of GPR109A, to suppress LPS-induced TNF-α production was determined in supernatants by ELISA. (B) Expression of maturation markers of stimulated DCs was analysed by flow cytometry. (A and B) Bar graphs represent means ± SEM of at least three experiments and are shown as fold change relative to control conditions. *$p<0.05$, ***$p<0.001$ based on paired student's T-test.

Supplementary tables

Supplementary Table 1. Primer sequences used for RT-qPCR.

Gene	Forward (5'-3')	Reverse (5'-3')
ACTB	GCTACGAGCTGCCTGACGG	CAGCGAGGCCAGGATGGAGCC
IL10	ACCTGCCTAACATGCTTCGAG	CCAGCTGATCCTTCATTTGAAAG
IDO1	GGTCTGGTGTATGAAGGGTTCTG	GAGGAACTGAGCAGCATGTCCT
TGFB1	CCCAGCATCTGCAAAGCTC	GTCAATGTACAGCTGCCGCA
RALDH1	TGGCTTATCAGCAGGAGTGT	ACCGTACTCTCCCAGTTCTCTTC
RALDH2	GAGCAGGGTCCCCAGATTGA	CCCAGTCCTTTGCCTCCACA
GPR41	TCTCAGCACCCTGAACTCCT	TTCTGCTCCTTCAGCTCCAT
GPR43	GCCTGGTGCTCTTCTTCATC	AGGTGGGACACGTTGTAAGG
GPR109	TGCCGCCCTTCCTGATGGACA	TGTTCAGGGCGTGGTGGGGA

6

Metabolic control of type 2 immunity

Leonard R. Pelgrom
Bart Everts

Review
Eur J Immunol. 2017 Aug;47(8):1266-1275
PMID: 28661041
DOI: 10.1002/eji.201646728

Abstract

Type 2 immune responses play key roles in protection against parasitic worm infections, whole-body metabolic homeostasis, wound healing, and the development of allergies. As a result, there is considerable interest in understanding the pathways that regulate type 2 immunity in order to identify strategies of targeting and controlling these responses. In recent years, it has become increasingly clear that the functional properties of immune cells, including those involved in type 2 immune responses, are dependent on the engagement of specific metabolic pathways such as aerobic glycolysis and fatty acid oxidation (FAO). We here discuss the latest insights in the metabolic regulation of immune cells that initiate type 2 immune responses, such as dendritic cells and innate lymphoid cells, as well as immune cells involved in the effector phase, like T helper 2 (Th2) cells, B cells and alternatively activated macrophages (M2 macrophages). Finally, we consider whether these findings may provide new prospects for the treatment of type 2 immune response-associated diseases.

Introduction

Type 2 immune responses are initiated by dendritic cells (DCs) that promote the differentiation of naïve CD4$^+$ T cells towards a T helper 2 (Th2) phenotype, which is characterized by the production of the prototypical type 2 cytokines: interleukin-4 (IL-4), IL-5, and IL-13 [1]. In some settings, type 2 innate lymphoid cells (ILC2s) and basophils contribute to this process by also presenting antigens to naïve T cells and by producing type 2 cytokines. IL-4, IL-5, and IL-13 play a central role in driving the humoral and cellular arms of type 2 immunity. IL-4 released in B-cell follicles by a specialized subset of Th2 cells, termed T follicular helper (Tfh) cells, promotes B cells to induce antibody class switching towards immunoglobulin E (IgE) as well as toward IgG4 in humans and IgG1 in mice [2]. Local release of IL-5 at the site of inflammation leads to the recruitment and activation of eosinophils which, similar to basophils and mast cells, release pre-formed granules with toxic proteins, histamine, and other vasoactive amines upon engagement of their high-affinity IgE receptors (FC epsilon receptor [FcεR]) by immune complexes of IgE [1]. In addition, these granulocytes produce bio-active lipids such as leukotrienes and prostaglandins, and a wide variety of cytokines. Finally, local release of both IL-4 and IL-13 induces the alternative activation of macrophages (M2 macrophages), a subset of macrophages that is known to assist in the killing of parasites, resolution of inflammation and repair of any tissue damage that has occurred [3]. However, these responses are also the main driver of allergic reactions that result in diseases such as asthma, rhinitis, and atopic dermatitis [1]. Given the vital contributions of each of these cells in the outcome of type 2 immune response-associated diseases, there is considerable interest in understanding the pathways that regulate their function in order to identify strategies of targeting and controlling type 2 immunity.

In recent years, it has become increasingly clear that immune cell differentiation, activation, proliferation, function, and longevity are underpinned by the engagement of specific core metabolic pathways. These core metabolic pathways include glycolysis, fatty acid synthesis, fatty acid oxidation (FAO), and mitochondrial oxidative phosphorylation (OXPHOS). For an introduction into these metabolic pathways we refer to a recent comprehensive review [4]. This has generated considerable enthusiasm for the rapidly expanding field of immunometabolism and has led to the emerging concept that the manipulation of immune cell metabolism could be a powerful and attractive tool to direct immune responses. In the context of type 2 immunity, the field of immunometabolism was in part ignited by a seminal study on macrophages in 2006 [5], which for the first time documented that M2 polarization of murine macrophages was supported by an increase in OXPHOS and FAO. This was very different from what was seen in classically activated macrophages (M1 macrophages) that instead shifted toward aerobic glycolysis during their polarization [5]. Since then, and in particular very recently, considerable progress has been made in delineating the different metabolic programs shaping the function of the various immune cells involved in type 2 immune responses. In this review we will discuss the latest insights in the metabolic regulation of type 2 immune cell biology and in addition explore whether targeting metabolic pathways could hold promise as an approach to treat diseases associated with a deregulated type 2 immunity.

Metabolism of immune cells involved in the priming of type 2 immune responses

Th2-priming dendritic cells

It has been shown that profound changes in cellular metabolism are integral to the activation and overall T-cell priming ability of DCs [6, 7]. Specifically, triggering of toll-like receptors (TLRs) on DCs, which is generally associated with an enhanced ability to prime CD8, Th1, or Th17 responses, rapidly increases the flux of glucose through the glycolytic pathway. This leads to an increase in pentose phosphate pathway (PPP) activity and citrate metabolism, which are both necessary for fatty acid synthesis [8]. Synthesis of new fatty acids then allows for the expansion of the endoplasmic reticulum, which is likely to be required for the production of effector molecules that are central to DC activation. In addition to these short-term effects, long-term TLR signaling inhibits mitochondrial respiration in DCs [9, 10] and therefore increases their dependence on glycolysis for the production of ATP. However, to date, little is known about the role of DC metabolism in Th2 priming. Some indirect evidence that lipid metabolism plays a role in DC-driven Th2 polarization comes from a handful of studies in which peroxisome proliferator-activated receptor gamma (PPAR-γ), a master regulator of lipid metabolism, was targeted in DCs [11-13]. For example, suppression of PPAR-γ through sirtuin-1-mediated deacetylation was found to be required for the Th2-priming capacity of murine DCs [13]. Consistent with this, DCs stimulated with the PPAR-γ agonist rosiglitazone were shown to inhibit the development of eosinophilic airway inflammation in a mouse model of asthma [11]. However, this effect appears to be secondary to the induction of regulatory T cells, rather than an inability to induce Th2 responses when PPAR-γ is activated [11, 12]. More recently, adenosine monophosphate-activated protein kinase (AMPK) signaling has been linked to the ability of DCs to induce Th2 differentiation [14]. AMPK is a sensor of intracellular adenosine nucleotide levels that during conditions of decreased ATP availability promotes FAO, mitochondrial OXPHOS and other forms of catabolic metabolism to generate more ATP [15]. In a model of murine *Nippostrongylus brasiliensis* infection, deletion of the AMPK alpha subunit in CD11c$^+$ cells resulted in the increased production of IL-12/23p40 by these cells and consequently, impaired type 2 immune responses and increased both worm burden and fecundity [14].

Finally, induction of Th2 polarization in mice was recently shown to be mediated by a specific subset of DCs [16], termed cDC2, which is dependent on the transcription factors KLF4 [16] and IRF4 [17] for its development. In myocytes, KLF4 has been implicated in mitochondrial biogenesis, mitophagy and the oxidation of both glucose and fatty acids [18], while IRF4 promotes the alternative activation of macrophages in an FAO-dependent manner [19]. Together, this makes it conceivable that Th2-priming DCs are characterized by, and rely on, a more oxidative-centered metabolism. However, evidence is still missing to support this. Future studies should focus on directly targeting the metabolic pathways involved in DC lipid and oxidative metabolism to more granularly define their importance for the Th2-priming capacity of DCs.

Type 2 innate lymphoid cells

So far, only a single study has explored the metabolic properties of ILC2s. Murine ILC2s were found to have both greater spare respiratory capacity (SRC) and glycolytic capacity than Th2 cells [20]. SRC is the extra capacity cells have to produce ATP via OXPHOS in response to stress and as such, is considered a marker for mitochondrial fitness. In addition, ILC2s, in contrast to other lymphocytes, were found to constitutively express high levels of arginase-1 (Arg1), an enzyme that converts argi- nine to urea and ornithine [20]. Importantly, Arg1 expression and enhanced bioenergetics appear to be functionally linked in ILC2s, since pharmacological inhibition of arginase with Nω-hydroxy- nor-arginine (nor-NOHA) was shown to reduce both maximal respiration and maximal glycolysis in these cells [20]. Although the mechanistic basis for this link was not explored, it is possible that ornithine derivatives could support OXPHOS. Ornithine can be converted into glutamate and subsequently into the TCA cycle-intermediate α-ketoglutarate (α-KG), which, if broken down completely in the TCA cycle, can generate 6.5 ATP molecules through OXPHOS [21] (Fig. 1A). Correspondingly, overexpression of arginase-2 in human bronchial epithelial cells increased mitochondrial oxygen consumption [22]. Inhibition of Arg1 in ILC2s also diminished their ability to produce ornithine-derived polyamines such as putrescine, spermidine, and spermine [20], which are known to be important for proliferation. In line with this, Arg1-defective ILC2s showed decreased proliferative potential [20]. Importantly, in this study, ILC-intrinsic deletion of Arg1 was found to diminish pathology in multiple murine models of lung inflammation [20], suggesting that Arg1 through regulation of cellular bioenergetics and polyamine synthesis underpins ILC2s function and thereby disease outcome. However, no role for Arg1 in ILC2 function or outcome of lung inflammation was found in another murine study [23]. This may possibly be explained by the fact that these studies used different approaches to conditionally delete Arg1 from ILC2s. Additional studies would be needed to reconcile these contradictory results and to definitively determine the link between Arg1, cellular metabolism, and ILC2 function.

ILC2s are considered the innate counterpart to Th2 cells as they share the ability to produce IL-5 and IL-13, and depend on the transcription factor GATA3 for their development. From a metabolic standpoint, this similarity may be extended to their shared requirement for mammalian target of rapamycin (mTOR) signaling in regulating their effector function. mTOR is a kinase that forms the core of two different complexes: mTORC1 and mTORC2, both of which promote anabolic metabolism, but also have distinct functions. mTORC1, of which Raptor is a key component, is known for its involvement in cell growth, while mTORC2, with Rictor as a key component, promotes cell survival and proliferation. The prototypical mTORC1 inhibitor rapamycin was shown to block murine ILC2 accumulation after intranasal administration of IL-33 and to diminish their production of IL-5 and IL-13 after restimulation with IL-33 ex vivo. This suggests that mTORC1 signaling is involved in murine ILC2 function [24] (Fig 1A). However, ILC2s are not unique among murine ILCs in their dependence on mTOR signaling, as ILC1s and ILC3s are almost completely absent in Nkp46-Mtor$^{-/-}$ mice [25]. Whether mTOR signaling is crucial for the development of ILCs from their progenitor, the common lymphoid progenitor (CLP), for mature ILC survival or both is still unclear. Rapamycin was found to skew the differentiation of ex vivo murine haematopoietic stem cells away from the CLP toward the common myeloid progenitor [26]. However, conditional deletion of mTOR in interferon-alpha-responsive murine cells increased the number of CLPs [27] and it was already known for a longer time that mouse models with constitutively active mTORC1 signaling have lower numbers of CLPs [28].

Altogether, these studies suggest that ILC2s, similar to other immune cells, depend on mTOR signaling for their development and function, but that they also may have a unique dependency on Arg1 to shape their metabolic profile and thereby their functional properties.

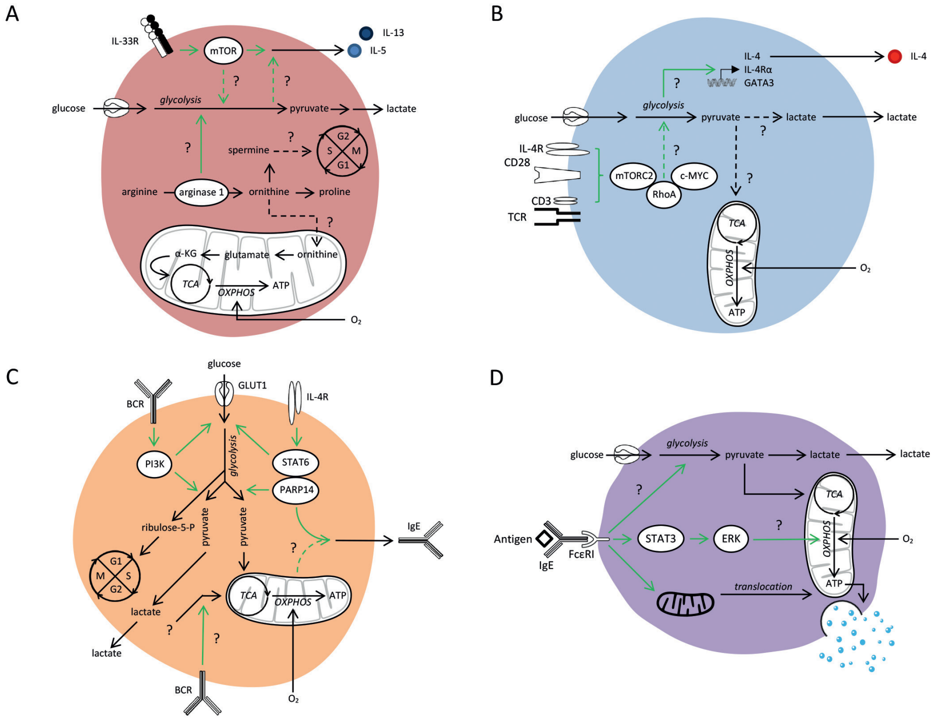
A
IL-33R
mTOR
IL-13
IL-5
?
?
glucose
glycolysis
pyruvate
lactate
?
spermine
?
G2
S
M
G1
arginine
arginase 1
ornithine
proline
?
α-KG
glutamate
ornithine
TCA
OXPHOS
ATP
O_2
B
IL-4
IL-4Rα
GATA3
IL-4
?
glucose
glycolysis
pyruvate
lactate
lactate
?
IL-4R
CD28
?
mTORC2
c-MYC
RhoA
?
CD3
TCR
TCA
OXPHOS
ATP
O_2
C
glucose
GLUT1
BCR
IL-4R
PI3K
glycolysis
STAT6
PARP14
ribulose-5-P
pyruvate
pyruvate
IgE
?
G1
M
S
G2
lactate
TCA
OXPHOS
ATP
lactate
?
?
BCR
O_2
D
glucose
glycolysis
pyruvate
lactate
lactate
?
Antigen
IgE
FcεRI
STAT3
ERK
?
TCA
OXPHOS
O_2
translocation
ATP

Figure 1. Metabolic characteristics of (A) ILC2s, (B) Th2 cells, (C) IgE-secreting B cells and (D) mast cells.

Proteins such as transcription factors and enzymes are circled. Green lines indicate signaling pathways, while black lines illustrate metabolic pathways. Lines with question marks represent not fully elucidated links.

Metabolism of cells involved in the effector phase of type 2 immune responses

T helper 2 cells

The relevance of cellular metabolism in T-cell activation, differentiation, and memory formation has been extensively studied in CD8$^+$ T cells (for a recent review see [29]). This significance is now also being unravelled for Th2 cells. In vitro-polarized murine Th2 cells show strongly enhanced glycolytic rates [30, 31]. Functionally, inhibition of glycolysis using 2-deoxyglucose (2-DG) diminished the expression of the transcription factor GATA3 [32], lowered the expression of the IL-4 receptor α chain (IL-4Rα) [32, 33] and blocked the production of IL-4 [32, 33] under Th2-polarizing conditions. Lowering glucose levels in the medium had a similar effect on IL-4Rα expression [33]. In contrast, inhibition of glycolysis did not affect the production of IFN-γ under Th1- polarizing conditions [32], suggesting that among Th cells, Th2 cells have a unique dependency on glycolysis for their effector function. In line with this, glycolytic rates seem to be higher in Th2 cells than Th1 and Th17 cells [30, 31]. The fate of glucose-derived pyruvate in these settings is yet to be elucidated, but the finding that Th2 cells have a higher mitochondrial oxygen consumption rate than Th1 cells [32], may indicate that pyruvate in Th2 cells is preferentially oxidized in the mitochondria to support OXPHOS. Moreover, Th2 cells from asthmatic individuals were shown to have a higher expression of carnitine palmitoyltransferase I isoform a (CPT1a), a transporter involved in the mitochondrial import of long-chain fatty acids, compared to Th2 cells from healthy controls [34]. This suggests that FAO-driven OXPHOS may also facilitate the effector functions of Th2 cells (Fig. 1B).

When looking for upstream metabolic regulators that are potentially involved in these Th2-specific metabolic adaptations, multiple studies support a role for mTORC2 signaling in the preferential differentiation of naïve T cells toward Th2 cells [32, 35-37]. For instance, conditional deletion of the GTPase RhoA, a downstream target of mTORC2, decreased glycolysis in, and IL-4 production by Th2 cells, while sparing glycolysis in, and IFN-γ production by Th1 cells [32]. Correspondingly, mice with a T-cell-specific deletion of RhoA were protected against the development of allergic asthma [32]. How RhoA promotes glycolysis remains to be determined. However, since RhoA is known to promote expression of transcription factor c-MYC [38], a master regulator of glycolysis [39], and expression of c-MYC in human primary Th2 cells was found to be positively associated with the allergic status of the individuals these cells were isolated from [34], makes it interesting to speculate that mTORC2 through activation of RhoA and c-MYC specifically controls the glycolytic reprogramming and effector function of Th2 cells, but not that of Th1 and Th17 cells (Fig. 1B).

From these studies a picture is emerging that mTORC2-driven glycolytic reprogramming plays a central role in supporting the differentiation and function of Th2 cells. It remains to be seen whether these findings are relevant for Tfh cells in the context of type 2 immune responses, as the metabolic properties of Tfh cells have only been studied during viral infection. In this setting, Tfh cells were found to have enhanced glycolytic rates compared to naïve CD4$^+$ T cells [40], but lower overall metabolic rates than Th1 cells [41].

B cells

Currently, no studies have specifically addressed whether there are metabolic requirements for the production of IgE. However, it is known that B-cell receptor (BCR) activation by cognate antigen induces surface glucose transporter 1 (GLUT1) expression and glucose uptake in murine splenic B cells in a phosphoinositide 3-kinase (PI3K)-dependent manner [42] (Fig. 1C). In this setting, large amounts of lactate are produced and glucose-derived carbons end up in the PPP. The PPP is an alternative glucose-fuelled metabolic pathway that branches off from glycolysis and serves to generate nicotinamide adenine dinucleotide phosphate (NAPDH) to support fatty acid synthesis and redox balance, and ribose-5-phosphate to support nucleotide synthesis. These nucleotides are needed for the DNA replication that occurs within 31–48 h after BCR activation [43]. This suggests that B-cell activation, similar to T-cell activation, results in increased aerobic glycolysis and PPP activity to support cellular proliferation. T-cell activation also increases the expression of amino acid transporters [29] and in line with this, B-cell activation also increases the expression of the small subunit 1 of the large neutral amino acids transporter (Slc7a5) and correspondingly increases leucine uptake [44]. However, in contrast to activated T cells, activated B cells maintain a balanced glycolysis/OXPHOS ratio [45]. If BCR activation is associated with aerobic glycolysis as described above, then likely other macromolecules such fatty acids or amino acids are needed to fuel the TCA cycle to accompany the observed increase in OXPHOS. However, the necessity for OXPHOS for BCR-induced B-cell activation is still uncertain and will require further research (Fig. 1C).

The main cytokine regulating the type 2 immune response-associated isotype switching is IL-4. Similar to BCR activation, IL-4 was found to induce surface GLUT1 expression, glucose uptake and glycolytic flux in murine splenic B cells [46, 47]. However, in contrast to BCR activation, IL-4 also induced the expression of citrate synthase, the first enzyme in the TCA cycle, and correspondingly increased glucose oxidation [46]. These effects were found to be dependent on STAT6-PARP14 [46] (Fig. 1C) and deletion of either proteins decreased the IgE production by IL-4-stimulated B cells [48]. Of note, while IL-4 increased glucose oxidation, FAO was unaffected [44].

Taken together, these studies suggest that B-cell activation and subsequent proliferation initially depend on aerobic glycolysis to support the increased activity of biosynthetic pathways such as the PPP. In addition, when exposed to IL-4, B cells might divert a part of the glucose toward OXPHOS to aid in IgE class switching. A first hint that the switching toward different antibody isotypes requires the engagement of distinct metabolic programs comes from one study, which reported that the inhibition of OXPHOS using rotenone had no effect on the production of IgM by murine splenic B cells that were exposed to LPS [45]. However, this awaits to be formally tested in more detailed metabolic studies.

Mast cells, basophils and eosinophils

The majority of studies dedicated to the cellular metabolism of granulocytic type 2 immune cells have focused on mast cells. Murine bone marrow-derived mast cells (BMMCs) that were sensitized with complexed IgE and then stimulated with antigen showed increased OXPHOS and glycolytic capacity [49]. The importance of glycolysis in mast cell effector function was supported by the finding that removing glucose from the media decreased histamine release by primary rat mast cells [50]. Increasing glucose oxidation at the expense of lactate production using the pyruvate dehydrogenase kinase inhibitor dicholoroacetate (DCA) was shown to decrease degranulation and IL-6 production by BMMCs [49], making it imaginable that during mast cell activation especially the rapid production of ATP that aerobic glycolysis can provide is important. However, this finding is hard to unify with the limited effect of 2-DG on these parameters in the same study.

In contrast, there appears to be a more coherent picture regarding the role of mitochondrial metabolism in mast cell effector functions. Human mast cells require the translocation of mitochondria into exocytosis sites for degranulation [51] (Fig. 1C). Loss of IgE/Ag-induced oxygen consumption by inhibiting STAT3 or ERK was associated with an abolishment of β-hexosaminidase release and TNF-α production in both BMMCs and rat basophilic leukaemia (RBL) cells, a model for mast cells [52]. Finally, direct inhibition of OXPHOS using rotenone blocked degranulation and lowered IL-6 production in BMMCs [49]. It is likely that OXPHOS fuelled by glucose oxidation rather than FAO is required for mast cell effector functions, as inhibition of pyruvate dehydrogenase (PDH) with CPI-613 lowered β-hexosaminidase release and cytokine production in RBL cells and human cord blood-derived mast cells [53], while blockade of FAO using the CTP1a inhibitor etomoxir did not affect mast cell functions [49]. As a whole, these studies suggest that glucose-fuelled OXPHOS is important for mast cell function. However, the role of glycolysis in mast cell biology warrants further investigation due to conflicting results from different studies (Fig. 1D).

The metabolic properties and requirements for basophil function are relatively unknown. Sumbayev and colleagues found that FcεR triggering on primary human basophils resulted in stabilization of hypoxia-inducible factor 1 alpha (HIF-1α) [54], which promotes the expression of genes involved in glycolysis [55]. Although silencing of HIF-1α in these cells impaired IgE-driven IL-4 release, it remains unclear which other effector functions are HIF-1α-dependent and whether these effects are secondary to a reduced glycolytic capacity.

Finally, there is a single study published in 1977 that interrogated the role of cellular metabolism in eosinophil biology [56]. David and colleagues reported that glycolysis, but not OXPHOS, was important for antibody-dependent, eosinophil-mediated damage of *Schistosoma mansoni* schistosomula. However, through which mechanism glycolysis underpins this effector function of eosinophils was not addressed and warrants further detailed analysis by taking advantage of more modern experimental techniques.

Collectively, this may suggest that basophils and eosinophils, similar to other granule-releasing immune cells, such as $CD8^+$ cytotoxic T lymphocytes, rely on glycolytic metabolism for the effective release of cytokines and enzyme containing granules [57]. In contrast, mast cells appear to primarily depend on mitochondrial respiration for this process. Interestingly, mast cells, as opposed to basophils or eosinophils, are long-lived cells and longevity at the cellular as well at the organismal level is known to be strongly supported by mitochondrial OXPHOS [58]. In this light, it is tempting to speculate that mast cells rely on oxidative metabolism for long-term survival and have come to co-opt this longevity-associated metabolic makeup to also support their effector functions.

Alternatively activated macrophages

The role of cellular metabolism in immune cell biology has been studied most extensively in macrophages. Already more than a decade ago, it was observed that M1 and M2 macrophages have very distinct metabolic properties on which they depend for their polarization. This has been reviewed in detail elsewhere [59] and we will here highlight only the most recent insights in M2 macrophage metabolism. It is well known that M2 macrophages are metabolically characterized by an increased expression of genes involved in FAO and OXPHOS, fatty acid uptake, mitochondrial mass and FAO-dependent mitochondrial oxygen consumption [5, 60]. Moreover, inhibition of fatty acid uptake by deleting CD36 [60], inhibition of lipolysis using Orlistat [60] or anti-lysosomal acid lipase (LAL) short hairpin RNA [60], and inhibition of FAO using etomoxir [5, 60] were all shown to prevent murine M2 polarization, while having little or no effect on M1 polarization. These murine data are supported by the finding that IL-4-stimulated human monocyte-derived macrophages (MDMs) from CD36-deficient patients have lower SRC and lower expression of the mannose receptor 1 than MDMs from a healthy control [60]. Together, these observations led to the initial concept that M2 polarization is solely fuelled by FAO and mitochondrial OXPHOS, thereby contrasting with the metabolic requirements for the polarization of M1 macrophages, which depends on a strong commitment to aerobic glycolysis.

However, more recently, several studies challenged this view and provide support for the concept that in addition to FAO-fuelled OXPHOS, glycolysis has also an important role in the alternative activation of macrophages. Murine M2 macrophages have an increased expression of genes involved in glycolysis [19], enhanced glycolytic capacity [19, 61] and glucose uptake [5, 19, 62] in comparison to unpolarized macrophages. Inhibition of glycolysis using 2-DG [19, 61, 63], or specifically glucose oxidation using UK5099 [19] or anti-mitochondrial pyruvate carrier 1 short hairpin RNA [19] all suppressed the IL-4-induced increase in mitochondrial oxygen consumption and expression of M2 markers such as RELMα [19] and Arg1 [61, 63]. Surprisingly, inhibition of fatty acid synthesis using TOFA mimicked these effects [19]. Based on these data, a model has been proposed in which glucose-derived carbons enter the TCA cycle to support mitochondrial citrate synthesis that is later used, following conversion into acetyl-CoA, for cytosolic fatty acid synthesis. Subsequently, these fatty acids can then be used for FAO-driven mitochondrial OXPHOS (Fig. 2, center). A similar atypical pathway has been suggested to operate in memory CD8$^+$ T cells [64]. It is possible that de novo fatty acid synthesis is required to produce ligands for lipid-dependent nuclear receptors such as PPARs [65-68] or contribute to ER stress [69, 70], which are both known to play a role in M2 polarization. However, this still remains to be addressed. In addition, it was recently shown that for the alternative activation of macrophages glycolysis-driven synthesis of acetyl-CoA is not only important through its use as a substrate for fatty acid synthesis, but also because it is used for histone acetylation and thereby epigenetic regulation of M2 marker gene expression [62] (Fig. 2, top right). Finally, glucose tracing studies in M2 macrophages have revealed that there is an increased flux of glucose carbons into the hexosamine biosynthesis pathway that, in combination with glutamine, generates UDP-GlcNAc, a sugar-donor required for protein and lipid O-and N-glycosylation (Fig. 2, bottom). Functionally this appears to be important, as inhibiting N-linked glycosylation using tunicamycin was shown to decrease M2 polarization [71], although the exact mechanism underlying this phenotype is still unclear.

More evidence for a role of glycolysis in the alternative activation of macrophages comes from studies investigating the role of mTORC1 and mTORC2 signaling pathways during M2 polarization. Both mTORC1 and mTORC2 are known to support glycolytic reprogramming [55] and in agreement with a role of glycolysis in the alternative activation of macrophages, both Raptor [62] and Rictor [19] were found to be crucial for the expression of a subset of M2 genes. Deletion of Rictor in macrophages (LysM-Cre) inhibited the increase in glycolysis that is associated with IL-4 stimulation and inhibited the concomitant increase in FAO-dependent mitochondrial oxygen consumption [19]. These mTORC2-driven metabolic changes were shown to be dependent on PI3K, AKT and IRF4.

Corresponding with a known role for M2 macrophages in the killing of parasites, tumor growth and adaptive thermogenesis, in LysM-Rictor$^{-/-}$ mice, infections with *Heligmosomoides polygyrus* [19] and *N. brasiliensis* [72] were more persistent, melanoma cells grew more slowly [19] and core body temperature was not maintained during cold challenge [72]. mTORC1 may contribute to M2 polarization through different mechanisms than mTORC2. Deletion of Raptor in macrophages inhibited the expression and IL-4-mediated activating-phosphorylation of ATP citrate lyase (Acly) [62], the cytosolic enzyme that converts citrate into acetyl-CoA. The increased availability of cytosolic acetyl-CoA during M2 polarization was found to facilitate histone acetylation of M2 genes and thereby to promote their expression [62]. This mTORC1-driven epigenetic change was shown to be dependent on AKT by operating upstream of mTORC1. Collectively, these studies suggest that both mTORC1 and mTORC2 signaling pathways are required for the alternative activation of macrophages, by each executing distinct parts of the metabolic program that supports M2 polarization. Of note, in addition to mTORC1 and mTORC2 co-operation, there is also some evidence for counter-regulation. Raptor-deficient M2 macrophages showed increased activity of N-myc downstream regulated gene 1 [19], a down-stream target of mTORC2, and conversely, macrophages with hyper-active mTORC1 signaling showed enhanced M1 polarization at the expense of M2 polarization [73]. This suggests that both mTORC1 and mTORC2 signaling pathways are active in M2 macrophages, but their activity needs to be tightly regulated for optimal M2 polarization [19].

Finally, there is a recent study that questions the importance of FAO in M2 polarization altogether. Murine macrophages that are deficient in CPT2, which in conjunction with CPT1 shuttles long-chain fatty acid into mitochondria, could still be polarized toward an M2 phenotype [74]. Moreover, the effect of the CPT1a inhibitor etomoxir on M2 polarization was still present, suggesting that etomoxir might have off-target effects [74]. This highlights the need for re-evaluation of some of the results derived from experiments in which only etomoxir was used to assess the role of FAO in M2 polarization and immune cell metabolism in general.

As a whole, these results illustrate that the role of FAO in M2 polarization is not as straightforward as thought and uncovered a previously unappreciated, but equally important role for glycolysis in the alternative activation of macrophages. Moreover, the observation that the difference between M1 and M2 macrophages in terms of metabolic phenotype is less distinct in human compared to murine macrophages [75], may point toward quantitative and possibly qualitative differences between the two species. More detailed comparative studies would be needed to carefully address these issues.

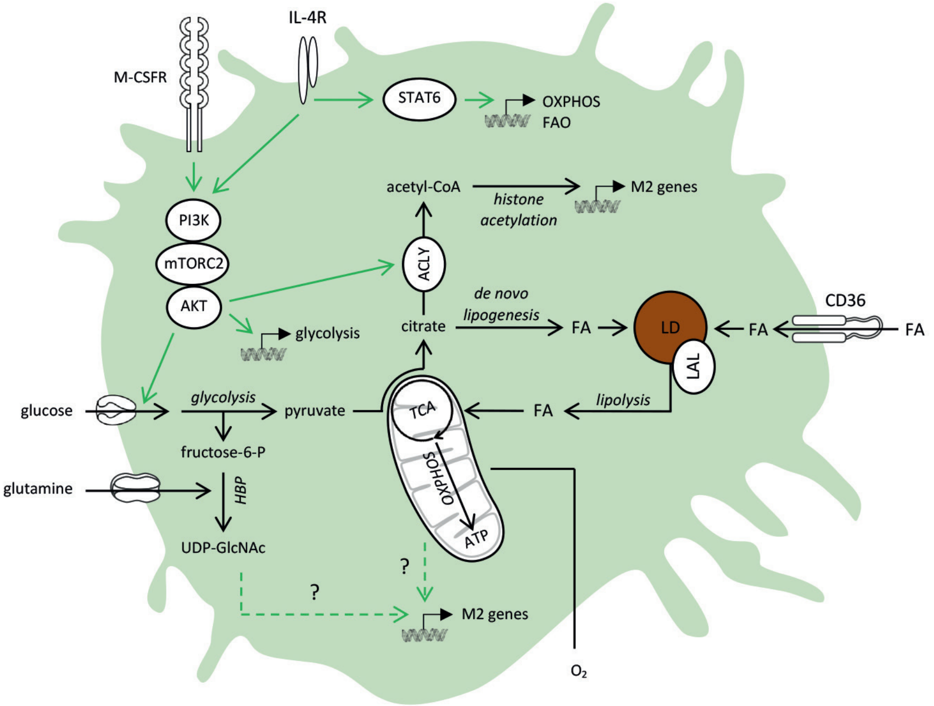
IL-4R
M-CSFR
STAT6
OXPHOS
FAO
acetyl-CoA
histone
acetylation
M2 genes
PI3K
mTORC2
AKT
ACLY
de novo
lipogenesis
CD36
FA
LD
LAL
glycolysis
citrate
FA
FA
FA
lipolysis
glucose
glycolysis
pyruvate
TCA
fructose-6-P
OXPHOS
glutamine
HBP
ATP
UDP-GlcNAc
?
?
M2 genes
O2

Figure 2. Metabolic pathways that support M2 macrophage polarization.

Proteins such as tran- scription factors and enzymes are circled. Green lines indicate signaling pathways, while black lines illustrate metabolic pathways. Lines with question marks represent not fully elucidated links.

Conclusion and future perspective

The burgeoning field of immunometabolism has generated many exciting new insights into how cellular metabolic pathways shape the function of immune cells, including those that are involved in type 2 immune responses. As many of the studies discussed in this review illustrate, it becomes increasingly clear that many type 2 immune cells (e.g. cDC2s, ILC2s, Th2 cells, and M2 macrophages) are characterized by, and are depend on, different metabolic programs than their type 1 immune cell counterparts (e.g. cDC1s, ILC1s, Th1 cells, and M1 macrophages). Moreover, several immune cells within the type 2 immune response network (i.e. Th2 cells [32], M2 macrophages [19, 61, 63], ILC2s [20], mast cells [49] and IL-4-stimulated B cells [46, 47] appear to share a common metabolic signature that is characterized by increased glycolysis as well as a concomitant higher mitochondrial oxygen consumption. Exceptions to this rule seem to be basophils and eosinophils, which are characterized by a more glycolysis-centered metabolism.

It remains to be determined why several type 2 immune cells seem to have a metabolic profile consisting of both increased glycolysis and OXPHOS. It is known that IL-4, and to a lesser extent IL-13, can induce these metabolic changes in immune cells. Given that most of these immune cells are exposed to IL-4 and IL-13 during type 2 immune responses, one could speculate that this profile is in part a reflection of metabolic imprinting by these cytokines. The ability to effectively engage both metabolic pathways may endow type 2 immune cells with the metabolic flexibility to use various substrates to meet their bioenergetics needs. This might allow them to maintain their effector functions during local fluctuations in nutrient availability. However, why this would be more important for type 2 immune cells than other types of immune cells is unclear. For M2 macrophages one could envision that an increased ability to oxidize lipids may be particularly important to perform their role in maintaining adipose tissues metabolic homeostasis and the repair of damaged tissues. In both situations, fat cells and dead cells release large quantities of lipids that need to be efficiently broken down by macrophages to prevent lipotoxiticy.

The observation that type 2 immune cells have metabolic properties distinct from each other, as well as from other types of immune cells, provides a potential window of opportunity for the metabolism-based treatment of type 2 immune response-associated diseases. Consistent with an important role of glycolysis in eosinophil and Th2-cell function, inhibiting the first step in glycolysis using 2-DG reduced the number of eosinophils and the levels of Th2 cytokines in the bronchoalveolar (BAL) fluid of mice with OVA-induced AAI, without affecting the infiltration of other immune cells and the production of IFN-γ, IL-17, and TGF- β [31, 57, 76]. In the same model, blocking the entry of glycolysis-derived pyruvate into the TCA cycle using CPI-613 decreased air-way resistance, which was associated with a reduction in the release of histamine by mast cells. However, CPI-613 also promoted the infiltration of eosinophils, macrophages, neutrophils, and lymphocytes into the BAL fluid [53]. Finally, the finding that ILC2s might rely on arginine metabolism for their function sheds interesting new mechanistic light on the long-appreciated beneficial effects of the arginase inhibitor nor-NOHA on asthma pathophysiology [77]. In line with the notion that nor-NOHA specifically targets Arg1 in ILC2s to reduce asthma, macrophage-intrinsic deletion of Arg1 did not impact pathology in murine models of air- way inflammation [20, 78, 79]. These studies provide interesting proof of principle that metabolic targeting of type 2 immune cells could hold promise as strategies to manipulate type 2 immunity for therapeutic gain. However, they also illustrate that targeting specific metabolic pathways in a limited number of cell types is necessary to prevent unwanted side-effects. More translational studies will be needed to address these challenges in the near future.

Most studies thus far have focused on core metabolic pathways to address the role of metabolism in type 2 immune cells. In addition, these studies have often been based on in vitro models which use culture conditions that may not necessarily mirror the metabolic microenvironment type 2 immune cells are exposed to in vivo. For instance, a high dependence on glycolysis may reflect more the adaptation to high glucose levels in the culture media rather than representing the natural condition. The recent development of more sensitive high-throughput metabolomics, proteomics and transcriptomics techniques in conjunction with more advanced mathematical and statistical modeling, will make it possible to characterize the metabolic properties and requirements of immune cells in unprecedented detail, both in vitro as well as in situ. These kinds of approaches will help to identify new metabolic pathways in type 2 immune cells that are unique for certain cells or effector functions and that then could be considered as novel therapeutic targets for the regulation of type 2 immunity. As such, we believe that this field can provide important contributions to the development of new treatment strategies that are needed to battle the sharp rise in type 2 immune response-associated diseases throughout the world, such as allergies and type 2 diabetes that are caused by either an overzealous or defective type 2 immunity respectively.

References

1. Wynn, T.A., *Type 2 cytokines: mechanisms and therapeutic strategies.* Nat Rev Immunol, 2015. **15**(5): p. 271-82.
2. Mestas, J. and C.C. Hughes, *Of mice and not men: differences between mouse and human immunology.* J Immunol, 2004. **172**(5): p. 2731-8.
3. Allen, J.E. and T.E. Sutherland, *Host protective roles of type 2 immunity: parasite killing and tissue repair, flip sides of the same coin.* Semin Immunol, 2014. **26**(4): p. 329-40.
4. O'Neill, L.A., R.J. Kishton, and J. Rathmell, *A guide to immunometabolism for immunologists.* Nat Rev Immunol, 2016. **16**(9): p. 553-65.
5. Vats, D., et al., *Oxidative metabolism and PGC-1beta attenuate macrophage-mediated inflammation.* Cell Metab, 2006. **4**(1): p. 13-24.
6. Everts, B. and E.J. Pearce, *Metabolic control of dendritic cell activation and function: recent advances and clinical implications.* Front Immunol, 2014. **5**: p. 203.
7. Pearce, E.J. and B. Everts, *Dendritic cell metabolism.* Nat Rev Immunol, 2015. **15**(1): p. 18-29.
8. Everts, B., et al., *TLR-driven early glycolytic reprogramming via the kinases TBK1-IKKvarepsilon supports the anabolic demands of dendritic cell activation.* Nat Immunol, 2014. **15**(4): p. 323-32.
9. Everts, B., et al., *Commitment to glycolysis sustains survival of NO-producing inflammatory dendritic cells.* Blood, 2012. **120**(7): p. 1422-31.
10. Pantel, A., et al., *Direct type I IFN but not MDA5/TLR3 activation of dendritic cells is required for maturation and metabolic shift to glycolysis after poly IC stimulation.* PLoS Biol, 2014. **12**(1): p. e1001759.
11. Hammad, H., et al., *Activation of peroxisome proliferator-activated receptor-gamma in dendritic cells inhibits the development of eosinophilic airway inflammation in a mouse model of asthma.* Am J Pathol, 2004. **164**(1): p. 263-71.
12. Khare, A., et al., *Cutting Edge: Dual Function of PPARgamma in CD11c+ Cells Ensures Immune Tolerance in the Airways.* J Immunol, 2015. **195**(2): p. 431-5.
13. Legutko, A., et al., *Sirtuin 1 promotes Th2 responses and airway allergy by repressing peroxisome proliferator-activated receptor-gamma activity in dendritic cells.* J Immunol, 2011. **187**(9): p. 4517-29.
14. Nieves, W., et al., *Myeloid-Restricted AMPKalpha1 Promotes Host Immunity and Protects against IL-12/23p40-Dependent Lung Injury during Hookworm Infection.* J Immunol, 2016. **196**(11): p. 4632-40.
15. Mihaylova, M.M. and R.J. Shaw, *The AMPK signalling pathway coordinates cell growth, autophagy and metabolism.* Nat Cell Biol, 2011. **13**(9): p. 1016-23.
16. Tussiwand, R., et al., *Klf4 expression in conventional dendritic cells is required for T helper 2 cell responses.* Immunity, 2015. **42**(5): p. 916-28.
17. Mildner, A. and S. Jung, *Development and function of dendritic cell subsets.* Immunity, 2014. **40**(5): p. 642-56.
18. Liao, X., et al., *Kruppel-like factor 4 is critical for transcriptional control of cardiac mitochondrial homeostasis.* J Clin Invest, 2015. **125**(9): p. 3461-76.

19. Huang, S.C., et al., *Metabolic Reprogramming Mediated by the mTORC2-IRF4 Signaling Axis Is Essential for Macrophage Alternative Activation.* Immunity, 2016. **45**(4): p. 817-830.
20. Monticelli, L.A., et al., *Arginase 1 is an innate lymphoid-cell-intrinsic metabolic checkpoint controlling type 2 inflammation.* Nat Immunol, 2016. **17**(6): p. 656-65.
21. Morris, S.M., Jr., *Arginine Metabolism Revisited.* J Nutr, 2016. **146**(12): p. 2579s-2586s.
22. Xu, W., et al., *Increased mitochondrial arginine metabolism supports bioenergetics in asthma.* J Clin Invest, 2016. **126**(7): p. 2465-81.
23. Bando, J.K., et al., *Type 2 innate lymphoid cells constitutively express arginase-I in the naive and inflamed lung.* J Leukoc Biol, 2013. **94**(5): p. 877-84.
24. Salmond, R.J., et al., *IL-33 induces innate lymphoid cell-mediated airway inflammation by activating mammalian target of rapamycin.* J Allergy Clin Immunol, 2012. **130**(5): p. 1159-1166.e6.
25. Marçais, A., et al., *The metabolic checkpoint kinase mTOR is essential for IL-15 signaling during the development and activation of NK cells.* Nat Immunol, 2014. **15**(8): p. 749-757.
26. Xia, P., et al., *Insulin-InsR signaling drives multipotent progenitor differentiation toward lymphoid lineages.* J Exp Med, 2015. **212**(13): p. 2305-21.
27. Guo, F., et al., *Mouse gene targeting reveals an essential role of mTOR in hematopoietic stem cell engraftment and hematopoiesis.* Haematologica, 2013. **98**(9): p. 1353-8.
28. Martelli, A.M., et al., *The emerging role of the phosphatidylinositol 3-kinase/Akt/mammalian target of rapamycin signaling network in normal myelopoiesis and leukemogenesis.* Biochim Biophys Acta, 2010. **1803**(9): p. 991-1002.
29. Buck, M.D., et al., *Mitochondrial Dynamics Controls T Cell Fate through Metabolic Programming.* Cell, 2016. **166**(1): p. 63-76.
30. Michalek, R.D., et al., *Cutting edge: distinct glycolytic and lipid oxidative metabolic programs are essential for effector and regulatory CD4+ T cell subsets.* J Immunol, 2011. **186**(6): p. 3299-303.
31. Shi, L.Z., et al., *HIF1alpha-dependent glycolytic pathway orchestrates a metabolic checkpoint for the differentiation of TH17 and Treg cells.* J Exp Med, 2011. **208**(7): p. 1367-76.
32. Yang, J.Q., et al., *RhoA orchestrates glycolysis for TH2 cell differentiation and allergic airway inflammation.* J Allergy Clin Immunol, 2016. **137**(1): p. 231-245.e4.
33. Yang, K., et al., *T cell exit from quiescence and differentiation into Th2 cells depend on Raptor-mTORC1-mediated metabolic reprogramming.* Immunity, 2013. **39**(6): p. 1043-56.
34. Seumois, G., et al., *Transcriptional Profiling of Th2 Cells Identifies Pathogenic Features Associated with Asthma.* J Immunol, 2016. **197**(2): p. 655-64.
35. Delgoffe, G.M., et al., *The kinase mTOR regulates the differentiation of helper T cells through the selective activation of signaling by mTORC1 and mTORC2.* Nat Immunol, 2011. **12**(4): p. 295-303.
36. Heikamp, E.B., et al., *The AGC kinase SGK1 regulates TH1 and TH2 differentiation downstream of the mTORC2 complex.* Nat Immunol, 2014. **15**(5): p. 457-64.

37. Lee, K., et al., *Mammalian target of rapamycin protein complex 2 regulates differentiation of Th1 and Th2 cell subsets via distinct signaling pathways.* Immunity, 2010. **32**(6): p. 743-53.
38. Sauzeau, V., et al., *A transcriptional cross-talk between RhoA and c-Myc inhibits the RhoA/Rock-dependent cytoskeleton.* Oncogene, 2010. **29**(26): p. 3781-92.
39. Wang, R., et al., *The transcription factor Myc controls metabolic reprogramming upon T lymphocyte activation.* Immunity, 2011. **35**(6): p. 871-82.
40. Zeng, H., et al., *mTORC1 and mTORC2 Kinase Signaling and Glucose Metabolism Drive Follicular Helper T Cell Differentiation.* Immunity, 2016. **45**(3): p. 540-554.
41. Ray, J.P., et al., *The Interleukin-2-mTORc1 Kinase Axis Defines the Signaling, Differentiation, and Metabolism of T Helper 1 and Follicular B Helper T Cells.* Immunity, 2015. **43**(4): p. 690-702.
42. Doughty, C.A., et al., *Antigen receptor-mediated changes in glucose metabolism in B lymphocytes: role of phosphatidylinositol 3-kinase signaling in the glycolytic control of growth.* Blood, 2006. **107**(11): p. 4458-65.
43. DeFranco, A.L., E.S. Raveche, and W.E. Paul, *Separate control of B lymphocyte early activation and proliferation in response to anti-IgM antibodies.* J Immunol, 1985. **135**(1): p. 87-94.
44. Cho, S.H., et al., *Germinal centre hypoxia and regulation of antibody qualities by a hypoxia response system.* Nature, 2016. **537**(7619): p. 234-238.
45. Caro-Maldonado, A., et al., *Metabolic reprogramming is required for antibody production that is suppressed in anergic but exaggerated in chronically BAFF-exposed B cells.* J Immunol, 2014. **192**(8): p. 3626-36.
46. Cho, S.H., et al., *Glycolytic rate and lymphomagenesis depend on PARP14, an ADP ribosyltransferase of the B aggressive lymphoma (BAL) family.* Proc Natl Acad Sci U S A, 2011. **108**(38): p. 15972-7.
47. Dufort, F.J., et al., *Cutting edge: IL-4-mediated protection of primary B lymphocytes from apoptosis via Stat6-dependent regulation of glycolytic metabolism.* J Immunol, 2007. **179**(8): p. 4953-7.
48. Cho, S.H., et al., *B cell-intrinsic and -extrinsic regulation of antibody responses by PARP14, an intracellular (ADP-ribosyl)transferase.* J Immunol, 2013. **191**(6): p. 3169-78.
49. Phong, B., et al., *Cutting Edge: Murine Mast Cells Rapidly Modulate Metabolic Pathways Essential for Distinct Effector Functions.* J Immunol, 2017. **198**(2): p. 640-644.
50. Takei, M. and K. Endo, *Histamine release and calcium concentrations in rat mast cells are dependent on intracellular ATP: effects of prostaglandin D2.* Prostaglandins Leukot Essent Fatty Acids, 1994. **50**(6): p. 357-62.
51. Zhang, B., et al., *Human mast cell degranulation and preformed TNF secretion require mitochondrial translocation to exocytosis sites: relevance to atopic dermatitis.* J Allergy Clin Immunol, 2011. **127**(6): p. 1522-31.e8.
52. Erlich, T.H., et al., *Mitochondrial STAT3 plays a major role in IgE-antigen-mediated mast cell exocytosis.* J Allergy Clin Immunol, 2014. **134**(2): p. 460-9.
53. Sharkia, I., et al., *Pyruvate dehydrogenase has a major role in mast cell function, and its activity is regulated by mitochondrial microphthalmia transcription factor.* J Allergy Clin Immunol, 2017. **140**(1): p. 204-214.e8.

54. Sumbayev, V.V., et al., *Involvement of hypoxia-inducible factor-1 HiF(1alpha) in IgE-mediated primary human basophil responses*. Eur J Immunol, 2009. **39**(12): p. 3511-9.
55. Weichhart, T., M. Hengstschlager, and M. Linke, *Regulation of innate immune cell function by mTOR*. Nat Rev Immunol, 2015. **15**(10): p. 599-614.
56. David, J.R., et al., *Antibody-dependent, eosinophil-mediated damage to 51Cr-labeled schistosomula of Schistosoma mansoni: effect of metabolic inhibitors and other agents which alter cell function.* J Immunol, 1977. **118**(6): p. 2221-9.
57. Cham, C.M., et al., *Glucose deprivation inhibits multiple key gene expression events and effector functions in CD8+ T cells*. Eur J Immunol, 2008. **38**(9): p. 2438-50.
58. Gubser, P.M., et al., *Rapid effector function of memory CD8+ T cells requires an immediate-early glycolytic switch*. Nat Immunol, 2013. **14**(10): p. 1064-72.
59. Mills, E.L. and L.A. O'Neill, *Reprogramming mitochondrial metabolism in macrophages as an anti-inflammatory signal*. Eur J Immunol, 2016. **46**(1): p. 13-21.
60. Huang, S.C., et al., *Cell-intrinsic lysosomal lipolysis is essential for alternative activation of macrophages.* Nat Immunol, 2014. **15**(9): p. 846-55.
61. Van den Bossche, J., et al., *Mitochondrial Dysfunction Prevents Repolarization of Inflammatory Macrophages*. Cell Rep, 2016. **17**(3): p. 684-696.
62. Covarrubias, A.J., et al., *Akt-mTORC1 signaling regulates Acly to integrate metabolic input to control of macrophage activation.* Elife, 2016. **5**.
63. Tan, Z., et al., *Pyruvate dehydrogenase kinase 1 participates in macrophage polarization via regulating glucose metabolism*. J Immunol, 2015. **194**(12): p. 6082-9.
64. O'Sullivan, D., et al., *Memory CD8(+) T cells use cell-intrinsic lipolysis to support the metabolic programming necessary for development.* Immunity, 2014. **41**(1): p. 75-88.
65. Kang, K., et al., *Adipocyte-derived Th2 cytokines and myeloid PPARdelta regulate macrophage polarization and insulin sensitivity*. Cell Metab, 2008. **7**(6): p. 485-95.
66. Odegaard, J.I., et al., *Macrophage-specific PPARgamma controls alternative activation and improves insulin resistance.* Nature, 2007. **447**(7148): p. 1116-20.
67. Odegaard, J.I., et al., *Alternative M2 activation of Kupffer cells by PPARdelta ameliorates obesity-induced insulin resistance*. Cell Metab, 2008. **7**(6): p. 496-507.
68. Szanto, A., et al., *STAT6 transcription factor is a facilitator of the nuclear receptor PPARγ-regulated gene expression in macrophages and dendritic cells*. Immunity, 2010. **33**(5): p. 699-712.
69. Oh, J., et al., *Endoplasmic reticulum stress controls M2 macrophage differentiation and foam cell formation.* J Biol Chem, 2012. **287**(15): p. 11629-41.
70. Shan, B., et al., *The metabolic ER stress sensor IRE1α suppresses alternative activation of macrophages and impairs energy expenditure in obesity.* Nat Immunol, 2017. **18**(5): p. 519-529.
71. Jha, A.K., et al., *Network integration of parallel metabolic and transcriptional data reveals metabolic modules that regulate macrophage polarization*. Immunity, 2015. **42**(3): p. 419-30.
72. Hallowell, R.W., et al., *mTORC2 signalling regulates M2 macrophage differentiation in response to helminth infection and adaptive thermogenesis.* Nat Commun, 2017. **8**: p. 14208.
73. Zhu, L., et al., *TSC1 controls macrophage polarization to prevent inflammatory disease.* Nat Commun, 2014. **5**: p. 4696.

74. Nomura, M., et al., *Fatty acid oxidation in macrophage polarization.* Nat Immunol, 2016. **17**(3): p. 216-7.
75. Namgaladze, D. and B. Brüne, *Fatty acid oxidation is dispensable for human macrophage IL-4-induced polarization.* Biochim Biophys Acta, 2014. **1841**(9): p. 1329-35.
76. Chang, C.H., et al., *Posttranscriptional control of T cell effector function by aerobic glycolysis.* Cell, 2013. **153**(6): p. 1239-51.
77. Maarsingh, H., J. Zaagsma, and H. Meurs, *Arginase: a key enzyme in the pathophysiology of allergic asthma opening novel therapeutic perspectives.* Br J Pharmacol, 2009. **158**(3): p. 652-64.
78. Barron, L., et al., *Role of arginase 1 from myeloid cells in th2-dominated lung inflammation.* PLoS One, 2013. **8**(4): p. e61961.
79. Cloots, R.H., et al., *Ablation of Arg1 in hematopoietic cells improves respiratory function of lung parenchyma, but not that of larger airways or inflammation in asthmatic mice.* Am J Physiol Lung Cell Mol Physiol, 2013. **305**(5): p. L364-76.

Acknowledgements

We thank B.M.F.W., M.Y., and B.G.A.G. for critical reading of the manuscript. This work was supported by an LUMC fellowship and Marie Curie CIG to B.E.

Conflict of interest

The authors declare no financial or commercial conflict of interest.

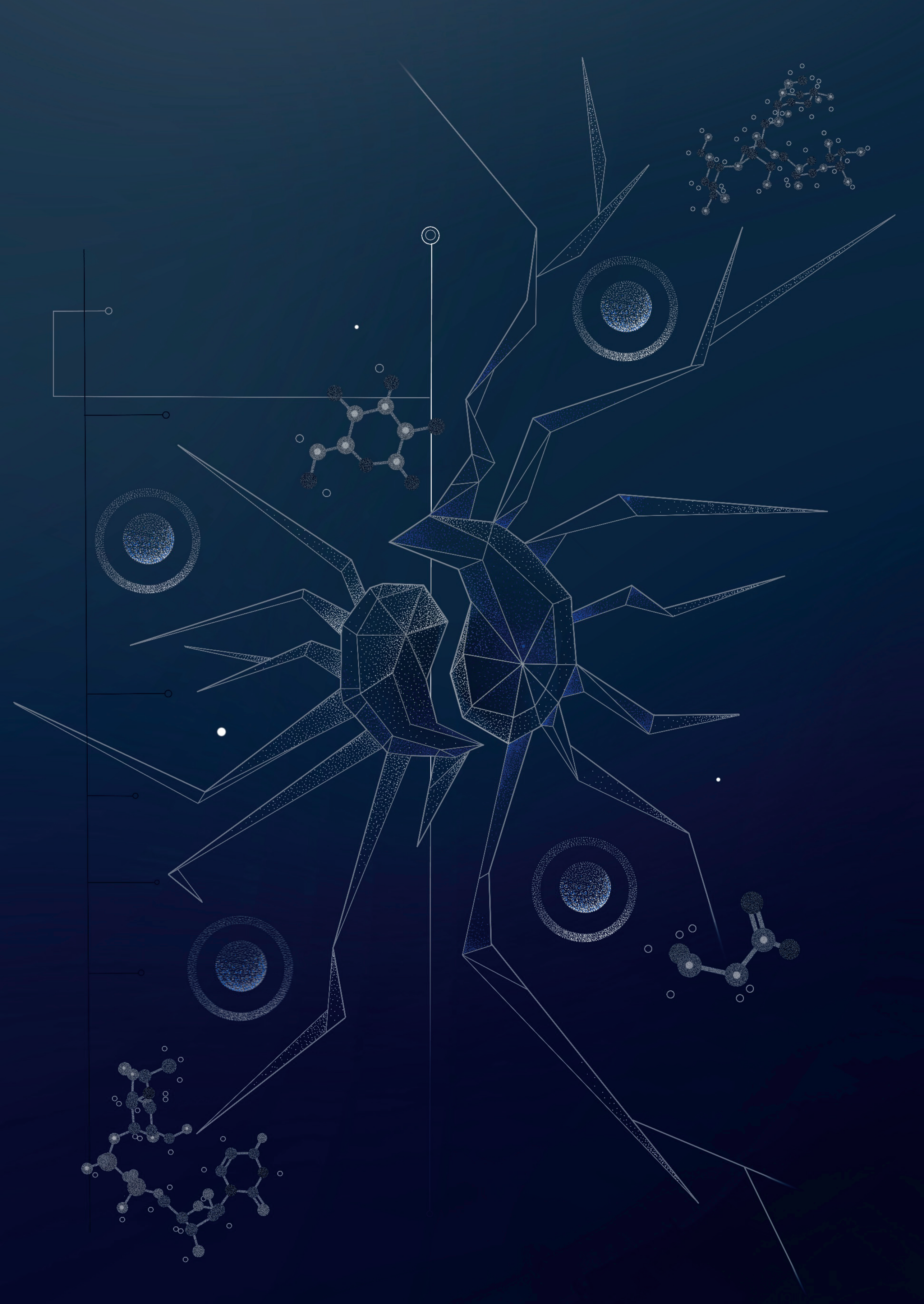

7

Protein O-GlcNAcylation and low glycolysis underpin Th2 polarization by dendritic cells

Leonard R. Pelgrom
Alexey A. Sergushichev
Marjolein Quik
Alwin J. van der Ham
Lisa W. Bloemberg
Beatrice M. F. Winkel
Gabriele Schramm
Cornelis H. Hokke
Meta Roestenberg
Maxim N. Artyomov
Bart Everts

Manuscript in preparation

Abstract

Activation of dendritic cells (DCs) for priming of T cell responses is dependent on rewiring of their cellular metabolism. However, the metabolic characteristics of and requirements for DCs to prime T helper 2 (Th2) responses are unknown. Using unbiased transcriptomics and non-targeted metabolomics we show here that helminth antigen-conditioned human DCs with the ability to drive Th2 polarization can be distinguished from unstimulated DCs and other Th-priming DCs by a unique metabolic signature of suppressed glycolytic activity, and elevated abundance of hexosamine biosynthesis pathway metabolites including UDP-GlcNAc which is the key substrate of O-GlcNAcylation, a post-translational modification of intracellular proteins. This metabolic reprogramming is functionally important specifically for priming of Th2 responses as suppression of glycolysis was sufficient to condition DCs for Th2 polarization. Furthermore, inhibition of O-GlcNAcylation in DCs impaired their ability to drive Th2, but not Th1 or Th17 responses. These findings were corroborated in experiments with DCs stimulated with allergens. Finally, a controlled human infection trial with the parasitic hookworm *Necator americanus* revealed a consistent increase in intracellular O-GlcNAcylation in circulating CD1c+ type 2 conventional DCs, but not in CD141+ cDC1s and CD123+ pDCs, providing credence for relevance of this pathway in humans. In summary, we uncovered a unique metabolic program in DCs selectively required for Th2 polarization which may aid in the development of therapeutic strategies aimed at modulating type 2 immunity.

Introduction

Type 2 immune responses are crucial for controlling parasitic helminth infections and mediating tissue repair. Additionally, they can confer protection against development of type 2 diabetes and atherosclerosis which is a major cause of cardiovascular disease. However, overzealous type 2 immunity can lead to allergies and support tumor growth [1]. This growing evidence of type 2 immunity's crucial role in the development and outcome of several important diseases signifies the importance of better understanding how they are initiated.

Dendritic cells (DCs) are the quintessential antigen presenting cell of the innate immune system. Antigen presentation and costimulatory signals provided by DCs allow them to induce T cell activation. Additionally, polarizing cytokines secreted by DCs instruct T cells to undergo specific differentiation programs [2]. As such, they play a key role in the initiation and regulation of type 2 immune responses by governing the priming and polarization of T helper (Th) 2 responses. The importance of DCs in type 2 immune responses indicates the need for better understanding of the mechanisms through which DCs initiate these responses, which could aid the development of novel therapeutic interventions for diseases in which type 2 immune responses are involved.

There is a longstanding interest in delineating signals, i.e. cytokines and membrane-bound proteins, expressed by DCs that instruct Th cells to initiate a certain differentiation program. These polarizing signals have been extensively characterized in the context of priming of Th1, Th17 and regulatory T (Treg) cell responses. However, for Th2-priming DCs these remain poorly defined. In part this stems from the fact that Th2-priming DCs do not appear to secrete polarizing cytokines analogous to IL-12, IL-23, or TGFβ that contribute to Th1, Th17 or Treg differentiation, respectively [3, 4].

Apart from studying immunological features to understand how DCs function, there is a growing appreciation that cellular metabolism plays a central role in regulation of DC biology [5, 6]. It is now clear that activation and their ability to prime T cell responses is accompanied by and underpinned by specific metabolic reprogramming [7]. Activation, migration, and production of pro-inflammatory cytokine production of DCs is dependent on aerobic glycolysis [8-11]. Moreover, evidence is emerging that the unique immunological signatures that differentiate DCs with different Th cell-priming capacities are paralleled and supported by distinct metabolic signatures [7]. The production of the Th1-priming cytokine interleukin (IL)-12 [8, 10, 11] and Th17-priming IL-6 are dependent on glycolysis [12]. The conditioning of human monocyte-derived DCs (moDCs) for a tolerogenic phenotype is also dependent on glycolysis [13, 14], either independently from [13] or coupled to high mitochondrial respiration [14], depending on the tolerogenic compounds used. Likewise, DCs that were rendered tolerogenic by the tumor microenvironment *in vivo*, relied on fatty acid oxidation for their ability to promote Treg responses [15]. On the other hand, the metabolic properties of Th2-priming DCs and the metabolic programs that support their ability to prime a Th2 response are still poorly defined. Thus far, the best metabolic description of DCs that can potentially prime Th2 cells comes from a recent study comparing the metabolism of *in vitro*-cultured murine DCs after conditioning with strong and weak stimuli [9]. In this study, stimulation with allergenic house dust mite led to an early induction of glycolysis, as did stimulation with bacterial lipopolysaccharides or yeast β-glucans that were depleted of their toll-like receptor (TLR) ligands (= tolerogenic DC associated). There were differences however in the metabolic signaling pathways associated and the duration of glycolytic reprogramming. Nevertheless, the T cell-priming capacity of these DCs and their dependence on unique metabolic states was not evaluated [9].

Therefore, in the present study, we set out to characterize the metabolic properties of Th2-priming DCs and define which metabolic programs license these cells for Th2 polarization. To this end, we used the combined experimental and computational pipeline of concordant metabolomics integration with transcription (CoMBI-T), previously applied in macrophages [16], to define the metabolic signature of human DCs conditioned to prime Th2 responses and to compare that to those of Th1- and Th17-priming DCs. We found that Th2-priming DCs can be distinguished from Th1- and Th17-priming DCs by their reduced glycolytic potential; a metabolic feature that in itself was sufficient to condition DCs for Th2 priming. Moreover, these Th2-priming DCs displayed a distinct metabolic signature of UDP-GlcNAc synthesis and O-GlcNAc transferase (OGT) enzyme expression. Blocking protein O-GlcNAcylation, either pharmacologically or genetically, selectively reduced the Th2-priming capacity of these DCs. Together, these findings define low glycolysis and protein O-GlcNAcylation as unique metabolic requirements for Th2 polarization by DCs. These requirements may be amenable for modulation in therapeutic settings to shape type 2 immune responses.

Results

Inhibition of glycolysis in DCs is associated with Th2 priming

As a model to study the metabolic properties of and requirements for Th2 polarization by DCs, we used the schistosome-derived glycoprotein omega-1 to condition moDCs for Th2 priming (Th2-DCs). Omega-1 is a well-studied and potent inducer of Th2 responses both *in vitro* and *in vivo* [17-19]. The transcriptome of these Th2-DCs was compared to those of unstimulated (iDCs), LPS+PolyIC-stimulated Th1-priming (Th1-DCs) and zymosan-stimulated Th17-priming DCs (Th17-DCs; Figure 1A-B and S1A-B). As previously reported, Th2-DCs did not display a strong upregulation of costimulatory molecules nor cytokine production, unlike Th1- and Th17- DCs (Figure S1C-F & [20]). In line with this muted activation profile, the transcriptome of Th2-DCs did not differ as much from iDCs as the transcriptomes of Th1-DCs and Th17-DCs. Nevertheless, the overall transcriptome of Th2-DCs was clearly distinct from iDCs (Figure 1C). Next, we generated transcriptional clusters with genes related to cellular metabolism that can be used to distinguish these DCs with distinct Th-priming capacities (Figure 1D). Pathway analysis was performed on overrepresented genes within those clusters to elucidate which metabolic pathways best represent these clusters. This analysis uncovered 4 metabolic clusters - in which genes related to glycolysis (Cluster 3), citrate metabolism (Cluster 8), glycerophospholipid metabolism (Cluster 9) and gonadotropin-releasing hormone (Cluster 11) were most significantly overrepresented - that could differentiate Th2-DCs from iDCs (Figure 1D). Of these clusters, only glycolysis (Figure 1E and S2A) and glycerophospholipid metabolism could be used to additionally distinguish Th2-DCs from Th1-DCs and Th17-DCs.

To establish the biological relevance of these findings we analyzed the glycolytic flux in differently conditioned DCs. Baseline rates of glycolysis were not significantly lower in Th2-DCs compared to iDCs as determined by extracellular flux (XF) analysis (Figure 1F) and lactate release (Figure 1G). Nonetheless, maximal glycolytic capacity (Figure 1F) and LPS-induced glycolytic reprogramming were impaired in Th2-DCs (Figure 1H-I). In contrast, Th1-DCs and Th17-DCs displayed strongly increased glycolytic rates, glycolytic capacity, and lactate release (Figure 1G). Th2-DCs did not compensate for a lower glycolytic flux by heightening the production of ATP through oxidative phosphorylation. In fact, consistent with the reduced expression of genes involved in TCA cycle metabolism (Figure S2B-C), Th2-DCs displayed the lowest mitochondrial respiratory activity of all DCs, both in terms of baseline and maximal respiration as well as oxygen consumption linked to ATP synthesis (Figure S3). This observation indicates a low overall bioenergetic status of Th2-DCs.

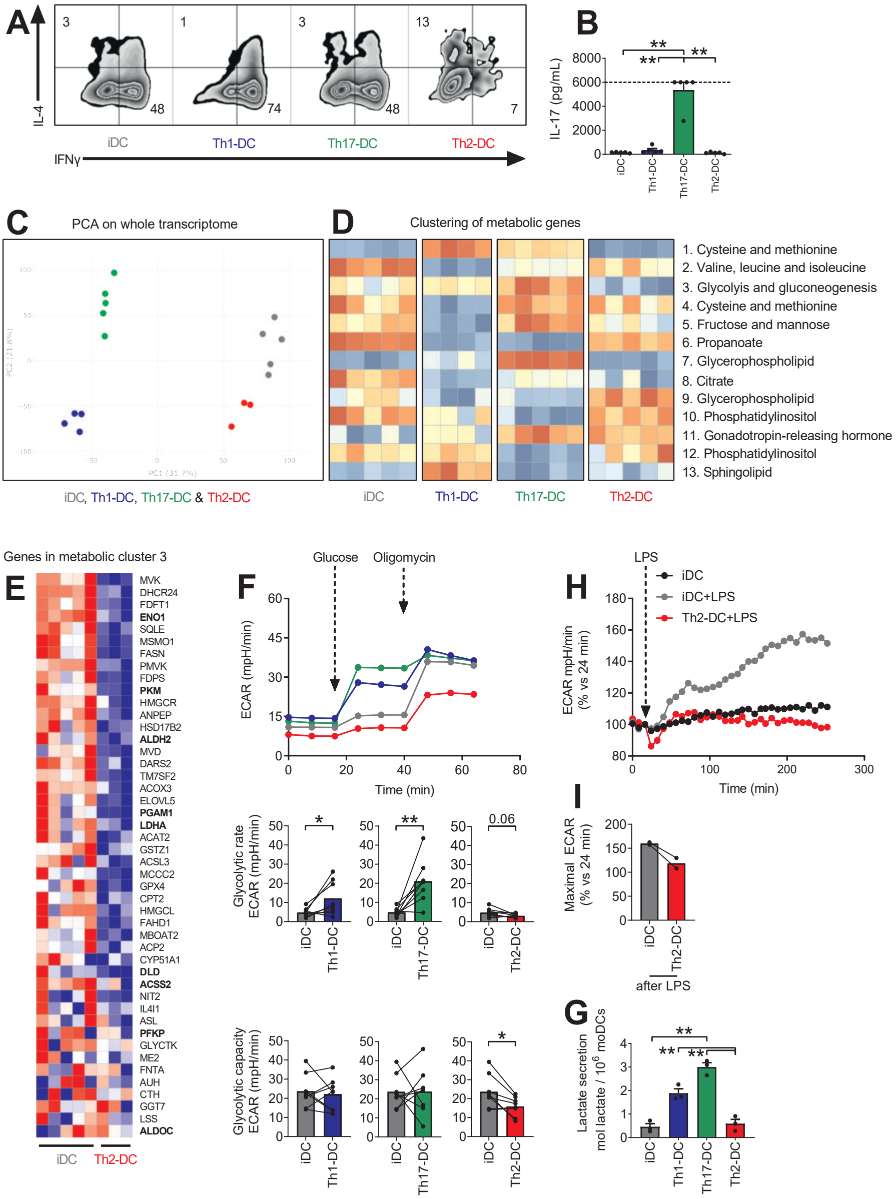
A
IL-4
IFNγ
3
48
1
74
3
48
13
7
iDC
Th1-DC
Th17-DC
Th2-DC
B
IL-17 (pg/mL)
8000
6000
4000
2000
0
**
**
**
iDC
Th1-DC
Th17-DC
Th2-DC
C
PCA on whole transcriptome
PC1 (31.7%)
PC2 (21.8%)
iDC, Th1-DC, Th17-DC & Th2-DC
D
Clustering of metabolic genes
1. Cysteine and methionine
2. Valine, leucine and isoleucine
3. Glycolyis and gluconeogenesis
4. Cysteine and methionine
5. Fructose and mannose
6. Propanoate
7. Glycerophospholipid
8. Citrate
9. Glycerophospholipid
10. Phosphatidylinositol
11. Gonadotropin-releasing hormone
12. Phosphatidylinositol
13. Sphingolipid
iDC
Th1-DC
Th17-DC
Th2-DC
Genes in metabolic cluster 3
E
MVK
DHCR24
FDFT1
ENO1
SQLE
MSMO1
FASN
PMVK
FDPS
PKM
HMGCR
ANPEP
HSD17B2
ALDH2
MVD
DARS2
TM7SF2
ACOX3
ELOVL5
PGAM1
LDHA
ACAT2
GSTZ1
ACSL3
MCCC2
GPX4
CPT2
HMGCL
FAHD1
MBOAT2
ACP2
CYP51A1
DLD
ACSS2
NIT2
IL4I1
ASL
PFKP
GLYCTK
ME2
FNTA
AUH
CTH
GGT7
LSS
ALDOC
iDC
Th2-DC
F
Glucose
Oligomycin
ECAR (mpH/min)
Time (min)
Glycolytic rate ECAR (mpH/min)
*
**
0.06
Glycolytic capacity ECAR (mpH/min)
*
iDC
Th1-DC
Th17-DC
Th2-DC
H
LPS
iDC
iDC+LPS
Th2-DC+LPS
ECAR mpH/min (% vs 24 min)
Time (min)
I
Maximal ECAR (% vs 24 min)
after LPS
G
Lactate secretion mol lactate / 10^6 moDCs
**
**
**

Figure 1. Inhibition of glycolysis in DCs is associated with Th2 priming.

Human moDCs were left untreated (iDC in grey) or stimulated for 24h with either LPS+PolyIC (Th1-DC in dark blue), zymosan (Th17-DC in green) or omega-1 (Th2-DC in red). Supernatants were then collected for determination of extracellular lactate (F) and DCs were set aside for either co-culture with allogeneic T cells (A-B), RNA-sequencing (C-E) and measurements of glycolysis using extracellular flux (XF) analysis (F, H-I).
(A) Representative histograms of T cell intracellular IFNγ and IL-4 that was analyzed by flow cytometry after a 6h stimulation with phorbol myristate acetate (PMA) and ionomycin. T cells used were naïve and the culture was 11 days.
(B) Co-culture with memory T cells. Supernatants were collected after 5 days and IL-17 concentrations was determined by ELISA.
(C) Principle component analysis on total transcriptome of differently conditioned DCs.
(D) Metabolic genes were selected out of the total transcriptome of differently conditioned DCs and used to form 13 clusters with maximal distinguishing power. Different clusters with distinct combination of genes were sometimes part of the same pathway in the KEGG database (e.g. cluster 1 and 4 = cysteine and methionine metabolism).
(E) Overview of genes in metabolic cluster 3. Genes that represented more in a DC type relative to the other are in red and genes that are represented less are in blue. Genes that are part of the KEGG pathway Glycolysis / Gluconeogenesis are highlighted in bold.
(F) Glycolytic stress test in Seahorse XF analyzer which consists of sequential injections of glucose and the ATP synthase inhibitor oligomycin after which extracellular medium acidification rate (ECAR) is measured as a proxy for glycolysis-derived lactate. Glycolytic rate = the difference before and after injection of glucose. Glycolytic capacity = the difference before injection glucose and after infection of oligomycin.
(G) Lactate concentration was determined by measuring absorbance of NADH at 340 nm after the reaction of lactate with NAD by reaction with NAD by lactate dehydrogenase into pyruvate and NADH.
(H-I) Real-time changes in the ECAR of DCs treated with LPS.
The number of independent experiments is represented by symbols in the graphs and shown as mean ± SEM; $*p < 0.05$, $**p < 0.01$

7

Inhibition of glycolysis in DCs is sufficient for Th2 priming

This association between reduced glycolysis in Th2-DCs and their Th2-priming capacity led us to ask if lower glycolytic engagement may be functionally linked to the Th2-priming capacity of these cells. Indeed, inhibition of glycolysis using 2-deoxyglucose (2-DG) – a competitive inhibitor of hexokinase, the first enzyme in glycolysis and the first rate-limiting step of this pathway - was in itself sufficient to condition both unstimulated and LPS-activated DCs for Th2 priming (2-DG-DCs; Figure 2A-B). This observation suggests an important functional role for this type of metabolic rewiring in Th2 priming by DCs. A common characteristic of Th2-priming DCs and prerequisite for efficient Th2 priming is low IL-12 expression [17-19, 21, 22]. Indeed, 2-DG-DCs secreted little IL-12 following CD40 ligation (Figure 2C). Furthermore, 2-DG-DCs selectively displayed increased CD86 surface expression (Figure 2E), which in some contexts has been implicated as a necessary costimulatory signal by DCs to mount Th2 responses *in vivo* [23, 24]. Taken together, these data show that lower glycolytic activity is one of the defining characteristics of Th2-priming DCs and suggest this is functionally linked to their ability to prime this Th cell response.

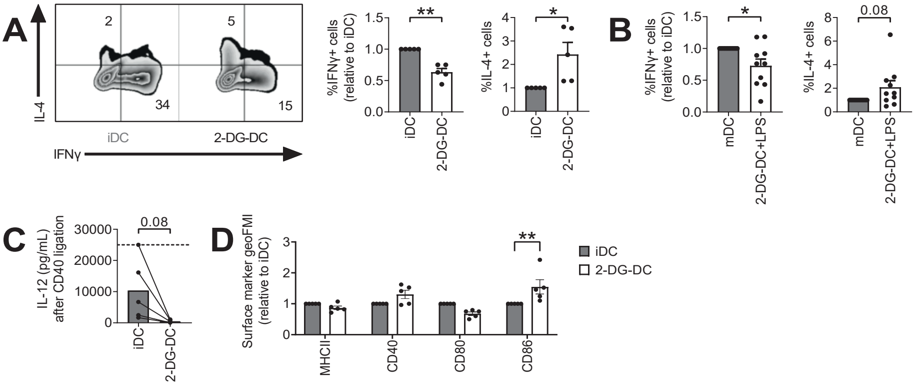

Figure 2. Inhibition of glycolysis in DCs is sufficient for Th2 priming.

Human moDCs were left untreated (iDC in grey) or stimulated for 24h with 2-deoxyglucose (2-DG-DC in white). Supernatants were then collected for determination of IL-10 secretion (D) and DCs were set aside for either co-culture with allogeneic T cells (A), determination of viability (B), IL-12p70 secretion after 24h co-culture with a CD40L expressing cell line (C) and maturation (E)
(A) On the left side, representative histograms of T cell intracellular IFNγ and IL-4 that was analyzed by flow cytometry after a 6h stimulation with phorbol myristate acetate (PMA) and ionomycin. T cells used were naïve and the culture was 11 days. On the right side, the percentages of T cells uniquely positive for either IFNγ or IL-4 are expressed relative to the iDC condition.
(B) Frequencies of dead DCs are enumerated using flow cytometry.
(C) Co-culture with CD40L expressing cell line. Supernatants were collected after 24 hours and IL-12p70 concentrations was determined by ELISA.
(D) Supernatants were collected after antigen stimulation and IL-10 concentrations was determined by ELISA.
(E) The expression of maturation makers – based on the geometric mean fluorescence – are shown relative to iDCs.
The number of independent experiments is represented by symbols in the graphs and shown as mean ± SEM; $*p < 0.05$, $**p < 0.01$

Enhanced hexosamine biosynthesis and O-GlcNAc transferase expression are unique to Th2-priming DCs

To further define and compare the metabolic characteristics of Th2-priming DCs, we additionally performed unbiased metabolomics using flow injection analysis mass spectrometry (FIA-MS) on the same cells that were used for RNA sequencing [16]. Metabolomics revealed only a handful of metabolites that significantly accumulated in Th2-DCs relative to iDCs. The majority of these are known substrates for glycosyltransferases (Fig 3A). To improve our chances of identifying important nodes of metabolic rewiring in a non-targeted manner, we performed an integrated network analysis of transcriptional and metabolomic data using our publicly available tool (GAM; [25]).

This integrated analysis corroborated results from our initial metabolic profiling based on transcriptomic data, as it identified a suppressed glycolytic pathway as one of the main metabolic signatures of Th2-DCs in comparison to iDCs (Figure 3B). However, this analysis now additionally uncovered a significantly upregulated metabolic module of metabolic enzymes and their substrates, which are involved in the post-translational modification of intracellular proteins by transfer of GlcNAc (i.e. O-GlcNAcylation) from uridine diphosphate N-acetylglucosamine (UDP-GlcNAc). Th2-DCs were found to express increased levels of the enzymes O-GlcNAc transferase (OGT) and O-GlcNAcase (OGA; encoded by the MGEA5 gene), which attach and remove O-GlcNAc moieties from proteins, respectively (Figure 3B and S4A). Their substrate/product UDP-GlcNAc was also elevated in Th2-DCs relative to iDCs, as was its precursor N-acetyl-glucsomine-1-phosphate. Finally, the abundance of several metabolites used in the hexosamine biosynthesis pathway (HBP) for the synthesis of UDP-GlcNAc were higher, including glutamine, glucose and acetyl-CoA (Figure 3B). These findings suggest that Th2-DCs specifically upregulate HBP flux to fuel O-GlcNAcylation. To better determine if this metabolic module is unique to Th2-DCs, we compared the mRNA expression of enzymes in the HBP and O-GlcNAcylation pathway between Th2- and Th1- and Th17-DCs. OGT mRNA was specifically upregulated in Th2-DCs compared to differently conditioned DCs, although this did not appear to translate into higher OGT protein expression 24 hours after stimulation with omega-1 (Figure S4B). In contrast, MGEA5 mRNA was upregulated in all Th-polarizing DCs compared to iDCs. Th2-DCs displayed higher expression of NAGK (also known as GNK) than Th1-DCs and Th17-DCs, while conversely, Th1-DCs and Th17-DCs showed higher expression of the rate-limiting enzymes of the HBP, GFPT1 and GFPT2 (also known as GFAT; Figure 3C). These data may suggest that Th2-DCs utilize different fuels for hexosamine synthesis than Th17- or Th1-DCs, as NAGK, the enzyme that mediates the conversion of glucosamine into glucosamine-6-phosphate, bypasses the need for glucose and glutamine by using glucosamine.

Taken together, these data show that in addition to suppressed glycolysis, Th2-priming DC are metabolically wired to increase synthesis of UDP-GlcNAc and other hexosamines, which may be used for supporting protein O-GlcNAcylation.

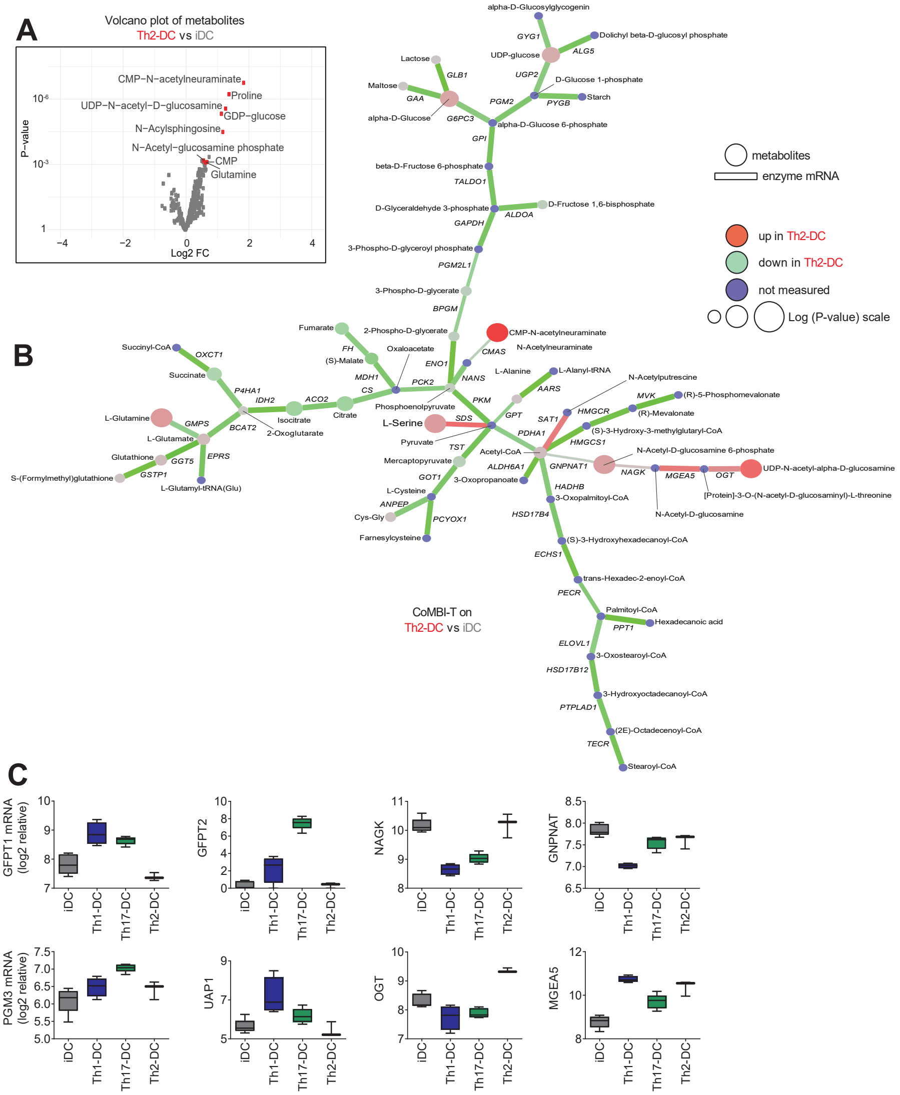
A
Volcano plot of metabolites
Th2-DC vs iDC
P-value
10^{-6}
10^{-3}
1
−4
−2
0
2
4
Log2 FC
CMP−N−acetylneuraminate
Proline
UDP−N−acetyl−D−glucosamine
GDP−glucose
N−Acylsphingosine
N−Acetyl−glucosamine phosphate
CMP
Glutamine
B
alpha-D-Glucosylglycogenin
GYG1
Dolichyl beta-D-glucosyl phosphate
ALG5
UDP-glucose
Lactose
GLB1
UGP2
D-Glucose 1-phosphate
Maltose
GAA
PGM2
Starch
PYGB
alpha-D-Glucose
G6PC3
alpha-D-Glucose 6-phosphate
GPI
beta-D-Fructose 6-phosphate
TALDO1
D-Glyceraldehyde 3-phosphate
D-Fructose 1,6-bisphosphate
ALDOA
GAPDH
3-Phospho-D-glyceroyl phosphate
PGM2L1
3-Phospho-D-glycerate
BPGM
Fumarate
2-Phospho-D-glycerate
CMP-N-acetylneuraminate
FH
Oxaloacetate
CMAS
N-Acetylneuraminate
(S)-Malate
ENO1
Succinyl-CoA
OXCT1
MDH1
PCK2
NANS
L-Alanine
L-Alanyl-tRNA
Succinate
CS
AARS
N-Acetylputrescine
P4HA1
IDH2
ACO2
PKM
MVK
(R)-5-Phosphomevalonate
Phosphoenolpyruvate
HMGCR
(R)-Mevalonate
L-Glutamine
GMPS
Isocitrate
Citrate
L-Serine
SDS
GPT
SAT1
BCAT2
2-Oxoglutarate
PDHA1
(S)-3-Hydroxy-3-methylglutaryl-CoA
L-Glutamate
Pyruvate
HMGCS1
EPRS
TST
Acetyl-CoA
N-Acetyl-D-glucosamine 6-phosphate
Glutathione
GGT5
Mercaptopyruvate
ALDH6A1
GNPNAT1
NAGK
MGEA5
OGT
UDP-N-acetyl-alpha-D-glucosamine
GSTP1
GOT1
3-Oxopropanoate
S-(Formylmethyl)glutathione
L-Glutamyl-tRNA(Glu)
HADHB
[Protein]-3-O-(N-acetyl-D-glucosaminyl)-L-threonine
L-Cysteine
3-Oxopalmitoyl-CoA
ANPEP
Cys-Gly
PCYOX1
HSD17B4
N-Acetyl-D-glucosamine
Farnesylcysteine
(S)-3-Hydroxyhexadecanoyl-CoA
ECHS1
trans-Hexadec-2-enoyl-CoA
CoMBI-T on
Th2-DC vs iDC
PECR
Palmitoyl-CoA
PPT1
Hexadecanoic acid
ELOVL1
3-Oxostearoyl-CoA
HSD17B12
3-Hydroxyoctadecanoyl-CoA
PTPLAD1
(2E)-Octadecenoyl-CoA
TECR
Stearoyl-CoA
metabolites
enzyme mRNA
up in Th2-DC
down in Th2-DC
not measured
Log (P-value) scale
C
GFPT1 mRNA (log2 relative)
GFPT2
NAGK
GNPNAT
PGM3 mRNA (log2 relative)
UAP1
OGT
MGEA5
iDC
Th1-DC
Th17-DC
Th2-DC

Figure 3. Integration of transcriptomic and metabolomic data reveals that enhanced hexosamine biosynthesis and O-GlcNAc transferase expression are unique to Th2-priming DCs.

Human moDCs were left untreated (iDC in grey) or stimulated for 24h with either LPS+PolyIC (Th1-DC in dark blue), zymosan (Th17-DC in green) or omega-1 (Th2-DC in red). DCs were then set aside for either flow injection analysis mass spectrometry (FIA-MS; A) or RNA-sequencing (C). Metabolomic and transcriptomic data sets were furthermore integrated using the GAM tool (B).
(A) Volcano plot showing metabolites differentially expressed between Th2-DC and iDC conditions. X axis shows log-fold change between Th2-DC and iDC conditions with positive values corresponding to metabolites upregulated in Th2-DCs. Y axis shows p value for corresponding metabolite. Top Th2-DC-specific metabolites are highlighted in red. (B) Most regulated subnetwork within the global human metabolic network that consists of enzymes and metabolites through the CoMBI-T profiling pipeline. Round nodes represent metabolites within core regulatory network. Enzymes are represented by square nodes. Differential expression of corresponding enzyme/metabolite is indicated by the size of the node, and fold-change by red (Th2-DC) to green (iDC) color scale. Enzymes in reactions with single product-substrate pair are represented by edges for visual convenience with thickness and color of the edge reflecting -log(p) and fold-change of differential expression correspondingly.
(C) Relative log mRNA expression of enzymes involved in protein O-GlcNAcylation (OGT and MGEA5) and the hexosamine biosynthesis pathway (HBP; rest) between differently conditioned DCs.

O-GlcNAcylation is required for Th2 priming by DCs but not for Th1 or Th17 priming

We next aimed to investigate if this signature of HBP activity and OGT expression was of functional importance to Th2-DCs. Inhibition of OGT using the pharmacological inhibitor ST045849 abolished the capacity of Th2-DCs to prime IL-4-producing Th2 cells, while the proportion of IFNγ-producing Th1 cells was not affected in these conditions (Figure 4A-B). Knockdown of OGT – using short interfering RNA – also abolished the Th2-priming capacity of Th2-DCs as well as their ability to suppress Th1 responses (Figure 4C). These T cells did not start producing IL-17 (Figure S5A) nor was their viability affected (Figure S5A-C). Importantly, OGT blockade in Th1- and Th17-DCs did not compromise their Th cell-polarizing ability (Figure 4D-E). This suggests a unique role for OGT-driven O-GlcNAcylation in the conditioning of DCs for Th2 priming. Interestingly, global protein O-GlcNAcylation levels as determined by flow cytometry (Figure 4F) and immunoblotting (Figure 4G) were similar between Th2-DCs and iDCs. This shows that the increased UDP-GlcNAc availability does not translate into an overall increased protein O-GlcNAcylation in Th2-DCs, but instead suggests that O-GlcNAcylation of a select number of proteins is potentially of importance for Th2 priming by DCs. UDP-GlcNAc can also serve as a substrate for N- and O-glycosylation. However, the N-glycosylation inhibitor tunicamycin did not affect the Th2-priming capacity of Th2-DCs (Figure 4A-B). Instead it specifically limited the ability of Th1-DCs to induce IFNγ production by T cells (Figure 4E) without promoting a switch to a different Th phenotype (Figure S5D-E). Neither ST045849 treatment, nor OGT silencing or tunicamycin treatment negatively impacted DC survival (Figure S5-F-G). Taken together, these data show that the transfer of GlcNAc from UDP-GlcNAc onto proteins by OGT is uniquely important for Th2 priming by DCs.

To start exploring mechanistically how O-GlcNAcylation in DCs is linked to their Th2-priming capacity, we first assessed whether silencing of OGT prevented surface marker expression or cytokine secretion by Th2-DCs. However, silencing of OGT did not change MHCII and CD40 surface expression (Figure S6A) nor IL-12 and IL-10 secretion (Figure S6A). Recent reports have implicated type I IFN signaling in DC-driven Th2 responses *in vivo* [24, 26]. Moreover, it was recently demonstrated that O-GlcNAcylation of mitochondrial anti-viral-signaling protein (MAVS) can enhance the interferon regulatory factor 3 (IRF3)-mediated production of type I IFNs [27]. Indeed, a non-targeted approach by performing gene set enrichment analysis on the differentially expressed genes between Th2-DCs and iDCs revealed type I interferon (IFN) signaling as the top pathway differentiating Th2-DCs from iDCs (Figure S6C). This may provide a first lead through which mechanism O-GlcNAcylation supports Th2 priming by DCs.

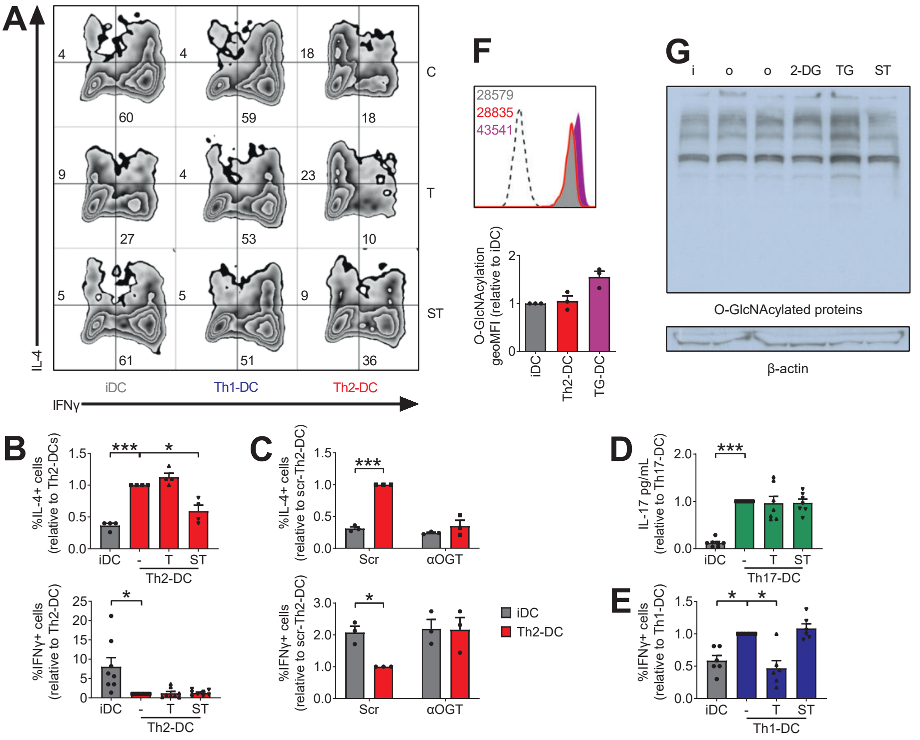

Figure 4. O-GlcNAcylation is required for Th2 priming by DCs but not for Th1 or Th17 priming.

Human moDCs were differentiated as normally (A-B, D-G) or short interfering RNA was introduced against O-GlcNAc transferase (OGT) at day 4 (C). Scrambled RNA was used as a control. At day 6, DCs were stimulated as normal with either LPS+PolyIC (Th1-DC in dark blue), zymosan (Th17-DC in green), omega-1 (Th2-DC in red / o), 2-deoxyglucose (2-DG-DC in white / 2-DG), Thiamet G (TG-DC in black / TG) or ST045849 (ST) for 24 hours, left untreated (iDC in grey / i), or first pre-incubated with inhibitors of O-GlcNAcylation (ST045849 [ST]), N-glycosylation (tunicamycin [T] for 30 minutes, or left untreated [C]. DCs were then set aside for either co-culture with allogeneic T cells (A-E) or determination of overall protein O-GlcNAcylation using flow cytometry (F) or western blotting (G).
(A) Representative histograms of T cell intracellular IFNγ and IL-4 that was analyzed by flow cytometry after a 6h stimulation with phorbol myristate acetate (PMA) and ionomycin. T cells used were naïve and the culture was 11 days.
(B-C, E) Co-culture with naïve T cells for 11 days. The percentages of T cells uniquely positive for either IFNγ or IL-4 are expressed relatively.
(D) Co-culture with memory T cells. Supernatants were collected after 5 days and IL-17 concentrations was determined by ELISA.
(F) Flow cytometry-based analysis of overall protein O-GlcNAcylation. Dotted line represents the fluorescence minus one control and Thiamet G – an inhibitor of O-GlcNAcase - was used a positive control.
(G) Western blot-based analysis of overall protein O-GlcNAcylation. Thiamet G was used a positive control and ST045849 - an inhibitor of O-GlcNAc transferase – was used as

a negative control. Beta-actin was taken along as housekeeping protein.

Allergen and 2-DG-driven Th2 priming by DCs depends on O-GlcNAcylation

To determine whether this metabolic profile of omega-1-conditioned DCs is a feature of Th2-priming DCs in general, we additionally assessed whether house dust mite allergen extract-conditioned DCs (HDM-DCs) would share the glycolytic and OGT sensitive profile of Th2-DCs conditioned with omega-1. On both accounts the HDM-DCs phenocopied omega-1-conditioned Th2-DCs, as conditioning with HDM also diminished the rapid induction of glycolysis by LPS (Figure 5A) and the Th2 priming-capacity of HDM-DCs was abolished by ST045849 (Figure 5B). Likewise, Th2 induction by 2-DG-DCs was impaired by OGT inhibition (Figure 5C), suggesting not only that O-GlcNAcylation in DCs is a general requirement for Th2-polarization, but also that reduction in glycolysis and O-GlcNAcylation are functionally linked.

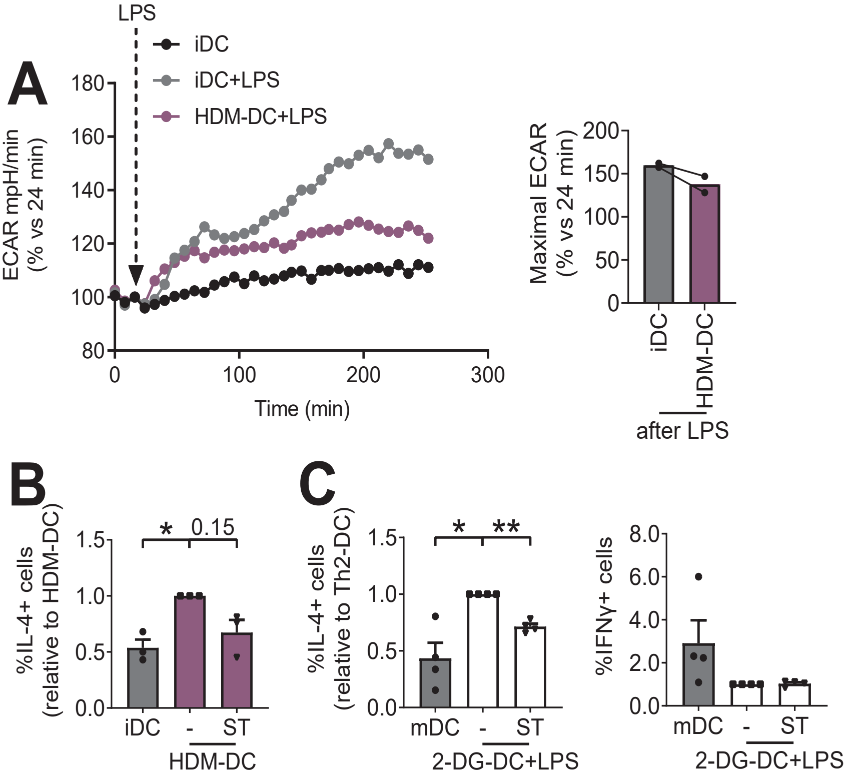

Figure 5. Allergen-induced Th2 priming by DCs also requires O-GlcNAcylation.

Human moDCs were left untreated (iDC in grey) or stimulated for 24h with house dust mite (HDM-DC in purple). DCs were then set aside for measurements of glycolysis using

extracellular flux (XF) analysis (A) or co-culture with allogeneic T cells (B).
(A) Co-culture with naïve T cells for 11 days. T cell intracellular IFNγ and IL-4 was analyzed by flow cytometry after a 6h stimulation with phorbol myristate acetate (PMA) and ionomycin. The percentages of T cells uniquely positive for IL-4 are expressed relatively.
(B) Real-time changes in the ECAR of DCs treated with LPS.
(C) Day 6 moDCs were stimulated either with LPS only (mDC in grey) or 2-deoxyglucose (2-DG-DC in white) in the presence of LPS. Some cells were first pre-incubated with an inhibitor of O-GlcNAcylation (ST045849 [ST]) for 30 minutes. The next day, DCs were set aside for co-culture with allogeneic T cells as in Figure 5A.

cDC2s from helminth infection individuals are characterized by increased protein O-GlcNAcylation

Finally, to study the *in vivo* relevance of our findings, we examined whether protein O-GlcNAcylation was affected in peripheral blood DCs of participants taking part in a controlled human infection (CHI) study using *Necator americanus* [28]. Eight weeks post infection, around the peak of the type 2 immune response as determined by eosinophilia (Figure 6A), protein O-GlcNAcylation was detected by flow cytometry. O-GlcNAcylation was increased in type 2 conventional DCs (cDC2s) - the subset that is classically associated with the priming of Th cell responses [29] - but not plasmacytoid DCs or cDC1s (Figure 6B). This increase shows that enhanced protein O-GlcNAcylation is also a characteristic of DCs during an active type 2 immune response in humans.

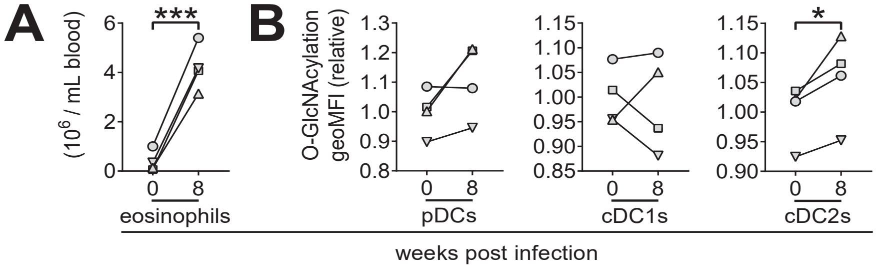

Figure 6. cDC2s from helminth infection individuals are characterized by increased O-GlcNAcylation.

Volunteers were infected with the hookworm *Nector americanus* for 8 weeks in a controlled human infection study. Induction of type 2 immune responses was determined by quantification of eosinophilia in blood using flow cytometry (A). Global protein O-GlcNAcylation in peripheral blood CD123+ plasmacytoid DCs (pDCs), CD141+ type 1 conventional DCs (cDC1s) and CD1c+ cDC2s was assessed using flow cytometry (B).

Discussion

Given the paucity in our understanding of the role of cellular metabolism in Th2 polarization by DCs, we aimed in the present study to identify metabolic properties that are unique to DCs that induce Th2 polarization and to determine the functional importance of those metabolic programs in DCs in priming this response. We found that Th2-priming DCs can be distinguished from immature iDCs, Th1- and Th17-priming DCs based on low glycolytic activity, a characteristic being in itself sufficient to endow DCs with Th2-polarizing ability. Another metabolic module that was found to not only define Th2-priming DCs, but also to be required for their ability to drive Th2 polarization, was the HBP and the associated process of O-GlcNAcylation. Importantly, we provide evidence that this relation between glycolysis, O-GlcNAcylation and Th2 priming extends beyond helminth antigen-conditioned *in vitro* Th2-DCs, as stimulation with allergenic HDM also impaired glycolytic flux and in addition promoted OGT-sensitive Th2 priming. Moreover, type 2 cDCs in peripheral blood from hookworm-infected individuals showed increased overall protein O-GlcNAcylation, while cDC1s and pDCs did not.

As opposed to DCs that prime Th1 or Th17 responses, Th2-priming DCs are commonly characterized by a muted activation phenotype and low expression of pro-inflammatory cytokines, of which particularly low IL-12 expression and low antigen presentation have been linked to their ability to prime Th2 responses [30]. Induction of aerobic glycolysis has been shown to be associated with and required for acquisition immunogenic DC activation and production of Th1-polarizing signals such as IL-12 [7, 8, 10]. Mechanistically, this has been linked to glycolysis-driven fatty acid synthesis that allows for ER/Golgi expansion in DCs after TLR ligation [8], which is thought necessary for optimal expression of costimulatory molecules and T cell-polarizing cytokines. Therefore, the impaired glycolytic potential of Th2-DCs we observed on our work may ‘lock’ them into a muted activation phenotype to allow for efficient Th2 priming. Indeed, inhibition of glycolysis itself made DCs refractory to secrete IL-12 following CD40 ligation and was sufficient to condition DCs for Th2 priming.

How omega-1 would suppress glycolysis is still unclear. It is a protein that bears N-glycans with terminal Lewis-X [fucosylated Galβ1-4(Fucα1-3)GlcNAc] motifs and has T2 ribonuclease (RNase) activity [17, 31]. Both protein glycosylation and RNase activity are required to drive Th2 responses [17]. One possibility is that omega-1 through its RNase activity and ability to suppress global protein synthesis also compromises the expression of glycolytic enzymes. In addition, it was recently reported that the triggering of galactose-type lectin receptor (MGL), which recognizes N-acetylgalactosamine (GalNAc) residues [32], reduces glycolysis in moDCs [33]. Although omega-1 recognition and internalization by DCs has been reported to be primarily mediated via the mannose receptor [17], it is conceivable it may also bind to macrophage galactose-type lectin receptor (MGL) through its terminal GalNAc residues that are present at a low frequency on its glycans [34]. Therefore, this omega-1-MGL interaction may additionally contribute to suppression of glycolysis in omega-1-conditioned moDCs.

The muted activation phenotype, underpinned by impaired glycolytic reprogramming, would be largely consistent with the ‘default concept’ [22, 35], which postulates that the absence of Th1-polarizing signals leads - by default - to a Th2 outcome [3]. However, this default concept has been challenged by studies showing a role for ligands of the Notch receptor (Jagged 1 and 2) and the TNF receptor superfamily (OX40L) in Th2 polarization by DCs in certain context [36-40], although blockade of these pathways did not prevent Th2 priming *in vivo* [41, 42]. Therefore, immunological signals that can uniformly distinguish Th2-priming DCs from other DCs are still unknown [4]. Here, we identified a positive metabolic signature that is unique for Th2-DCs defined by elevated levels of HBP metabolites and OGT mRNA. Although we did not find increased total O-GlcNAcylation in Th2-DCs after 24 hours of conditioning, the fact that Th2-DCs were singularly sensitive to OGT inhibition – both pharmacologically and genetically – indicates that some proteins need to be O-GlcNAcylated for a proper activation of a Th2-priming program in these DCs to ensue.

A key question is how O-GlcNAcylation underpins the ability of DCs to prime Th2 responses. The investigation of how O-GlcNAcylation - as a post-translational modification of proteins - effects the function of immune cells is still in its infancy, but is gaining traction [43]. The role of O-GlcNAcylation has been more exhaustively studied in cancer where it has an important function in the glycolytic reprogramming of cancer cells [44]. Key enzymes in glycolysis such as hexokinase (HK), phosphofructokinase (PFK) and pyruvate kinase isozyme M2 (PKM2) can all be O-GlcNAcylated, resulting in change in glycolytic flux [45]. Whether a similar functional connection between O-GlcNAcylation and inhibition in glycolysis exists in human DCs remains to be determined. However, since pharmacological inhibition of OGT did not rescue omega-1-mediated suppression of IL-12 production, which we show is a consequence of low glycolytic rates, this seems unlikely.

Possibly a more plausible explanation for how O-GlcNAcylation may regulate Th2 priming by DCs, comes from our transcriptomic analysis identifying type I IFN signaling as the top pathway that could distinguish Th2-DCs from iDCs. Recent studies have reported that type I IFN signaling in cDCs is required for Th2 induction *in vivo* in several murine models of type 2 immunity [24, 26] and

MAVS - as a central adaptor molecule required for production of type I IFNs - depends on O-GlcNAcylation for its activity [27, 46, 47]. Therefore, a role for O-GlcNAcylation in conditioning DCs for Th2 priming through control of type 1 IFN signaling is conceivable. Further work is needed to determine a possible relation between O-GlcNAcylation, type I IFN-related cytokine production and Th2 priming by DCs.

Another observation was that Th2 priming following pharmacological inhibition of glycolysis in DCs was largely dependent on O-GlcNAcylation. In T cells, it has been shown that high rates of anaerobic glycolysis limits flux of glucose-derived metabolites into the HBP and thereby UDP-GlcNAc synthesis. Conversely, suppression of glycolysis allows for redirection of glucose into the HBP resulting in enhanced UDP-GlcNAc [48]. Also in liver, neuronal and lung cancer cell lines, this inverse relation has been reported with increases in OGT expression and protein O-GlcNAcylation after glucose deprivation [49-52]. This makes it conceivable that in Th2-DCs, active suppression of glycolysis may not only be a prerequisite for Th2 induction by limiting their IL-12 expression and restricting overall maturation, but also for increased HBP flux, UDP-GlcNAc synthesis and O-GlcNAcylation. This subsequently provides a yet to be identified additional signal(s) that license(s) DCs to prime a Th2 response as discussed above.

Finally, we extend our *in vitro* observations to primary DCs in humans, by showing that cDC2s from individuals taking part in a controlled human hookworm infection trial, displayed increased intracellular O-GlcNAcylation levels during the peak of their type 2 immune response. The finding that this change in O-GlcNAcylation was only consistently observed in CD1c+ cDC2s, but not cDC1s or pDCs, and the knowledge that particularly this DC subset has been linked to regulation of Th cell responses in humans [53-55], provides a first indication that O-GlcNAcylation is also important for DCs to drive Th2 responses in the context of human helminth infection. Further studies are warranted to test this hypothesis and assess the functional relevance of this increased O-GlcNAcylation signature in Th cell polarization by cDC2s.

In summary, we identified HBP, O-GlcNAcylation and low glycolysis as key metabolic processes that uniquely define Th2-priming DCs and that underpin their ability to prime this response. How these different processes exactly interact is not yet clear. More research is needed to elucidate this interplay and how Th2-priming DCs maintain essential HBP flux in the context of suppressed glycolysis. However, their unique characteristics of high HBP engagement and protein O-GlcNAcylation can provide an opportunity for DC manipulation of their Th2-priming capacity through targeting these pathways without affecting Th1- or Th17-priming.

References

1. Gause, W.C., C. Rothlin, and P. Loke, *Heterogeneity in the initiation, development and function of type 2 immunity.* Nat Rev Immunol, 2020. **20**(10): p. 603-614.
2. Kapsenberg, M.L., *Dendritic-cell control of pathogen-driven T-cell polarization.* Nat Rev Immunol, 2003. **3**(12): p. 984-93.
3. MacDonald, A.S. and R.M. Maizels, *Alarming dendritic cells for Th2 induction.* J Exp Med, 2008. **205**(1): p. 13-7.
4. Schuijs, M.J., H. Hammad, and B.N. Lambrecht, *Professional and 'Amateur' Antigen-Presenting Cells In Type 2 Immunity.* Trends Immunol, 2019. **40**(1): p. 22-34.
5. O'Neill, L.A. and E.J. Pearce, *Immunometabolism governs dendritic cell and macrophage function.* J Exp Med, 2016. **213**(1): p. 15-23.
6. Pearce, E.J. and B. Everts, *Dendritic cell metabolism.* Nat Rev Immunol, 2015. **15**(1): p. 18-29.
7. Patente, T.A., L.R. Pelgrom, and B. Everts, *Dendritic cells are what they eat: how their metabolism shapes T helper cell polarization.* Curr Opin Immunol, 2019. **58**: p. 16-23.
8. Everts, B., et al., *TLR-driven early glycolytic reprogramming via the kinases TBK1-IKKvarepsilon supports the anabolic demands of dendritic cell activation.* Nat Immunol, 2014. **15**(4): p. 323-32.
9. Guak, H., et al., *Glycolytic metabolism is essential for CCR7 oligomerization and dendritic cell migration.* Nat Commun, 2018. **9**(1): p. 2463.
10. Krawczyk, C.M., et al., *Toll-like receptor-induced changes in glycolytic metabolism regulate dendritic cell activation.* Blood, 2010. **115**(23): p. 4742-9.
11. Thwe, P.M., et al., *Cell-Intrinsic Glycogen Metabolism Supports Early Glycolytic Reprogramming Required for Dendritic Cell Immune Responses.* Cell Metab, 2017. **26**(3): p. 558-567.e5.
12. Fliesser, M., et al., *Hypoxia-inducible factor 1alpha modulates metabolic activity and cytokine release in anti-Aspergillus fumigatus immune responses initiated by human dendritic cells.* Int J Med Microbiol, 2015. **305**(8): p. 865-73.
13. Ferreira, G.B., et al., *Vitamin D3 Induces Tolerance in Human Dendritic Cells by Activation of Intracellular Metabolic Pathways.* Cell Rep, 2015. **10**(5): p. 711-725.
14. Malinarich, F., et al., *High mitochondrial respiration and glycolytic capacity represent a metabolic phenotype of human tolerogenic dendritic cells.* J Immunol, 2015. **194**(11): p. 5174-86.
15. Zhao, F., et al., *Paracrine Wnt5a-beta-Catenin Signaling Triggers a Metabolic Program that Drives Dendritic Cell Tolerization.* Immunity, 2018. **48**(1): p. 147-160.e7.
16. Jha, A.K., et al., *Network integration of parallel metabolic and transcriptional data reveals metabolic modules that regulate macrophage polarization.* Immunity, 2015. **42**(3): p. 419-30.
17. Everts, B., et al., *Schistosome-derived omega-1 drives Th2 polarization by suppressing protein synthesis following internalization by the mannose receptor.* J Exp Med, 2012. **209**(10): p. 1753-67, s1.
18. Everts, B., et al., *Omega-1, a glycoprotein secreted by Schistosoma mansoni eggs, drives Th2 responses.* J Exp Med, 2009. **206**(8): p. 1673-80.

19. Steinfelder, S., et al., *The major component in schistosome eggs responsible for conditioning dendritic cells for Th2 polarization is a T2 ribonuclease (omega-1).* J Exp Med, 2009. **206**(8): p. 1681-90.
20. Hilligan, K.L., et al., *Dermal IRF4+ dendritic cells and monocytes license CD4+ T helper cells to distinct cytokine profiles.* Nat Commun, 2020. **11**(1): p. 5637.
21. Hussaarts, L., et al., *Rapamycin and omega-1: mTOR-dependent and -independent Th2 skewing by human dendritic cells.* Immunol Cell Biol, 2013. **91**(7): p. 486-9.
22. Hussaarts, L., M. Yazdanbakhsh, and B. Guigas, *Priming dendritic cells for th2 polarization: lessons learned from helminths and implications for metabolic disorders.* Front Immunol, 2014. **5**: p. 499.
23. Janss, T., et al., *Interferon response factor-3 promotes the pro-Th2 activity of mouse lung CD11b(+) conventional dendritic cells in response to house dust mite allergens.* Eur J Immunol, 2016. **46**(11): p. 2614-2628.
24. Webb, L.M., et al., *Type I interferon is required for T helper (Th) 2 induction by dendritic cells.* Embo j, 2017. **36**(16): p. 2404-2418.
25. Sergushichev, A.A., et al., *GAM: a web-service for integrated transcriptional and metabolic network analysis.* Nucleic Acids Res, 2016. **44**(W1): p. W194-200.
26. Connor, L.M., et al., *Th2 responses are primed by skin dendritic cells with distinct transcriptional profiles.* J Exp Med, 2017. **214**(1): p. 125-142.
27. Song, N., et al., *MAVS O-GlcNAcylation Is Essential for Host Antiviral Immunity against Lethal RNA Viruses.* Cell Rep, 2019. **28**(9): p. 2386-2396.e5.
28. Hoogerwerf, M.A., et al., *New Insights Into the Kinetics and Variability of Egg Excretion in Controlled Human Hookworm Infections.* J Infect Dis, 2019. **220**(6): p. 1044-1048.
29. Eisenbarth, S.C., *Dendritic cell subsets in T cell programming: location dictates function.* Nat Rev Immunol, 2019. **19**(2): p. 89-103.
30. van Panhuys, N., F. Klauschen, and R.N. Germain, *T-cell-receptor-dependent signal intensity dominantly controls CD4(+) T cell polarization In Vivo.* Immunity, 2014. **41**(1): p. 63-74.
31. Dunne, D.W., F.M. Jones, and M.J. Doenhoff, *The purification, characterization, serological activity and hepatotoxic properties of two cationic glycoproteins (alpha 1 and omega 1) from Schistosoma mansoni eggs.* Parasitology, 1991. **103 Pt 2**: p. 225-36.
32. Meevissen, M.H., et al., *Specific glycan elements determine differential binding of individual egg glycoproteins of the human parasite Schistosoma mansoni by host C-type lectin receptors.* Int J Parasitol, 2012. **42**(3): p. 269-77.
33. Zaal, A., et al., *Activation of the C-Type Lectin MGL by Terminal GalNAc Ligands Reduces the Glycolytic Activity of Human Dendritic Cells.* Front Immunol, 2020. **11**: p. 305.
34. Meevissen, M.H., et al., *Structural characterization of glycans on omega-1, a major Schistosoma mansoni egg glycoprotein that drives Th2 responses.* J Proteome Res, 2010. **9**(5): p. 2630-42.
35. Jankovic, D., et al., *In the absence of IL-12, CD4(+) T cell responses to intracellular pathogens fail to default to a Th2 pattern and are host protective in an IL-10(-/-) setting.* Immunity, 2002. **16**(3): p. 429-39.

36. Amsen, D., et al., *Instruction of distinct CD4 T helper cell fates by different notch ligands on antigen-presenting cells*. Cell, 2004. **117**(4): p. 515-26.
37. Balic, A., et al., *Selective maturation of dendritic cells by Nippostrongylus brasiliensis-secreted proteins drives Th2 immune responses*. Eur J Immunol, 2004. **34**(11): p. 3047-59.
38. de Kleer, I.M., et al., *Perinatal Activation of the Interleukin-33 Pathway Promotes Type 2 Immunity in the Developing Lung*. Immunity, 2016. **45**(6): p. 1285-1298.
39. Ito, T., et al., *TSLP-activated dendritic cells induce an inflammatory T helper type 2 cell response through OX40 ligand*. J Exp Med, 2005. **202**(9): p. 1213-23.
40. Willart, M.A., et al., *Interleukin-1α controls allergic sensitization to inhaled house dust mite via the epithelial release of GM-CSF and IL-33*. J Exp Med, 2012. **209**(8): p. 1505-17.
41. Chu, D.K., et al., *IL-33, but not thymic stromal lymphopoietin or IL-25, is central to mite and peanut allergic sensitization*. J Allergy Clin Immunol, 2013. **131**(1): p. 187-200.e1-8.
42. Tu, L., et al., *Notch signaling is an important regulator of type 2 immunity*. J Exp Med, 2005. **202**(8): p. 1037-42.
43. Quik, M., C.H. Hokke, and B. Everts, *The role of O-GlcNAcylation in immunity against infections*. Immunology, 2020. **161**(3): p. 175-185.
44. Jozwiak, P., et al., *O-GlcNAcylation and Metabolic Reprograming in Cancer*. Front Endocrinol (Lausanne), 2014. **5**: p. 145.
45. Yi, W., et al., *Phosphofructokinase 1 glycosylation regulates cell growth and metabolism*. Science, 2012. **337**(6097): p. 975-80.
46. Li, T., et al., *O-GlcNAc Transferase Links Glucose Metabolism to MAVS-Mediated Antiviral Innate Immunity*. Cell Host Microbe, 2018. **24**(6): p. 791-803.e6.
47. Seo, J., et al., *O-Linked N-Acetylglucosamine Modification of Mitochondrial Antiviral Signaling Protein Regulates Antiviral Signaling by Modulating Its Activity*. Front Immunol, 2020. **11**: p. 589259.
48. Araujo, L., et al., *Glycolysis and glutaminolysis cooperatively control T cell function by limiting metabolite supply to N-glycosylation*. Elife, 2017. **6**.
49. Cheung, W.D. and G.W. Hart, *AMP-activated protein kinase and p38 MAPK activate O-GlcNAcylation of neuronal proteins during glucose deprivation*. J Biol Chem, 2008. **283**(19): p. 13009-20.
50. Kang, J.G., et al., *O-GlcNAc protein modification in cancer cells increases in response to glucose deprivation through glycogen degradation*. J Biol Chem, 2009. **284**(50): p. 34777-84.
51. Taylor, R.P., et al., *Up-regulation of O-GlcNAc transferase with glucose deprivation in HepG2 cells is mediated by decreased hexosamine pathway flux*. J Biol Chem, 2009. **284**(6): p. 3425-32.
52. Taylor, R.P., et al., *Glucose deprivation stimulates O-GlcNAc modification of proteins through up-regulation of O-linked N-acetylglucosaminyltransferase*. J Biol Chem, 2008. **283**(10): p. 6050-7.
53. Bachem, A., et al., *Superior antigen cross-presentation and XCR1 expression define human CD11c+CD141+ cells as homologues of mouse CD8+ dendritic cells*. J Exp Med, 2010. **207**(6): p. 1273-81.

54. Leal Rojas, I.M., et al., *Human Blood CD1c(+) Dendritic Cells Promote Th1 and Th17 Effector Function in Memory CD4(+) T Cells*. Front Immunol, 2017. **8**: p. 971.
55. Yin, X., et al., *Human Blood CD1c+ Dendritic Cells Encompass CD5high and CD5low Subsets That Differ Significantly in Phenotype, Gene Expression, and Functions.* J Immunol, 2017. **198**(4): p. 1553-1564.
56. Vincent, E.E., et al., *Mitochondrial Phosphoenolpyruvate Carboxykinase Regulates Metabolic Adaptation and Enables Glucose-Independent Tumor Growth.* Mol Cell, 2015. **60**(2): p. 195-207.
57. Gainullina, A., et al., *Open Source ImmGen: network perspective on metabolic diversity among mononuclear phagocytes*. bioRxiv, 2020.
58. Ulland, T.K., et al., *TREM2 Maintains Microglial Metabolic Fitness in Alzheimer's Disease.* Cell, 2017. **170**(4): p. 649-663.e13.
59. Pelgrom, L.R., A.J. van der Ham, and B. Everts, *Analysis of TLR-Induced Metabolic Changes in Dendritic Cells Using the Seahorse XF(e)96 Extracellular Flux Analyzer.* Methods Mol Biol, 2016. **1390**: p. 273-85.

Methods

Isolation of peripheral blood mononuclear cells

Peripheral venous blood, from buffy coats provided by Sanquin (Amsterdam, The Netherlands), was divided in conical 50 mL tubes (#227261, Greiner) with 20 mL of room temperature venous blood diluted 1:1 with room temperature HBSS (#14170-088, Gibco) per tube. This solution was gently mixed before addition of 13 mL room temperature Ficoll (#17-1440-02, GE healthcare) underneath the blood:HBSS. Alternatively, all liquids were used cold, but temperatures were never mixed. Peripheral blood mononuclear cells (PBMCs) were concentrated into a ring by density centrifugation at 400g with low brake for 25 minutes at room temperature. The rings were transferred using a Pasteur pipette (#861172001, Sarstedt) to new 50 mL tubes to which HBSS supplemented with 1% v/v heat-inactivated fetal calf serum (HI-FCS; #S-FBS-EU-015, Serana, Pessin, Germany) was added up to 50 mL. Blood platelets were removed by two rounds of centrifugation at 200g with normal brake for 20 minutes at room temperature. Finally, the PBMCs were resuspended in a home-made cell separation buffer (MACS buffer = PBS [from LUMC pharmacy] supplemented with 0.5% BSA [fraction V, #10735086001, Roche, Woerden, The Netherlands] and 2 mM EDTA [#15575-038, Thermo]) that was sterilized using a 0.22 µm filter system (#431097, Corning).

Monocyte-derived dendritic cell culture

PBMCs were counted using an in-house Türk solution (= 50 mg gentian violet, 5 mL glacial acetic acid and 500 mL H_20) and brought to a concentration of 10^7 cells per 95 µL of MACS buffer. Monocytes were isolated by addition of 5 µL of CD14 MACS beads (#120-007-943, Miltenyi) per 10^7 cells, mixing well, incubating for 15 minutes at 4 degrees Celsius and column sorting using LS columns (#130-042-401, Miltenyi) according to the manufacturer's protocol provided with the beads. Whole PBMCs, CD14- flow through and CD14+ monocyte fractions were set aside to check for purity, which routinely was >95%. Monocytes were brought to 400 cells per µL in ice-cold monocyte-derived dendritic cell (moDC) differentiation medium (= no additives RPMI [naRPMI; #42401-042, Invitrogen] supplemented with 10% HI-FCS, 2 mM L-glutamine [#G-8540-100g, Sigma], 100 U/mL penicillin [#16128286, Eureco-pharma , Ridderkerk, The Netherlands] and 100 µg/mL streptomycin [#S9137, Sigma] that together formed our general human immune cell RPMI for metabolism work or ‘himRPMI’ and also 10 ng/mL of human recombinant granulocyte/macrophage colony-stimulating factor (GM-CSF; #PHC2013, Biosource) and 0.86 ng/mL of human recombinant IL-4 (#204-IL, R&D systems) was added for moDC differentiation. The media was kept cold to prevent monocytes sticking to the plastic tube. Monocytes were usually plated at 2 million cells per 5 mL of media in 6-well plates (#140675, Nunc) and after 2 or 3 days, the top half of the medium was carefully removed and replaced by 2.5 mL of fresh medium complemented with 20 ng/mL of GM-CSF and 1.72 ng/mL of IL-4 to maintain the concentrations of differentiating cytokines.

O-GlcNAc transferase knockdown

At day 4 of the culture, the cells were harvested, washed with PBS, brought to a concentration of 1.1x10^6 cells per 100 µL and split into 1.5 mL Eppendorf tubes with 100 µL of cell solution. Shortly before transfection by electroporation, tubes were spun down, cell pellets were carefully pipetted dry, pellets were reconstituted in 100 µL of resuspension buffer and 10 µL of 455 nM siRNA was added (anti-OGT [#M-019111-00-0005, Darmacon, Lafayette, Colorado, United States] or scrambled control [#D-001206-13-05, Darmacon]). Electroporation as described here was performed using the 100 µL variant (#MPK10096, Invitrogen) of the Neon Transfection System (#MPK5000, Invitrogen) and a complementary pipette (#MPP100, Invitrogen) with the following settings: 1600 V, 20 ms and one pulse. Immediately after electroporation, the cells were transferred to 5 mL of 10% HI-FCS RPMI-1640 with 2 mM glutamine but without further additions. Importantly, the media contained no antibiotics at this stage. Electroporation tips were re-used to a maximum of three times for the same target. Later, the cells were plated at 200 cells per µL in, if cell numbers allowed it, 6-well plates again. The next morning, the media was re-supplemented with penicillin, streptomycin, rGM-CSF and rIL-4. At day 6, the cells were handled as normally. Reconstituting the pellet in a total volume of 110 µL helped prevent sucking up air bubbles into the electroporation tip, which is crucial. Minimizing time spend in the resuspension buffer helped with cell viability. Silencing efficiency was determined by qPCR on 6 days old cells and was routinely greater than 80%.

DC stimulation and analysis of activation

Day 5-7 moDCs were harvested without discarding the differentiation media and replated in 96-well plates (#167008, Nunc) at 5-10x10^4 cells per 100 µL of the same media and left to rest for 2-3 hours. Alternatively, cells were plated in 200 µL and the next day the top half of the medium was carefully removed. Inhibitors were added 30 minutes prior to antigen stimulation and the cells were kept for a total of 24 hours in a 5% CO2 and 37 degrees Celsius cell incubator. Inhibitors included: 5-10 mM of 2-deoxyglucose (2-DG; in mQ water; #D8375-1g, Sigma), 20 µM ST045849 (ST; in DMSO; #6775, Tocris) and 10 µM Thiamet G (TG; in DMSO; #13237, Cayman Chemical, Ann Arbor, Michigan, United States). Antigens included 100 ng/mL of ultrapure lipopolysaccharides (LPS; *Escherichia coli* 0111 B4 strain, #tlrl-3pelps, InvivoGen), 20 µg/mL of polyinosinic:polycytidylic acid (PolyIC; high molecular weight, #TLRL-PIC, InvivoGen), 20-50 µg/mL of zymosan (#Z4250, Sigma), 250-500 ng/mL of omega-1 (in-house), 25-50 µg/mL of soluble egg antigen (SEA; *Schistosoma mansoni* Puerto Rican strain, in-house) and 10 µg/mL of house dust mite (HDM; Greer, lot number: 305470). Supernatants were collected after 24 hours and IL-10 and IL-12p70 concentrations were determined using ELISA. Alternatively, 10.000 24h-stimulated DCs were co-cultured with 10.000 J558-CD40L cells - a CD40L-expressing cell line – for another 24 hours before determination of cytokine concentrations. Viability, differentiation markers and expression of costimulatory molecules were determined using flow cytometry on a FACSCanto II.

Analysis of blood DCs from a controlled human hookworm infection trial.

Peripheral venous blood was drawn from healthy volunteers prior to and 8 weeks after infection with *Necator americanus*, as part of a controlled human infection trial (NCT03126552) [28]. PBMCs were isolated as described above and cryopreserved in liquid nitrogen until later analysis.

Preparation of Schistosoma mansoni soluble egg antigens and omega-1

S. mansoni eggs were isolated and processed into a SEA preparation as described previously [18]. Protein concentration was determined using a bicinchoninic acid (BCA) protein assay kit (Pierce, #PIER23225). Endotoxin contamination was determined by a direct comparison of SEA batches to LPS in a TLR4-transfected Human Embryonic Kidney 293 (HEK) reporter cell line, in which IL-8 secretion by 5x10^8 HEK cells after stimulation with 10 µg of SEA is expected to be similar or less than after stimulation with 1-3 ng/mL of LPS. Omega-1 was purified from SEA as described [18].

T cell polarization

Naïve CD4 T cells for assessment of DC capacity for Th1/2 polarization were isolated from allogeneic buffy coat PBMCs using a naïve human CD4 T cell isolation kit (#480042, BioLegend). Memory CD4 T cells for assessment of DC capacity for Th17 reactivation were isolated using a human CD4 T cell isolation kit (#130-096-533, Miltenyi) followed by a combination of anti-CD45RO-PE (UCHL1 clone; #R0843, Dako) and anti-PE microbeads (#130-048-801) to eliminate naïve CD4 T cells. For Th1/2 polarization, 5.000 DCs that were stimulated for 24h were co-cultured with 20.000 allogeneic naïve CD4 T cells in the presence of 20 pg/mL Staphylococcal Enterotoxin B (SEB; #S4881, Sigma) in a cell culture treated flat-bottom 96 well plate. After 5-7 days, cells were transferred to a flat-bottom 24 well plate well containing 1 mL of media that was supplemented with 42 IU/mL recombinant human IL-2 (#202-IL, R&D systems). 2 days later, 1 mL of fresh media with IL-2 was added and cell cultures were split into two. Cells were restimulated at approximately 11 days with 100 ng/mL phorbol myristate acetate (PMA) and 2 µg/mL ionomycin for a total 6 hours, of which the last 4 hours in the presence of 10 μg/mL brefeldin A (#B-7651, Sigma). Cells were stained with Aqua LIVE/DEAD and fixed with formalin as described in the next section before permeabilization with a permeabilization buffer (#00-8333-56, Thermo) according to the manufacturer's recommendation. Production of IL-4 and IFNγ was determined using flow cytometry. For Th17 reactivation, 2.000 stimulated DCs were co-cultured with 20.000 allogeneic memory CD4 T cells in IMDM (#12-722F, Lonza) supplemented with 10% HI-FCS, 100 U/mL penicillin and 100 μg/mL streptomycin in the presence of 10 pg/mL SEB in a flat-bottom 96 well plate. Supernatants were collected after 5 days and IL-17 concentration was determined using ELISA.

Flow cytometry

In general, single cell suspensions underwent viability staining for 20 minutes at room temperature using the LIVE/DEAD™ Fixable Aqua Dead Cell Stain Kit (#L34957, Thermo) 1:400 in PBS and fixation for 15 minutes at room temperature using 1.85% formaldehyde (F1635, Sigma) in PBS before surface staining with antibodies in a non-sterile version of the in-house cell separation buffer (=FACS buffer) for 30 minutes at 4 degrees Celsius. Alternatively, cells were acquired unfixed in FACS buffer with 7-AAD (#00-6993-50, eBioscience) 1:50 to distinguish live from dead cells. Compensation was done using single staining on beads (#552843, BD Biosciences or 552845, BD Biosciences or #A10346, Invitrogen)

For detection of protein O-GlcNAcylation in moDCs, cells underwent Aqua viability staining for 30 minutes on ice and fixation for 60 minutes at 4 degrees using the Foxp3 / Transcription Factor Staining Buffer Set (#00-5523-00, eBioscience). Afterwards, cells were further permeabilized by first resuspending them in 20 μL of ice-cold PBS and then adding 180 μL of ice-cold absolute methanol (90% end concentration; #1.06009, Merck). Methanol was added carefully to prevent leaking of methanol out of the pipette tips and overflowing of the well plates. Cells were fixed for at least 10 minutes at -20 degrees Celsius up to overnight. Methanol was washed away with FACS buffer at least two times before staining O-GlcNAcylation, CD1a and CD14 to prevent interaction with methanol sensitive fluorochromes. Cells were analyzed on a FACSCanto II.

To assess levels of O-GlcNAcylation in DCs subsets in frozen human blood, PBMCs were thawed and first live stained for the following surface markers during the fixable Aqua stain: CD3/CD56/CD19, which were used as exclusion markers, and HLA-DR and CD11c, which in combination with CD123, CD141, and CD1c were used to identify pDCs, cDC1s and cDC2s respectively. Cells were then washed in PBS and fixed with an Intracellular Fixation & Permeabilization Buffer Set (#88-8824-00, eBioscience) for 1 h at 4 degrees Celsius. Cells we washed again in PBS and subsequently permeabilized using the same set before a second staining for O-GlcNAcylation as described above. Cells were analyzed on an LSR-II.

All samples were run on a FACSCanto II or LSR-II (both BD Biosciences) and analyzed using FlowJo (Version 10, TreeStar, Meerhout, Belgium).

Antibodies

The antibodies used in this study can be found in supplementary table 1.

RNA sequencing and metabolomics

moDCs from three 6-well plates were pooled, centrifuged and resuspended in 1 mL himRPMI. 300 µL was used for mRNA extraction, 300 µL was used for metabolite extraction, 300 µL was used for extracellular flux (XF) analysis and the remaining 100 µL was used for cell counting, analysis of DC activation and T cell polarization. Cell numbers for mRNA extraction and metabolite extraction ranged between 0.3-1.1 million cells.

mRNA was extracted with oligo-dT beads (Invitrogen) and libraries were prepared and quantified as described before [56].

Extraction of metabolites was done according to the recommendations of General Metabolomics (Boston, Massachusetts, USA) specifically for extraction of polar metabolites from adherent mammalian cell culture. Briefly, cells were transferred to 1.5 mL Eppendorfs, centrifuged, washed using a warm ammonium carbonate wash solution (75 mM ammonium carbonate [#A9516, Sigma] in HLPC-grade water and pH 7.4 titrated with HLPC-grade formic acid) and resuspended in a 70 degrees Celsius 70% ethanol extraction solvent (70% v/v absolute ethanol [#100983.1000, Merck] in HLPC-grade water). After exactly 3 minutes, the extracts were transferred to other, pre-chilled Eppendorfs in a dry-ice bed. The first group of Eppendorfs were washed with a second volume of extraction solvent that was immediately transferred to the second group of Eppendorfs. Combined extracts were then centrifuged at 14.000 rpm for 10 minutes at 4 degrees Celsius or colder, after which a fixed volume of the extract supernatant was collected – without disturbing any pelleted material – and transferred to a third group of Eppendorfs, also pre-chilled and in a dry-ice bed. The materials were stored at -80 degrees Celsius before shipping processing by General Metabolics as described in [16].

RNA-seq and metabolic network analysis

RNA-seq libraries were sequenced using paired-end sequencing, second read (read-mate) was used for sample demultiplexing. Reads were aligned to the GRCh37 assembly of human genome using STAR aligner. Aligned reads were quantified using quant3p script (https://github.com/ctlab/quant3p) to account for specifics of 3′ sequencing with protein-coding subset of Gencode gene annotation. DESeq2 was used for differential expression analysis. Metabolic network clustering analysis was done with GAM-clustering method [57] based on gene expression profiles and metabolic network based on KEGG database. Metabolic module for Th2-DC vs iDC comparison was done using GATOM method as described in Ulland et al. [58] based on both DESeq2-based differential expression results for genes and limma-based differential analysis results for metabolites.

Extracellular flux analysis

For real-time metabolic analysis on live cell, DCs were resuspended in Seahorse media (= unbuffered RPMI [#R1383-10X1L, Sigma] of which the pH was set to 7.4 using 37% HCl (#1.00317.1000, Merck) before sterilization using a 0.22 μm filter system that was supplemented with 5% HI-FCS and plated in XF cell culture plates (part of pack #102416-100, Agilent, Amstelveen, The Netherlands) at 5x10^4 cells per 180 μL of Seahorse media. The plate was quickly spun down to facilitate the adherence of cells to the bottom of the well and then, the cells were rested for 1 hour in a special 0% CO_2 cell incubator at 37 degrees Celsius. This rest time is also needed for the evaporation of remaining CO_2 in the media, which can acidify the unbuffered media. To facilitate the adherence of semi-adherent DCs even more, the assay plate wells were coated beforehand with 25 μL of 50 μg/mL Poly-D-Lysine hydrobromide (PDL; diluted in mQ water; # A-003-E, Merck) for a minimum of 1 hour at 37 degrees Celsius, after which the PDL was pipetted away and the wells were washed using 200 μL of mQ water and subsequent air-drying. MilliQ water is preferred over PBS here as air-drying PBS residues might result in crystal formation. During the rest, pre-hydrated XF cartridges were filled with 10x concentrated assay reagents in Seahorse media that did not contain HI-FCS for sequential injections of glucose (10 mM end; port A; #G8644-100mL, Sigma), oligomycin (1 μM end; port B; #11342, Cayman Chemical), fluoro-carbonyl cyanide phenylhydrazone (FCCP, 3 μM end; port C; # C2920-10MG, Sigma), and finally, rotenone/antimycin A (1/1 μM end; port D; #R8875-1G/#A8674-25MG, Sigma). The manufacturer recommended the removal of HI-FCS from the injection solution to prevent clogging of the injection ports. Oxygen consumption rates (OCR) and extracellular acidification rates (ECAR) were recorded with the XF96e Extracellular Flux analyser (Agilent) and analyzed using Wave Desktop (Version 2.6, Agilent). Immediately after the run, XF culture plates were collected from the analyser, supernatants were carefully pipetted away, cells were washed gently with PBS, lysed in 25 μL of a RIPA-like buffer (50 mM Tris-HCl [pH 7.4], 150 mM NaCl and 0.5% SDS) and the plate was stored at -20 degrees Celsius for later protein content quantification using bicinchoninic acid protein assay kit (BCA; #PIER23225, Pierce) according to the manufacturer's recommendations.

Glycolytic rate = increase in ECAR in response to injection A. Glycolytic capacity = increase in ECAR in response to injection A and injection B. Baseline OCR = difference in OCR between readings following port A injection and readings after port D injection. Spare OCR is difference between basal and maximum OCR, which is calculated based on the difference in OCR between readings following port C injection and readings after port A injection. ATP production = difference in OCR between readings following port A injection and readings after port B injection. Proton leak = difference in OCR between readings following port B injection and after port D injection. A more detailed description of this procedure can be found somewhere else [59].

Western blotting

DCs were washed twice with PBS before being lysed in EBSB buffer (8% [w/v] glycerol, 3% [w/v] SDS and 100 mM Tris–HCl [pH 6.8]). Lysates were immediately boiled for 5 min and their protein content was determined using a BCA kit. Protein was separated by SDS-PAGE followed by transfer to a PVDF membrane. Protein content of 1 million moDCs that were stimulated for 24h but not recounted before lysis in 150 µL was approximately 0.5 mg/mL. Usually 10 µg of protein was added to each lane. Membranes were blocked for 1 h at room temperature in TTBS buffer (20 mM Tris-HCl [pH 7.6], 137 mM NaCl, and 0.25% [v/v] Tween 20) containing 5% (w/v) fat free milk and incubated overnight with primary antibodies. The primary antibodies used were O-GlcNAc (RL2 clone; 1:1000, #?, company?), OGT (D1D8Q clone; 1:1000; #24083S, Cell Signaling and beta-actin (AC-15 clone; 1:10.000; #A5441, Sigma). The membranes were then washed in TTBS buffer and incubated with horseradish peroxidase-conjugated secondary antibodies for 2 h at room temperature. After washing, blots were developed using enhanced chemiluminescence.

qPCR

RNA was extracted from snap-frozen pulsed DCs. The isolation of mRNA was performed according to manufacturer's instruction using micro RNA Plus kit (Qiagen). cDNA was synthesized with reverse transcriptase kit (Promega) and PCR amplification by the SYBER Green method were done using CFX (Biorad). Specific primers for detected genes are as follows: human OGT forward is AGAAGGGCAGTGTTGCTGAAG and reverse is TGATATTGGCTAGGTTATTCAGAGAGTCT. The cycle threshold (Ct) value is defined as the number of PCR cycles in which the fluorescence signal exceeds the detection threshold value. The normalized amount of targeted mRNA (Nt) was calculated from Ct value obtained for both target and ACTB mRNA (served as housekeeping gene) with the equation Nt=2Ct(β-actin)-Ct(target). Relative mRNA expression was obtained by setting Nt in control as 1 in each experiment and for each donor.

Quantification and statistical analysis

Statistical analysis as specified in figure legends were performed with Prism 9 (GraphPad software Inc.). Graphs with 2 bars were analyzed with the paired Student's t test, while graphs with more than 2 bars were analyzed with the repeated measures analysis of variance (ANOVA) corrected for multiple comparisons using Sidak's multiple comparison test. A p value < 0.05 was considered significant (* for $p < 0.05$, ** for $p < 0.01$ and *** for $p < 0.001$).

Acknowledgements

This work was supported by an LUMC fellowship and a VENI grant (#91614087 by Netherlands Organisation for Scientific Research) awarded to BE.

Author contributions

LP, MQ, AvdH, LB and BW performed experiments. LP, AS and BE analyzed experiments. GS provided omega-1. MR provided PBMCs from the controlled human hookworm infection trial. LP, CH, MA and BE designed experiments. BE conceived and supervised the study and wrote the manuscript together with LP.

Conflict of interest

The authors declare that no competing financial interests exist in relation to the work described.

Supplemental figures

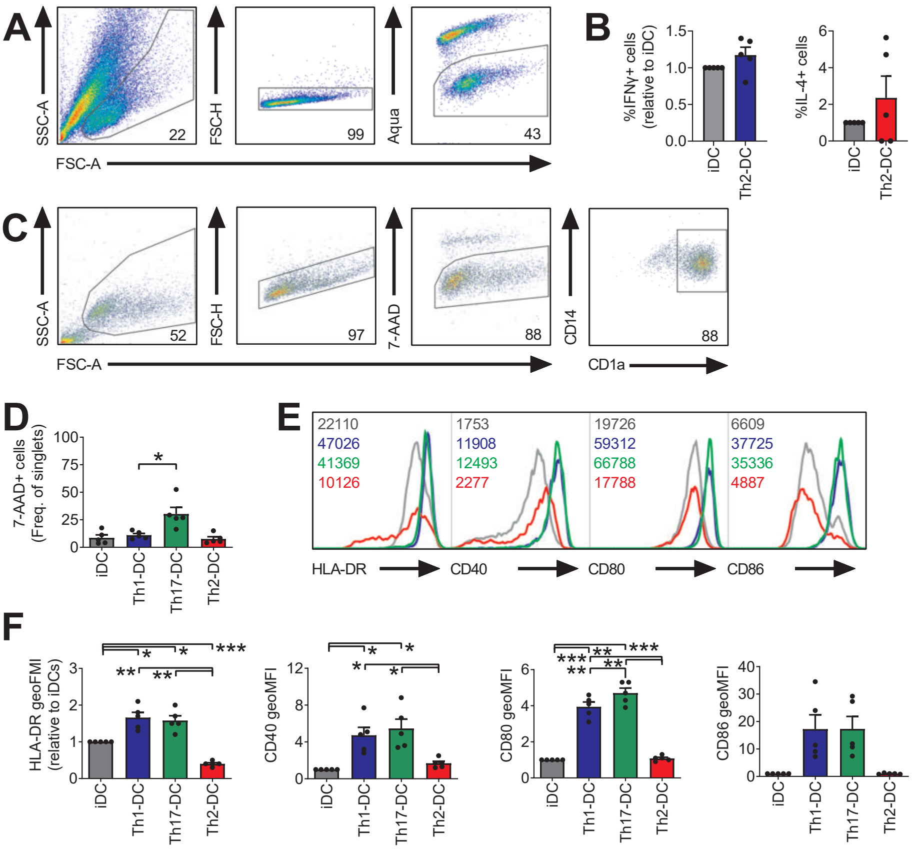

Figure S1.

Human moDCs were left untreated (iDC in grey) or stimulated for 24h with either LPS+PolyIC (Th1-DC in dark blue), zymosan (Th17-DC in green) or omega-1 (Th2-DC in red). DCs were then set aside for determination of viability (D) and maturation (E-F) using flow cytometry (C). If DC quality was sufficient, they were furthermore co-cultured with allogeneic naïve T cells for 11 days. T cell cytokine production was assessed using intracellular cytokine staining (B) using flow cytometry (A).

(A) Flow gating strategy for live T cells in 11-day old cultures of DCs and T cells by sequential gating for lymphocytes, singlets and live cells.

(B) The percentages of T cells uniquely positive for either IFNγ or IL-4 are expressed relative to the iDC condition.

(C) Flow gating strategy for live differentiated DCs by sequential gating for myeloid cells, singlets, live cells and CD1a+CD14intermediate cells after 6 days of differentiation - in the presence of GM-CSF and IL-4 - followed by 24 hours of stimulation with antigens.

(D) Frequencies of dead DCs are enumerated.

(E-F) The expression of maturation makers – based on the geometric mean fluorescence

– are shown in representative histograms with representative absolute values in E) and enumerated relative to iDCs in F).
The number of independent experiments is represented by symbols in the graphs and shown as mean ± SEM; *p < 0.05, **p < 0.01, ***p < 0.001

Gene set enrichment analysis
on genes in metabolic cluster 3 using pathways supplied by the Kegg database

A

Gene set description	# genes in overlap (k)	FDR q-value
Glycolysis / Gluconeogenesis	8	$2.18\ e^{-13}$
Terpenoid backbone biosynthesis	6	$2.5\ e^{-13}$
Steroid biosynthesis	6	$4.11\ e^{-13}$
Valine, leucine and isoleucine degradation	7	$7.75\ e^{-13}$
Pyruvate metabolism	6	$7.52\ e^{-11}$
Fatty acid metabolism	5	$1.63\ e^{-8}$
Peroxisome	5	$3.39\ e^{-7}$
Propanoate metabolism	4	$6.81\ e^{-7}$
Glutathione metabolism	4	$3.37\ e^{-6}$
Biosynthesis of unsaturated fatty acids	3	$2.32\ e^{-5}$

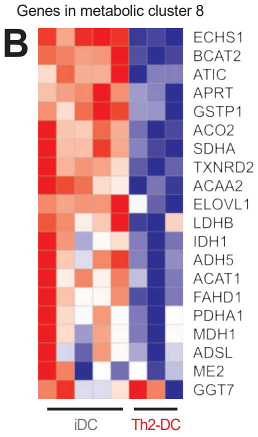

Gene set enrichment analysis
on genes in metabolic cluster 8 using pathways supplied by the Kegg database

C

Gene set description	# genes in overlap (k)	FDR q-value
Citrate cycle (TCA cycle)	6	$6.94\ e^{-13}$
Pyruvate metabolism	5	$7.22\ e^{-10}$
Fatty acid metabolism	4	$2.01\ e^{-7}$
Valine, leucine and isoleucine degradation	4	$2.01\ e^{-7}$
Gloxylate and dicarboxylate metabolism	3	$1.71\ e^{-6}$
Propanoate metabolism	3	$1.3\ e^{-5}$
Butanoate metabolism	3	$1.3\ e^{-5}$
Glutathione metabolism	3	$3.7\ e^{-5}$
Glycolysis / Gluconeogenesis	3	$6.32\ e^{-5}$
Valine, leucine and isoleucine biosynthesis	2	$2.04\ e^{-4}$

Figure S2.

Human moDCs were left untreated (iDC in grey) or stimulated for 24h with either LPS+PolyIC (Th1-DC in dark blue), zymosan (Th17-DC in green) or omega-1 (Th2-DC in red). DCs were then set aside for RNA-sequencing. Metabolic genes were selected out of the total transcriptome of differently conditioned DCs and used to form 13 clusters with maximal distinguishing power. Pathway analysis was done on the genes in these metabolic clusters. Top pathways in cluster 3 (A) and 8 (C) are shown here, as well as an overview of genes in metabolic cluster 8 (B).
The number of independent experiments is represented by blocks in the heat map.

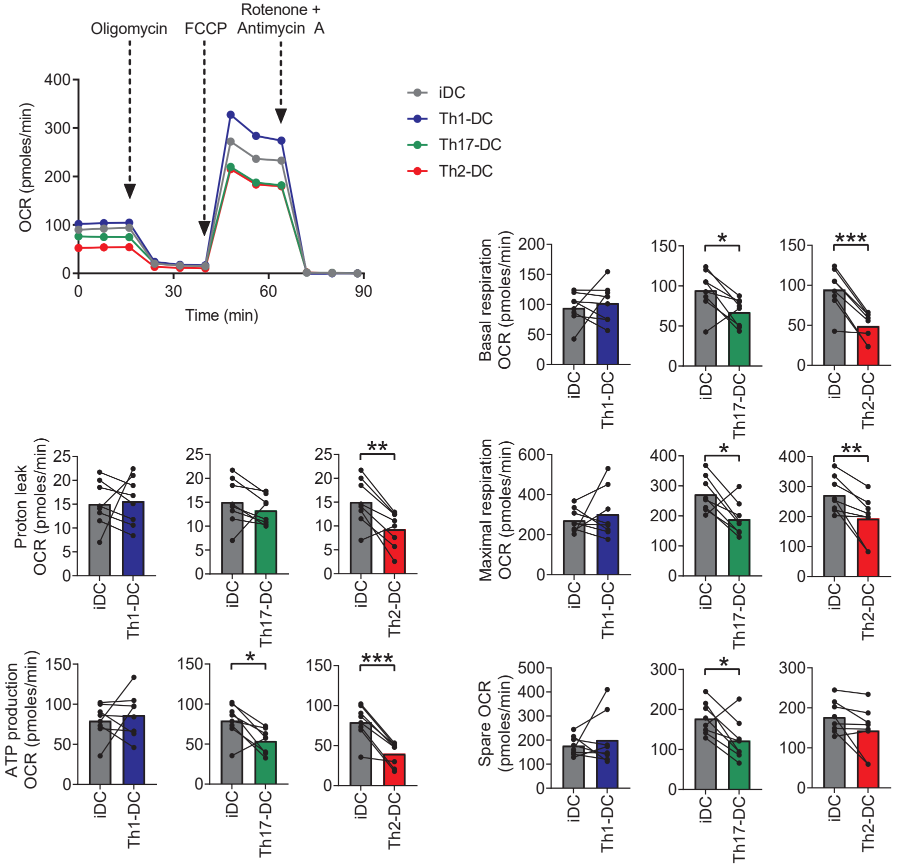

Figure S3.

Human moDCs were left untreated (iDC in grey) or stimulated for 24h with either LPS+PolyIC (Th1-DC in dark blue), zymosan (Th17-DC in green) or omega-1 (Th2-DC in red). DCs were then set aside for measurements of mitochondrial respiration using extracellular flux (XF) analysis.
Mitochondrial stress test in Seahorse XF analyzer which consists of sequential injections of oligomycin, FCCP and Rotenone + Antimycin A. Measurements of mitochondrial respiration were determined after subtraction of non-mitochondrial oxygen consumption = oxygen consumption rate (OCR) after injection of Rotenone + Antimycin A Basal respiration = OCR before injection of oligomycin. Max respiration = OCR after injection of FCCP. Spare OCR = difference basal and max respiration. Proton leak = OCR after injection of oligomycin. (Mitochondrial) ATP production = the difference before and after injection of oligomycin.
The number of independent experiments is represented by symbols in the graphs and shown as mean ± SEM; $*p < 0.05$, $**p < 0.01$, $***p < 0.001$

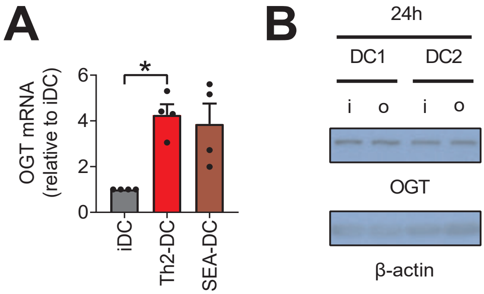

Figure S4.

Human moDCs were left untreated (iDC in grey / i) or stimulated for 24h with either omega-1 (Th2-DC in red / o) or *Schistosoma mansoni* soluble egg antigens (SEA-DC). DCs were then set aside for qPCR (A) or western blotting (B).
(A) Proteins were visualized by western blotting using antibodies against O-GlcNAc transferase (OGT) and beta-actin. Beta-actin was taken along as housekeeping protein.
(B) The mRNA expression of OGT was determined.
The number of independent experiments is represented by symbols in the graphs and shown as mean ± SEM; *p < 0.05

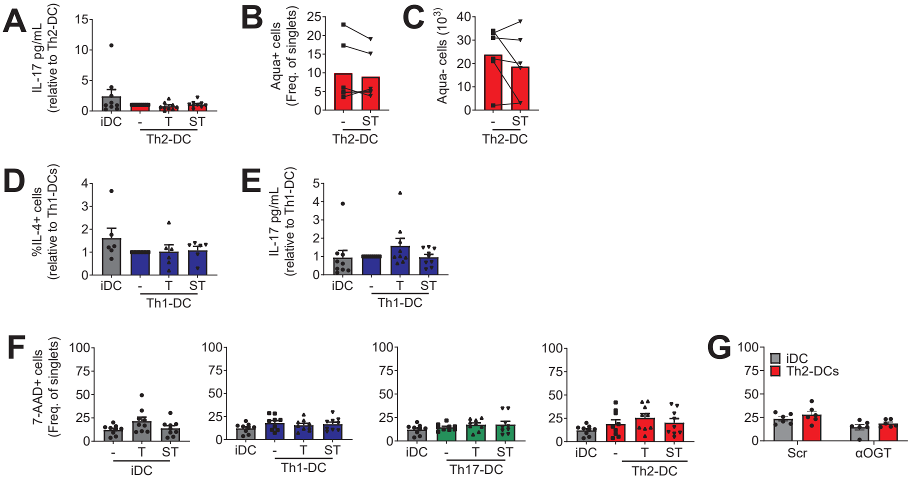

Figure S5.

Human moDCs were differentiated as normally (A-F) or short interfering RNA was introduced against O-GlcNAc transferase (OGT) at day 4 (G). Scrambled RNA was used as a control. At day 6, DCs were stimulated as normal with either LPS+PolyIC (Th1-DC in dark blue), zymosan (Th17-DC in green), omega-1 (Th2-DC in red) for 24 hours or left untreated (iDC in grey). DCs were then set aside for co-culture with allogeneic T cells (A-E) or viability was determined using flow cytometry (F-G).
(A, E) Co-culture with memory T cells. Supernatants were collected after 5 days and IL-17 concentrations was determined by ELISA.
(B-D) Co-culture with naïve T cells for 11 days. T cell viability (B) and numbers (C) were determined using flow cytometry. T cell intracellular IFNγ and IL-4 was analyzed by flow cytometry after a 6h stimulation with phorbol myristate acetate (PMA) and ionomycin (D). The percentages of T cells uniquely positive for either IL-4 are expressed relatively.
(F-G) Frequencies of dead DCs are enumerated.
The number of independent experiments is represented by symbols in the graphs and shown as mean ± SEM.

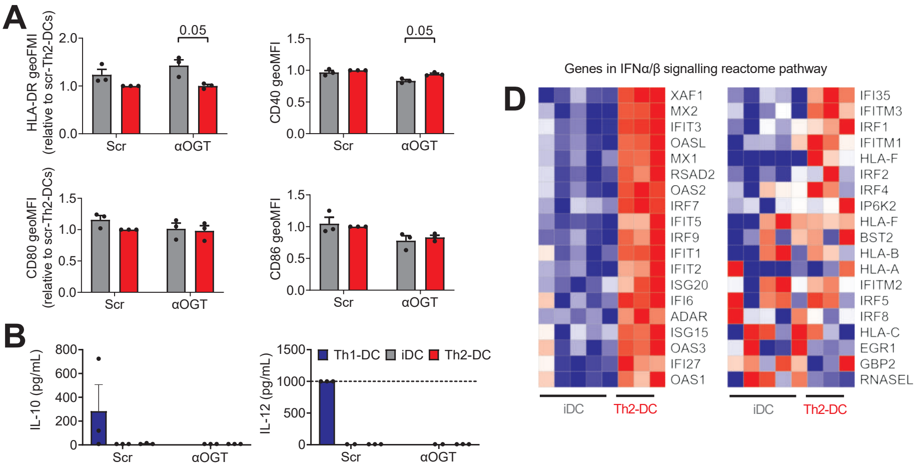

C

Reactome pathway analysis on top 200 DEGs up in Th2-DCs vs iDCs

Index	Name	Adjusted p-value	Combined score
1	Interferon alpha/beta signaling	1.25E-13	801.78
2	Interferon Signaling	5.04E-15	472.38
3	TRAIL signaling Homo sapiens	0.006402	441.63
4	CASP8 activity is inhibited	0.02344	239.56
5	Regulation by c-FLIP	0.02131	239.56
6	Dimerization of procaspase-8	0.01953	239.56
7	NF-kB activation through FADD/RIP-1 pathw ay mediated by caspase-8 and -10	0.02386	212.59
8	ISG15 antiviral mechanism	0.00001262	212.54
9	Antiviral mechanism by IFN-stimulated genes	0.00001052	212.54
10	Interferon gamma signaling	0.000012	185.78

Figure S6.

Human moDCs were differentiated as normally (C) or short interfering RNA was introduced against O-GlcNAc transferase (OGT) at day 4 (A-B). Scrambled RNA was used as a control. At day 6, DCs were stimulated as normal with omega-1 (Th2-DC in red) for 24 hours or left untreated (iDC in grey). Supernatants were then collected for determination of IL-10 and IL-12p70 secretion (B) and DCs were set aside for RNA-sequencing (C) and determination of maturation (A).
(A) The expression of maturation makers – based on the geometric mean fluorescence – are shown relative to iDCs.
(B) IL-10 and IL-12p70 concentrations was determined by ELISA.
(C) Top pathways are shown of pathway analysis on total transcriptome of differently conditioned DCs.
The number of independent experiments is represented by symbols in the graphs and shown as mean ± SEM.

Supplementary tables

Table 1. Antibodies used in study.

Target	Clone	Conjugate	Source	Identifier	Dilution
IL-4	8D4-8	PE	BD Biosciences	554516	1:250
IFNγ	25723.11	FITC	BD Biosciences	340449	1:20
CD16/32	Polyclonal	Pure	eBiosciences	14-9161	1:100
CD1a	BL6	PE	Beckman Coulter	A07742	1:50
CD14	MφP9	PerCP	BD Biosciences	345786	1:50
CD86	2331	PE-Cy7	BD Biosciences	561128	1:120
CD40	5C3	APC	BD Biosciences	555591	1:50
HLA-DR	LN3	APC-eF780	eBiosciences	47-9956	1:250
CD80	L307.4	HV450	BD Biosciences	560442	1:1000
O-GlcNAc	RL2	APC	Novus	NB300-524APC	1:4000
HLA-DR	G46-6	BV605	BD Biosciences	562844	1:50
CD1c	L161	BV711	BioLegend	331535	1:100
CD141	M80	BV421	BioLegend	344113	1:800
CD11c	B-ly6	PE-Cy7	BD Biosciences	561356	1:300
CD123	7G3	FITC	BD Biosciences	558663	1:50
CD56	B159	PE	BD Biosciences	555516	1:50
CD19	HIB19	PE	BioLegend	302207	1:100
CD3	UCHT1	PE	BioLegend	300407	1:50

8

LKB1 expressed in dendritic cells governs the development and expansion of thymus-derived regulatory T cells

Leonard R. Pelgrom
Thiago A. Patente
Alexey Sergushichev
Ekaterina Esaulova
Frank Otto
Arifa Ozir-Fazalalikhan
Hendrik J. P. van der Zande
Alwin J. van der Ham
Stefan van der Stel
Maxim N. Artyomov
Bart Everts

Cell Res. 2019 May;29(5):406-419
PMID: 30940876
DOI: 10.1038/s41422-019-0161-8

Introduction

Dendritic cells (DCs) form a central link between innate and adaptive immunity and are crucial for initiation and regulation of T cell responses both under inflammatory conditions as well as during steady state. DCs are also key regulators of immune homeostasis and maintenance of immune tolerance by governing the development of regulatory T cells (Tregs). Tregs can be induced in the thymus, referred to as thymic-derived Tregs (tTregs), as well as in the periphery (pTregs) from naïve T cells [1]. tTregs are characterized by a TCR repertoire that predominantly recognizes self-antigens and are important to maintain self-tolerance and to prevent auto-immunity [2]. pTregs, on the other hand, are thought to primarily govern tolerogenic responses against foreign antigens and microbes [3]. Whereas the mechanisms through which pTregs are induced in the periphery by DCs are fairly well characterized [4], the pathways through which DCs control tTreg development and homeostasis are still poorly defined.

There is a growing appreciation that activation and effector function of immune cells, including that of DCs, are dependent on reprogramming of intracellular metabolic pathways [5, 6]. Primarily in vitro studies have shown that an immunogenic phenotype of DCs induced by Toll-like receptor (TLR) activation depends on a glycolysis-driven anabolic program [7, 8], while a more catabolic type of metabolism is linked to quiescent and tolerogenic DCs, characterized by increased fatty acid oxidation and mitochondrial oxidative phosphorylation (OXPHOS) [8-10]. However, to what extent catabolic vs. anabolic metabolism of DCs regulates the balance between tolerogenic and immunogenic properties of DCs under physiological conditions, remains to be determined.

The tumor suppressor liver kinase B1 (LKB1, encoded by *Stk11*) is a bioenergetic sensor that controls cell metabolism and growth. LKB1 has several downstream targets, but it is most well known for being a key upstream activator of AMP-activated kinase (AMPK). Under low intracellular ATP levels, as a result of insufficient oxygen and/or nutrient availability to fuel mitochondrial OXPHOS and glycolysis to generate ATP, LKB1 phosphorylates AMPK. This allows AMPK to activate catabolic mitochondrial metabolism and to suppress anabolic sugar and lipid metabolic pathways to conserve energy and restore cellular bioenergetic homeostasis [11]. The role of LKB1 as a tumor suppressor has been well appreciated as germline mutations in *Stk11* are responsible for the inherited cancer disorder Peutz-Jeghers Syndrome [12] and as LKB1 is commonly mutated in various types of cancer [13]. More recently a picture is emerging that LKB1 also plays a key role in regulation of the immune system. For example, LKB1 was shown to be required for haematopoietic stem cell maintenance [14, 15] and T cell development in the thymus [16]. It is also crucial for metabolic and functional fitness of Tregs [17, 18] and can dampen pro-inflammatory responses in macrophages [19]. However, the physiological role of LKB1 in regulating metabolic and functional properties of DCs has not yet been explored.

We here report that loss of LKB1 in DCs results in disruption of mitochondrial fitness and enhanced immunogenic properties of these cells in vivo. Surprisingly, however, loss of LKB1 also greatly enhances the capacity of CD11b$^+$ DCs in the thymus to promote the generation of functional Tregs, through enhanced mTOR signalling and phospholipase C β1-driven CD86 expression. Our findings reveal a central role for LKB1 in DC metabolism and immune homeostasis, as it — depending on the context — acts as a critical brake on the immunogenic and tolerogenic properties of DCs.

Results

LKB1 promotes mitochondrial fitness in DCs and retains them in a quiescent state

To study the physiological role of LKB1 in the biology of DCs, *Stk11*$^{flox/flox}$ mice were crossed to *Itgax*^{cre} mice to generate mice with a selective deficiency for LKB1 in CD11c$^+$ cells. cDCs from the conditional knockout mice (CD11c$^{\Delta LKB1}$) showed a near complete loss of LKB1 expression (Fig. 1a). Furthermore, all major splenic DC subsets were present in similar frequencies and numbers as in Cre$^-$ littermates (CD11c^{WT}) (Fig. 1b, c; Supplementary information, Fig. S1a, b), suggesting loss of LKB1 has no major impact on DC homeostasis. Given the importance of LKB1 in cellular metabolism, we next assessed several mitochondrial parameters of, and glucose uptake by, splenic DC subsets. Consistent with previous reports, we found that cDC1s displayed higher mitochondrial mass, membrane potential and reactive oxygen species production compared to cDC2s [20, 21] (Fig. 1d). Interestingly, a marked defect in mitochondrial mass, membrane potential and reactive oxygen species production could be observed in both cDC subsets and pDCs from CD11c$^{\Delta LKB1}$ mice in spleen (Fig. 1d; Supplementary information, Fig. S2a) and LNs (Supplementary information, Fig. S2b, c), while glucose uptake was enhanced in the cDC2s due to LKB1 deficiency (Fig. 1e). We additionally characterized in vivo Flt3L-expanded splenic cDC subsets metabolically (Supplementary information, Fig. S3a). Although similar to unexpanded splenic cDCs, these cells displayed defects in several mitochondrial parameters (Supplementary information, Fig. S3b). No significant alterations in mitochondrial respiration could be observed due to loss of LKB1 (Supplementary information, Fig. S3d, e). Moreover, consistent with increased glucose uptake by unexpanded splenic cDC2s, glucose uptake (Supplementary information, Fig. S3c) and glycolytic rates (Supplementary information, Fig. S3f, g) were increased in Flt3L-expanded cDC2s, but not in cDC1s, from CD11c$^{\Delta LKB1}$ mice. Moreover, bone marrow-derived DCs (GMDCs) generated from CD11c$^{\Delta LKB1}$ mice showed metabolic alterations, characterized by reduced baseline mitochondrial respiration and spare respiratory capacity (Supplementary information, Fig. S4), suggesting an important role for LKB1 in maintaining mitochondrial fitness in various DCs subsets.

Phenotypically, cDCs, but not pDCs, from CD11c$^{\Delta LKB1}$ mice displayed an increased expression of several activation markers in spleen and LNs (Fig. 1f; Supplementary information, Fig. S5a-c) and had an altered cytokine production profile at steady state with lower TNF production but higher IL-6 secretion by cDC2s (Fig. 1g). It should be noted that we cannot rule out the possibility that the absence of a strong phenotype in pDCs may be the result of incomplete deletion of LKB1, due to intermediate CD11c and thereby Cre expression. In addition, analysis of peripheral lymph nodes (LNs) revealed a significantly increased accumulation of migratory DCs. On the other hand, frequencies and numbers of resident DC populations were in general not increased by LKB1 deficiency (Fig. 1h; Supplementary information, Fig. S5d, e), except for the number of inguinal LN-resident DCs (Fig. 1h), which went along with an increase in overall cell numbers in this LN in CD11c$^{\Delta LKB1}$ mice (Supplementary information, Fig. S5f). Together, with strongly upregulated CCR7 expression by migratory DCs (Supplementary information, Fig. S5g), this points towards enhanced baseline migration towards lymphoid organs by tissue-derived DCs when LKB1 is lost. Indeed, subcutaneously injected GMDCs from CD11c$^{\Delta LKB1}$ mice, which also expressed higher levels of CCR7 than their WT counterparts (Fig. 2a), accumulated more rapidly in draining LNs (Fig. 2b, c). Together, this suggests that LKB1 signalling is important for restricting spontaneous activation and migration of DCs under steady state conditions.

LKB1 limits the T cell-priming capacity of DCs

Next, we aimed to address how the loss of LKB1 would affect the T cell-priming capacities of DCs. To this end, we adoptively transferred GMDCs, pulsed in vitro with OVA and LPS, into footpads of recipient mice and analysed the T cell response in the draining LNs 7 days later (Fig. 2d). Compared to WT GMDCs, immunization with LKB1-deficient GMDCs resulted in a significantly greater expansion of effector CD44^{+}CD62L^{-}CD4^{+} and CD8^{+} T cells (Fig. 2e, h) and OVA-specific CD8^{+} T cells (Fig. 2f). Furthermore, enhanced production of IFN-γ by CD8^{+} T cells (Fig. 2g) and IFN-γ and IL-17 by CD4^{+} T cells (Fig. 2i–k) was also observed. Likewise, OVA-pulsed primary splenic cDC1s and cDC2s isolated from CD11c$^{\Delta LKB1}$ mice induced stronger in vitro proliferation of CD8^{+} (OT-I) and CD4^{+} (OT-II) T cells, respectively (Supplementary information, Fig. S6a–c), of which the latter also produced more IL-4 and IL-17 (Supplementary information, Fig. S6d). These data indicate that LKB1, by limiting DC activation in a cell-intrinsic manner, functions as a brake on the overall T cell-priming capacities of DCs.

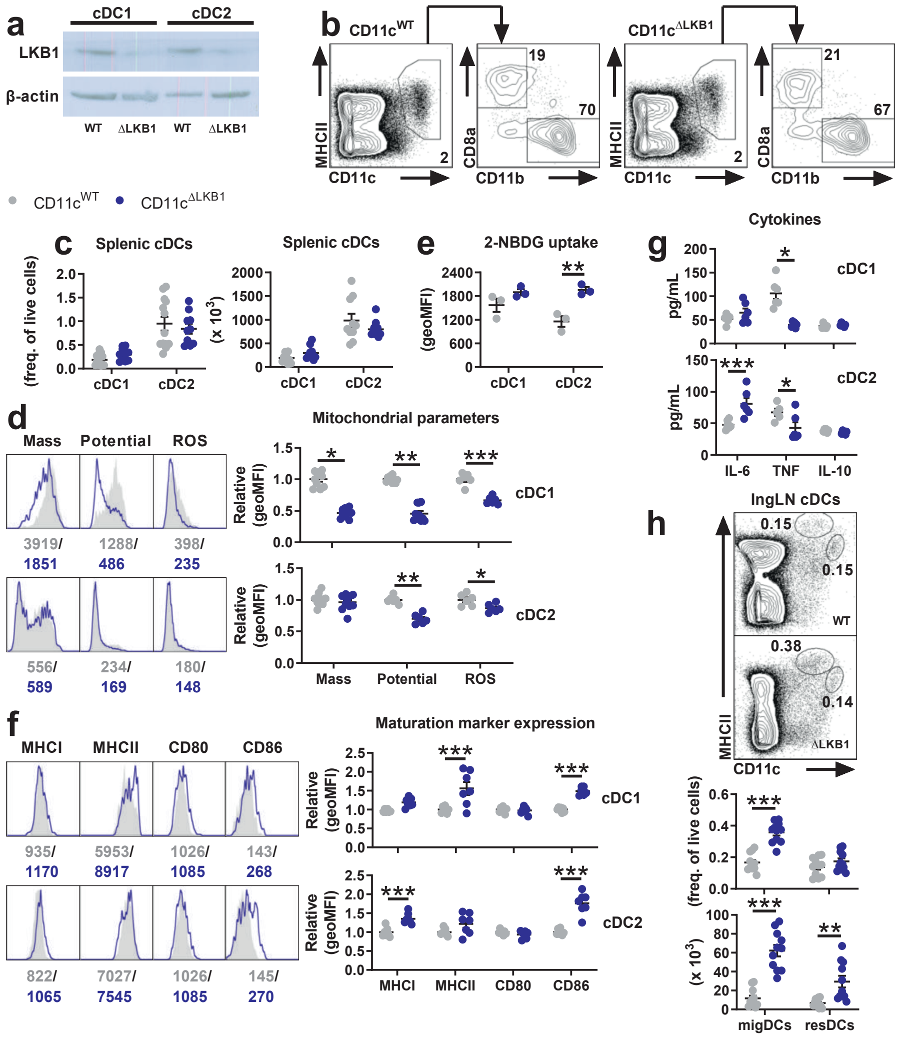
a
cDC1
cDC2
LKB1
β-actin
WT
ΔLKB1
WT
ΔLKB1
b
CD11c^WT
MHCII
CD11c
2
CD8a
CD11b
19
70
CD11c^ΔLKB1
MHCII
CD11c
2
CD8a
CD11b
21
67
● CD11c^WT ● CD11c^ΔLKB1
c
Splenic cDCs
(freq. of live cells)
2.0
1.5
1.0
0.5
0.0
cDC1
cDC2
Splenic cDCs
(x 10^3)
2000
1500
1000
500
0
cDC1
cDC2
e
2-NBDG uptake
(geoMFI)
2400
1800
1200
600
0
**
cDC1
cDC2
g
Cytokines
pg/mL
200
150
100
50
0
*
cDC1
150
100
50
0
***
*
cDC2
IL-6
TNF
IL-10
d
Mass
Potential
ROS
3919/
1851
1288/
486
398/
235
556/
589
234/
169
180/
148
Mitochondrial parameters
Relative (geoMFI)
1.5
1.0
0.5
0.0
*
**
***
cDC1
*
**
cDC2
Mass
Potential
ROS
h
IngLN cDCs
0.15
0.15
WT
0.38
0.14
ΔLKB1
MHCII
CD11c
(freq. of live cells)
0.6
0.4
0.2
0.0
***
(x 10^3)
100
80
60
40
20
0
***
**
migDCs
resDCs
f
MHCI
MHCII
CD80
CD86
935/
1170
5953/
8917
1026/
1085
143/
268
822/
1065
7027/
7545
1026/
1085
145/
270
Maturation marker expression
Relative (geoMFI)
2.5
2.0
1.5
1.0
0.5
0.0
***
***
cDC1
***
***
cDC2
MHCI
MHCII
CD80
CD86

Figure. 1 LKB1 promotes mitochondrial fitness in DCs and retains them in a quiescent state.

a Flt3L-expanded cDC1s and cDC2s were sorted from spleens of WT (CD11c^{WT}) and *Itgax*^{cre}*Stk11*$^{fl/fl}$ (CD11c$^{\Delta LKB1}$) mice before immunoblot analysis of LKB1 and β-actin. **b, c** Splenic cDC1s and cDC2s were identified as CD11c^{+}MHCII^{+}CD8a^{+} (or CD11c^{+}MHCII^{+}XCR1^{+}) and CD11c^{+}MHCII^{+}11b^{+} (CD11c^{+}MHCII^{+}CD172a^{+}) respectively as shown in representative flow cytometric plots ((**b**), see Supplementary information, Figure S1a for full gating). Percentages ((**c**), left) and absolute numbers ((**c**), right) were quantified. **d** Representative histograms (left) and relative expression (right) of mitochondrial mass, membrane potential and ROS production in splenic cDC1s (top) and cDC2s (bottom), as analysed by flow cytometry. **e** Uptake of a fluorescent glucose analogue by splenic cDCs detected using flow cytometry. **f** Representative histograms (left) and relative surface expression (right) of indicated markers by splenic cDC1s (top) and cDC2s (bottom). **g** Flt3L-expanded splenic cDC1s (top) and cDC2s (bottom) were sorted from spleens and put into culture. 16 h later, supernatants were harvested and analysed for indicated cytokines by cytokine bead array. **h** Migratory and resident DCs in the inguinal LN were identified as CD11c^{+}MHCII^{hi} and CD11c^{hi}MHCII^{+} respectively as shown in representative flow cytometric plots (top), and percentages (middle) and absolute numbers (bottom) were quantified. Data are pooled from 3 (**c, h**), 2 (**d, f, g**)2 or 1 (**e**) (independent) experiment(s) with three to four mice and shown as mean ± SEM; $*p < 0.05$, $**p < 0.01$, $***p < 0.001$

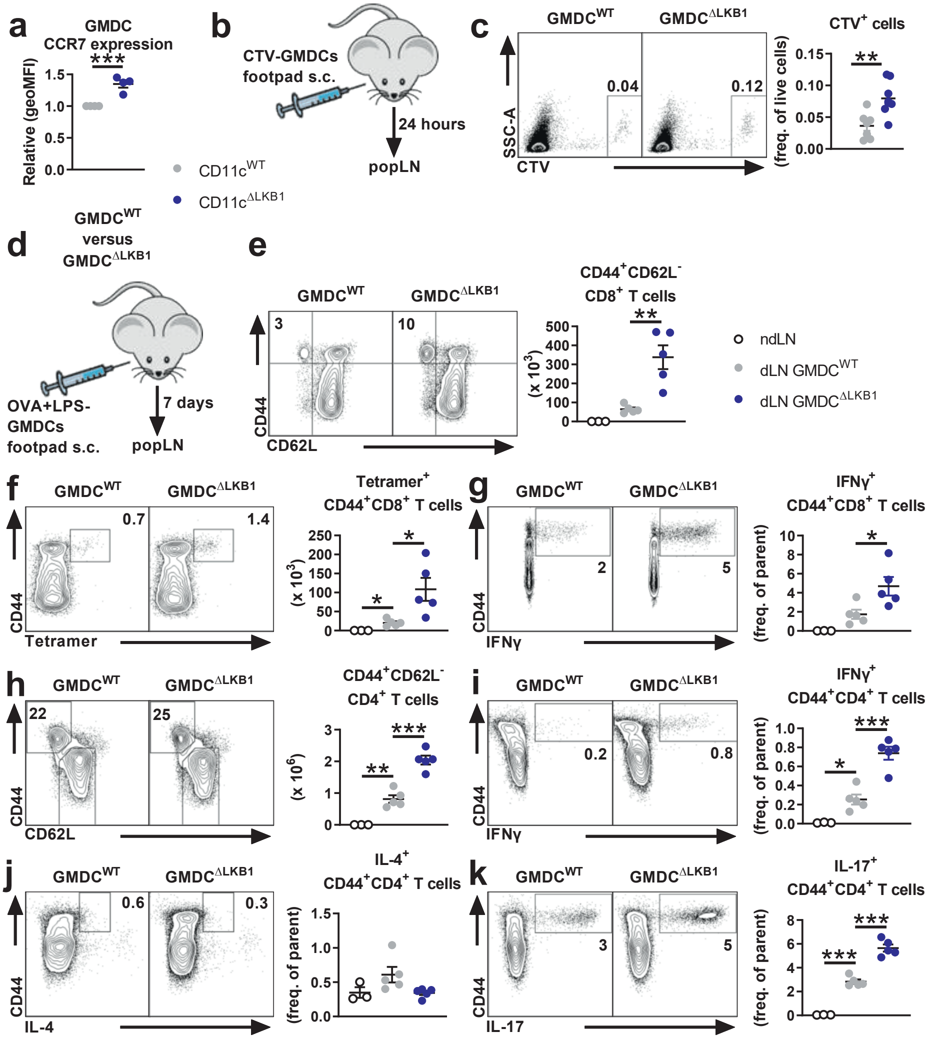
a
GMDC
CCR7 expression
***
Relative (geoMFI)
1.5
1.0
0.5
0.0
● CD11c^WT
● CD11c^ΔLKB1
b
CTV-GMDCs
footpad s.c.
24 hours
popLN
c
GMDC^WT
GMDC^ΔLKB1
0.04
0.12
SSC-A
CTV
CTV⁺ cells
**
(freq. of live cells)
0.15
0.10
0.05
0.00
d
GMDC^WT
versus
GMDC^ΔLKB1
OVA+LPS-
GMDCs
footpad s.c.
7 days
popLN
e
GMDC^WT
GMDC^ΔLKB1
3
10
CD44
CD62L
CD44⁺CD62L⁻
CD8⁺ T cells
**
(x 10³)
500
400
300
200
100
0
○ ndLN
● dLN GMDC^WT
● dLN GMDC^ΔLKB1
f
GMDC^WT
GMDC^ΔLKB1
0.7
1.4
CD44
Tetramer
Tetramer⁺
CD44⁺CD8⁺ T cells
*
*
(x 10³)
250
200
150
100
50
0
g
GMDC^WT
GMDC^ΔLKB1
2
5
CD44
IFNγ
IFNγ⁺
CD44⁺CD8⁺ T cells
*
(freq. of parent)
10
8
6
4
2
0
h
GMDC^WT
GMDC^ΔLKB1
22
25
CD44
CD62L
CD44⁺CD62L⁻
CD4⁺ T cells
**
***
(x 10⁶)
3
2
1
0
i
GMDC^WT
GMDC^ΔLKB1
0.2
0.8
CD44
IFNγ
IFNγ⁺
CD44⁺CD4⁺ T cells
*
***
(freq. of parent)
1.0
0.8
0.6
0.4
0.2
0.0
j
GMDC^WT
GMDC^ΔLKB1
0.6
0.3
CD44
IL-4
IL-4⁺
CD44⁺CD4⁺ T cells
(freq. of parent)
1.5
1.0
0.5
0.0
k
GMDC^WT
GMDC^ΔLKB1
3
5
CD44
IL-17
IL-17⁺
CD44⁺CD4⁺ T cells
***
***
(freq. of parent)
8
6
4
2
0

Figure. 2 LKB1 limits the T cell-priming capacity of DCs.

a Surface expression of CCR7 on GM-CSF-cultured BM-derived DCs (GMDCs) from CD11c^{WT} and CD11c$^{\Delta LKB1}$ mice as analysed by flow cytometry. **b, c** CTV-labeled GMDCs from CD11c^{WT} and CD11c$^{\Delta LKB1}$ mice were injected into footpads of WT mice. 24 h later, migrated GMDCs were quantified in draining popliteal LNs by flow cytometry. **d–k** GMDCs were stimulated for 6 hours with OVA and LPS and then, injected into footpads of WT mice. 7 days later, T cell responses were evaluated in draining popliteal LNs by flow cytometry (**e–k**). **e** Frequencies of CD44$^+$CD62L$^-$ effector CD8$^+$ T cells are shown in representative flow cytometry plots (left) and enumerated (right). **f** Frequencies of CD44$^+$ OVA-specific CD8$^+$ T cells, based on KbOva tetramer, are shown in representative flow cytometry plots (left) and enumerated (right). **g** Popliteal LN cells were stimulated with PMA/Ionomycin in the presence of ΩBrefeldin A and CD8$^+$ T cells were analysed for expression of indicated cytokines as shown in representative flow cytometry plots (left) and enumerated (right). **h** Frequencies of CD44$^+$CD62L$^-$ effector CD4$^+$ T cells are shown in representative flow cytometry plots (left) and enumerated (right). **i–k** Popliteal LN cells were stimulated as in (**g**) and CD4$^+$ T cells were analysed for expression of indicated cytokines as shown in representative flow cytometry plots (left) and enumerated (right). Data are pooled from 4 independent experiments (**a**), 2 independent experiments with four mice (**c**) or 1 experiment with five mice (**e–k**) and shown as mean ± SEM; $*p < 0.05$, $**p < 0.01$, $***p < 0.001$

CD11c$^{\Delta LKB1}$ mice have impaired responses to immunization and are less capable of controlling tumor growth due to a DC-extrinsic immune suppressive environment

Given the increased pro-inflammatory properties of LKB1-deficient DCs, we hypothesized that CD11c$^{\Delta LKB1}$ mice would mount stronger immune responses in response to immunization. However, unexpectedly, in a model of subcutaneous immunization (Fig. 3a), CD11c$^{\Delta LKB1}$ mice showed impaired antigen-specific CD8$^+$ T cell responses (Fig. 3d) and reduced production of IFN-γ by both CD8$^+$ (Fig. 3b) and CD4$^+$ T cells (Fig. 3c). Consistent with these data, we found that CD11c$^{\Delta LKB1}$ mice challenged with a B16 melanoma tumor (Fig. 3e), for which both CD4$^+$ and CD8$^+$ T cell responses are required for anti-tumor immunity [22], had a more rapid outgrowth of those tumors than CD11c^{WT} mice (Fig. 3f). These data together suggest that despite the pro-inflammatory signature of DCs present in CD11c$^{\Delta LKB1}$ mice, these mice display an immune-suppressed phenotype.

To reconcile these at first sight contradictory observations, we hypothesized that there may be additional changes in the overall immunological profile of CD11c$^{\Delta LKB1}$ mice outside the DC compartment that counteract the increased immunogenic properties of LKB1-deficient DCs, and could account for the immune-suppressed phenotype. To explore the possibility that the immune-suppressive environment could be DC extrinsic in these mice, we adoptively transferred WT GMDCs, pulsed in vitro with OVA and LPS, into footpads of either CD11c^{WT} or CD11c$^{\Delta LKB1}$ mice and subsequently analysed T cell responses in these mice (Fig. 3g). We observed a reduced ability to prime effector T cell responses by WT DCs in the CD11c$^{\Delta LKB1}$ mice compared to CD11c^{WT} mice, as evidenced by lower cytokine production in primed T cells (Fig. 3h, i), providing support for the existence of an DC-extrinsic immune-suppressive environment in CD11c$^{\Delta LKB1}$ mice.

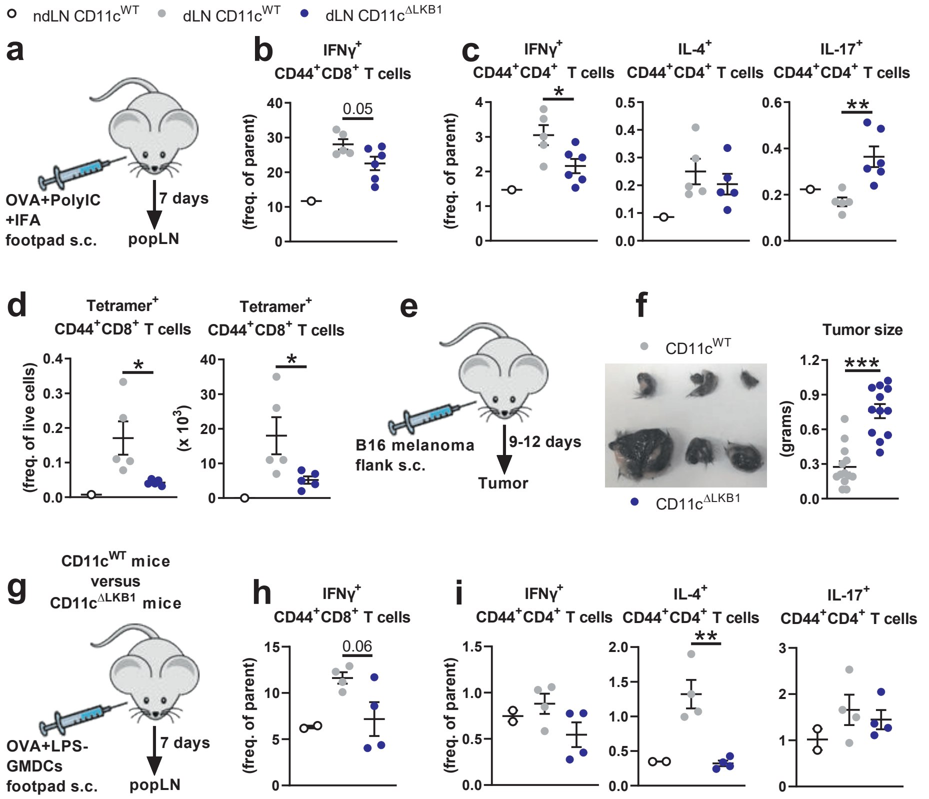

Figure. 3 CD11c$^{\Delta LKB1}$ mice have impaired responses to immunization and are less capable of controlling tumor growth.

a–d CD11c^{WT} and CD11c$^{\Delta LKB1}$ mice were immunized with Poly (I:C) and OVA in incomplete Freund's adjuvant into the footpad. 7 days later, T cell responses were evaluated in draining popliteal LNs by flow cytometry. **b, c** Popliteal LN cells were stimulated with PMA/Ionomycin in the presence of Brefeldin A and CD8$^+$ T cells (**b**) and CD4$^+$ T cells (**c**) were analysed for expression of indicated cytokines by flow cytometry. **d** Percentages (left) and absolute numbers (right) of CD44$^+$ OVA-specific CD8$^+$ T cells, based on KbOva tetramer, were quantified by flow cytometry. **e, f** B16 melanoma tumour cells were injected into the flank of CD11c^{WT} and CD11c$^{\Delta LKB1}$ mice and tumour weight was determined 9 to 12 days later. **g–i** GMDCs were stimulated for 6 h with OVA and LPS and then, injected into footpads of CD11c^{WT} and CD11c$^{\Delta LKB1}$ mice. 7 days later, T cell responses were evaluated in draining popliteal LNs by flow cytometry (**h, i**). Popliteal LN cells were stimulated as in (**c**) and CD8$^+$ T cells (**h**) and CD4$^+$ T cells (**i**) were analysed for expression of indicated cytokines. Data are pooled from 4 independent experiments with three to four mice (**f**) or1 experiment with four to five mice (**b–d, h, i**) and shown as mean ± SEM; $*p < 0.05$, $**p < 0.01$, $***p < 0.001$

LKB1-deficiency in DCs results in a dramatically expanded functional Treg pool in vivo that is associated with protection against allergic asthma

Given the well-established critical role of Tregs in regulation and suppression of immune responses, we wondered whether alterations in the Treg compartment could provide an explanation for the immune-suppressed phenotype of CD11c$^{\Delta LKB1}$ mice. When we analysed the T cell pool of naïve CD11c$^{\Delta LKB1}$ mice, we found a dramatically expanded pool, both in frequencies and numbers, of Foxp3^{+} Tregs in spleen and peripheral LNs relative to CD11c^{WT} mice (Fig. 4a). In comparison to Tregs from CD11c^{WT} mice, these Tregs expressed increased levels of immune-suppressive markers glucocorticoid-induced TNFR family-related gene (GITR), cytotoxic T lymphocyte-associated antigen 4 (CTLA4) and activation marker CD44, but lower levels of CD25 (Fig. 4b), an expression profile that has been linked to effector (e)Tregs [23]. Moreover, on a per cell basis, Tregs from CD11c$^{\Delta LKB1}$ mice showed an enhanced capacity to suppress bystander T cell proliferation in vitro (Fig. 4c, d). To further characterize the Tregs from these mice, we analyzed and compared the TCR repertoire of CD25^{hi}CD4^{+} Tregs from CD11c$^{\Delta LKB1}$ and CD11c^{WT} mice. The distribution of the most frequently used V and J genes from both TCRα and β was similar between Tregs from CD11c$^{\Delta LKB1}$ and CD11c^{WT} mice (Supplementary information, Fig. S7), suggesting no major differences between the TCR repertoire of the Tregs from the two mouse strains. This indicates that 1) the expanded Treg pool in CD11c$^{\Delta LKB1}$ mice is not due to selective outgrowth of Tregs with particular antigen specificity and 2) the increased suppressive function of Tregs in CD11c$^{\Delta LKB1}$ mice is not the result of altered antigen specificity, but more likely a consequence of potentiated antigen-independent bystander suppression due to increased expression of immunoregulatory markers [24-26].

To assess whether this increased functional Treg pool in CD11c$^{\Delta LKB1}$ mice could also be associated with a beneficial effect on disease outcome, we challenged mice with house dust mite to induce allergic asthma (Fig. 5a), which is a Type 2 immunity-driven disease model in which Tregs can provide protection against allergic inflammation [27]. CD11c^{WT} mice were highly susceptible to induction of HDM-driven allergic asthma, as evidenced by increased cellular infiltrate in the bronchioalveolar lavage (BAL) (Fig. 5b), increased accumulation of eosinophils in BAL and lung (Fig. 5c–e), and strong antigen-specific production of the Type 2 cytokines IL-4, IL-5, IL-10 and IL-13 by immune cells in the lung-draining mediastinal LN (Fig. 5f). Remarkably, CD11c$^{\Delta LKB1}$ mice were totally resistant to developing this allergic response (Fig. 5b–e), which corresponded with significantly increased frequencies of Tregs in lungs and medLNs both before and after HDM challenge (Fig. 5g, h). This shows that in vivo LKB1 signalling in DCs is crucial for limiting excessive Treg induction, which is correlated with susceptibility to allergic asthma as a model of an inflammatory disease.

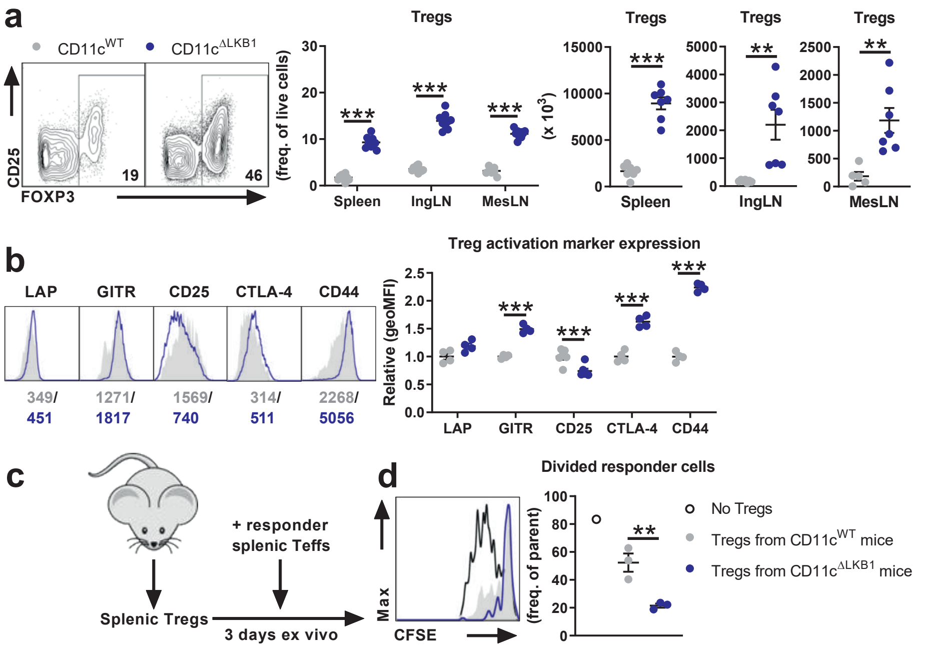

Figure. 4 LKB1-deficiency in DCs results in a dramatically expanded functional Treg pool in vivo.

a Tregs in spleens, inguinal LNs and mesenteric LNs from CD11c^{WT} and CD11c$^{\Delta LKB1}$ mice were identified as CD3$^+$CD4$^+$FOXP3$^+$ as shown in representative flow cytometry plots from the spleen (left). Frequencies (middle) and absolute numbers (right) were quantified by flow cytometry. **b** Representative histograms (left) and relative surface expression (right) are shown of indicated markers by splenic Tregs. **c, d** T cell suppression assay, in which the ability of CD25^{hi}CD4$^+$ T cells sorted from spleens of CD11c^{WT} and CD11c$^{\Delta LKB1}$ mice to suppress anti-CD3- and splenocyte-induced proliferation of CFSE-labeled CD25$^-$CD4$^+$ T cells as responder cells was evaluated. Proliferation of responder cells was evaluated by CFSE dilution after 3 days as shown in a representative histogram (left) and quantified (right). Data are pooled from 2 to 3 independent experiments with three to four mice (**a**), 1 experiment with four mice (**b**) or is a representative of 2 independent experiments (**d**) and shown as mean ± SEM; *$p < 0.05$, **$p < 0.01$, ***$p < 0.001$

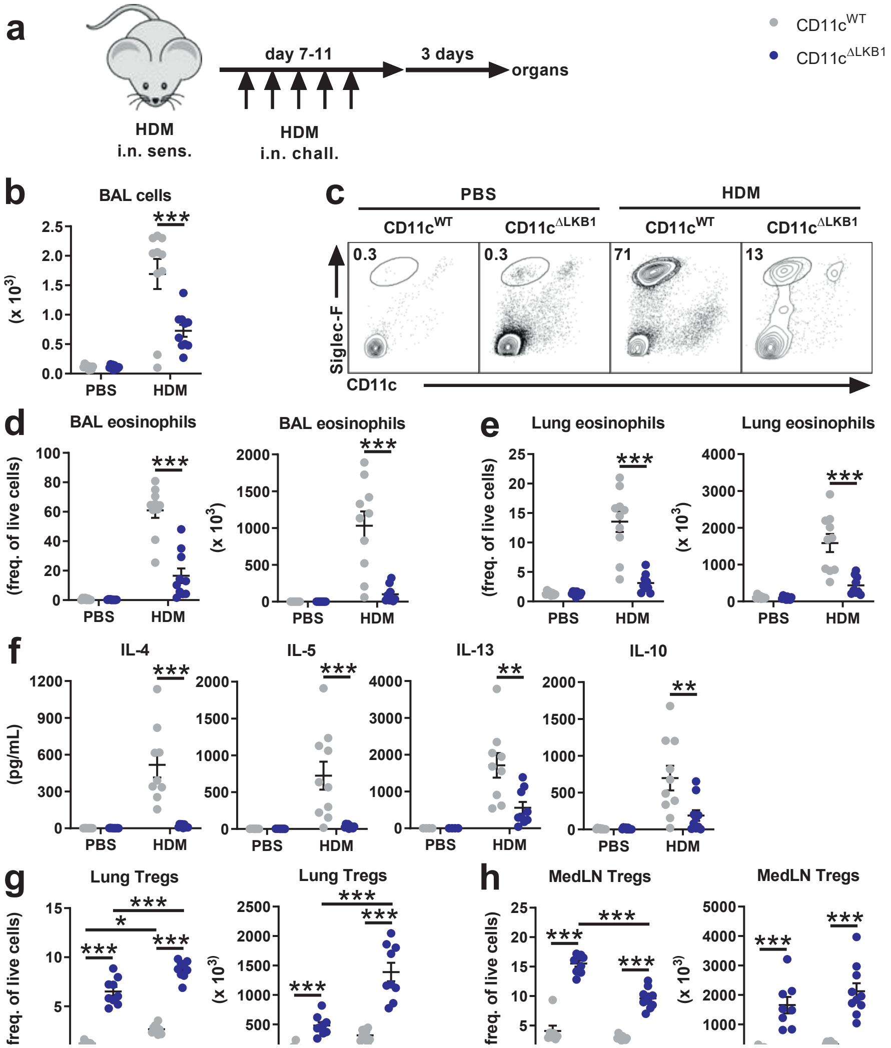

Figure. 5 LKB1-deficiency in DCs protects mice from allergic asthma.

a–h CD11c^{WT} and CD11c$^{\Delta LKB1}$ mice were sensitized by intranasal application of HDM and 1 week later challenged for 5 consecutive days. 3 days after the challenge, allergic airway inflammation was evaluated in bronchoalveolar lavage (BAL), lungs and lung-draining mediastinal LNs by flow cytometry. **b** Inflammatory cell recruitment was determined in BAL by cell counts. **c–e** Eosinophils were identified as Siglec-F$^+$CD11c$^-$ as shown in representative flow cytometry plots from the BAL (**c**). BAL eosinophil percentages ((**d**), left) and absolute numbers ((**d**), right) and lung eosinophil percentages ((**e**), left) and absolute numbers ((**e**), right) were quantified. **f** Mediastinal LN cells were restimulated with HDM and 3 days later, supernatants were harvested and analysed for indicated cytokines by cytokine bead array. **g, h** Tregs identified as CD3$^+$CD4$^+$FOXP3$^+$. Lung Tregs percentages ((**g**), left) and absolute numbers ((**g**), right) and MedLN Treg percentages ((**h**), left) and absolute numbers ((**h**), right) were quantified. Data are pooled from 2 independent experiments with three to five mice and shown as mean ± SEM; *$p < 0.05$, **$p < 0.01$, ***$p < 0.001$

LKB1 restricts the ability of thymic CD11b$^+$ cDC2s to drive tTreg generation

Tregs can originate from the thymus (tTregs) as well as develop from naïve T cells in the periphery (pTregs). Under steady state conditions, tTregs can be identified based on the expression of Helios [28, 29]. We observed that a higher frequency and number of Tregs from CD11c$^{\Delta LKB1}$ mice expressed Helios than their counterparts in CD11c^{WT} mice, suggesting that Tregs from CD11c$^{\Delta LKB1}$ mice are of thymic origin (Fig. 6a). Consistent with this notion, we observed increased frequencies and numbers of Tregs in the thymus of adult CD11c$^{\Delta LKB1}$ mice (Fig. 6b), despite a normal distribution of thymocyte subsets (Supplementary information, Fig. S8a), although it cannot be ruled out that pTregs circulating through the thymus could also potentially contribute to this phenotype [30]. However, we found that at 6 days after birth, which is just after the start of tTreg development in mice [31], the frequencies and numbers of Tregs were higher in thymi of CD11c$^{\Delta LKB1}$ mice (Fig. 6c), but not in spleens (Supplementary information, Fig. S8b). Together, these data provide support for the notion that the phenotype of accumulated Tregs in CD11c$^{\Delta LKB1}$ mice is initiated in the thymus, concurrent with the beginning of natural tTreg development. Moreover, given the eTreg-like features of tTregs from CD11c$^{\Delta LKB1}$ mice, and the highly proliferative nature of eTregs [23], we wondered whether in addition to increased tTreg output from thymus, enhanced peripheral proliferation of tTregs is occurring, which could contribute to the enlarged Treg pool in these mice. Indeed, in LNs from adult CD11c$^{\Delta LKB1}$ mice, we found a significantly higher frequency of Ki67$^+$ Tregs compared to WT mice (Supplementary information, Fig. S8c), although this was not clearly seen in spleens. In addition, we found that in in vitro cultures of peripheral tTregs with splenic DCs, Tregs proliferated faster when cocultured with cDC2s isolated from CD11c$^{\Delta LKB1}$ mice than from WT counterparts (Supplementary information, Fig. S8d). Of note, cDC1s did not show a difference in this assay. These data indicate that, in addition to increased tTreg output from thymus, enhanced peripheral proliferation of tTregs may contribute to the observed tTreg accumulation in CD11c$^{\Delta LKB1}$ mice.

Next, we aimed to further understand how loss of LKB1 in DCs enhanced Treg output from the thymus. Three major DC subsets have been described to be present in the thymus: CD8a$^+$ cDC1s, CD11b$^+$ cDC2s and pDCs, all of which have, depending on the model studied, been implicated in tTreg development [32-35]. We found that cDC2s, but not cDC1s or pDCs, were present in an approximately two-fold higher frequency in thymi of CD11c$^{\Delta LKB1}$ compared to CD11c^{WT} mice (Fig. 6d; Supplementary information, Fig. S9a), although due to reduced total cell number of thymi from CD11c$^{\Delta LKB1}$ mice, total cDC2 numbers were not elevated (Fig. 6d; Supplementary information, Fig. S9b). The increased frequency of cDC2s in thymi CD11c$^{\Delta LKB1}$ mice correlated with a higher surface expression of CCR7 selectively on these DCs (Supplementary information, Fig. S9c). Ki67 staining was similar between cDC2s from thymi of CD11c$^{\Delta LKB1}$ and CD11c^{WT} mice, indicating no differences in proliferative rates (Supplementary information, Fig. S9d). In addition, consistent with what was observed for splenic cDCs, thymic cDCs from CD11c$^{\Delta LKB1}$ mice had reduced mitochondrial mass and membrane potential (Supplementary information, Fig. S9e).

tTregs have been shown to primarily develop from immature single positive (SP) CD4$^+$ CD25$^-$ thymocytes [31]. To identify which DC subset(s) may drive the enhanced tTreg generation, we used an ex vivo DC-thymocyte coculture model [35], in which we assessed the ability of different thymic DC subsets to induce expression of Foxp3$^+$ in SP CD4$^+$ CD25$^-$GFP$^-$ thymocytes sorted from foxp3-GFP/DTR (DEREG) mice (Supplementary information, Fig. S10a, d). Given the rarity of thymic DCs, in vivo Flt3L-expanded thymic DC subsets were used for these experiments. Consistent with a previous report using this model [35], we found that cDC2s from CD11c^{WT} mice tended to have a superior ability to induce Foxp3$^+$ Tregs from Foxp3$^-$ thymocytes, over cDC1s and pDCs (Fig. 6e, f). Importantly, cDC2s isolated from CD11c$^{\Delta LKB1}$ mice showed a further enhanced capacity to generate Foxp3$^+$ Tregs from Foxp3$^-$ thymocytes (Fig. 6f). Concomitantly, some additional expansion of Foxp3$^-$ T cells could be observed (Supplementary information, Fig. S10b). The tTreg-generating ability of the other two DC subsets was unaffected by loss of LKB1 (Fig. 6f). Moreover, doubling the number cDC2s from CD11c$^{\Delta LKB1}$ mice in these cultures, to mimic the increased frequency of cDC2s found in thymi of these mice, further boosted tTreg output (Fig. 6g). This would suggest that both cell-intrinsic differences and changes in frequency of cDC2s as a consequence of LKB1 deficiency could account for the increased tTreg generation. Of note, in analogous cocultures of splenic DCs with splenic naïve conventional CD25$^-$GFP$^-$CD4$^+$ T cells (Supplementary information, Fig. S10c) or of OVA-peptide pulsed splenic DCs with naïve OVA-specific OT-II CD4$^+$ T cells (data not shown), no differential induction of Foxp3$^+$ Tregs could be observed. Together, these findings suggest that LKB1 signalling in DCs is critically important for selectively keeping tTreg generation in check, specifically by limiting the ability of thymic cDC2s to promote tTreg generation.

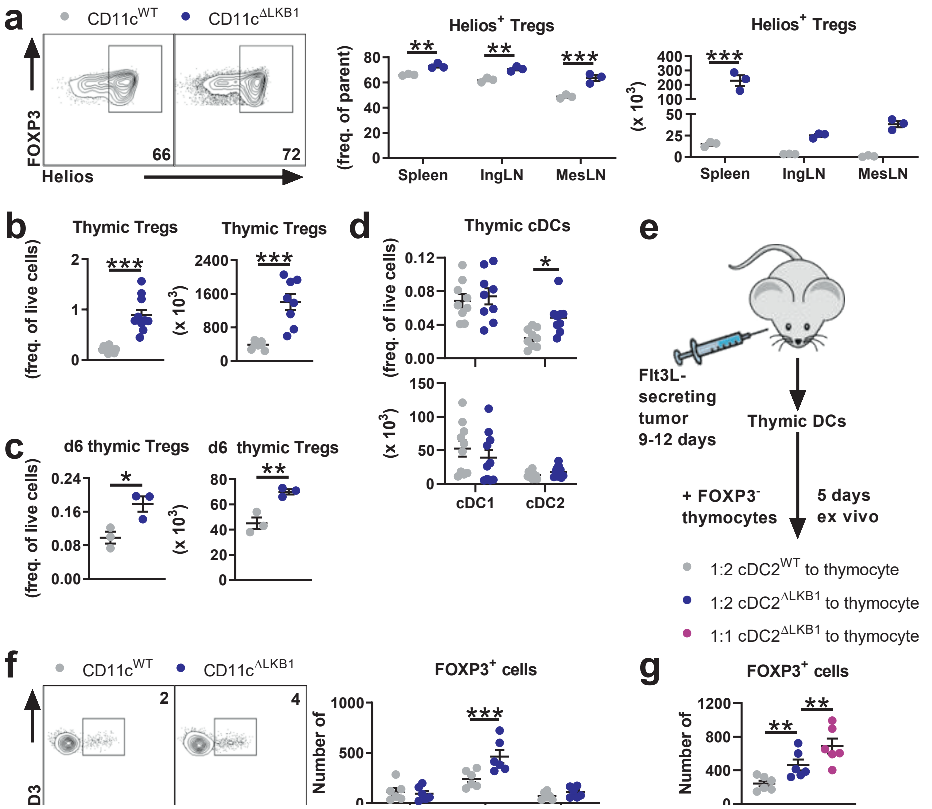

Figure. 6 LKB1 restricts the ability of thymic CD11b^{+} cDC2s to drive tTreg generation.

a Intracellular Helios expression in Tregs identified as CD3^{+}CD4^{+}FOXP3^{+} from indicated peripheral organs of CD11c^{WT} and CD11c$^{\Delta LKB1}$ mice as shown in representative flow cytometry plots of splenic Tregs (left). Percentages (middle) and absolute numbers (right) were quantified by flow cytometry. **b** Percentages (left) and absolute numbers (right) of Tregs in thymi of CD11c^{WT} and CD11c$^{\Delta LKB1}$ mice were quantified. **c** Percentages (left) and absolute numbers (right) of Tregs in thymi of 6 days old CD11c^{WT} and CD11c$^{\Delta LKB1}$ pups were quantified. **d** Thymic cDC1s and cDC2s were identified as CD11c^{+}MHCII^{+}CD8a^{+} (or CD11c^{+}MHCII^{+}XCR1^{+}) and CD11c^{+}MHCII^{+}11b^{+} (CD11c^{+}MHCII^{+}CD172a^{+}) respectively (see Supplementary information, Figure S1a for gating strategy), and percentages (top) and absolute numbers (bottom) were quantified. **e, f** Flt3L-expanded thymic cDC1s, cDC2s and pDCs, the last identified as Siglec-H^{+}CD11c^{int}, were sorted and cocultured in the presence of IL-7 with GFP^{-}CD25^{-} single positive CD4^{+} thymocytes sorted from DEREG mice. After 5 days, frequencies of newly generated GFP^{+}(FOXP3^{+}) cells were determined as shown in representative flow cytometric plots of cocultures with thymic cDC2s ((**f**), left) and enumerated ((**f**), right). **g** Coculture as in (**f**) but with double amount of thymic cDC2s. Data are pooled from 3 (**b, d**), 2 (**f, g**) or 1 (**a, c**) (independent) experiment(s) with three to four mice and shown as mean ± SEM; *$p < 0.05$, **$p < 0.01$, ***$p < 0.001$

LKB1 signalling restricts tTreg generation by thymic cDC2 by limiting mTOR, calcium signalling and expression of CD86

Finally, we aimed to delineate the underlying immunological and molecular mechanism(s) through which LKB1 limits thymic cDC2s to promote generation of tTregs. We found either very low or no difference in mRNA expression of cytokines linked to fostering tTreg development [36-38], including IL-2, IL-7, IL-15 and TGFβ1/2, between thymic cDC2s from CD11c$^{\Delta LKB1}$ and CD11c^{WT} mice (Fig. 7a). However, we did find a selective increase in expression of CD86 on both Flt3L-expanded and unexpanded thymic cDC2s from CD11c$^{\Delta LKB1}$ mice (Fig. 7b; Supplementary information, Fig. S11a). Increased expression of CD86 on thymic cDC2s from CD11c$^{\Delta LKB1}$ mice was already evident at day 6 after birth (Supplementary information, Fig. S11b), which coincides with the initiation of the increased tTreg output from the thymus in these mice. The frequencies of these DCs were not yet increased on day 6 (Supplementary information, Fig. S11c). Costimulation provided by CD80 and CD86 is known to be crucial for tTreg development as tTreg generation in CD80/86 or CD28 KO mice is severely compromised [39, 40]. Importantly, addition of low doses of neutralizing anti-CD86 to cDC2:thymocyte cocultures as described in Fig. 6g — to reduce, but not entirely block CD86-mediated costimulation — selectively counteracted the enhanced tTreg-generating ability of LKB1-deficient cDC2s, back to levels similar to those induced by WT cDC2s (Fig. 7c), suggesting that the increased CD86 expression accounts for the observed phenotype.

The most well-characterized substrate through which LKB1 regulates cellular functions and metabolism is AMPK, which mediates its effects through its catalytic α–subunit [41]. Of the two α–subunit isoforms that exist, myeloid cells express only AMPKα1 [42]. To assess whether LKB1 controls the tTreg-generating ability of thymic cDC2s through AMPK signalling, we crossed *Prkaa1*$^{flox/flox}$ mice (encoding AMPKα1) with *Itgax*^{cre} mice (CD11c$^{\Delta AMPK\alpha1}$). Thymic DCs from both CD11c$^{\Delta LKB1}$ (Supplementary information, Fig. S11d) and CD11c$^{\Delta AMPK\alpha1}$ (Supplementary information, Fig. S11e) mice showed a comparable defect in AMPK signalling, which was measured by phosphorylation of the bona fide AMPK substrate ACC at serine 79. Surprisingly, however, in contrast to what we found in CD11c$^{\Delta LKB1}$ mice, Treg populations in both spleens and thymi from CD11c$^{\Delta AMPK\alpha1}$ mice were similar in size to that of CD11c^{WT} mice (Supplementary information, Fig. S11f), demonstrating that the observed Treg phenotype in CD11c$^{\Delta LKB1}$ mice is driven in an AMPK-independent manner. Of note, metabolic changes observed in DCs from CD11c$^{\Delta LKB1}$ mice, were not seen in DCs from CD11c$^{\Delta AMPK\alpha1}$ mice, indicating that LKB1-induced metabolic properties in DCs are also mediated independently from AMPK (Supplementary information, Fig. S11g, h). In an attempt to identify how LKB1 regulates the tTreg-generating ability of thymic cDC2s independently from AMPK, the transcriptome of thymic cDC2s from CD11c$^{\Delta LKB1}$ mice was analysed and compared to that of the other thymic DC subsets, as well as to those from CD11c^{WT} mice. This revealed that loss of LKB1 had the largest impact on the transcriptome of cDC2s, in comparison to cDC1s and pDCs, resulting in total of 70 significantly differentially expressed genes between KO and WT cDC2s (Fig. 7d; Supplementary information, Fig. S12). The single most strongly upregulated gene (800 fold) in LKB1-deficient cDC2s was *plcb1*, which encodes phospholipase C β1 (PLC-β1) (Fig. 7d). PLC, by activation of inositol trisphosphate receptor (IP3R), promotes calcium release and signalling in cells, which has been shown to be crucial for DC activation, migration and T cell priming [43]. Consistent with this increased expression of PLC-β1, we found elevated baseline calcium levels in thymic LKB1-deficient cDC2s (Fig. 7e). When we lowered PLC activity, using low doses of a PLC inhibitor, or inhibited IP3R in LKB1-deficient cDC2s, the increased CD86 expression was selectively reduced in LKB1-deficient cDC2s (Fig. 7f, g), which concordantly resulted in a reduction of their tTreg-generating ability to similar levels as thymic LKB1-sufficient cDC2s (Fig. 7h). In addition, gene set enrichment analysis for biological processes indicated increased translational activity in LKB1-deficient cDC2s (Supplementary information, Fig. S13a). The mammalian target of rapamycin (mTOR) signalling pathway is an important positive regulator of translation and its activation is antagonized by AMPK signalling [44]. Consistent with impaired AMPK signalling and an increased translational signature, thymic DCs from CD11c$^{\Delta LKB1}$ mice displayed heightened mTOR signalling as determined by phosphorylation of S6 on serine 235 and 236 (Supplementary information, Fig. S13b). Blocking of mTOR did not significantly reduce CD86 expression in LKB1-deficient cDC2s (Supplementary information, Fig. S13c). However, it did result in a significant reduction of their tTreg-generating ability, back to similar levels as LKB1-sufficient cDC2s (Supplementary information, Fig. S13d), suggesting a role for enhanced mTOR signalling in this phenotype independent from regulation of CD86. These observations indicate that LKB1, independently from AMPK, keeps tTreg generation in check by limiting mTOR signalling and calcium signalling-induced costimulation by thymic cDC2s.

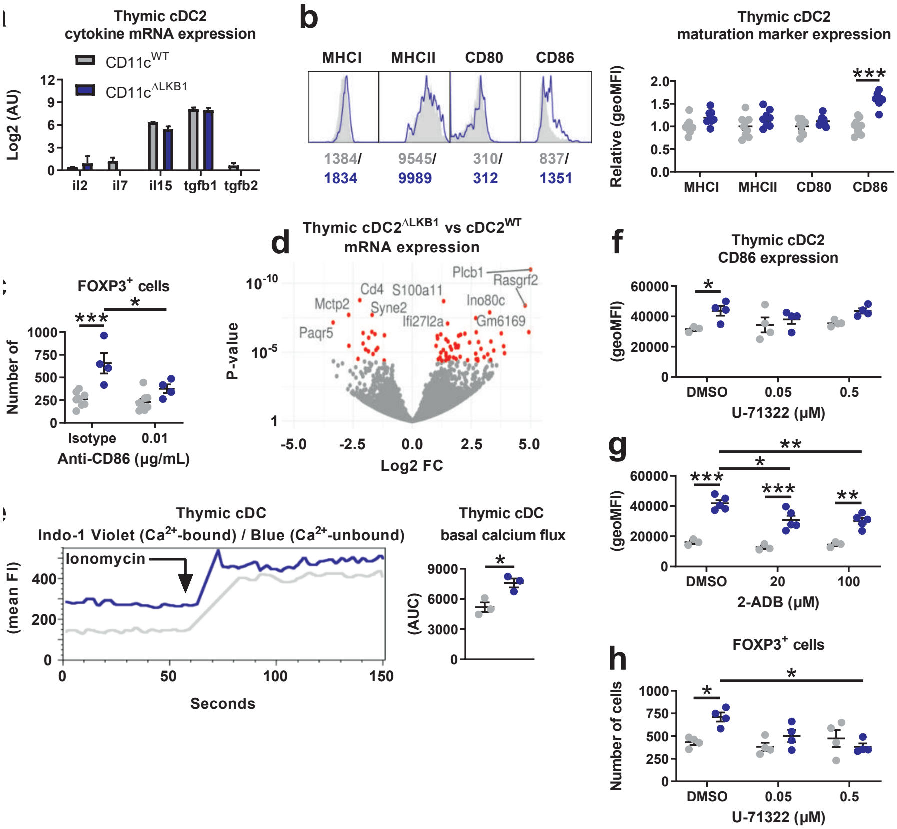
Thymic cDC2
cytokine mRNA expression
CD11c^{WT}
CD11c$^{\Delta LKB1}$
Log2 (AU)
12
9
6
3
0
il2
il7
il15
tgfb1
tgfb2
b
MHCI
MHCII
CD80
CD86
1384/
1834
9545/
9989
310/
312
837/
1351
Thymic cDC2
maturation marker expression
Relative (geoMFI)
2.0
1.5
1.0
0.5
0.0
MHCI
MHCII
CD80
CD86
***
FOXP3^{+} cells
Number of
1000
750
500
250
0
***
*
Isotype
0.01
Anti-CD86 (μg/mL)
d
Thymic cDC2$^{\Delta LKB1}$ vs cDC2^{WT}
mRNA expression
P-value
10^{-10}
10^{-5}
1
-5.0
-2.5
0.0
2.5
5.0
Log2 FC
Plcb1
Rasgrf2
Cd4
S100a11
Mctp2
Syne2
Ino80c
Ifi27l2a
Gm6169
Paqr5
f
Thymic cDC2
CD86 expression
(geoMFI)
60000
40000
20000
0
*
DMSO
0.05
0.5
U-71322 (μM)
g
(geoMFI)
60000
40000
20000
0
**
*
***
***
**
DMSO
20
100
2-ADB (μM)
Thymic cDC
Indo-1 Violet (Ca^{2+}-bound) / Blue (Ca^{2+}-unbound)
(mean FI)
Ionomycin
400
200
0
0
50
100
150
Seconds
Thymic cDC
basal calcium flux
(AUC)
9000
6000
3000
0
*
h
FOXP3^{+} cells
Number of cells
1000
750
500
250
0
*
*
DMSO
0.05
0.5
U-71322 (μM)

Figure. 7 LKB1 signalling restricts thymic cDC2-induced tTreg generation by limiting calcium signalling and expression of CD86.

a RNAseq-based relative mRNA expression of indicated genes from sorted Flt3L-expanded LKB1-deficient thymic cDC2s vs. Flt3L-expanded WT thymic cDC2s. **b** Representative histograms (left) and relative surface expression (right) are shown of indicated markers by Flt3L-expanded thymic cDC2s. **c** Flt3L-expanded thymic cDC2s were sorted and cocultured with GFP-FOXP3^{-}CD25^{-} single positive CD4^{+} thymocytes sorted from DEREG mice in the presence of IL-7 with or without anti-CD86. After 5 days, newly generated GFP-FOXP3^{+} cells were enumerated. **d** Volcano plot shows genes differentially expressed between Flt3L-expanded LKB1-deficient thymic cDC2s vs. Flt3L-expanded WT thymic cDC2s. x axis shows log-fold change in expression between LKB1-deficient and WT thymic cDC2s. y axis shows p value for corresponding gene. Significantly differentially expressed genes are highlighted in red. **e** Calcium flux in CD11c-MACSed Flt3L-expanded thymic total cDCs from CD11c^{WT} and CD11c$^{\Delta LKB1}$ mice. The bridged gap indicates the addition of Ionomycin. Basal calcium flux = 30 s before addition of Ionomycin. **f** Thymic single cell suspensions from Flt3L-treated mice were treated with the phospholipase C (PLC) inhibitor U-71322 for 30 min, washed, and 18 h later, CD86 surface expression on cDC2s was determined by flow cytometry. **g** As in (**f**) but with the IP3R inhibitor 2-ADB instead of U-71322. **h** as in (**c**) but with 30 min pre-treatment with U-71322 instead of anti-CD86. Data are pooled from 3 independent experiments with three mice (**b**), 2 independent experiments with one to three mice (c, h) or 1 experiment with three to five mice (**a, d, f, g**) and shown as mean ± SEM; $*p < 0.05$, $**p < 0.01$, $***p < 0.001$

Discussion

LKB1 is a central regulator of cellular metabolism and growth. Despite the growing appreciation for a key role of metabolic reprogramming in shaping the functional properties of DCs, the role of LKB1 in DC metabolism and biology has thus far not been explored. We here discovered a crucial role for LKB1 in governing mitochondrial fitness, and in putting a brake on DC activation, migration and T cell priming. Interestingly, we provide evidence that while loss of LKB1 results in enhanced immunogenicity of DCs in the periphery, this phenotype of enhanced maturation also licences CD11b^{+} DCs to increase thymic Treg development and expansion under homeostatic conditions. Our data suggest that this tTreg accumulation has a dominant immunosuppressive effect on any pro-inflammatory immune response induced in these mice as illustrated by a reduced capacity to control tumor growth and by protection against developing allergic asthma. This reveals that LKB1 serves as an important rheostat in DCs to maintain immune homeostasis by governing the balance between pro-inflammatory and regulatory T cell responses.

Although LKB1 has been shown to be required for haematopoietic stem cell and Treg survival and maintenance [14, 15, 17, 18], we did not observe gross alterations in DC frequencies and numbers in CD11c$^{\Delta LKB1}$ mice, suggesting

LKB1 is dispensable for these processes in DCs. Possibly, the fact that DCs are shorter-lived [45], makes them less reliant on LKB1-dependent processes that support longevity. Metabolically, LKB1-deficiency resulted in reduction of mitochondrial fitness parameters in multiple DC subsets across several organs, which was accompanied by increased glycolytic rates. Since we previously found that DC activation depends on a switch to glycolytic metabolism and not on OXPHOS [7, 8], LKB1 may contribute to maintaining DCs in a quiescent state by stimulating mitochondrial oxidative metabolism and reducing aerobic glycolysis. To what extent this is AMPK- dependent remains to be determined, but the fact that other studies have documented a more pro-inflammatory phenotype of DCs in which AMPK was silenced [8, 42, 46], would indicate at least a partial dependence on AMPK. However, $CD11c^{\Delta AMPK\alpha1}$ mice did not phenocopy the metabolic changes in DCs, nor enhanced Treg accumulation seen in $CD11c^{\Delta LKB1}$ mice, clearly demonstrating additional AMPK-independent LKB1-driven effects on DC biology, as further discussed below.

Despite the increased immunogenic potential of LKB1-deficient DCs, $CD11c^{\Delta LKB1}$ mice were protected against allergic asthma and were less capable of controlling tumor growth. Our data suggest that this is due to a dramatic expansion of $Foxp3^+$ Tregs with an effector (eTreg) phenotype, characterized by high expression of immunosuppressive markers and enhanced suppressive function. The observations that 1) a higher frequency of Tregs express Helios in naïve $CD11c^{\Delta LKB1}$ mice, 2) Tregs were found to present in higher frequencies in thymi but not yet in spleens of newborn mice, and 3) only thymic DCs, but not splenic DCs, from $CD11c^{\Delta LKB1}$ mice showed enhanced capacity to promote Treg differentiation, provide strong support for the notion that the observed accumulation of Tregs stems from increased tTreg output and not from enhanced conversion of pTregs from naïve T cells in the periphery. Moreover, our data suggest that tTreg proliferation is additionally stimulated in the periphery, which may further contribute to the observed enhanced accumulation of Tregs in $CD11c^{\Delta LKB1}$ mice. Finally, it should be noted that our experimental model cannot formally rule out that loss of LKB1 in $CD11c^+$ cells other than DCs, such as macrophages, may play a role in the accumulated tTreg phenotype. However, this is unlikely as it has been shown that macrophages play no significant role in development of tTregs [47].

Several studies have highlighted the importance of thymic DCs in contributing to tTreg development [32-35], presumably by presenting self-antigen to positively selected, immature $CD4^+$ SP thymocytes in the medullar regions of the thymus [48]. However, the precise mechanisms and the relative contributions of different DC subsets in regulating thymic tTreg development are not well understood. In line with others [35], we here identified thymic $CD11b^+$ cDC2s, to have a superior ability to promote Treg expansion from CD4$^+$ SP thymocytes ex vivo. Importantly, in keeping with the observation that LKB1 deficiency induced the largest number of transcriptional changes in thymic cDC2, loss of LKB1 further potentiated the capacity specifically of thymic CD11b$^+$ cDC2s to promote tTreg generation. In these cultures, we used CD4$^+$ SP CD25$^-$GFP$^-$ thymocytes sorted from foxp3-GFP/ DTR (DEREG) mice with the aim to test de novo induction of tTregs by these DCs. However, DEREG mice have been reported to have a small proportion of Foxp3$^+$ cells that do not express GFP [49]. We therefore cannot formally exclude the possibility that some of the tTregs arising from our ex vivo coculture experiments, originate from a few CD25$^-$Foxp3$^+$ tTreg precursors that may have been present in the sorted CD4$^+$ SP CD25$^-$GFP$^-$ thymocytes. Yet, given that Foxp3 expression by thymocytes in the absence of CD25 expression renders them highly apoptotic [50], it is unlikely that these cells are a major contributor to the CD25$^+$GFP$^+$Foxp3$^+$ tTreg pool we evaluated as a readout in these cultures. Finally, it should be noted that, thymic cDC2s were expanded in vivo with Flt3L-secreting tumor before use in ex vivo culture systems. We currently do not know whether these DCs are functionally identical to those in unmanipulated mice. Therefore, additional studies, using genetic approaches that selectively target LKB1 in cDC2s in situ, are warranted to unequivocally demonstrate that tTreg expansion observed in CD11c$^{\Delta LKB1}$ mice is mediated by cDC2s in vivo.

tTreg development is commonly thought to be favored by engagement of TCRs with relatively high affinity to self-antigens, somewhere between the affinity required for positive selection of conventional T cells and the affinity leading to negative selection [48]. Our observation that Tregs from CD11c^{WT} and CD11c$^{\Delta LKB1}$ have similar TCR repertoires, makes it unlikely that enhanced tTreg generation in CD11c$^{\Delta LKB1}$ mice is due to an altered repertoire of peptides presented by thymic cDC2s that favor Treg-promoting high affinity MHCII:peptide:TCR interactions. Instead, we found an increased expression of CD86 on cDC2s from CD11c$^{\Delta LKB1}$ mice, which underpins the enhanced capacity of these cells to promote tTreg generation. CD86 and CD80-dependent costimulation has been shown to be a prerequisite for tTreg development and has been suggested to provide signals — independently from TCR stimulation — that facilitate Treg differentiation early during development rather than fostering Treg generation through promoting the proliferative expansion of Treg precursors [39, 51-53]. Our data extend these observations by revealing that costimulation is not only permissive for, but may also, when increased, result in potentiation of tTreg generation. Further studies will be required to gain insight into the mechanism through which CD86-mediated costimulation by LKB1-deficient cDC2s results in enhanced tTreg development. In addition, we found an increased frequency of cDC2s in the thymus, which when mimicked in the ex vivo DC:thymocyte cultures, further enhanced tTreg generation. Thymic cDC2s develop extrathymically and migrate to the thymus where they can locally proliferate [54]. Although the role for CCR7 in migration of DCs to the thymus is not fully understood, the observation that thymic cDC2s from CD11c$^{\Delta LKB1}$ mice expressed higher levels of CCR7, but did not show increased Ki67 staining, may suggest that the higher frequency of these cells in the thymus can be explained by enhanced migration. We hypothesize that this increased DC frequency in the thymus results in more frequent and/or higher affinity TCR interactions [48], that together with increased CD86 expression, can further contribute to the enhanced tTreg generation in CD11c$^{\Delta LKB1}$ mice. Taken together, our work suggests that both cell-intrinsic differences and changes in frequency of cDC2s as a consequence of LKB1 deficiency can account for the increased tTreg generation and output. This reveals a central role of LKB1 in tTreg homeostasis by specifically restricting the ability of thymic cDC2s to drive tTreg development.

Interestingly, we show that deficiency of AMPKα1 in DCs does not lead to enhanced Treg accumulation, arguing against a role for AMPK in restricting LKB1-driven tTreg generation. Instead we found that loss of LKB1 resulted in increased PLC-β1 expression and baseline calcium levels. In line with the well-described role for PLC-induced calcium signalling in DC activation and migration [43], pharmacological inhibition of PLC or IP3R, partially reverted increased CD86 expression as well as the enhanced ability of thymic LKB1-deficient cDC2s to support tTreg development. However, given the potential off target effects of inhibitors, additional studies using genetic approaches are warranted to further corroborate these results. Thus far, LKB1 signalling has not been implicated in regulation of calcium signalling. Additional studies will be needed to reveal the underlying pathway through which LKB1 controls PLC-β1 expression and calcium signalling. It is likely to involve one or more of the AMPK-related kinases, which are also substrates of LKB1 and are known to mediate several LKB1-driven cellular processes [55]. In this respect, MAP/microtubule affinity-regulating kinases and salt-inducible kinases might be interesting candidates as they have been shown to mediate the AMPK-independent immunological changes driven by LKB1 in Tregs [17]. In addition, loss of LKB1 in thymic cDC2s resulted in increased mTOR activation which was also required for the increased ability of these cells to support tTreg development. Whether or how there is crosstalk between mTOR and PLC-β1-mediated calcium signalling in thymic cDC2s to regulate tTreg development remains to be determined. Given that PLC-γ1 signalling can promote mTOR activation in tumor cells [56], it is tempting to speculate that mTOR is a downstream target of PLC-β1 signalling to control tTreg development by thymic cDC2s. Collectively, our findings, revealing a key role for LKB1 in the regulation of DC function that is independent from AMPK, are largely consistent with, and add to the growing body of literature documenting AMPK-independent functions for LKB1 in the biology of other immune cells such as haematopoietic stem cells [14, 15], Tregs [17, 18] and macrophages [19].

Taken together, our current work reveals a crucial role for LKB1 in preventing DCs from going into functional overdrive, which at peripheral sites, translates into limiting their capacity to mature, migrate and prime pro-inflammatory T cells responses, and in the thymus, into restricting generation of tTregs. The observations of an increased inflammatory phenotype of DCs and concomitant accumulation of Tregs in CD11c$^{\Delta LKB1}$ mice, share similarities with what has been observed in mice with a DC-specific deletion of A20, a negative regulator of TLR signalling [57]. However, those mice were highly susceptible to developing systemic auto-immunity due to the fact that, in contrast to our murine model, Tregs only started to accumulate later in life (>20 weeks of age). Nonetheless, it is conceivable that both their and our observations, although with different kinetics, represent a common phenomenon of a feedback regulatory loop between DCs and Tregs described by Nussenzweig et al., [58] in which immunological effects of decreased or increased DC numbers and/or activation are counterbalanced by the concomitant shrinkage or expansion of the Treg pool, respectively, in an attempt to maintain immune homeostasis. In conclusion, we discovered a central role for LKB1 in governing DC-driven immunity and tolerance, which provides novel mechanistic insights into how tolerance vs. immunity are controlled and identifies the LKB1 signalling axis as a potentially promising target for therapeutic interventions.

References

1. Abbas, A.K., et al., *Regulatory T cells: recommendations to simplify the nomenclature*. Nat Immunol, 2013. **14**(4): p. 307-8.
2. Josefowicz, S.Z., L.F. Lu, and A.Y. Rudensky, *Regulatory T cells: mechanisms of differentiation and function.* Annu Rev Immunol, 2012. **30**: p. 531-64.
3. Bilate, A.M. and J.J. Lafaille, *Induced CD4+Foxp3+ regulatory T cells in immune tolerance*. Annu Rev Immunol, 2012. **30**: p. 733-58.
4. Domogalla, M.P., et al., *Tolerance through Education: How Tolerogenic Dendritic Cells Shape Immunity.* Front Immunol, 2017. **8**: p. 1764.
5. Buck, M.D., et al., *Metabolic Instruction of Immunity.* Cell, 2017. **169**(4): p. 570-586.
6. Pearce, E.J. and B. Everts, *Dendritic cell metabolism*. Nat Rev Immunol, 2015. **15**(1): p. 18-29.
7. Everts, B., et al., *TLR-driven early glycolytic reprogramming via the kinases TBK1-IKKvarepsilon supports the anabolic demands of dendritic cell activation.* Nat Immunol, 2014. **15**(4): p. 323-32.
8. Krawczyk, C.M., et al., *Toll-like receptor-induced changes in glycolytic metabolism regulate dendritic cell activation.* Blood, 2010. **115**(23): p. 4742-9.
9. Ferreira, G.B., et al., *Vitamin D3 Induces Tolerance in Human Dendritic Cells by Activation of Intracellular Metabolic Pathways*. Cell Rep, 2015. **10**(5): p. 711-725.
10. Malinarich, F., et al., *High mitochondrial respiration and glycolytic capacity represent a metabolic phenotype of human tolerogenic dendritic cells*. J Immunol, 2015. **194**(11): p. 5174-86.
11. Lin, S.C. and D.G. Hardie, *AMPK: Sensing Glucose as well as Cellular Energy Status*. Cell Metab, 2017.
12. Hemminki, A., et al., *A serine/threonine kinase gene defective in Peutz-Jeghers syndrome*. Nature, 1998. **391**(6663): p. 184-7.
13. Shorning, B.Y. and A.R. Clarke, *Energy sensing and cancer: LKB1 function and lessons learnt from Peutz-Jeghers syndrome*. Semin Cell Dev Biol, 2016. **52**: p. 21-9.
14. Gurumurthy, S., et al., *The Lkb1 metabolic sensor maintains haematopoietic stem cell survival*. Nature, 2010. **468**(7324): p. 659-63.
15. Nakada, D., T.L. Saunders, and S.J. Morrison, *Lkb1 regulates cell cycle and energy metabolism in haematopoietic stem cells*. Nature, 2010. **468**(7324): p. 653-8.
16. Cao, Y., et al., *LKB1 regulates TCR-mediated PLCγ1 activation and thymocyte positive selection*. Embo j, 2011. **30**(10): p. 2083-93.
17. He, N., et al., *Metabolic control of regulatory T cell (Treg) survival and function by Lkb1*. Proc Natl Acad Sci U S A, 2017. **114**(47): p. 12542-12547.
18. Yang, K., et al., *Homeostatic control of metabolic and functional fitness of Treg cells by LKB1 signalling*. Nature, 2017.
19. Liu, Z., et al., *Liver kinase B1 suppresses lipopolysaccharide-induced nuclear factor κB (NF-κB) activation in macrophages*. J Biol Chem, 2015. **290**(4): p. 2312-20.
20. Du, X., et al., *Hippo/Mst signalling couples metabolic state and immune function of CD8alpha(+) dendritic cells*. Nature, 2018.
21. Kratchmarov, R., et al., *Metabolic control of cell fate bifurcations in a hematopoietic progenitor population*. Immunol Cell Biol, 2018. **96**(8): p. 863-871.

22. Goldszmid, R.S., et al., *Dendritic cells charged with apoptotic tumor cells induce long-lived protective CD4+ and CD8+ T cell immunity against B16 melanoma*. J Immunol, 2003. **171**(11): p. 5940-7.
23. Smigiel, K.S., et al., *CCR7 provides localized access to IL-2 and defines homeostatically distinct regulatory T cell subsets*. J Exp Med, 2014. **211**(1): p. 121-36.
24. Karim, M., et al., *CD25+CD4+ regulatory T cells generated by exposure to a model protein antigen prevent allograft rejection: antigen-specific reactivation in vivo is critical for bystander regulation*. Blood, 2005. **105**(12): p. 4871-7.
25. Sakaguchi, S., et al., *Regulatory T cells: how do they suppress immune responses?* Int Immunol, 2009. **21**(10): p. 1105-11.
26. Thornton, A.M. and E.M. Shevach, *Suppressor effector function of CD4+CD25+ immunoregulatory T cells is antigen nonspecific*. J Immunol, 2000. **164**(1): p. 183-90.
27. Kearley, J., D.S. Robinson, and C.M. Lloyd, *CD4+CD25+ regulatory T cells reverse established allergic airway inflammation and prevent airway remodeling*. J Allergy Clin Immunol, 2008. **122**(3): p. 617-24.e6.
28. Thornton, A.M., et al., *Expression of Helios, an Ikaros transcription factor family member, differentiates thymic-derived from peripherally induced Foxp3+ T regulatory cells*. J Immunol, 2010. **184**(7): p. 3433-41.
29. Zabransky, D.J., et al., *Phenotypic and functional properties of Helios+ regulatory T cells*. PLoS One, 2012. **7**(3): p. e34547.
30. Thiault, N., et al., *Peripheral regulatory T lymphocytes recirculating to the thymus suppress the development of their precursors*. Nat Immunol, 2015. **16**(6): p. 628-34.
31. Fontenot, J.D., et al., *Developmental regulation of Foxp3 expression during ontogeny*. J Exp Med, 2005. **202**(7): p. 901-6.
32. Hu, Z., et al., *CCR7 Modulates the Generation of Thymic Regulatory T Cells by Altering the Composition of the Thymic Dendritic Cell Compartment*. Cell Rep, 2017. **21**(1): p. 168-180.
33. Martín-Gayo, E., et al., *Plasmacytoid dendritic cells resident in human thymus drive natural Treg cell development*. Blood, 2010. **115**(26): p. 5366-75.
34. Perry, J.S.A., et al., *Distinct contributions of Aire and antigen-presenting-cell subsets to the generation of self-tolerance in the thymus*. Immunity, 2014. **41**(3): p. 414-426.
35. Proietto, A.I., et al., *Dendritic cells in the thymus contribute to T-regulatory cell induction*. Proc Natl Acad Sci U S A, 2008. **105**(50): p. 19869-74.
36. Konkel, J.E., et al., *Thymocyte apoptosis drives the intrathymic generation of regulatory T cells*. Proc Natl Acad Sci U S A, 2014. **111**(4): p. E465-73.
37. Vang, K.B., et al., *IL-2, -7, and -15, but not thymic stromal lymphopoeitin, redundantly govern CD4+Foxp3+ regulatory T cell development*. J Immunol, 2008. **181**(5): p. 3285-90.
38. Weist, B.M., et al., *Thymic regulatory T cell niche size is dictated by limiting IL-2 from antigen-bearing dendritic cells and feedback competition*. Nat Immunol, 2015. **16**(6): p. 635-41.
39. Hinterberger, M., G. Wirnsberger, and L. Klein, *B7/CD28 in central tolerance: costimulation promotes maturation of regulatory T cell precursors and prevents their clonal deletion*. Front Immunol, 2011. **2**: p. 30.

40. Salomon, B., et al., *B7/CD28 costimulation is essential for the homeostasis of the CD4+CD25+ immunoregulatory T cells that control autoimmune diabetes*. Immunity, 2000. **12**(4): p. 431-40.
41. Ross, F.A., C. MacKintosh, and D.G. Hardie, *AMP-activated protein kinase: a cellular energy sensor that comes in 12 flavours*. Febs j, 2016. **283**(16): p. 2987-3001.
42. Nieves, W., et al., *Myeloid-Restricted AMPKalpha1 Promotes Host Immunity and Protects against IL-12/23p40-Dependent Lung Injury during Hookworm Infection*. J Immunol, 2016. **196**(11): p. 4632-40.
43. Shumilina, E., S.M. Huber, and F. Lang, *Ca2+ signaling in the regulation of dendritic cell functions*. Am J Physiol Cell Physiol, 2011. **300**(6): p. C1205-14.
44. Weichhart, T., M. Hengstschlager, and M. Linke, *Regulation of innate immune cell function by mTOR*. Nat Rev Immunol, 2015. **15**(10): p. 599-614.
45. Chen, M., et al., *Regulation of the lifespan in dendritic cell subsets*. Mol Immunol, 2007. **44**(10): p. 2558-65.
46. Carroll, K.C., B. Viollet, and J. Suttles, *AMPKalpha1 deficiency amplifies proinflammatory myeloid APC activity and CD40 signaling*. J Leukoc Biol, 2013. **94**(6): p. 1113-21.
47. Guerri, L., et al., *Analysis of APC types involved in CD4 tolerance and regulatory T cell generation using reaggregated thymic organ cultures*. J Immunol, 2013. **190**(5): p. 2102-10.
48. Hsieh, C.S., H.M. Lee, and C.W. Lio, *Selection of regulatory T cells in the thymus*. Nat Rev Immunol, 2012. **12**(3): p. 157-67.
49. Schallenberg, S., et al., *Vagaries of fluorochrome reporter gene expression in Foxp3+ regulatory T cells*. PLoS One, 2012. **7**(8): p. e41971.
50. Tai, X., et al., *Foxp3 transcription factor is proapoptotic and lethal to developing regulatory T cells unless counterbalanced by cytokine survival signals*. Immunity, 2013. **38**(6): p. 1116-28.
51. Lio, C.W., et al., *CD28 facilitates the generation of Foxp3(-) cytokine responsive regulatory T cell precursors*. J Immunol, 2010. **184**(11): p. 6007-13.
52. Tai, X., et al., *CD28 costimulation of developing thymocytes induces Foxp3 expression and regulatory T cell differentiation independently of interleukin 2*. Nat Immunol, 2005. **6**(2): p. 152-62.
53. Williams, J.A., et al., *Thymic medullary epithelium and thymocyte self-tolerance require cooperation between CD28-CD80/86 and CD40-CD40L costimulatory pathways*. J Immunol, 2014. **192**(2): p. 630-40.
54. Li, J., et al., *Thymus-homing peripheral dendritic cells constitute two of the three major subsets of dendritic cells in the steady-state thymus*. J Exp Med, 2009. **206**(3): p. 607-22.
55. Lizcano, J.M., et al., *LKB1 is a master kinase that activates 13 kinases of the AMPK subfamily, including MARK/PAR-1*. Embo j, 2004. **23**(4): p. 833-43.
56. Dai, L., et al., *Phosphoinositide-specific phospholipase Cγ1 inhibition induces autophagy in human colon cancer and hepatocellular carcinoma cells*. Sci Rep, 2017. **7**(1): p. 13912.
57. Kool, M., et al., *The ubiquitin-editing protein A20 prevents dendritic cell activation, recognition of apoptotic cells, and systemic autoimmunity*. Immunity, 2011. **35**(1): p. 82-96.

58. Liu, K., et al., *In vivo analysis of dendritic cell development and homeostasis*. Science, 2009. **324**(5925): p. 392-7.
59. Vincent, E.E., et al., *Mitochondrial Phosphoenolpyruvate Carboxykinase Regulates Metabolic Adaptation and Enables Glucose-Independent Tumor Growth*. Mol Cell, 2015. **60**(2): p. 195-207.
60. Love, M.I., W. Huber, and S. Anders, *Moderated estimation of fold change and dispersion for RNA-seq data with DESeq2*. Genome Biol, 2014. **15**(12): p. 550.
61. Sergushichev, A.A., et al., *GAM: a web-service for integrated transcriptional and metabolic network analysis*. Nucleic Acids Res, 2016. **44**(W1): p. W194-200.
62. Fabregat, A., et al., *Reactome graph database: Efficient access to complex pathway data*. PLoS Comput Biol, 2018. **14**(1): p. e1005968.
63. Subramanian, A., et al., *Gene set enrichment analysis: a knowledge-based approach for interpreting genome-wide expression profiles*. Proc Natl Acad Sci U S A, 2005. **102**(43): p. 15545-50.
64. Bolotin, D.A., et al., *MiXCR: software for comprehensive adaptive immunity profiling*. Nat Methods, 2015. **12**(5): p. 380-1.
65. Nazarov, V.I., et al., *tcR: an R package for T cell receptor repertoire advanced data analysis*. BMC Bioinformatics, 2015. **16**(1): p. 175.
66. Pelgrom, L.R., A.J. van der Ham, and B. Everts, *Analysis of TLR-Induced Metabolic Changes in Dendritic Cells Using the Seahorse XF(e)96 Extracellular Flux Analyzer*. Methods Mol Biol, 2016. **1390**: p. 273-85.

Materials and methods

Mice

Itgax^{cre}*Stk11*$^{fl/fl}$ (LKB1) (17591855; 12226664), *Itgax*^{cre}*Prkaa1*$^{fl/fl}$ (AMPKα1) (21124450), Foxp3-DTR/EGFP (DEREG) (17200412), OVA-specific CD4^{+} T cell receptor transgenic mice (OT-II), or OVA- specific CD8^{+} T cell receptor transgenic mice (OT-I), and WT male and female mice, all on a C57BL/6 background, were purchased from The Jackson Laboratory and crossed, housed and bred at the LUMC, Leiden, The Netherlands, under SPF conditions. Animal experiments were performed when the mice were between 2–6 days or 8–16 weeks old, all in accordance with local government regulations and the EU Directive 2010/63EU and Recommendation 2007/526/EC regarding the protection of animals used for experimental and other scientific purposes, as well as approved by the Dutch Central Authority for Scientific Procedures on Animals (CCD) (animal license number AVD116002015253).

Flt3L-secreting B16 melanoma cells

Flt3L-secreting B16 melanoma cells were kindly provided by Dr. Edward Pearce and passaged every 3–4 days using a Trypsin-EDTA solution (Sigma, Zwijndrecht, The Netherlands) followed by replating in T175 culture flasks at 2 × 10^{6} cells in 35 mL of medium comprised of DMEM High Glucose (Biowest, Nuaillé, France) supplemented with 10% FCS (Capricorn, Den Haag, The Netherlands), 100 U/mL penicillin (Eureco-pharma, Ridderkerk, The Netherlands) and 100 µg/mL streptomycin (Sigma).

Generation of BM-derived DCs

BM cells were flushed from femurs and plated in 6-well plate at 2× 10^{6} cells in 3–6 mL of medium comprised of RMPI-1640 (Gibco, Bleiswijk, The Netherlands) supplemented with 5% FCS (Gibco), 50 µM β-mercaptoethanol (Sigma), 100 U/mL penicillin (Eureco-pharma), 100 µg/mL streptomycin (Sigma) and 20 ng/mL of GM-CSF (PeproTech, Hamburg, Germany) for 8 days, with a medium change on day 4 and day 7. Subsequently, non-adherent GMDCs were used for various assays.

In vivo DC expansion, isolation and sorting

To expand the number of DCs in mice, Flt3L-secreting B16 melanoma cells were harvested and washed using phenol red-free HBSS (Gibco) before subcutaneous injection of 2 × 10^{6} cells in 100 µL of HBSS into the flank of mice. Nine to twelve days later, lymphoid organs were harvested, placed in 500 µL medium (with Ca^{2+}), mechanically disrupted, digested by addition of 50 µL medium (with Ca^{2+}) supplemented with Collagenase D (Roche, Woerden, The Netherlands, end concentration of 1 mg/mL) and DNase I (Sigma, end concentration of

2000 U/mL) and incubation for 20 min at 37 °C. Upon completion of digestion, single-cell suspensions were subjected to red blood cell lysis (inhouse; 0.15 M NH4Cl, 1 mM KHCO3, 0.1 mM EDTA [Sigma] in ddH2O) and filtered with a 100 µm sterile filter before counting. From these suspensions, DC populations were further enriched by positive isolation with CD11c$^-$ Microbeads (Miltenyi, Leiden, The Netherlands) and sorting in cDC1 (CD8a$^+$CD11c$^+$MHCII$^+$), cDC2 (CD11b$^+$CD11c$^+$MHCII$^+$) and pDC (Siglec-H$^+$CD11c^{int}) subsets on a BD FACSAria using a 85 µm nozzle at 45 PSI. Subsequently, sorted DCs were used for various assays.

Western blotting

Sorted Flt3L-expanded splenic cDCs were washed twice with PBS before being lysed in EBSB buffer (8% [w/v] glycerol, 3% [w/v] SDS and 100 mM Tris-HCl [pH 6.8]). Lysates were immediately boiled for 5 min and their protein content was determined using a bicinchoninic acid protein assay kit (Pierce). Proteins were separated by SDS-PAGE followed by transfer to a PVDF membrane. Membranes were blocked for 1 h at room temperature in TTBS buffer (20 mM Tris-HCl [pH 7.6], 137 mM NaCl, and 0.25% [v/v] Tween 20) containing 5% (w/v) fat free milk and incubated overnight with primary antibodies. The primary antibodies used were: anti-LKB1 (Ley 37D/G6) (1:1000) (Santa Cruz) and anti-β-actin (AC-15) (1:2000) (Sigma). The membranes were then washed in TTBS buffer and incubated with horseradish peroxidase-conjugated secondary antibodies for 2 h at room temperature. After washing, blots were developed using enhanced chemiluminescence.

DC cytokine analysis

For cytokine production, 3 × 10^5 expanded DCs in 200 µL of medium were settled in a flat-bottom 96-well plate and stimulated with Poly(I:C) (InvivoGen, Toulouse, France) or LPS (ultrapure, InvivoGen). Sixteen hours later, supernatants were collected for cytokine analysis by cytokine bead array.

DC migration assay

For DC migration assays, GMDCs were harvested on day 8, labelled with CTV according to the manufacture's recommendation (1 µM, Invitrogen, Bleiswijk, The Netherlands), and washed using phenol red-free HBSS (Gibco) before subcutaneous injection of 5 × 10^5 cells in 40 µL of HBSS into the footpad of mice. Twenty-four hours later, the number of migrated CTV-labeled GMDCs was assessed in the draining popliteal lymph nodes (popLNs)

In vitro T cell priming assay

OT-II cells were negatively isolated with a $CD4^+$ T cell Isolation Kit (Miltenyi) and OT-I cells were positively isolated with anti-mouse CD8a-PE (eBioscience, Bleiswijk, The Netherlands) followed by anti-PE MicroBeads (Miltenyi). 5×10^3 DCs were settled in a round-bottom 96-well plate, pulsed with 100 µg/mL of OVA (InvivoGen) in combination with LPS for 5 h, and washed before adding 5×10^4 CFSE-labeled OT cells in 200 µL of medium. After 3 days for the OT-I cells and 4 days for the OT-II cells, cells were harvested and analyzed for proliferation by assessing CFSE dilution and for cytokine production by intracellular cytokine analysis by flow cytometry which was done by incubating the cells in PMA/Ionomycin (Sigma) in the presence of Brefeldin A (Sigma) for 4 h before viability staining and fixation.

In vivo T cell priming following footpad immunization

In vitro-cultured GMDCs were pulsed with 100 µg/mL OVA (InvivoGen) and 100 ng/mL LPS (ultrapure, InvivoGen) for 6 h, after which cells were washed and used for subcutaneous immunization in the hind footpads of mice (5×10^5 DCs/footpad). Alternatively, mice were subcutaneously immunized with OVA and Poly (I:C) emulsified in 30 µL of incomplete Freunds' adjuvant (IFA, InvivoGen) in the hind footpad. Seven days later, draining popliteal LNs were harvested and OVA-specific $CD8^+$ T cell response was determined by flow cytometry. $CD4^+$ and $CD8^+$ T cell cytokine production was determined by flow cytometry after incubating the cells in PMA/Ionomycin (Sigma) in the presence of Brefeldin A (Sigma) for 4 h before viability staining and fixation.

In vitro T cell suppression assay

T cell suppression assays were performed in round-bottom 96-well plates with 2×10^4 sorted splenic $CD4^+CD25^-$ T cells labelled with CFSE according to the manufacturer's recommendations (0.5 µM, Sigma) as responder cells, activated by 5 µg/mL of anti-CD3 (BD Pharmingen, Vianen, The Netherlands), and cultured in the presence of 8×10^4 irradiated (3000 RAD) splenocytes, acting as antigen-presenting cells. 5×10^3 $CD4^+CD25^+$ T cells as suppressors sorted from $CD11c^{WT}$ or $CD11c^{\Delta LKB1}$ mice were added and then cultured for 3 days after which CFSE dilution was assessed by flow cytometry.

In vitro Treg proliferation assay

5×10^4 $CD4^+CD8^-GFP^+CD25^+$ splenocytes, sorted from DEREG mice and labelled with CTV according to the manufacturer's recommendations, were cultured in round-bottom 96-well plates together with 25×10^3 Flt3L-expanded splenic DC subsets sorted from $CD11c^{WT}$ or $CD11c^{\Delta LKB1}$ mice, in the presence of 100 U/mL of recombinant human IL-2 (R&D systems). 4 days later, CTV dilution was assessed by flow cytometry.

In vitro Treg induction assay

In vitro Treg induction assays were performed in round-bottom 96-well plates with 1 × 10^4 sorted Flt3L-expanded thymic or splenic DC subsets and 2 × 10^4 sorted $CD4^+CD8^-GFP^-CD25^-$ thymocytes or splenocytes from DEREG mice, unless different ratios are specifically mentioned, in the presence of 10 ng/mL of IL-7 (PeproTech) for 5 days. To determine the contribution of CD86 on DCs, anti-CD86 (BioLegend, Koblenz, Germany) or its isotype control (BioLegend) were added during the entire culture. To determine the contribution of phospholipase C, calcium or mTOR signalling in DCs, the DCs were incubated for 30 min with the phospholipase C inhibitor U 71322 (Abcam, Cambridge, The Netherlands), inositol trisphosphate receptor (IP3R) inhibitor 2-aminoethyl diphenylborinate (2-ADB, Sigma) or rapamycin (Cal-biochem), respectively, and washed before adding the thymocytes in the presence of 150 ng/mL Flt3L (eBioscience). On day 5, the number of GFP^+ Tregs in the culture was assessed by flow cytometry. For ex vivo assessment of the effect of these inhibitors on CD86 expression in thymic cDC2s, 1 × 10^6 thymocyte single-cell suspensions were incubated for 30 min with U-71322, 2-ADB or rapamycin and washed before culture in the presence of 150 ng/ mL Flt3L. 18 h later, CD86 expression on thymic cDC2s was assessed by flow cytometry.

House dust mite-induced allergic asthma model

Allergic airway inflammation was induced by sensitizing mice via intranasal administration of 1 μg HDM (Greer, London, United Kingdom) in 50 μL of PBS. One week later, these mice were challenged for 5 consecutive days via intranasal administration of 10 μg HDM in 50 μL of PBS. On day 15, bronchoalveolar lavage (BAL) fluid, lung, and lung-draining mediastinal LNs (med LNs) were obtained to determine inflammatory cell recruitment. BAL was performed by instilling the lungs with 3 × 1 mL aliquots of sterile PBS (Braun, Oss, The Netherlands). For single-cell suspensions of whole lung tissue, lungs were perfused with sterile PBS via the right ventricle to clear leukocytes and erythrocytes from the pulmonary circulation. Lung and medLN homogenization was performed as described above. Eosinophilia was assessed in BAL and lungs by flow cytometry as a readout for allergic inflammation. To assess HDM-specific T cell responses, single cell suspensions of 3 × 10^5 isolated leukocytes of medLNs were added to a round-bottom 96-well plate with 10 μL HDM in 200 μL of medium. Plates were incubated at 37 °C in 5% CO2 for 3 days after which supernatants were analysed for cytokines by cytokine bead array.

Melanoma tumor model

Mice were challenged with 1 × 10^5 OVA-expressing B16 melanoma cells intradermally on the flank. Nine to twelve days later, mice were sacrificed and tumor weight was determined.

Flow cytometry

Enzymatically digested cell suspensions were stained for 20 min at room temperature using a Fixable Aqua Dead Cell Stain Kit (Invitrogen) and unless sorted or calcium flux assessed, fixed for 10 min at 37 °C using a 4% methanol-free formaldehyde solution (Polysciences, Edenkoben, Germany for pACC [Ser79] detection) or 1 h at 4 °C using a FOXP3/Transcription Factor Staining Buffer Set (Invitrogen, for FOXP3 detection) or 15 min at room temperature using a 1.85% formaldehyde PBS solution (Sigma, for everything else). For detection of pACC (Ser79), cell suspensions were permanently permeabilised using 100% methanol for at least 10 min at −20 °C. Afterwards, cell suspensions were stained in PBS supplemented with 0.5% BSA (Roche) and 2 mM EDTA (Sigma) and antibodies for 30 min at 4 °C. For detection of FOXP3 and intracellular cytokines, cell suspensions were stained in Permeabilization Buffer (eBioscience) instead of supplemented PBS. Mitochondrial mass, membrane potential and ROS were quantified by staining with MitoTracker Green (20 nM, Invitrogen), TMRM (20 nM, Invitrogen) and MitoSOX (5 µM, Invitrogen) for 30 min at 37 °C before staining with other antibodies. Phosphorylated ACC (Ser79) and S6 (Ser235/236) were stained for 1 h at room temperature before staining with other antibodies. The second round of staining included goat anti-rabbit-AF647 to detect the unconjugated rabbit anti-pACC (Ser79). All samples were run on a FACSCanto II or BD LSR II and analysed using FACS Diva 8 (all BD Biosciences) and FlowJo (Version 9.5, TreeStar).

Antibodies

The antibodies used in this study were as follows: anti-CD3-eF450, anti-CD4-PE-Cy7, anti-CD11b-PE-Cy7, anti-CD11c-PE-Cy7, anti-CD40, anti-CD44, anti-CD62L, anti-CD80, anti-CD152 (CTLA-4), anti-FOXP3, anti-IFN-γ-FITC and IFN-γ-PE-Cy7, anti-IL-17A and anti-MHCII all from eBioscience. Anti-CD3-BV605, anti-CD8a, anti-CD64, anti-CD86-APC-Fire 750, anti-CD103, anti-CD172a, anti-CD197 (CCR7), anti-CD326 (EpCAM), anti-Helios, anti-Ki67, anti-LAP (TGF-β1), anti-H2-Kb (MHCI) and anti-XCR1 all from BioLegend. Anti-CD4-BV650, anti-CD11c-HV450, anti-CD25, anti-CD86-PE, anti-IFN-γ-APC-Cy7, anti-IL-4, anti-Siglec-F and anti-pS6 (Ser235/236) all from BD Biosciences (Vianen, The Netherlands). Anti-CD11b-PerCP-Cy5.5 from BD Pharmingen. Anti-pACC (Ser79) from Cell Signaling (Leiden, The Netherlands). Anti-rabbit from Invitrogen. H-2Kb/OVA (SIINFEKL) MHC Tetramer made inhouse.

Cytometric bead array

Cell culture supernatants were analyzed for IL-1b, IL-4, IL-5, IL-6, IL- 10, IL-13 and TNF using the Cytokine Bead Array (BD Biosciences) according to the manufacturer's recommendation.

RNA and TCR sequencing

mRNA from 0.5 to 1 × 10^5 sorted thymic DC subsets or splenic and thymic $CD8^-CD4^+CD25^{hi}$ Tregs was extracted with oligo-dT beads (Invitrogen), and libraries were prepared and quantified as described before [59]. Raw and processed data were deposited to Gene Expression Omnibus. Differential gene expression analysis was carried out with DESeq2 package [60], pre-ranked gene set enrichment analysis was done using fgsea package [61] with Reactome database [62], MSigDB Hallmarks collection [63] and Gene Ontology database (The Gene Ontology Consortium, 2017). T cell receptor alpha and beta chain clonality was assessed using the MiXCR tool [64] using standard parameters of the RNA-seq workflow. TCR clonality was analyzed using the R package tcR [65].

Extracellular flux analysis

Extracellular Flux Analysis was performed as described before [66]. Briefly, DCs were resuspended in unbuffered RPMI-1640 (Sigma), which was filtered through a 0.22 µm filter system (Corning, Amsterdam, The Netherlands), the pH was set to 7.4 using 37% HCl, and was supplemented with 5% FCS. Cells were settled (70.000 GMDCs or 175.000 cDCs) on a 96-well assay plate (Agilent, Amstelveen, The Netherlands) and rested at 37 °C in 0% CO2 for 1h. OCR and ECAR were recorded with the XF96e Extracellular Flux analyser (Agilent) and analysed using Wave Desktop (Version 2.6, Agilent). Subsequently extracellular acidification rate (ECAR) and oxygen consumption rate (OCR) were analyzed in response to glucose (10 mM; port A; Sigma), oligomycin (1 µM; port B; Cayman Chemical, Ann Arbor, Michigan, United States), fluoro-carbonyl cyanide phenylhydrazone (FCCP, 3 µM; port C; Sigma), and rotenone/antimycin A (1/1 µM; port D; Sigma). Glycolytic rate = increase in ECAR in response to injection A. Baseline OCR = difference in OCR between readings following port A injection and readings after port D injection. Spare OCR is difference between basal and maximum OCR, which is calculated based on the difference in OCR between readings following port C injection and readings after port A injection.

Calcium flux assay

To assess intracellular calcium flux in DCs, MACS-isolated $CD11c^+$ cells from the thymus were washed with PBS (with Ca^{2+}/Mg^{2+}) supplemented with 1% FCS. 2 uM of Indo-1 AM (Invitrogen) was added to 500 µL of PBS 1% FCS (with Ca^{2+}/Mg^{2+}) for up to 2 × 10^6 cells. Cells were incubated for 45 min at 37

°C in the dark and then washed with cold PBS (with Ca^{2+}/Mg^{2+}) and resuspended in 500 µL cold PBS (with Ca^{2+}/Mg^{2+}). The cells were reheated for 5 min to 37 °C before assessing calcium flux. Calcium flux was then assessed by flow cytometry analysing Indo-1 ratio over a time course of 30 s basal measurement and 30 s following Ionoymcin (Sigma) stimulation.

Quantification and statistical analysis

Statistical analysis, as specified in figure legends, were performed with Prism 7 (GraphPad software). Data were analysed with the non-paired Student's t test for 2 bars or the two-way ANOVA corrected for multiple comparisons using Sidak's multiple comparison test for 2 or more groups. p values < 0.05 were considered significant (*$p < 0.05$, **$p < 0.01$, ***$p < 0.001$).

Acknowledgements

This work was supported by an LUMC and Marie Curie fellowship awarded to B.E.

Author contributions

B.E., L.R.P., T.A.P., A.J.v.d.H., F.O., H.v.d.Z., S.v.d.S., A.S., A.O.-F. and E.E. performed experiments; B.E., M.N.A., L.R.P., A.S. and E.E. designed and analyzed experiments; B.E. conceived and supervised the study and wrote the manuscript together with L.R.P.

Competing interests

The authors declare no competing interests.

Supplemental figures

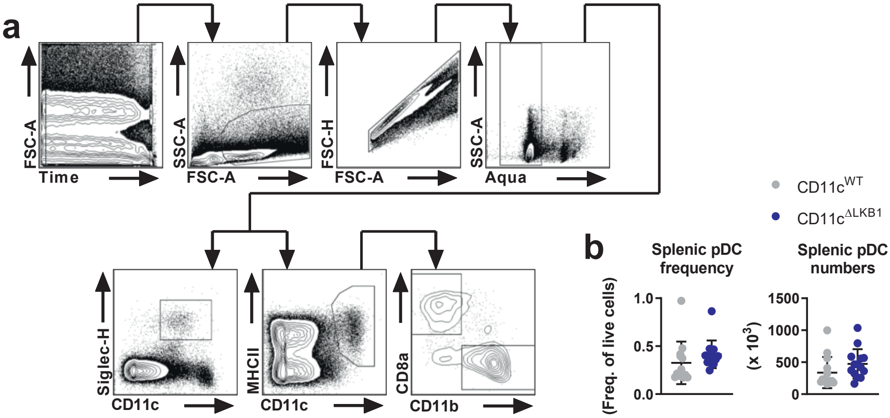

Figure S1. Gating strategy for splenic DCs.

a Extended gating strategy of splenic and thymic DCs is shown. Events were captured after the flow stream had stabilized (panel 1). Live/dead exclusions was performed through both FSC-A/SSC-A exclusion (panel 2) and Aqua staining of dead cells (panel 4). Doublets were excluded using FSC-A/FSC-H (panel 3). Plasmacytoid DCs (pDCs) were identified as Siglec-H$^+$CD11c^{int} (panel 5) and conventional DCs (cDCs) as CD11c$^+$MHCII$^+$ (panel 6). Two major subsets of splenic and thymic cDCs are shown (CD8a$^+$ or XCR1$^+$ and CD11b$^+$ or CD172a$^+$ in panel 7). **b** Splenic pDC percentage (left) and absolute number (right) data were pooled and quantified from 4 independent experiments with three to four mice and shown as mean ± SEM.

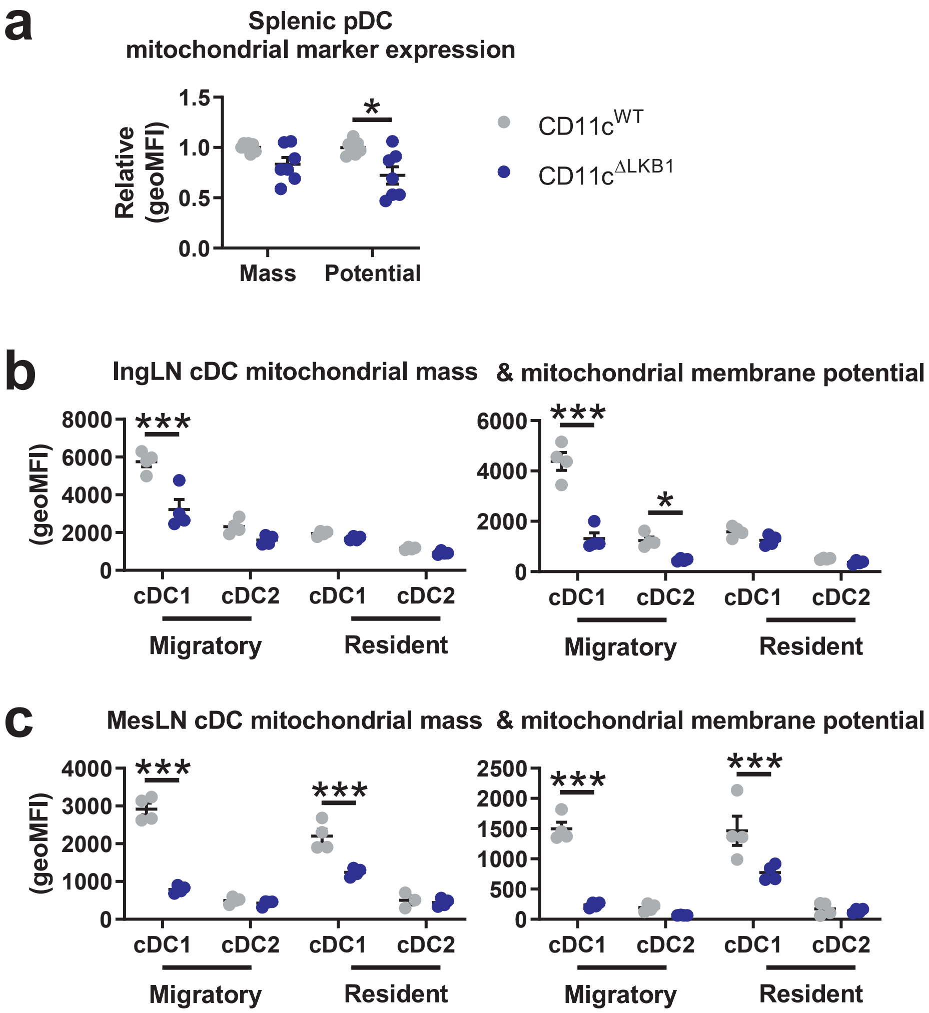

Figure S2. LKB1 deficiency reduces mitochondrial metabolism of DCs in LNs.

a splenic pDCs were identified as Siglec-H^{+}CD11c^{int} and relative expression of mitochondrial mass and membrane potential was determined by flow cytometry. **b** inguinal LN cDC1s and cDC2s were identified as CD11c^{+}MHCII^{+}EpCAM^{-}XRC1^{+} and CD11c^{+}MHCII+EpCAM^{-}CD172a^{+} respectively and relative expression of mitochondrial mass (left) and membrane potential (right) was determined by flow cytometry. **c** mesenteric LN cDC1s and cDC2s were identified as CD11c^{+}MHCII^{+}XRC1^{+} and CD11c^{+}MHCII^{+}CD172a^{+} respectively and relative expression of mitochondrial mass (left) and membrane potential (right) was determined by flow cytometry. Data are pooled from 2 (**a**) or 1 (**b-c**) (independent) experiment(s) with three to four mice and shown as mean ± SEM; *p < 0.05, ***p < 0.001.

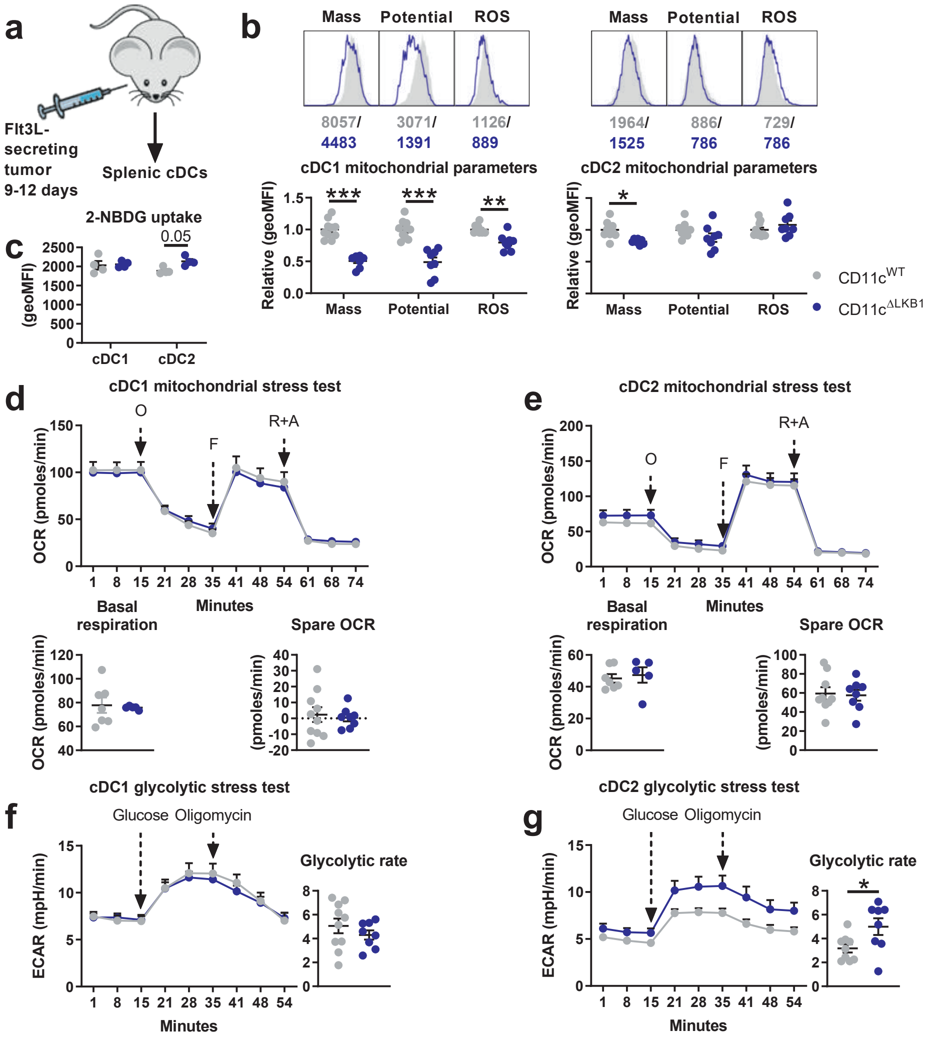

Figure S3. Effects of LKB1 deficiency on DC metabolism.

a Model of in vivo DC expansion. **b** Representative histograms (top) and relative expression (bottom) are shown of mitochondrial mass, membrane potential and ROS production in Flt3L-expanded splenic cDC1s (top) and cDC2s (bottom) by flow cytometry. **c** Uptake of a fluorescent glucose analog by Flt3L-expanded splenic cDCs using flow cytometry. **d** Real-time mitochondrial respiration (top) in sorted Flt3L-expanded splenic cDC1s, starting from basal respiration and after the sequential addition of oligomycin (complex V inhibition), FCCP (maximal respiration induction) and rotenone/antimycin A (electron transport chain inhibition). Baseline OCR (bottom left) = difference in OCR between basal respiration and after rotenone/antimycin A. Spare OCR (bottom right) = difference between basal and maximal respiration. **e** Real-time mitochondrial respiration (top), baseline OCR (bottom left) and spare OCR (bottom right) in sorted Flt3L-expanded splenic cDC2s as in (**d**). **f** Real-time glycolysis (left) in sorted Flt3L-expanded splenic cDC1s, starting from basal extracellular acidification rate (ECAR), in which the cells were incubated in glucose-free medium, followed by the sequential addition of glucose (glycolysis induction) and oligomycin (maximal glycolysis induction). Glycolytic rate (right) = increase in ECAR in response to glucose. **g** Real-time glycolysis (left) and glycolytic rate (right) in sorted Flt3L- expanded splenic cDC2s as in (**f**). Data are pooled from 3 (**d-g**), 2 (**b**) or 1 (**c**) independent experiment(s) with three to four mice and shown as mean ± SEM; *p < 0.05, ***p < 0.001.

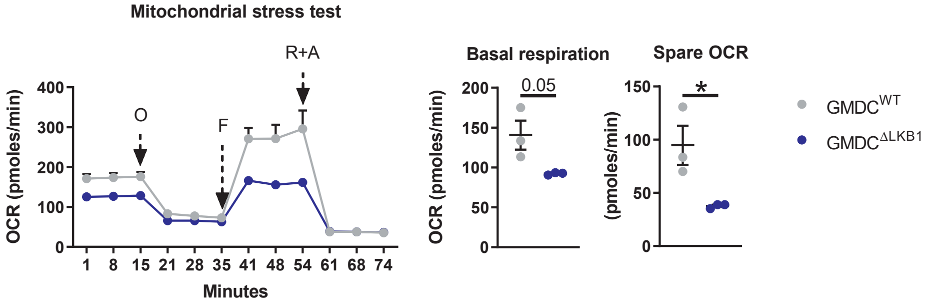

Figure S4. LKB1 deficiency impairs mitochondrial metabolism of GMDCs.

Real-time mitochondrial respiration (left) in GM-CSF-cultured BM-derived DCs (GMDCs) from $CD11c^{WT}$ and $CD11c^{\Delta LKB1}$ mice, starting from basal respiration and after the sequential addition of oligomycin (complex V inhibition), FCCP (maximal respiration induction) and rotenone/antimycin A (electron transport chain inhibition). Basal respiration (middle) = difference in OCR between basal respiration and after rotenone/antimycin A. Spare OCR (right) = difference between basal and maximal respiration. Data is from 1 experiment with three mice and shown as mean ± SEM; *p < 0.05.

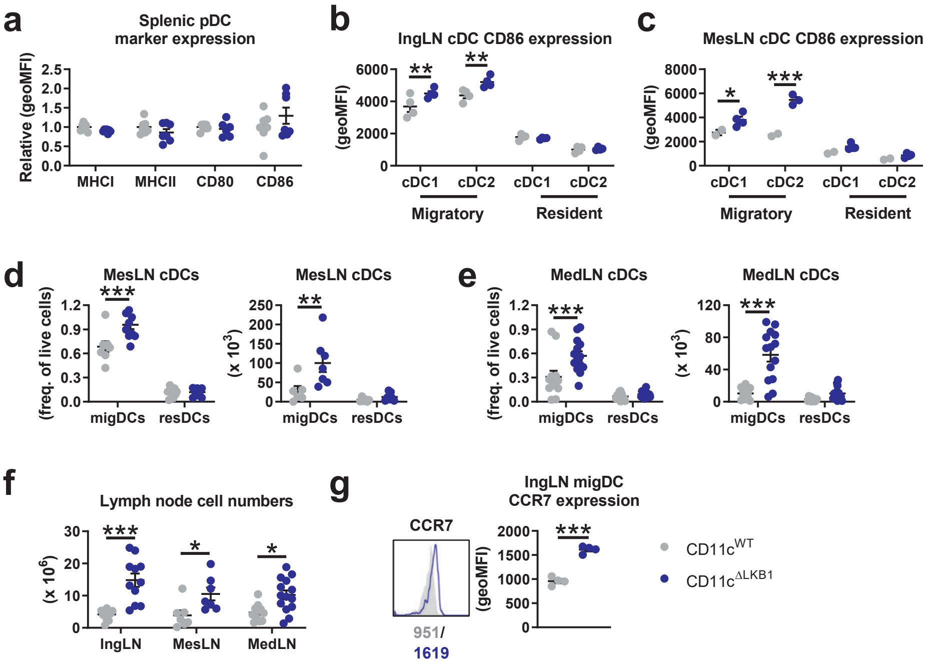

Figure S5. LKB1 deficiency alters phenotype and abundance of peripheral DCs.

a-c Relative surface expression is shown of indicated markers by splenic pDCs (**a**), inguinal LN cDCs (**b**) and mesenteric LN cDCs (**c**) by flow cytometry. d Migratory and resident DCs in the mesenteric LN were identified as CD11c$^+$MHCII^{hi} and CD11c^{hi}MHCII$^+$ respectively and percentages (left) and absolute numbers (right) were quantified. **e** Migratory and resident DCs in the mediastinal LN were identified as CD11c$^+$MHCII^{hi} and CD11c^{hi}MHCII$^+$ respectively and percentages (left) and absolute numbers (right) were quantified. **f** Thymic cell numbers were determined by cell counts. **g** Surface expression of CCR7 on migratory DCs in the inguinal LN as analysed by flow cytometry. Data are pooled from 3 (**d-f**), 2 (**a**) or 1 (**b-c, g**) (independent) experiment(s) with three to four mice and shown as mean ± SEM; *$p < 0.05$, **$p < 0.01$, ***$p < 0.001$.

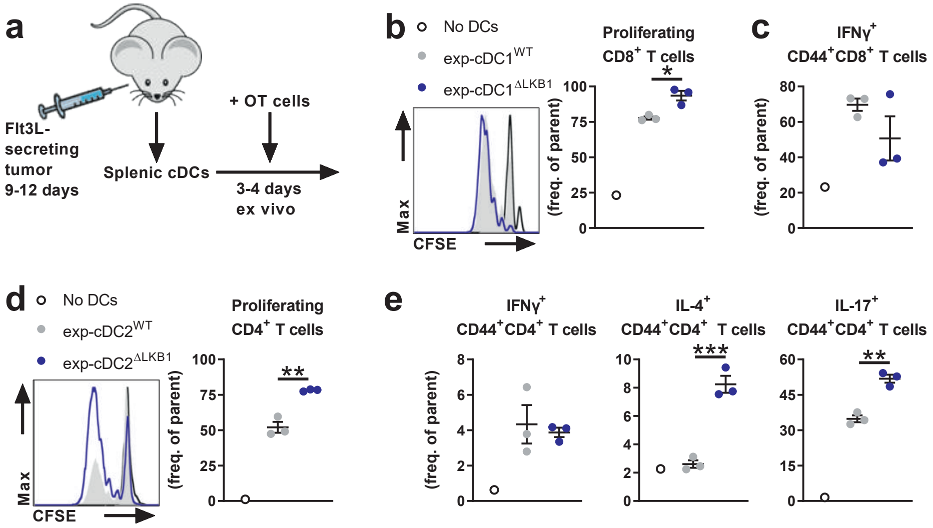

Figure S6. LKB1 deficiency enhances T cell priming by DCs in vitro.

a-e Flt3L-expanded splenic cDC1s and cDC2s were sorted and pulsed with OVA and LPS for 5 hours and then, MACS-isolated CFSE-labeled OVA-specific OT-I and OT-II T cells were added to these cDC1s and cDC2s respectively. 3 days later, cDC1 + OT-I cultures were stimulated with PMA/Ionomycin in the presence of Brefeldin A and proliferation was evaluated by CFSE dilution as shown in a representative histogram (**b**, left) and quantified (**b**, right) and CD8$^+$ T cells were analysed for expression of indicated cytokines by flow cytometry (**c**). 4 days later, proliferation (**d**) and cytokine expression of CD4$^+$ T cells (**e**) in cDC2 + OT-II cultures were analyzed as in (**b-c**). Data is from 1 experiment with three mice and shown as mean ± SEM; *p < 0.05, **p < 0.01, ***p < 0.001.

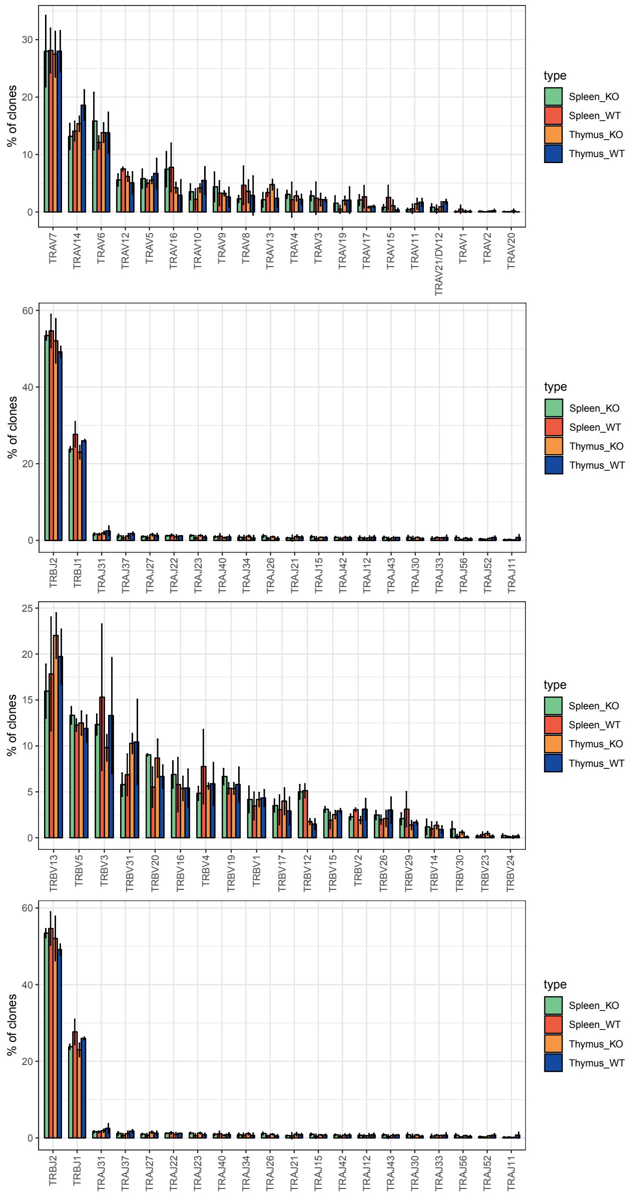

Figure S7. TCR repertoire of Tregs from CD11c$^{\Delta LKB1}$ and CD11c^{WT} mice is comparable.

Tregs were identified as CD3^{+}CD4^{+}CD8^{-}CD25^{hi} cells and sorted from the spleens and thymi of CD11c^{WT} (WT) and CD11c$^{\Delta LKB1}$ (KO) mice before T cell receptor alpha chain variable (TRAV) segment, alpha chain joining (TRAJ) segment, beta chain variable (TRBV) segment and beta chain joining (TRBJ) segment clonality was assessed. Data are from two to three mice and shown as mean ± SEM.

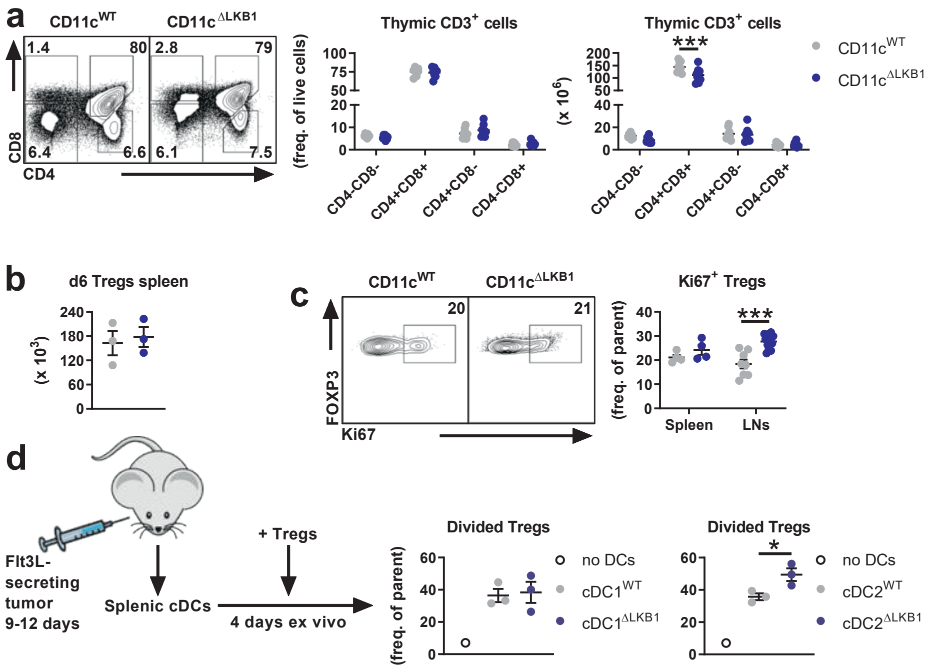

Figure S8. Comparison of cellular composition of thymus and peripheral Treg proliferation in CD11c$^{\Delta LKB1}$ and CD11c^{WT} mice.

a Visualisation (left), quantification (middle) and enumeration (right) of thymocytes from CD11c^{WT} and CD11c$^{\Delta LKB1}$ mice based on CD8a and CD4 expression by flow cytometry. **b** Enumeration of Tregs identified as CD3^{+}CD4^{+}FOXP3^{+} in spleens of 6 days old CD11c^{WT} and CD11c$^{\Delta LKB1}$ mice pups by flow cytometry. **c** Representative flow cytometry plots of proliferating splenic Tregs (left), based on intracellular Ki67 expression, and percentages of proliferation Tregs from spleens and LNs (inguinal, mesenteric and mediastinal; right) were quantified by flow cytometry. **d** Flt3L-expanded splenic cDC1s and cDC2s were sorted and cocultured in the presence of IL-2 with CTV-labeled splenic GFP-FOXP3^{+}CD25^{+} CD4^{+} T cells sorted from DEREG mice. After 4 days, proliferation was evaluated by CTV dilution and quantified by flow cytometry.

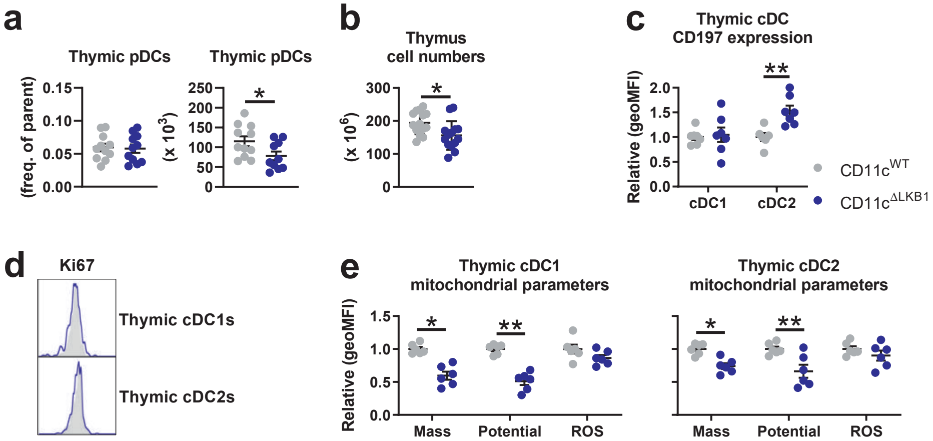

Figure S9. Phenotypic and metabolic comparison of thymic DC subsets from CD11c$^{\Delta LKB1}$ and CD11c^{WT} mice.

a Thymic pDCs were identified as Siglec-H^{+}CD11c^{int} and percentages (left) and absolute numbers (right) were quantified. **b** Thymic cell numbers were determined by cell counts. **c** Relative surface expression of CCR7 on thymic cDCs as analysed by flow cytometry. **d** Representative flow cytometry plots of proliferating thymic cDC1s (top) and cDC2s (bottom) based on intracellular Ki67 expression. **e** Expression is shown of mitochondrial mass, membrane potential and ROS production in thymic cDC1s (left) and cDC2s (right) from CD11c^{WT} and CD11c$^{\Delta LKB1}$ mice as analyzed by flow cytometry. Data are pooled from 3 (**a-b**) or 2 (**c-e**) independent experiments with three to four mice or is a representative of 2 independent experiments (d) and shown as mean ± SEM; *p < 0.05, **p < 0.01.

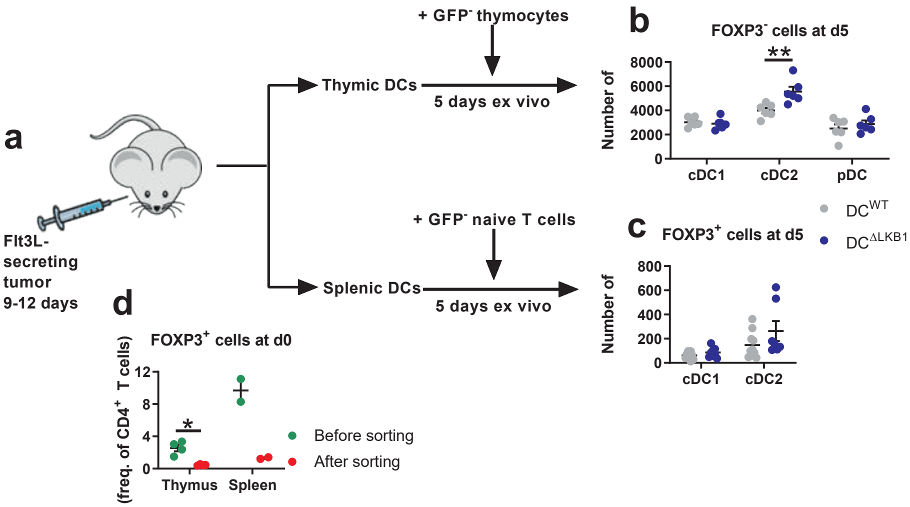

Figure S10. Description of ex vivo thymocyte-thymic DCs coculture model.

a-d Flt3L-expanded thymic cDC1s, cDC2s and pDCs were sorted from CD11c^{WT} and CD11c$^{\Delta LKB1}$ mice and cocultured in the presence of IL-7 with GFP-FOXP3^{-}CD25^{-} single positive CD4^{+} thymocytes sorted from DEREG mice. After 5 days, GFP-FOXP3^{-} cells were enumerated (**b**). Alternatively, Flt3L-expanded splenic cDC1s and cDC2s were sorted and cocultured in the presence of IL-7 with splenic GFP-FOXP3^{-}CD25^{-} CD4^{+} T cells. After 5 days, newly generated GFP-FOXP3^{+} cells were enumerated (**c**). **d** Quantification of FOXP3^{+} cells remaining in sorted GFP-FOXP3^{-} fractions from DEREG mice and were used for coculture in the corresponding Figures 6f-g and Supplementary figures S10b-c as analysed by flow cytometry. Data are pooled from 3 (**c**) or 2 (**b**) independent experiments with three to four mice, or 2-4 independent experiments with one mice (**d**) and shown as mean ± SEM; *$p < 0.05$, **$p < 0.01$, ***$p < 0.001$.

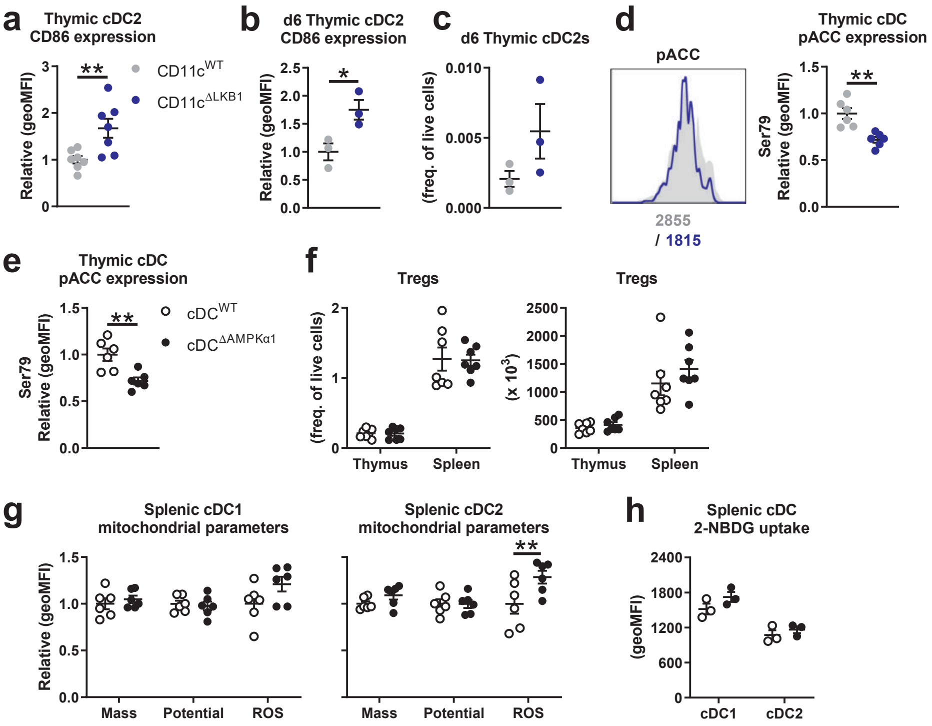

Figure S11. CD11c$^{\Delta AMPK\alpha1}$ mice do not recapitulate the metabolic and immunological phenotype seen in CD11c$^{\Delta LKB1}$ mice.

a-b Relative surface expression is shown of CD86 on cDC2s in thymi from adult CD11c^{WT} and CD11c$^{\Delta LKB1}$ mice (**a**) and in thymi of 6 days old CD11c^{WT} and CD11c$^{\Delta LKB1}$ pups (**b**) by flow cytometry. **c** total number of cDC2s in thymi from 6 days old CD11c^{WT} and CD11c$^{\Delta LKB1}$ mice (same as in **b**) by flow cytometry. **d-e** Flow cytometry-based analysis of ACC phosphorylation on serine 79 in thymic total cDCs from CD11c^{WT} and CD11c$^{\Delta LKB1}$ (**d**) and CD11c^{WT} and CD11c$^{\Delta AMPK\alpha1}$ (**e**). **f** Tregs in spleens and thymi from CD11c^{WT} and CD11c$^{\Delta AMPK\alpha1}$ mice were identified as CD3$^+$CD4$^+$FOXP3$^+$ and frequencies (middle) and absolute numbers (right) were quantified by flow cytometry. **g** Relative expression is shown of mitochondrial mass, membrane potential and ROS production in splenic cDC1s (left) and cDC2s (right) from CD11c^{WT} and CD11c$^{\Delta AMPK\alpha1}$ mice as analyzed by flow cytometry. **h** Uptake of a fluorescent glucose analog by splenic cDCs from CD11c^{WT} and CD11c$^{\Delta AMPK\alpha1}$ mice using flow cytometry. Data are pooled from 2 (**a,d,e**) or 1 (**b,c,f-h**) (independent) experiment(s) with three to four mice and shown as mean ± SEM; $*p < 0.05$, $**p < 0.01$.

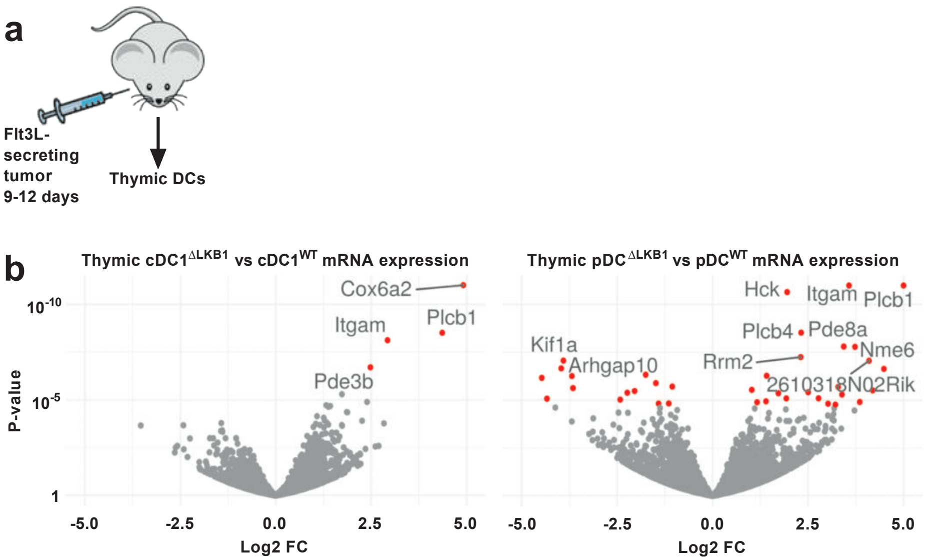

Figure S12. Loss of LKB1 results in transcriptional changes in thymic pDCs and cDC1s.

a-b Volcano plot shows genes differentially expressed between Flt3L-expanded LKB1-deficient thymic cDC21 versus Flt3L-expanded WT thymic cDC21s (left) and between Flt3L-expanded LKB1-deficient thymic pDCs versus Flt3L-expanded WT thymic pDCs (right). x axis shows log-fold change in expression between LKB1-deficient and WT thymic cDC2s. y axis shows p value for corresponding gene. Significantly differentially expressed genes are highlighted in red (**b**). Data are from 1 experiment with three mice.

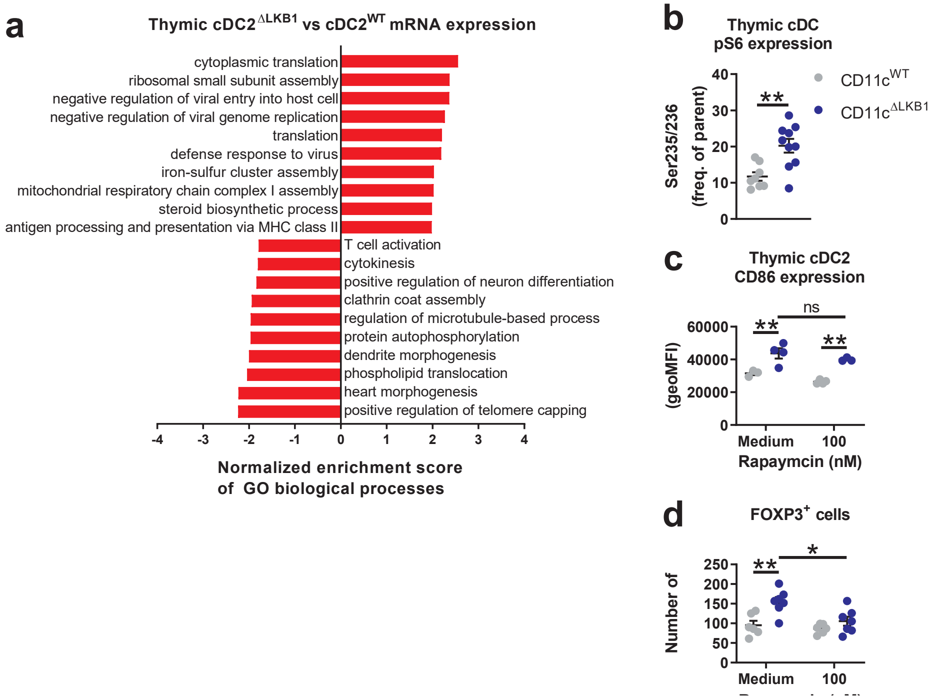

Figure S13. Increased mTOR signalling contributes to enhanced tTreg differentiation by LKB1- deficient thymic cDC2s.

a Gene set enrichment analysis of GO biological processes based on comparison of RNAseq data from Flt3L-expanded LKB1-deficient thymic cDC2s versus Flt3L-expanded WT thymic cDC2s. **b** Flow cytometry-based analysis of S6 phosphorylation on serine 235/236 in thymic total cDCs from CD11c$^{\mathrm{WT}}$ and CD11c$^{\Delta\mathrm{LKB1}}$. **c** Thymic single cell suspensions from Flt3L-treated mice were treated with the mTORC1 inhibitor Rapamycin for 30 minutes, washed, and 18 hours later, CD86 surface expression on cDC2s was determined by flow cytometry. **d** Flt3L- expanded thymic cDC2s were sorted and treated with Rapamycin for 30 minutes, washed, and cocultured in the presence of IL-7 with GFP-FOXP3$^-$CD25$^-$ single positive CD4$^+$ thymocytes sorted from DEREG mice. After 5 days, newly generated GFP-FOXP3$^+$ cells were enumerated. Data are pooled from 3 (**b**), 2 (**d**) or a representative of 2 (**c**) independent experiments with three to four mice and shown as mean ± SEM; **p < 0.01.

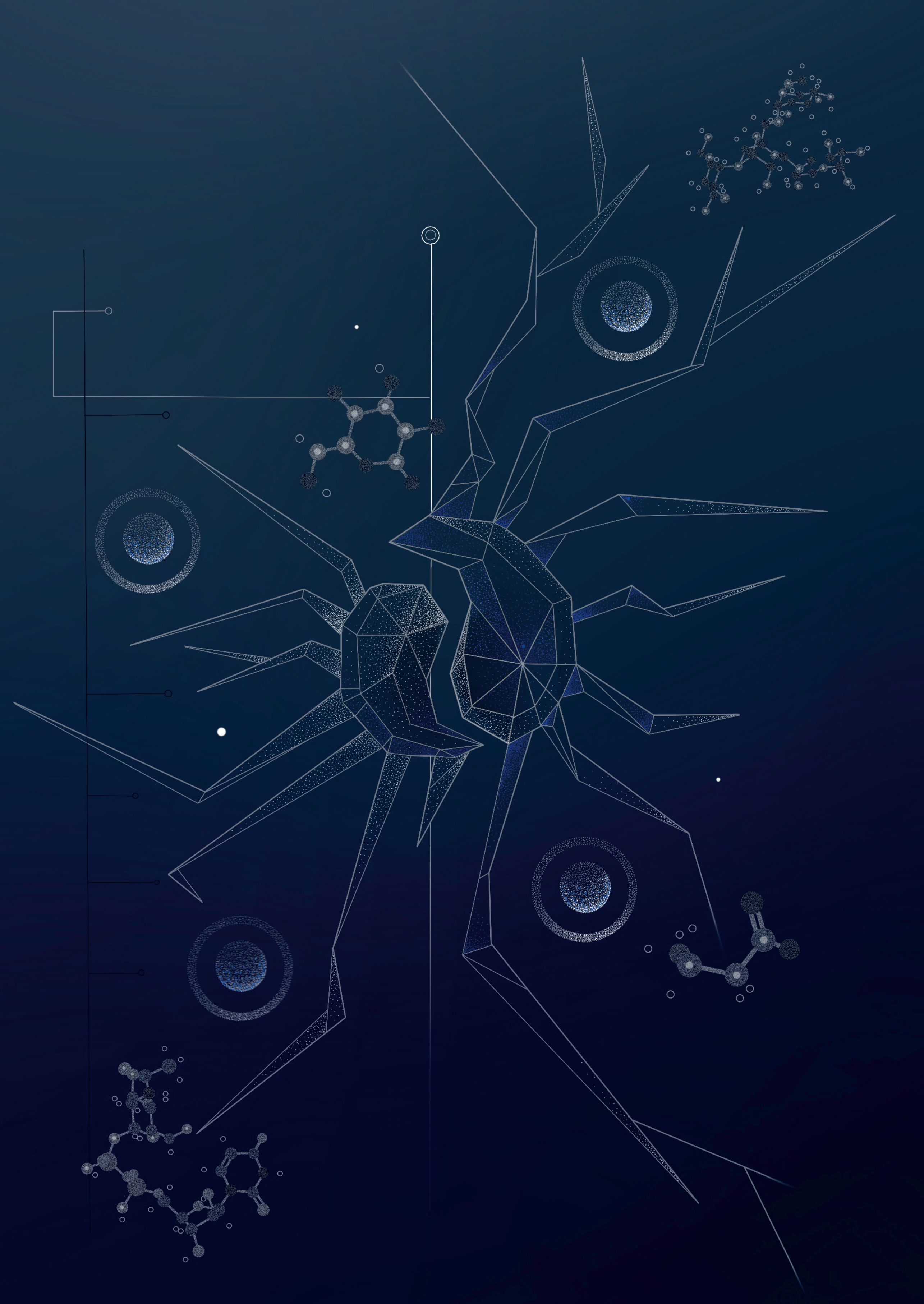

9

mTORC1 signalling in antigen-presenting cells of the skin restrains CD8+ T cell priming

Leonard R. Pelgrom
Thiago A. Patente
Frank Otto
Lonneke V. Nouwen
Arifa Ozir-Fazalalikhan
Alwin J. van der Ham
Hendrik J.P. van der Zande
Ramon Arens
Bart Everts

Under revision

Abstract

Mechanistic target of rapamycin complex 1 (mTORC1), a key sensor and regulator of cellular metabolism, has primarily been shown *in vitro* to affect various aspects of dendritic cell (DC) biology. However, our understanding of how mTORC1 regulates DC metabolism and their T cell-priming capacity *in vivo* remains limited. Here, using mice deficient in mTORC1 component raptor in DCs (CD11c$^{\Delta raptor}$), we found that loss of mTORC1 primarily compromises glucose uptake, mitochondrial fitness and cellular maturation, particularly MHCI expression, of type 1 conventional DCs from lymphoid organs. Nonetheless, antigen-specific CD8+ T cell responses to infection were not compromised and even enhanced following skin immunization in CD11c$^{\Delta raptor}$ mice. This was associated with potentiated costimulatory molecule expression and IL-12 production specifically by Langerhans cells in CD11c$^{\Delta raptor}$ mice. Together, this work reveals distinct roles for mTORC1 in orchestrating the immunogenicity of different antigen presenting cell subsets, which may have implications for vaccination practices.

Introduction

Dendritic cells (DCs) of the innate immune system are uniquely equipped to present antigens to T cells and to provide costimulatory signals and cytokines for T cell activation and polarization. This gives them a central role in the establishment of protective adaptive immunity following infections and after vaccination. In addition, their ability to prime regulatory T cells and their ability to induce anergy to host self-antigens, make them critical regulators of tolerance [1]. DCs patrol tissues until they recognize exogenous or endogenous danger signals with their pattern recognition receptors, after which they undergo rapid changes in their biology that enable them to efficiently migrate to lymphoid tissues and instruct T cells there for the appropriate immune response [2]. As these changes require concomitant changes in their metabolism [3], manipulation of DC metabolism may become an attractive therapeutic strategy for controlling the outcome of immune responses.

The mechanistic (formerly mammalian) target of rapamycin (mTOR) coordinates intracellular metabolism with environmental inputs that include nutrients, growth factors and immunological cues such as cytokines. It is a protein complex that exists in two distinct forms with either raptor (mTOR complex 1 [mTORC1]) or rictor (mTORC2) as one if its core components. Activity of mTORC1 is associated with increased protein synthesis, metabolism of lipids, nucleotides and glucose, and reduced autophagy; while mTORC2 signalling governs proliferation, survival, and cytoskeletal remodelling. Of the two, mTORC1 has been investigated most thoroughly, due to the discovery in the early 1970s of the compound ‘rapamycin’, which gave the complex it inhibited its name [4]. mTORC1 signalling has been shown to be vital for the metabolic reprogramming of various immune cells and in particular for the initial activation, proliferation, differentiation and effector function acquisition of lymphocytes [5].

The role of mTORC1 in DC biology has been extensively studied *in vitro*, and the outcome of mTORC1 inhibition in these cells seems to be context and species dependent [6, 7]. In vivo transferred murine bone marrow-derived DCs (BMDCs), that were generated *in vitro* using granulocyte-macrophage colony-stimulating factor (GM-CSF [GMDCs]), were shown to prime stronger CD8+ T cell responses after toll-like receptor (TLR)-activated in the presence of rapamycin [8-10]. This was associated with increased autophagy [10], a switch from anaerobic glycolysis to oxidative phosphorylation [11], and increased longevity and maintenance of high costimulatory molecule expression [8]. These latter two effects are likely the result of autocrine signalling by nitric oxide (NO) [12, 13], so whether these findings translate to conventional DCs (cDCs) that express little NO *in vivo* [14] is currently unclear.

Thus far, *in vivo* studies using CD11c-cre raptor$^{fl/fl}$ mice that display a selective loss of mTORC1 signalling in CD11c-expressing cells, which is largely restricted to DCs, revealed that maintenance of CD103+ type 1 cDCs (cDC1s) in the lungs [15] and Langerhans cells (LCs) in the skin and to a lesser degree in draining lymph nodes [16], was dependent on mTORC1 signalling. In addition, frequencies of CD8+ cDC1s in the spleen and CD11b+ cDC2s in the lamina propria can be modulated by loss of mTORC1 signalling [17], although the changes in DC homeostasis were not nearly as affected as in the lungs [15]. Functionally, mice with a CD11c-specific mTOR deletion, in which both mTORC1 and mTORC2 signalling is compromised, were found to have an antigen presenting cell (APC) compartment in the lung with an altered cellular metabolism, which was associated with a reduced capacity to mount a CD8+ T cell response upon viral infection and directly responsible for a shift from mounting a type 2 to type 17 immune response following allergen challenge [15]. However, whether these effects are a consequence of a defect in mTORC1, mTORC2 signalling, or both, remains unclear. Hence the specific role of mTORC1 signalling in DCs in regulating their metabolic and T cell-priming phenotype *in vivo* remains to be addressed.

In the current study, we found that the loss of raptor, a key component of mTORC1, in DCs compromises the maturation of various DC subsets in the spleen and skin draining lymph nodes, which was apparent during steady state conditions, systemic infection and local immunization. Especially the surface expression of the major histocompatibility complex I (MHCI) was reduced, which was associated with selective metabolic defects in cDC1s. Nevertheless, the priming of CD8+ T cells was not impaired but rather potentiated following subcutaneous (s.c.) immunization. This latter finding was associated specifically with enhanced IL-12 production and costimulatory molecule surface expression by LCs. Together, these data provide new insights into APC subset-specific effects of mTORC1 signalling and how this controls T cell responses *in vivo*, with a potential role for mTORC1 in restricting LC-dependent CD8+ T cell priming.

Results

mTORC1 signalling impacts glucose uptake and MHCI expression by splenic cDC1s

Mice with a conditional deletion of raptor in CD11c-expressing cells (CD11c$^{\Delta raptor}$ mice) displayed decreased steady state phosphorylation of ribosomal protein S6, a downstream target of the mammalian target of rapamycin complex 1 (mTORC1) that contains raptor, in both type 1 (cDC1) and type 2 splenic conventional DCs (cDC2) (Figure 1B). In contrast to what was previously reported [17], the frequency and numbers of splenic cDC1s were similar between CD11c-cre negative raptor$^{fl/fl}$ (CD11c^{WT}) and CD11c$^{\Delta raptor}$ littermates (Figure 1A,C). However, we did observe changes in splenic cDC1 metabolism. In keeping with reports that splenic cDC1s are more metabolically active than splenic cDC2s [18], we found splenic cDC1s to have higher uptake of the fluorescent glucose analogue 2-NBDG than other splenic DC subsets (Figure 1D). And consistent with a well described role for mTORC1 signalling in supporting glycolysis [4-7], we found that conditional deletion of raptor lowered 2-NBDG uptake in cDC1s, but not in cDC2s and pDCs (Figure 1D). Loss of raptor did not affect mitochondrial mass and membrane potential of any DC subset in the spleen (Figure 1E). Given the importance of glycolysis in DC activation [19-21], we next investigated whether the selective reduction of 2-NBDG uptake in raptor-deficient cDC1s was accompanied by changes in surfaces markers related to DC activation. Conditional deletion of raptor in splenic cDCs primarily resulted in an impaired activation profile of splenic cDC1s of which a decrease in MHCI surface expression was most prominent (Figure 1F).

Figure legends

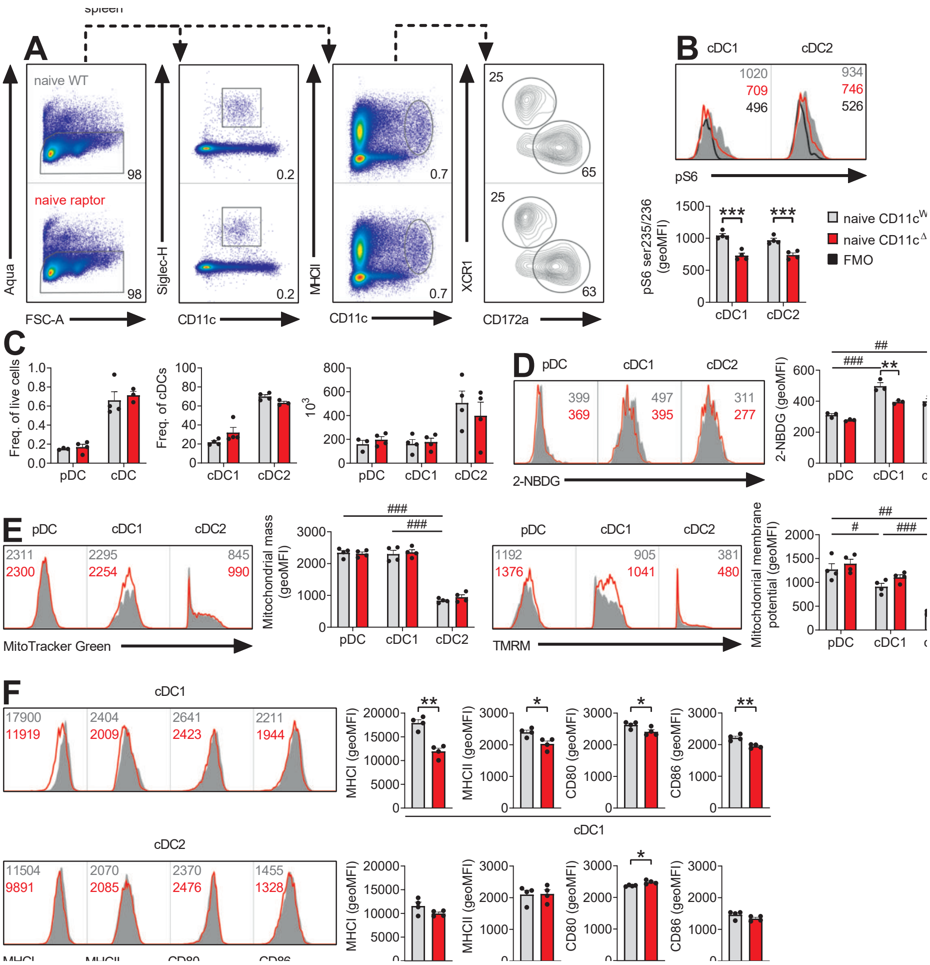

CD8+ T cell priming in response to, and host protection against listeria infection is intact in mice with raptor-deficient APCs

Given the critical role for MHCI in the priming and maintenance of CD8+ T cells by DCs, we next assessed whether the reduced expression of MHCI on raptor-deficient splenic cDCs would affect the CD8+ T cell pool in CD11c$^{\Delta raptor}$ mice. Indeed, in naïve CD11c$^{\Delta raptor}$ mice, antigen-experienced effector (EFF; CD44+CD62L-) CD8+ T cells were reduced in blood and central memory (CM; CD44+CD62L+) CD8+ T cells were reduced spleen, despite normal T cell development in the thymus (Figure 2A and S1A-B).

Figure 1. mTORC1 signalling is required for glucose uptake by splenic cDC1s and their MHCI expression.

(A) Flow gating strategy for splenic DC subsets by sequential gating of intact cells (forward scatter area [FSC-A] versus side scatter area [SSC-A], not shown), singlets (FSC-A versus forward scatter height [FSC-H], not shown), live cells (Aqua- cells in panel 1), pDCs (CD11c+ versus Siglec-H+ cells in panel 2) and cDCs (CD11c++ versus MHCII+ cells in panel 3), cDC1s (XCR1+ or CD8+ versus CD172a- or CD11b- cells in panel 4) and cDC2s (XCR1- or CD8- versus CD172a+ or CD11b+ cells in panel 4). (B) Flow cytometry-based analysis of S6 phosphorylation on serine 235/236 in splenic cDCs from CD11c^{WT} mice in grey, CD11c$^{\Delta raptor}$ mice in red and a Fluorescence Minus One (FMO) control in black. (C) Frequencies and numbers of splenic DC subsets as gated in A) are enumerated. (D) Flow cytometry-based analysis of overall metabolic pathway engagement by splenic DC subsets using the fluorescent glucose analogue 2-NBDG. (E) Flow cytometry-based analysis of mitochondrial mass and mitochondrial membrane potential in splenic DC subsets using MitoTracker Green and TMRM respectively. (F) Flow cytometry-based analysis of MHCI, MHCII, CD80 and CD86 surface protein expression on splenic cDCs. Data are from 1 out of 2 representative experiments using 3-4 mice per group and shown as mean ± SEM; $*p < 0.05$, $**p < 0.01$, $***p < 0.001$ when comparing samples between CD11c^{WT} and CD11c$^{\Delta raptor}$ mice; $\#\#p < 0.01$, $\#\#\#p < 0.001$ when comparing populations within CD11c^{WT} mice.

Next, to determine whether CD8+ T cell responses in CD11c$^{\Delta raptor}$ mice would be similarly compromised in response to infection, mice were challenged with a live-attenuated strain of *Listeria monocytogenes* expressing ovalbumin (Lm-dActA-OVA). *L. monocytogenes* is a facultative intracellular bacterium that primarily infects the spleen and liver and largely depends on splenic cDC1s for the efficient priming of protective CD8+ T cell responses [22]. While the infection elicited a clear expansion of CD44+CD62L- effector CD8+ T cells in control mice, this was less pronounced in the spleens of CD11c$^{\Delta raptor}$ mice after infection (Figure 2B-C). However, within this effector pool, the frequency of OVA-specific CD8+ T cells was increased in these mice. This resulted in a similar overall number of OVA-specific CD8+ T cells in the spleens of infected WT and CD11c$^{\Delta raptor}$ mice (Figure 2D). The expansion of CD44+ effector CD4+ T cells was affected to a lesser degree (Figure 2C) and their capacity to produce cytokines was unaltered (Figure S1C). In contrast, the production of the prototypical CD8+ cytotoxic T cell (CTL) cytokine interferon-gamma (IFNγ) by CD44+ CD8+ T cells in spleens from CD11c$^{\Delta raptor}$ mice after *ex vivo* restimulation with OVA was higher than that of CD8+ T cells from CD11c^{WT} mice (Figure 2E). Together, this suggests that the ability of CD11c$^{\Delta raptor}$ mice to mount antigen-specific CD8+ T cell responses to Lm-dActA-OVA infection was not compromised.

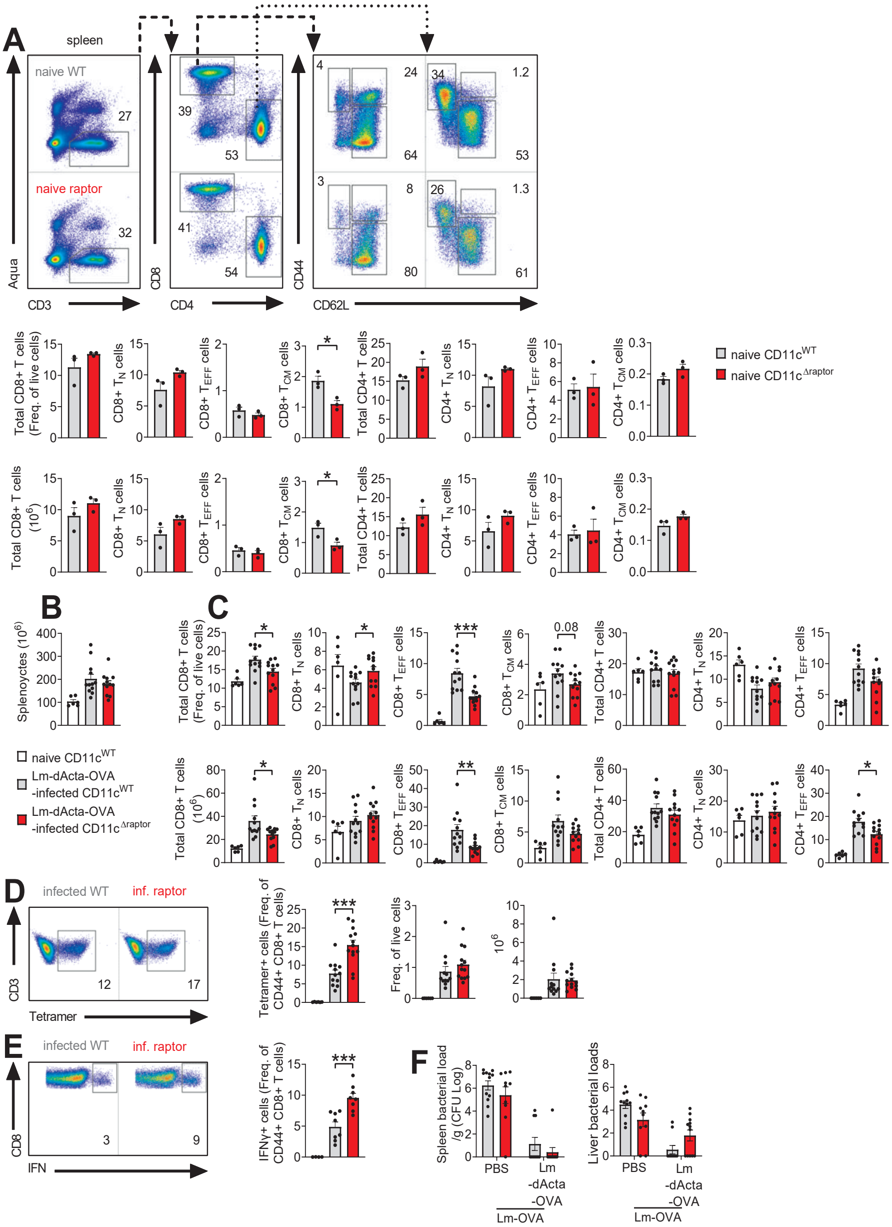
A
spleen
naive WT
naive raptor
27
32
39
53
41
54
4
24
64
34
1.2
53
3
8
80
26
1.3
61
Aqua
CD3
CD8
CD4
CD44
CD62L
Total CD8+ T cells (Freq. of live cells)
CD8+ T_N cells
CD8+ T_{EFF} cells
CD8+ T_{CM} cells
Total CD4+ T cells
CD4+ T_N cells
CD4+ T_{EFF} cells
CD4+ T_{CM} cells
Total CD8+ T cells (10^6)
*
naive CD11c^{WT}
naive CD11c$^{\Delta raptor}$
B
Splenocytes (10^6)
C
Total CD8+ T cells (Freq. of live cells)
Total CD8+ T cells (10^6)
*
***
**
0.08
naive CD11c^{WT}
Lm-dActa-OVA -infected CD11c^{WT}
Lm-dActa-OVA -infected CD11c$^{\Delta raptor}$
D
infected WT
inf. raptor
12
17
CD3
Tetramer
Tetramer+ cells (Freq. of CD44+ CD8+ T cells)
Freq. of live cells
10^6
***
E
infected WT
inf. raptor
3
9
CD8
IFN
IFNγ+ cells (Freq. of CD44+ CD8+ T cells)
***
F
Spleen bacterial load /g (CFU Log)
Liver bacterial loads
PBS
Lm -dActa -OVA
Lm-OVA

Figure 2. CD8+ T cell priming in response to Listeria infection and host protection is intact in mice with raptor-deficient APCs.

(A) On the top a gating strategy for splenic T cell subsets by sequential gating of intact cells (forward scatter area [FSC-A] versus side scatter area [SSC-A], not shown), singlets (FSC-A versus forward scatter height [FSC-H], not shown), live cells (Aqua- cells in panel 1), live T cells (CD3+ versus Aqua- cells in panel 1), total CD4 T cells (CD4+ versus CD8+ in panel 2) and total CD8+ T cells (CD4- versus CD8+ in panel 2), naïve CD8+ T cells (CD8+ TN; CD62L+ versus CD44- in panel 3) and effector CD8+ T cells (CD8+ TEFF; CD62L- versus CD44+ in panel 3) and central memory CD8+ T cells (CD8+ TCM; CD62L+CD44+ in panel 3), and naïve CD4 T cells (CD4+ TN; CD62L+CD44- in panel 4) and effector CD4 T cells (CD4+ TEFF; CD62L- versus CD44+ in panel 4) and central memory CD4+ T cells (CD4+ TCM; CD62L+CD44+ in panel 4). Antigen-experienced T cells (TAE) are the sum of TEFF and TCM subsets. Frequencies and numbers of splenic T cells are enumerated on the bottom. (B-E) CD11c^{WT} and CD11c$^{\Delta raptor}$ mice were infected with 5x10^6 Lm-dActa-OVA i.v. and splenic T cell responses were analysed 7 days later by flow cytometry. (B) Total cell numbers in spleen. (C) Frequencies and numbers of splenic CD8+ T cell subsets as analysed by flow cytometry. Representative histograms are in Figure S1A. (D) Frequencies and numbers of OVA-specific CD8+ TAE cells based on K^{b}OVA-tetramer staining as analysed by flow cytometry. (E) Splenocytes were stimulated with SIINFEKL in the presence of Brefeldin A and analysed for OVA-specific IFNγ production by CD8+ TAE cells using flow cytometry. (F) Mice were infected with 5x106 Lm-dActa-OVA by retro-orbital i.v. injection and challenged 21 days later with 5x104 Lm-OVA. The burden of LM-OVA in spleen and liver were determined on day 24. Data are from 2 experiments using 1-3 mice per group (A), 3 experiments using 1-4 mice per group (B-E, although E misses 1 experiment due to failed T cell marker staining), or 2 experiments using 5-7 mice per group (F). Data shown as mean ± SEM; *p < 0.05, ***p < 0.001 when comparing samples between CD11c^{WT} and CD11c$^{\Delta raptor}$ mice.

To assess whether the differences between the CD8+ T cell compartments of CD11c^{WT} and CD11c$^{\Delta raptor}$ mice following a primary infection with attenuated Lm-dActA-OVA would affect protective immunity against a secondary infection with a replication competent strain (Lm-OVA), mice were infected as before and subsequently challenged with Lm-OVA three weeks later. Right before challenge (d20 post primary infection) no differences in frequencies of circulating CM or effector OVA-specific CD8+ T cells between CD11c^{WT} and CD11c$^{\Delta raptor}$ mice were observed (Figure S1D). Moreover, 3 days following challenge infection (d24 post primary infection) frequencies of effector, antigen-experienced (AE; CD44+) CD8+ T cells in blood and spleen were comparable between CD11c^{WT} and CD11c$^{\Delta raptor}$ mice (Figure S1D). In line with these results, the bacterial loads in spleen and liver did not significantly differ between the two groups (Figure 2F), suggesting that CD8+ T cell memory formation and protective immunity to *L. monocytogenes* rechallenge was not affected by the loss of raptor in CD11c-expressing cells.

mTORC1 signalling is dispensable for longevity, maturation duration and production of IL-12 and IL-10 by TLR-stimulated splenic DCs

To mechanistically understand how CD11c$^{\Delta raptor}$ mice generated increased frequencies of antigen-specific and IFNγ-producing CD8+ T cells in response to *L. monocytogenes* infection, despite having splenic cDC1s with decreased surface expression of MHCI, we first assessed whether infection restored or even further enhanced levels of MHCI on these DCs. However, raptor-deficient splenic cDC1s maintained a decreased surface expression of MHCI following infection with Lm-dActA-OVA (Figure 3A). Since cross-presentation by DCs has been demonstrated to contribute to proper priming of CD8+ T cell responses against *L. monocytogenes* infection [23] and that autophagy, a process known to be enhanced by mTORC1 inhibition [4], can promote cross-presentation [24], we tested whether this was enhanced in DCs lacking raptor. However, the capacity of raptor-deficient cDC1s to cross-present soluble antigen - as assessed by their ability to present the H-2Kb-restricted OVA$_{257-264}$ short peptide (SIINFEKL) on MHCI following exposure to a synthetic long peptide (SLP) variant that contains this epitope (SLP-OVA) - was lower than that of their CD11c^{WT} counterparts (Figure 3B).

As rapamycin can promote GMDC longevity and sustain high costimulatory molecules expression after TLR stimulation [8], we next assessed survival and/or maturation comparing splenic cDCs from CD11c^{WT} and CD11c$^{\Delta raptor}$ mice following *ex vivo* TLR stimulation of whole splenocyte cultures for several days. However, no differences in survival (Figure S2A) or maturation (Figure S2B) were observed. As it has been shown that also IL-12 production by cDC1s can play a key role in the production of IFNγ by CD8+ T cells [25] and - primarily based on mouse GMDCs culture and human primary DC data - it is known that mTORC1 signalling can limit the production of IL-12 by DCs [6], we additionally tested whether there was a difference in IL-12p40/p70 production between splenic cDCs from CD11c^{WT} and CD11c$^{\Delta raptor}$ mice. However, IL-12 production by splenic cDCs from naïve CD11c$^{\Delta raptor}$ and CD11c$^{\Delta raptor}$ mice that were stimulated *ex vivo* with TLR ligands was comparable (Figure 3C). Alternatively, rapamycin-sensitive IL-10 production by DCs can limit CD8+ T cell priming independent of IL-12 production [26] and because conditional deletion of raptor in CD11c-expressing cells has been shown to abolish the steady state production of IL-10 by DCs and macrophages from the small intestine [17], we went on to determine whether there was a difference in IL-10 secretion between sorted splenic cDC1s and cDC2s from CD11c^{WT} and CD11c$^{\Delta raptor}$ mice, in which the DC numbers were expanded *in vivo* using Flt3L. However, the IL-10 production after *ex vivo* stimulation with the TLR3 ligand PolyIC was not significantly different (Figure 3D). More importantly, when we immunized recipient mice with these cDC1s, no differences were observed in their CD8+ T cell priming capacity (Figure 3E-H).

Taken together, these data suggest that raptor deficiency in cDC1s compromises MHCI expression and cross presentation, without significantly affecting longevity, maturation duration, cytokine production and CD8+ T cell priming.

mTORC1 signalling is required for maintenance of mitochondrial mass in skin migratory cDC1s and supports maturation of both migratory cDC subsets

mTOR signalling impacts DC biology differently depending on the tissue the DCs reside in [15], which made us wonder if DCs in other lymphoid tissues than the spleen, such as skin draining lymph nodes (sdLNs), would be similarly affected by loss of raptor with respect to their metabolic and immunogenic phenotype. Phosphorylation of ribosomal protein S6 showed a trend to be decreased in raptor-deficient cDCs from sdLNs (Figure 4B and S3A), suggesting a functional loss of raptor also in these DCs. This loss might potentiate their migration under steady state conditions as both the frequency and number of migratory cDCs (migDCs) were higher in sdLNs from CD11c$^{\Delta raptor}$ mice compared to CD11c^{WT} mice (Figure 4A,C). In contrast, resident DC (resDC) homeostasis was unchanged (Figure 4A,C). Like splenic cDC1s, skin migDC1s showed high 2-NBDG uptake, high mitochondrial mass and high membrane potential, of which the former was reduced by loss of raptor (Figure 4D-E and S3B). Moreover, like in the spleen, raptor deficiency more severely blunted maturation of sdLN migDC1 than that of sdLN migDC2s, as evaluated by the decreased surface expression of MHCI, MHCII, CD86 and CD80 on migDC1s versus MHCI and MHCII on migDC2s (Figure 4F and S3C). Together, these data reveal that also in skin-draining LNs the phenotype of cDC1s is more severely impacted by loss of raptor than that of cDC2s.

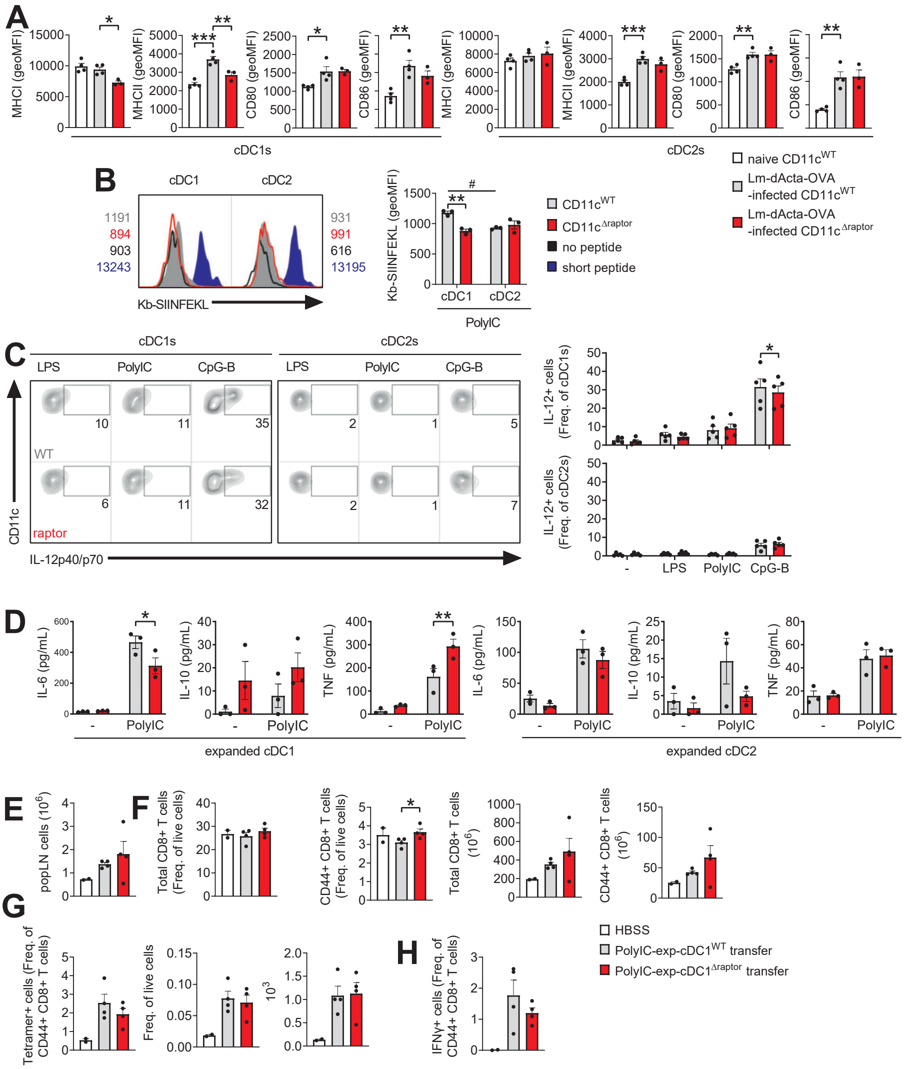
A
MHCI (geoMFI)
MHCII (geoMFI)
CD80 (geoMFI)
CD86 (geoMFI)
cDC1s
cDC2s
☐ naive CD11c^{WT}
▨ Lm-dActa-OVA -infected CD11c^{WT}
🟥 Lm-dActa-OVA -infected CD11c$^{\Delta raptor}$
B
cDC1
cDC2
1191
894
903
13243
931
991
616
13195
Kb-SIINFEKL
Kb-SIINFEKL (geoMFI)
#
PolyIC
▨ CD11c^{WT}
🟥 CD11c$^{\Delta raptor}$
■ no peptide
■ short peptide
C
cDC1s
cDC2s
LPS
PolyIC
CpG-B
WT
raptor
CD11c
IL-12p40/p70
10
11
35
2
1
5
6
11
32
2
1
7
IL-12+ cells (Freq. of cDC1s)
IL-12+ cells (Freq. of cDC2s)
-
LPS
PolyIC
CpG-B
D
IL-6 (pg/mL)
IL-10 (pg/mL)
TNF (pg/mL)
-
PolyIC
expanded cDC1
expanded cDC2
E
popLN cells (10^6)
F
Total CD8+ T cells (Freq. of live cells)
CD44+ CD8+ T cells (Freq. of live cells)
Total CD8+ T cells (10^6)
CD44+ CD8+ T cells (10^6)
G
Tetramer+ cells (Freq. of CD44+ CD8+ T cells)
Freq. of live cells
10^3
H
IFNγ+ cells (Freq. of CD44+ CD8+ T cells)
☐ HBSS
▨ PolyIC-exp-cDC1^{WT} transfer
🟥 PolyIC-exp-cDC1$^{\Delta raptor}$ transfer
*
**
***

Figure 3. mTORC1 signalling is dispensable for longevity, maturation duration and production of IL-12 and IL-10 by TLR-stimulated splenic DCs.

(A) CD11c^{WT} and CD11c$^{\Delta raptor}$ mice were infected with 2.5x10^5 Lm-dActA-OVA by retro-orbital i.v. injection and splenic cDCs surface protein expression of indicated surface markers was analysed 1 day later by flow cytometry. (B) Flow cytometry-based analysis of cross presentation in splenic cDCs from CD11c^{WT} mice in grey, CD11c$^{\Delta raptor}$ mice, a no antigen negative control in black and a SIINFEKL positive control in blue. (C) Splenocytes from naïve WT and CD11c$^{\Delta raptor}$ mice were stimulated with either 100 ng/mL LPS, 10 µg/mL PolyIC or 5 µg/mL CpG-B and all in the presence of Brefeldin A and analysed for production of IL-12p40/p70 by splenic cDCs using flow cytometry. (D) In vivo Flt3L-expanded splenic cDC1s and cDC2s were sorted using a flow cytometer and put into culture with or without PolyIC. Supernatants were harvested 16 hours later and analysed for indicated cytokines by cytokine bead array. (E-H) In vivo Flt3L-expanded splenic cDC1s were sorted and conditioned with OVA and PolyIC for 5 hours *ex vivo* before transfer into recipient mice by footpad injection. CD8+ T cell responses were evaluated in draining popliteal LNs (popLNs) 7 days later by flow cytometry. (E) Number of cells in popLNs. (F) Frequencies and numbers of total CD8+ T cells and antigen-experienced (CD44+) CD8+ T cells (CD8+ TAE) as analysed by flow cytometry. (G) Frequencies and numbers of OVA-specific CD8+ TAE cells based on K^{b}OVA-tetramer staining as analysed by flow cytometry. (H) Splenocytes were stimulated with SIINFEKL in the presence of Brefeldin A and analysed for OVA-specific IFNγ production by CD8+ TAE cells using flow cytometry. Data are from 1 experiment using 4 mice per group (A), 1 experiment using 3 mice per group (B) 5 experiments using 1 mouse per group (C), 1 experiment using 3 mice per group (D), or 1 experiment using 2-4 mice per group (E-H). Data shown as mean ± SEM; $*p < 0.05$, $**p < 0.01$, $***p < 0.001$ when comparing samples between CD11c^{WT} and CD11c$^{\Delta raptor}$ mice; $\#p < 0.05$ when comparing populations within CD11c^{WT} mice.

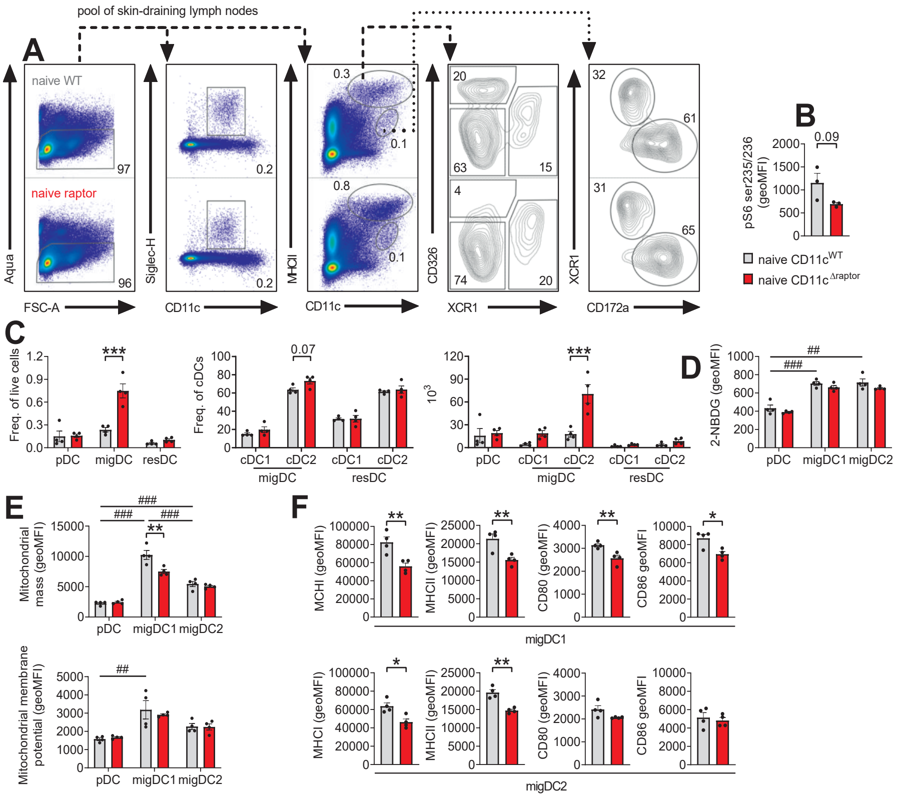
pool of skin-draining lymph nodes
A
naive WT
naive raptor
97
96
0.2
0.2
0.3
0.1
0.8
0.1
20
63
15
4
74
20
32
61
31
65
Aqua
FSC-A
Siglec-H
CD11c
MHCII
CD11c
CD326
XCR1
XCR1
CD172a
B
pS6 ser235/236 (geoMFI)
2000
1500
1000
500
0
0.09
naive CD11c^{WT}
naive CD11c$^{\Delta raptor}$
C
Freq. of live cells
1.2
0.9
0.6
0.3
0.0
***
pDC
migDC
resDC
Freq. of cDCs
100
80
60
40
20
0
0.07
cDC1
cDC2
cDC1
cDC2
migDC
resDC
10^3
120
90
60
30
0
***
pDC
cDC1
cDC2
cDC1
cDC2
migDC
resDC
D
2-NBDG (geoMFI)
1000
800
600
400
200
0
##
###
pDC
migDC1
migDC2
E
Mitochondrial mass (geoMFI)
15000
10000
5000
0
###
###
###
**
pDC
migDC1
migDC2
Mitochondrial membrane potential (geoMFI)
5000
4000
3000
2000
1000
0
##
pDC
migDC1
migDC2
F
MCHI (geoMFI)
100000
80000
60000
40000
20000
0
**
MHCII (geoMFI)
25000
20000
15000
10000
5000
0
**
CD80 (geoMFI)
4000
3000
2000
1000
0
**
CD86 geoMFI
10000
8000
6000
4000
2000
0
*
migDC1
MHCI (geoMFI)
100000
80000
60000
40000
20000
0
*
MHCII (geoMFI)
25000
20000
15000
10000
5000
0
**
CD80 (geoMFI)
4000
3000
2000
1000
0
CD86 geoMFI
10000
8000
6000
4000
2000
0
migDC2

Figure 4. mTORC1 signalling is required for maintenance of mitochondrial mass in skin migratory cDC1s and supports maturation of both migratory cDC subsets.

(A) Flow gating strategy for LCs and DC subsets in sdLNs by sequential gating of intact cells (forward scatter area [FSC-A] versus side scatter area [SSC-A], not shown), singlets (FSC-A versus forward scatter height [FSC-H], not shown), live cells (Aqua- cells in panel 1), pDCs (CD11c+ versus Siglec-H+ cells in panel 2) and migratory APCs (CD11c+ versus MHCII++ cells in panel 3) and resDCs (CD11c+ versus MHCI+ cells in panel 3), LCs (XCR1- versus CD326+ cells in panel 4) and migDC1s (XCR1+ versus CD326- in panel 4) and migDC2s (XCR1- versus CD326- in panel 4), and resDC1s (CD172a- versus XCR1+ cells in panel 5) and resDC2s (CD172a+ versus XCR1- cells in panel 5). (B) Flow cytometry-based analysis of S6 phosphorylation on serine 235/236 in total migDCs from skin draining lymph nodes (sdLNs) out of CD11c^{WT} mice in grey, CD11c$^{\Delta raptor}$ mice in red and a Fluorescence Minus One (FMO control in black). Representative histograms are in Figure S3A. sdLNs were a pool of brachial, axillary and inguinal LNs. (C) Frequencies and numbers of DC subsets in sdLNs as gated in A) are enumerated. Migratory DCs are migAPCs minus LCs. (D) Flow cytometry-based analysis of overall metabolic pathway engagement by sdLN DC subsets using the fluorescent glucose analogue 2-NBDG. Representative histograms are in Figure S3B. (E) Flow cytometry-based analysis of mitochondrial mass and mitochondrial membrane potential in sdLN DC subsets using MitoTracker Green and TMRM respectively. Representative histograms are in Figure S3B. (F) Flow cytometry-based analysis of MHCI, MHCII, CD80 and CD86 surface protein expression on sdLN migDCs. Representative histograms are in Figure S6C. Data are from 1 out of 2 representative experiments using 4 mice per group and shown as mean ± SEM; *p < 0.05, **p < 0.01, ***p < 0.001 when comparing samples between WT and CD11c$^{\Delta raptor}$ mice; ##p < 0.01, ###p < 0.001 when comparing populations within CD11c^{WT} mice.

mTORC1 signalling in CD11c-expressing cells limits CD8+ T cell priming following subcutaneous immunization

Because raptor-deficient sdLN migDC1s and migDC2s displayed a weaker maturation profile, we first investigated if the T cell compartment in sdLNs from CD11c$^{\Delta raptor}$ mice was changed under steady state conditions. Like in the circulation, the frequency of effector T cells was reduced in sdLNs from naïve CD11c$^{\Delta raptor}$ mice compared to CD11c^{WT} mice (Figure 5A).

sdLN migDC2s from CD11c$^{\Delta raptor}$ mice express reduced MHCII (Figure 4F), which has been implicated in favouring the priming of CD4+ T helper 2 (Th2) cells [27]. In addition, pharmacological inhibition of mTORC1 in human monocyte-derived DCs has been shown to enhance their Th2-priming capacity *in vitro* [28]. Hence, we next investigated whether Th2 priming was altered in CD11c$^{\Delta raptor}$ mice following footpad injection with a soluble antigen extract of *Schistosoma mansoni* eggs (SEA). However, the secretion of canonical type 2 cytokines such as IL-4, IL-5, and IL-13 by sdLN cells from CD11c^{WT} and CD11c$^{\Delta raptor}$ mice was comparable after *ex vivo* antigen-specific restimulation (Figure 5B). Moreover, Th2 responses were not different between CD11c^{WT} and CD11c$^{\Delta raptor}$

mice during systemic *S. mansoni* infection, as evaluated by the production of type 2 cytokines by CD44+CD4+ cells in the liver and draining hepatic lymph node (Figure S4), which are major sites of T cell priming during schistosomiasis [29]. Together, these data suggest that mTORC1 signalling in CD11c-expressing cells is not important for the generation of Th2 cell responses.

Finally, we assessed whether the reduced activation profile of sdLN migDC1s in CD11c$^{\Delta raptor}$ mice would affect CD8+ T cell priming following s.c. immunization. Mice were immunized with the TLR9 ligand CpG-B in combination with a synthetic 43-mer long peptide form the human papillomavirus (HPV) E7 protein that contains the immunodominant and H-2Db-restricted epitope RAHYNIVTF (E7-SLP), a combination that predominantly activates cDC1s and requires cross-presentation for priming of CD8+ T cells [30]. This resulted in enhanced frequencies and numbers of E7-specific CD8+ T cells in sdLNs from CD11c$^{\Delta raptor}$ mice compared to sdLNs from their CD11c^{WT} littermates (Figure 5C-D), as well as enhanced IFNγ production by these cells after *ex vivo* antigen-specific restimulation (Figure 5E-F). These effects were independent of antigen or TLR stimulus, as enhanced IFNγ production by CD8+ T cells and trends towards higher frequencies and numbers of antigen-specific CD8+ T cells were also observed in CD11c$^{\Delta raptor}$ mice after immunization with CpG-B with full length OVA (Figure 5G-J) or PolyIC with E7-SLP (Figure 5K-L).

mTORC1 signalling supports activation of migratory skin DCs but constrains activation of Langerhans cells in response to subcutaneous immunization

To find a mechanistic basis for the enhanced IFNγ production by CD8+ T cells in CD11c$^{\Delta raptor}$ mice after s.c. immunization, we assessed whether loss of raptor affected maturation, cytokine production and/or migration of sdLN migDCs in response to these immunizations. However, immunization with either PolyIC or CpG-B did not restore or further enhance the maturation of raptor-deficient migDCs *in vivo* (Figure 6A and S5A-B). Little IL-12p40/p70 production by migDCs was measured *ex vivo* following immunization *in vivo* (Figure S5C) and also the IL-12 production by migDCs from naïve CD11c^{WT} and CD11c$^{\Delta raptor}$ mice that were stimulated *ex vivo* with several TLR ligands was comparable (Figure 6B and S5D). No differences were found in the frequencies and numbers of Fluorescein isothiocyanate (FITC)+ skin migratory cDC1s and cDC2s in draining inguinal LNs from CD11c$^{\Delta raptor}$ mice and their CD11c^{WT} littermates 24 hours after inflammatory FITC painting of the flank (Figure 6C). Moreover, 72h after FITC painting, frequencies, numbers and maturation of these cells were not affected by loss of raptor (Figure 6C and S5E), suggesting that longevity of activated migDCs and their maintenance of high costimulatory molecule expression is not differentially impacted between raptor competent and raptor-deficient cells. More importantly, this also suggests that CD11c-expressing cells other than migDCs may underlie the observed potentiated CD8+ T cell priming in CD11c$^{\Delta raptor}$ mice after s.c. immunization.

In the light of these findings, we turned our attention to Langerhans cells (LCs), which are another important group of professional APCs in the skin, that have migratory, T helper cell priming and CTL priming capacity [31]. Notably, LCs also express high levels of CD11c and may therefore be affected in this model. In line with work showing that LCs depend on mTORC1 signalling for their survival [16], we found that deletion of raptor in CD11c-expressing cells decreased steady state phosphorylation of ribosomal protein S6 in LCs from sdLNs (Figure S6A). This resulted in CD24+CD326+XCR1- LCs (Figure S6B) to be strongly reduced in frequency within the migratory APC gate (Figure 4A and S6C). However, due to the overall increased migratory APC pool size (Figure 4A,C) the total number of LCs in sdLNs was not different between CD11c^{WT} and CD11c$^{\Delta raptor}$ mice (Figure S6C). Moreover, the migratory capacity of LCs was intact after loss of raptor (Figure 6D). Loss of raptor decreased 2-NBDG uptake by LCs (Figure S6D) without affecting mitochondrial mass (Figure S6E), mitochondrial membrane potential (Figure S6E) in steady state conditions. Immunologically, a higher surface expression of costimulatory markers CD70 and CD80 could be observed on LCs from CD11c$^{\Delta raptor}$ mice compared to LCs from CD11c^{WT} mice after s.c. immunization with either PolyIC or CpG-B (Figure 6E and S5B). Moreover, these raptor-deficient LCs showed an approximately 2-fold higher production of IL-12 (Figure 6F and S5D). The production of IL-12 after stimulation with LPS was, however, not affected (Figure 6F). In line with this, s.c. immunization with LPS+OVA did, in contrast to immunizations with PolyIC or CpG (Figure 5), not result in enhanced IFNγ production by CD8+ T cells (Figure S6F,G). Finally, the reduced MHCI expression under steady state conditions by raptor-deficient LCs was restored to WT levels after TLR stimulation (Figure 6E). Correspondingly, cross presentation of soluble OVA SLP antigen was, in contrast to migDC1s, not significantly compromised in LCs from CD11c$^{\Delta raptor}$ mice (Figure 6G). This was associated with increased expression of autophagy marker LC3 in raptor-deficient LCs, but not in migDCs, relative to their raptor sufficient counterparts (Figure 6H-I). Taken together, these findings in the LC compartment may explain the enhanced CD8+ T cell response in CD11c$^{\Delta raptor}$ mice after s.c. immunization.

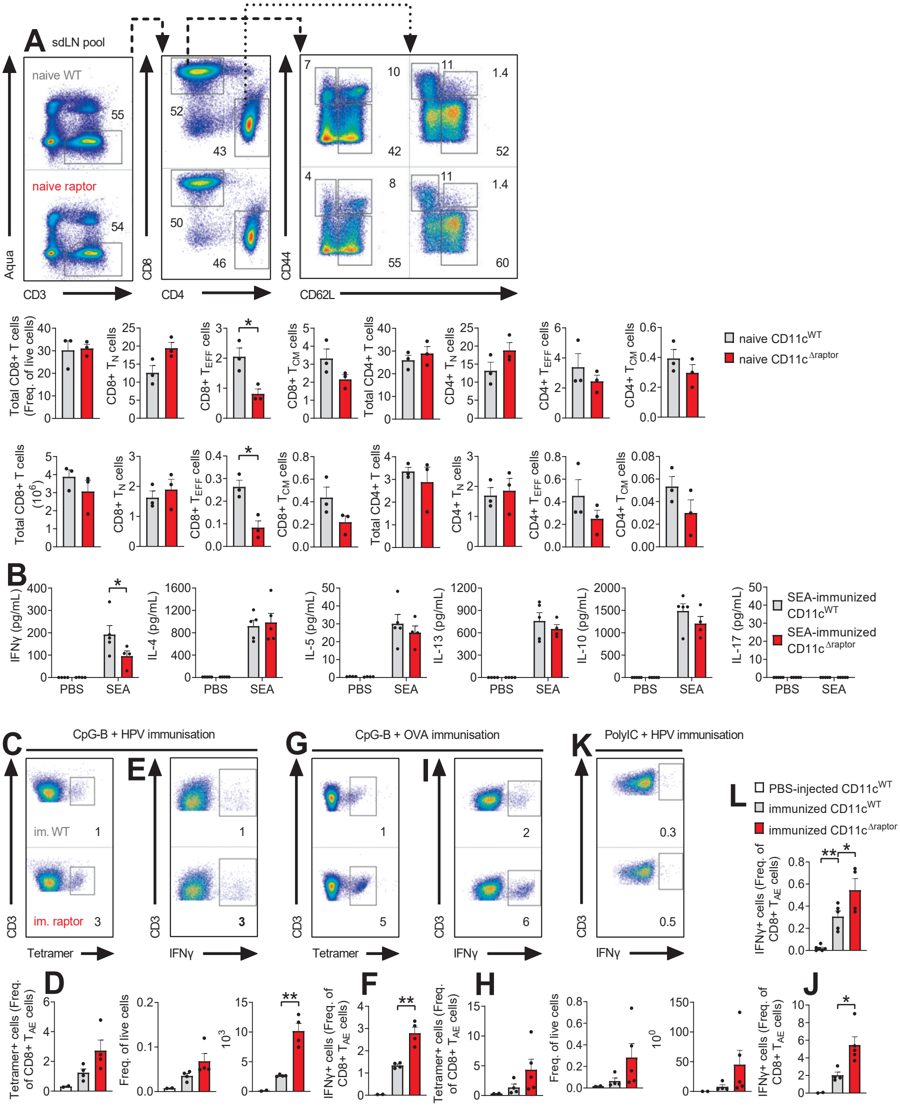
A
sdLN pool
naive WT
naive raptor
55
54
52
43
50
46
7
10
42
4
8
55
11
1.4
52
11
1.4
60
Aqua
CD3
CD8
CD4
CD44
CD62L
Total CD8+ T cells (Freq. of live cells)
CD8+ T_N cells
CD8+ T_EFF cells
CD8+ T_CM cells
Total CD4+ T cells
CD4+ T_N cells
CD4+ T_EFF cells
CD4+ T_CM cells
Total CD8+ T cells (10^6)
naive CD11c^WT
naive CD11c^Δraptor
*
B
IFNγ (pg/mL)
IL-4 (pg/mL)
IL-5 (pg/mL)
IL-13 (pg/mL)
IL-10 (pg/mL)
IL-17 (pg/mL)
PBS
SEA
SEA-immunized CD11c^WT
SEA-immunized CD11c^Δraptor
C
CpG-B + HPV immunisation
E
G
CpG-B + OVA immunisation
I
K
PolyIC + HPV immunisation
im. WT
im. raptor
1
3
1
3
1
5
2
6
0.3
0.5
CD3
Tetramer
IFNγ
L
PBS-injected CD11c^WT
immunized CD11c^WT
immunized CD11c^Δraptor
IFNγ+ cells (Freq. of CD8+ T_AE cells)
**
D
F
H
J
Tetramer+ cells (Freq. of CD8+ T_AE cells)
Freq. of live cells
10^3
10^0
IFNγ+ cells (Freq. of CD8+ T_AE cells)

Figure 5. mTORC1 signalling in CD11c-expressing cells limits CD8+ T cell priming following subcutaneous immunization but not Th2 polarization.

(A) On the top a gating strategy for T cell subsets in skin-draining lymph nodes (sdLNs; pool of brachial, axillary and inguinal LNs) as shown in Figure 2A. Frequencies and numbers of splenic T cells are enumerated on the bottom. (B) $CD11c^{WT}$ and $CD11c^{\Delta raptor}$ mice were immunized with *S. mansoni* soluble egg antigens (SEA) by s.c. footpad injection and draining popLNs were collected 7 days later. popLN single cell suspensions were put into culture for 3 days with or without SEA. Supernatants were harvested and analysed for indicated cytokines by cytokine bead array. (C-F) Mice were immunized with HPV SLP and 25 µg of CpG-B by s.c. tailbase injection and T cell responses in draining inguinal lymph nodes (ingLNs) were analysed 7 days later by flow cytometry. (C,D) Representative histograms, frequencies and numbers of E7-specific CD8+ TAE cells based on D^bE7-tetramer staining as analysed by flow cytometry. (E,F) IngLN cells were stimulated with E7-SLP in the presence of Brefeldin A and analysed for HPV-specific IFNγ production by CD8+ TAE cells using flow cytometry. (G-J) Mice were immunized with OVA and 25 µg of CpG-B by s.c. footpad injection and T cell responses in draining popLNs were analysed 7 days later by flow cytometry. (G,H) Representative histograms, frequencies and numbers of OVA-specific CD8+ TAE cells based on K^bOVA-tetramer staining as analysed by flow cytometry. (I,J) popLN cells were stimulated with SIINFEKL in the presence of Brefeldin A and analysed for OVA-specific IFNγ production by CD8+ TAE cells using flow cytometry. (K,L) Mice were immunized with HPV and 25 µg of PolyIC by s.c. tailbase injection and T cell responses in draining ingLNs were analysed 7 days later by flow cytometry. ingLN cells were stimulated with E7-SLP in the presence of Brefeldin A and analysed for E7-specific IFNγ production by CD8+ TAE cells using flow cytometry. Data are from 1 experiment using 3 mice per group (A), 1 experiment using 4-5 mice per group (B), 1 experiment using 2-4 mice per group (C-F), 1 experiment using 2-5 mice per group (G-J) or 1 experiment using 2 lymph nodes from 2-3 mice per group (K-L). Data shown as mean ± SEM; $*p < 0.05$, $**p < 0.01$ when comparing samples between $CD11c^{WT}$ and $CD11c^{\Delta raptor}$ mice.

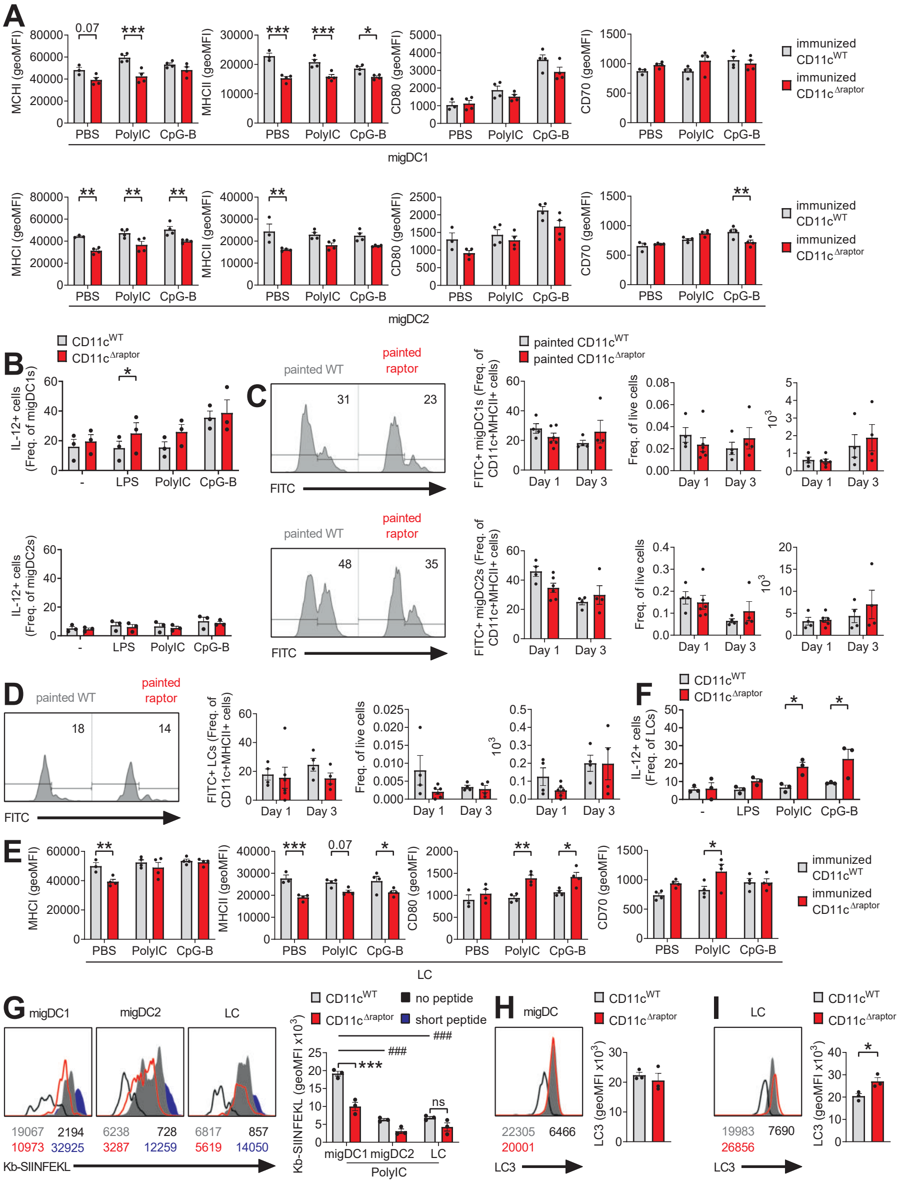
A
MCHI (geoMFI)
MHCII (geoMFI)
CD80 (geoMFI)
CD70 (geoMFI)
0.07
***
*
PBS PolyIC CpG-B
migDC1
immunized CD11c^WT
immunized CD11c^Δraptor
MHCI (geoMFI)
**
migDC2
B
CD11c^WT
CD11c^Δraptor
IL-12+ cells (Freq. of migDC1s)
IL-12+ cells (Freq. of migDC2s)
- LPS PolyIC CpG-B
C
painted WT
painted raptor
31
23
48
35
FITC
painted CD11c^WT
painted CD11c^Δraptor
FITC+ migDC1s (Freq. of CD11c+MHCII+ cells)
FITC+ migDC2s (Freq. of CD11c+MHCII+ cells)
Freq. of live cells
10^3
Day 1 Day 3
D
painted WT
painted raptor
18
14
FITC
FITC+ LCs (Freq. of CD11c+MHCII+ cells)
Freq. of live cells
10^3
Day 1 Day 3
F
CD11c^WT
CD11c^Δraptor
IL-12+ cells (Freq. of LCs)
- LPS PolyIC CpG-B
E
MHCI (geoMFI)
MHCII (geoMFI)
CD80 (geoMFI)
CD70 (geoMFI)
PBS PolyIC CpG-B
LC
immunized CD11c^WT
immunized CD11c^Δraptor
G
migDC1
migDC2
LC
19067 2194
10973 32925
6238 728
3287 12259
6817 857
5619 14050
Kb-SIINFEKL
CD11c^WT
CD11c^Δraptor
no peptide
short peptide
Kb-SIINFEKL (geoMFI x10^3)
###
***
ns
migDC1 migDC2 LC
PolyIC
H
migDC
22305 6466
20001
LC3
LC3 (geoMFI x10^3)
CD11c^WT
CD11c^Δraptor
I
LC
19983 7690
26856
LC3
LC3 (geoMFI x10^3)
CD11c^WT
CD11c^Δraptor

Figure 6. mTORC1 signalling supports activation of migratory skin DCs but constrains activation of Langerhans Cells in response to subcutaneous immunization.

(A,E) CD11c^{WT} and CD11c$^{\Delta raptor}$ mice were immunized with either 25 µg of CpG-B or 25 µg of PolyIC by s.c. tailbase injection and (A) migDC1 and migDC2, and (E) LC maturation in draining inguinal lymph nodes (ingLNs) was analysed 24 hours later by flow cytometry. Representative histograms are in Figure S8B. (B,F) IngLN cells from naïve WT and CD11c$^{\Delta raptor}$ mice were stimulated with either 10 µg/mL PolyIC or 5 µg/mL CpG-B and all in the presence of Brefeldin A and analysed for production of IL-12p40/p70 by (B) migDC1s and migDC2s, and (H) LCs using flow cytometry. Representative histograms are in Figure S8C. (C,D) Mice were painted on their flank with inflammatory FITC paint and FITC+ migAPC migration was analysed on the indicated days by flow cytometry. (G) Flow cytometry-based analysis of cross presentation in sdLN migAPCs from CD11c^{WT} mice in grey, CD11c$^{\Delta raptor}$ mice in red, a no antigen negative control in black and a SIINFEKL positive control in blue. (H-I) Flow cytometry-based analysis of the autophagy marker Light Chain 3 (LC3) in sdLN migDCs (H) and LCs (I) from WT mice in grey CD11c$^{\Delta raptor}$ mice in red and a fluorescence minus one (FMO; no primary antibody) control in black. Data are from 1 experiment using 2 lymph nodes from 2 mice per group (A,E), 3 experiments using 1 mouse per group (B,F), 1 out of 2 representative experiments using 4-6 mice per group (C-D) or 1 experiment using 3 mice (G-I). Data shown as mean ± SEM; $*p < 0.05$, $**p < 0.01$, $***p < 0.001$ when comparing samples between CD11c^{WT} and CD11c$^{\Delta raptor}$ mice; $\#\#\#p < 0.001$ when comparing populations within CD11c^{WT} mice.

Discussion

In the present study we aimed to determine how mTORC1 regulates DC metabolism and their T cell priming capacity *in vivo*. We show that the metabolic and immunological phenotype of professional APCs are differently affected by loss of mTORC1 signalling depending on their origin and location. Apart from compromised MHCI expression, homeostasis and activation of splenic cDCs was only minimally affected by deletion of raptor. On the other hand, raptor deficiency resulted in a greater abundance of migDCs in skin-draining LNs with a strongly reduced maturation profile, with the notable exception of LCs which showed increased expression of the costimulatory molecules and IL-12. These latter findings were associated with a potentiated ability of CD11c$^{\Delta raptor}$ mice to mount CD8 T cell responses following s.c. immunization. Together, these data highlight distinct effects of mTORC1 signalling inhibition on different APC subsets and may suggest that mTORC1 acts as a negative regulator of CD8 T cell priming selectively in LCs.

We found that splenic CD8+ cDC1s display higher uptake of the fluorescent glucose analogue 2-NBDG, and increased mitochondrial mass and membrane potential than splenic CD11b+ cDC2s. This is in line with a recent study that reported splenic CD8+ cDC1s to have higher mitochondrial respiration, glycolytic flux, mitochondrial mass, and membrane potential than their CD8- counterpart [18]. This unique metabolic profile of splenic cDC1s was reported to depend on the Hippo pathway kinases Mst1 and Mst2 and was important for their function, which was illustrated by the fact that these DCs were much more sensitive to metabolic inhibitors such as metformin and 2-deoxyglucose than cDC2s [18]. We now report that also skin migratory cDC1s have relative high 2-NBDG uptake, mitochondrial mass and membrane potential, although the 2-NBDG uptake was similarly high in migDC1s and migDC2s. Consistent with a well described role for mTORC1 signalling in supporting glycolysis, mitochondrial biogenesis and preventing mitophagy in myeloid cells [7], 2-NBDG uptake and mitochondrial mass were reduced following loss of mTORC1 signalling. Interestingly, the former occurred specifically in splenic cDC1s while the latter happened explicitly in skin migDC1. How mTORC1 differentially affects the metabolism of DCs at different locations is currently unclear, but is likely to be influenced by local nutrient and growth factor availability which both are important determinants of mTORC1 activity.

Moreover, we found that raptor-deficient cDCs show a consistent reduction in MHCI surface expression at steady state conditions, while homeostasis, migration, costimulatory molecule expression and cytokine production are minimally affected. Although an important role for mTORC1 in the processing and presentation of antigens in the context of MHCII has been well established [3, 32], its role in antigen presentation in the context of MHCI is less well-defined. Stable MHCI surface expression is dependent on the transcription of MHCI and the availability of high affinity peptides, which under steady state are commonly derived from proteasome mediated degradation of cytosolic proteins [33]. The synthesis of these proteins [34] and the expression and activity of the proteasome [35] can be positively regulated by active mTORC1 signalling. Treatment of tumour cells with rapamycin indeed reduced the intracellular peptide pool and consequently the surface MHCI expression [34]. Additionally, mTORC1 inhibition is well known to promote autophagy which can reduce MHCI surface levels by mediating their degradation following endocytosis [36]. Such studies might provide an explanation for the reduced surface expression of MHCI on raptor-deficient DCs at steady state. Lower baseline MHCI expression on raptor-deficient DCs did not however translate into an impaired ability of CD11c$^{\Delta raptor}$ mice to mount CD8+ T cell responses to foreign antigens. This was apparent during both systemic (listeria infection) and local (s.c. immunization) immunological challenge. In fact, antigen-specific CD8+ T cell responses in CD11c$^{\Delta raptor}$ mice were even potentiated following s.c. immunization. While our data suggest that the latter observation - as discussed in more detail below – may stem from alterations in skin-resident LC function, the intact CD8+ T cell priming after listeria infection is likely to have a different basis. *L.*

monocytogenes primarily infects splenic macrophages and liver Kupffer cells. However, cDC1s are also directly infected and serve as a critical entry point to establish infection [37]. Following internalization, the bacteria can escape from phagosomes and access the host cytosol for replication. Hence, it has been shown that listeria-derived antigens from both exogenous/vacuolar and cytosolic origin can be presented in MHCI, via cross and direct presentation, respectively [23, 38]. Our observation that cross-presentation is not enhanced in raptor-deficient splenic cDC1s, might indicate that instead presentation of cytosolic listeria-derived antigens is enhanced. mTORC1 inhibition is well known to promote autophagy, a process that has been shown to be activated as a host protective mechanism to promote breakdown of intracellular bacteria [10], including listeria [39], and to facilitate generation of peptides for presentation on MHCI [40]. Further studies are required to determine whether enhanced presentation of listeria-derived antigens, as a consequence of increased autophagy, can compensate for overall lower MHCI expression and explain the uncompromised ability of CD11c$^{\Delta raptor}$ mice to mount antigen-specific CD8+ T cell responses following listeria infection.

Other aspects of DC biology - including longevity, the magnitude and duration of expression of costimulatory markers, cytokine expression and migration - that could potentially explain the differences in CD8+ T cell phenotype between CD11c^{WT} and CD11c$^{\Delta raptor}$ mice, were not substantially different between TLR-stimulated DCs from CD11c^{WT} and CD11c$^{\Delta raptor}$ mice both *in vivo* and *ex vivo*. This is at odds with *in vitro* studies showing that TLR-activated GMDCs display increased mitochondrial respiration, survival and duration of costimulatory molecule expression after treatment with rapamycin, which translated into an enhanced CD8+ T cell priming capacity following adoptive transfer *in vivo* [8-10]. This may in part be explained by different biological consequences of long-term deletion versus acute pharmacological inhibition. In addition, one well known difference between TLR-activated GMDCs and cDCs is that GMDCs, but not cDCs, express inducible nitric oxide (NO) synthase (iNOS) and produces NO in an mTOR-dependent manner, while the latter does not [14]. NO has been shown to poison mitochondrial respiration of GMDCs in an autocrine manner [12] and in line with this, beneficial effects of mTOR inhibition on GMDC immunogenicity were reported as secondary to reduced iNOS expression and NO production [13, 19]. This likely explains why loss of mTORC1 signalling in cDCs had less effect on these parameters. Consistent with a lack of clear immunological differences between splenic cDC1s from CD11c^{WT} and CD11c$^{\Delta raptor}$ mice, we found that raptor competent and raptor-deficient PolyIC-activated splenic cDC1s were equally capable of inducing antigen-specific CD8+ T cell responses after adoptive transfer *in vivo*.

In search for an alternative explanation for the potentiated antigen-specific CD8+ T cell response following s.c. immunization in CD11c$^{\Delta raptor}$ mice, we found that loss of raptor in CD11c-expressing cells selectively augmented the activation of LCs reflected by increased expression of CD80, CD70 and IL-12 following immunization with either PolyIC or CpG. In addition, we observed that LC frequencies, but not total numbers, were significantly reduced in sdLNs. Our findings are largely consistent with earlier studies showing that LCs are critically dependent on raptor for their homeostasis in skin epidermis and dermis, but their frequencies are less negatively affected by raptor deficiency in draining lymph nodes [16]. In addition, LC-specific deletion of p14, a protein required for mTORC1 activation, resulted in stronger activation as determined by CD86 and MHCII expression [41]. However, the consequences of these phenotypes for *in vivo* T cell priming were not evaluated in these studies. Another interesting observation was that TLR stimulation recovered the defect in MHCI expression by LCs from CD11c$^{\Delta raptor}$ mice, which was still reduced on cDCs from those same LNs. Likewise, in contrast to migratory cDCs lacking raptor, the cross-presentation ability of LCs was not compromised. This was associated with increased expression of LC3, marking enhanced autophagic activity in raptor-deficient LCs. Since autophagy can promote cross-presentation, it is tempting to speculate that the increased activation of autophagy due to loss of mTORC1 signalling may help to restore MHCI surface expression on LCs by facilitating cross-presentation. This uncompromised MHCI expression by raptor-deficient LCs, together with increased expression of IL-12 and costimulation, in particular provided by CD70 - signals which are known to underpin CTL priming and IFNγ-production [25, 42] - strongly point towards a central role for LCs in driving the potentiated antigen-specific CD8+ T cell response following s.c. immunization in CD11c$^{\Delta raptor}$ mice. Murine LCs are generally considered to have inferior cross-presenting potential compared to murine cDC1s and human LCs [31] and this is reflected in their transcriptome [43]. Moreover, they have also been shown dispensable for the generation of CD8+ CTLs in response to infections [31], such as herpes simplex virus [44], *Candida albicans* [45] and pox vaccinia virus [46]. Nonetheless, this does not exclude the possibility that the augmented activation profile of LCs from CD11c$^{\Delta raptor}$ mice can directly contribute to the observed enhanced CD8+ T cell priming *in vivo*. This would be supported by our observations that IL-12 production by LCs was increased after *ex vivo* stimulation with ligands for TLR3 and TLR9 but not TLR4, which was mirrored by higher frequencies of antigen-specific CD8+ T cell responses following immunization with ligands for TLR3 and TLR9 as adjuvant but not TLR4. Together, our data support the idea that LCs play a key role in the potentiated antigen-specific CD8+ T cell response in CD11c$^{\Delta raptor}$ mice following s.c. immunization. An intriguing question that remains to be answered is why loss of raptor has such strikingly divergent effects on LC and cDC biology. Possibly the potentiating effects of loss of raptor selectively on LC activation, but not cDCs, could be explained by studies showing that beta-catenin, which is constitutively active and required for LC differentiation but dispensable for dermal DC differentiation [47], has anti-inflammatory effects on DCs through activation of mTORC1 [26]. This would render LCs particularly sensitive to effects of mTORC1 inhibition. Further studies are warranted to better understand the differential effects mTORC1 signalling on DCs versus LCs.

Our observations highlight that pharmacological inhibition of mTORC1 may be a viable means to boost cellular immunity following vaccination. Interestingly, since LCs have also been reported to promote CD4+ T follicular helper cell differentiation, germinal center formation and humoral responses in a variety of settings [48-52], not only cellular, but also humoral immune responses may benefit from local mTORC1 inhibition in response to vaccination and clearly warrants further study. In summary, we provide evidence for distinct effects of mTORC1 signalling in different APC subsets plays on their ability to prime cytotoxic T cell responses, with selectively an inhibitory role for mTORC1 in this process in LCs, which may have implications for vaccination practices.

References

1. Kapsenberg, M.L., *Dendritic-cell control of pathogen-driven T-cell polarization*. Nat Rev Immunol, 2003. **3**(12): p. 984-93.
2. Eisenbarth, S.C., *Dendritic cell subsets in T cell programming: location dictates function*. Nat Rev Immunol, 2019. **19**(2): p. 89-103.
3. Patente, T.A., L.R. Pelgrom, and B. Everts, *Dendritic cells are what they eat: how their metabolism shapes T helper cell polarization*. Curr Opin Immunol, 2019. **58**: p. 16-23.
4. Saxton, R.A. and D.M. Sabatini, *mTOR Signaling in Growth, Metabolism, and Disease*. Cell, 2017. **168**(6): p. 960-976.
5. Jones, R.G. and E.J. Pearce, *MenTORing Immunity: mTOR Signaling in the Development and Function of Tissue-Resident Immune Cells*. Immunity, 2017. **46**(5): p. 730-742.
6. Snyder, J.P. and E. Amiel, *Regulation of Dendritic Cell Immune Function and Metabolism by Cellular Nutrient Sensor Mammalian Target of Rapamycin (mTOR)*. Front Immunol, 2018. **9**: p. 3145.
7. Weichhart, T., M. Hengstschlager, and M. Linke, *Regulation of innate immune cell function by mTOR*. Nat Rev Immunol, 2015. **15**(10): p. 599-614.
8. Amiel, E., et al., *Inhibition of mechanistic target of rapamycin promotes dendritic cell activation and enhances therapeutic autologous vaccination in mice*. J Immunol, 2012. **189**(5): p. 2151-8.
9. Jagannath, C. and P. Bakhru, *Rapamycin-induced enhancement of vaccine efficacy in mice*. Methods Mol Biol, 2012. **821**: p. 295-303.
10. Jagannath, C., et al., *Autophagy enhances the efficacy of BCG vaccine by increasing peptide presentation in mouse dendritic cells*. Nat Med, 2009. **15**(3): p. 267-76.
11. Amiel, E., et al., *Mechanistic target of rapamycin inhibition extends cellular lifespan in dendritic cells by preserving mitochondrial function*. J Immunol, 2014. **193**(6): p. 2821-30.
12. Everts, B., et al., *Commitment to glycolysis sustains survival of NO-producing inflammatory dendritic cells*. Blood, 2012. **120**(7): p. 1422-31.
13. Lawless, S.J., et al., *Glucose represses dendritic cell-induced T cell responses*. Nat Commun, 2017. **8**: p. 15620.
14. Thwe, P.M. and E. Amiel, *The role of nitric oxide in metabolic regulation of Dendritic cell immune function*. Cancer Lett, 2018. **412**: p. 236-242.
15. Sinclair, C., et al., *mTOR regulates metabolic adaptation of APCs in the lung and controls the outcome of allergic inflammation*. Science, 2017.
16. Kellersch, B. and T. Brocker, *Langerhans cell homeostasis in mice is dependent on mTORC1 but not mTORC2 function*. Blood, 2013. **121**(2): p. 298-307.
17. Ohtani, M., et al., *Cutting edge: mTORC1 in intestinal CD11c+ CD11b+ dendritic cells regulates intestinal homeostasis by promoting IL-10 production*. J Immunol, 2012. **188**(10): p. 4736-40.
18. Du, X., et al., *Hippo/Mst signalling couples metabolic state and immune function of CD8alpha(+) dendritic cells*. Nature, 2018.

19. Everts, B., et al., *TLR-driven early glycolytic reprogramming via the kinases TBK1-IKKvarepsilon supports the anabolic demands of dendritic cell activation.* Nat Immunol, 2014. **15**(4): p. 323-32.
20. Guak, H., et al., *Glycolytic metabolism is essential for CCR7 oligomerization and dendritic cell migration.* Nat Commun, 2018. **9**(1): p. 2463.
21. Thwe, P.M., et al., *Cell-Intrinsic Glycogen Metabolism Supports Early Glycolytic Reprogramming Required for Dendritic Cell Immune Responses.* Cell Metab, 2017. **26**(3): p. 558-567.e5.
22. Chávez-Arroyo, A. and D.A. Portnoy, *Why is Listeria monocytogenes such a potent inducer of CD8+ T-cells?* Cell Microbiol, 2020. **22**(4): p. e13175.
23. Reinicke, A.T., et al., *Dendritic cell cross-priming is essential for immune responses to Listeria monocytogenes.* PLoS One, 2009. **4**(10): p. e7210.
24. Mintern, J.D., et al., *Differential use of autophagy by primary dendritic cells specialized in cross-presentation.* Autophagy, 2015. **11**(6): p. 906-17.
25. Mashayekhi, M., et al., *CD8α(+) dendritic cells are the critical source of interleukin-12 that controls acute infection by Toxoplasma gondii tachyzoites.* Immunity, 2011. **35**(2): p. 249-59.
26. Fu, C., et al., *beta-Catenin in dendritic cells exerts opposite functions in cross-priming and maintenance of CD8+ T cells through regulation of IL-10.* Proc Natl Acad Sci U S A, 2015. **112**(9): p. 2823-8.
27. van Panhuys, N., F. Klauschen, and R.N. Germain, *T-cell-receptor-dependent signal intensity dominantly controls CD4(+) T cell polarization In Vivo.* Immunity, 2014. **41**(1): p. 63-74.
28. Hussaarts, L., et al., *Rapamycin and omega-1: mTOR-dependent and -independent Th2 skewing by human dendritic cells.* Immunol Cell Biol, 2013. **91**(7): p. 486-9.
29. Pearce, E.J. and A.S. MacDonald, *The immunobiology of schistosomiasis.* Nat Rev Immunol, 2002. **2**(7): p. 499-511.
30. Maynard, S.K., et al., *Vaccination with synthetic long peptide formulated with CpG in an oil-in-water emulsion induces robust E7-specific CD8 T cell responses and TC-1 tumor eradication.* BMC Cancer, 2019. **19**(1): p. 540.
31. Kaplan, D.H., *Ontogeny and function of murine epidermal Langerhans cells.* Nat Immunol, 2017. **18**(10): p. 1068-1075.
32. Sukhbaatar, N., M. Hengstschlager, and T. Weichhart, *mTOR-Mediated Regulation of Dendritic Cell Differentiation and Function.* Trends Immunol, 2016. **37**(11): p. 778-789.
33. Williams, A., C.A. Peh, and T. Elliott, *The cell biology of MHC class I antigen presentation.* Tissue Antigens, 2002. **59**(1): p. 3-17.
34. Reits, E.A., et al., *Radiation modulates the peptide repertoire, enhances MHC class I expression, and induces successful antitumor immunotherapy.* J Exp Med, 2006. **203**(5): p. 1259-71.
35. Zhang, Y., et al., *Coordinated regulation of protein synthesis and degradation by mTORC1.* Nature, 2014. **513**(7518): p. 440-3.
36. Loi, M., et al., *Macroautophagy Proteins Control MHC Class I Levels on Dendritic Cells and Shape Anti-viral CD8(+) T Cell Responses.* Cell Rep, 2016. **15**(5): p. 1076-1087.

37. Edelson, B.T., et al., *CD8α(+) dendritic cells are an obligate cellular entry point for productive infection by Listeria monocytogenes.* Immunity, 2011. **35**(2): p. 236-48.
38. Villanueva, M.S., A.J. Sijts, and E.G. Pamer, *Listeriolysin is processed efficiently into an MHC class I-associated epitope in Listeria monocytogenes-infected cells.* J Immunol, 1995. **155**(11): p. 5227-33.
39. Riebisch, A.K., et al., *Autophagy-A Story of Bacteria Interfering with the Host Cell Degradation Machinery.* Pathogens, 2021. **10**(2).
40. Fiegl, D., et al., *Amphisomal route of MHC class I cross-presentation in bacteria-infected dendritic cells.* J Immunol, 2013. **190**(6): p. 2791-806.
41. Sparber, F., et al., *The late endosomal adaptor molecule p14 (LAMTOR2) represents a novel regulator of Langerhans cell homeostasis.* Blood, 2014. **123**(2): p. 217-27.
42. Rowley, T.F. and A. Al-Shamkhani, *Stimulation by soluble CD70 promotes strong primary and secondary CD8+ cytotoxic T cell responses in vivo.* J Immunol, 2004. **172**(10): p. 6039-46.
43. Artyomov, M.N., et al., *Modular expression analysis reveals functional conservation between human Langerhans cells and mouse cross-priming dendritic cells.* J Exp Med, 2015. **212**(5): p. 743-57.
44. Allan, R.S., et al., *Epidermal viral immunity induced by CD8alpha+ dendritic cells but not by Langerhans cells.* Science, 2003. **301**(5641): p. 1925-8.
45. Igyártó, B.Z., et al., *Skin-resident murine dendritic cell subsets promote distinct and opposing antigen-specific T helper cell responses.* Immunity, 2011. **35**(2): p. 260-72.
46. Seneschal, J., X. Jiang, and T.S. Kupper, *Langerin+ dermal DC, but not Langerhans cells, are required for effective CD8-mediated immune responses after skin scarification with vaccinia virus.* J Invest Dermatol, 2014. **134**(3): p. 686-694.
47. Yasmin, N., et al., *β-Catenin promotes the differentiation of epidermal Langerhans dendritic cells.* J Invest Dermatol, 2013. **133**(5): p. 1250-9.
48. Bouteau, A., et al., *DC Subsets Regulate Humoral Immune Responses by Supporting the Differentiation of Distinct Tfh Cells.* Front Immunol, 2019. **10**: p. 1134.
49. Levin, C., et al., *Critical Role for Skin-Derived Migratory DCs and Langerhans Cells in T(FH) and GC Responses after Intradermal Immunization.* J Invest Dermatol, 2017. **137**(9): p. 1905-1913.
50. Marschall, P., et al., *Dual function of Langerhans cells in skin TSLP-promoted T(FH) differentiation in mouse atopic dermatitis.* J Allergy Clin Immunol, 2020.
51. Yao, C., et al., *Skin dendritic cells induce follicular helper T cells and protective humoral immune responses.* J Allergy Clin Immunol, 2015. **136**(5): p. 1387-97.e1-7.
52. Zimara, N., et al., *Langerhans cells promote early germinal center formation in response to Leishmania-derived cutaneous antigens.* Eur J Immunol, 2014. **44**(10): p. 2955-67.
53. Poussin, M.A. and H. Goldfine, *Evidence for the involvement of ActA in maturation of the Listeria monocytogenes phagosome.* Cell Res, 2010. **20**(1): p. 109-12.
54. Pelgrom, L.R., et al., *LKB1 expressed in dendritic cells governs the development and expansion of thymus-derived regulatory T cells.* Cell Res, 2019. **29**(5): p. 406-419.
55. Everts, B., et al., *Omega-1, a glycoprotein secreted by Schistosoma mansoni eggs, drives Th2 responses.* J Exp Med, 2009. **206**(8): p. 1673-80.

Materials and methods

Mice

Itgax-cre Rptor-fl/fl (CD11c-cre raptor-fl/fl or CD11c$^{\Delta raptor}$ mice), transgenic with OVA specific CD4 T cells (OT-II), transgenic with OVA specific CD8+ T cells (OT-I) and wild type (WT) mice, both male and female and all on a C57BL/6J background, were bred under SPF conditions at the Leiden University Medical Center (LUMC), Leiden, The Netherlands. Mice were culled through cervical dislocation. Anaesthesia with isoflurane was used for *L. monocytogenes* infection and ketamine with either dexdomitor or xylazine was used for *S. mansoni* infection. Animal experiments were performed when the mice were between 8-16 weeks old. Animal experiments were performed in accordance with local government regulations, EU Directive 2010/63EU and Recommendation 2007/526/EC regarding the protection of animals used for experimental and other scientific purposes, as well as approved by the Dutch Central Authority for Scientific Procedures on Animals (CCD). Animal license number AVD116002015253.

Digestion of murine tissues

Lymphoid organs were collected in 500 µL of no additives media (naRPMI = RPMI-1640 supplemented with GlutaMAX™ [#61870-010 or alternatively 61870036, Gibco, Bleiswijk, The Netherlands], which should contain Ca^{2+} for the collagenase) in a plate and mechanically disrupted using the back-end of a syringe before addition of 50 µL of a digestion media (dRPMI = naRPMI supplemented with 11x collagenase D (#11088866001, Roche, Woerden, The Netherlands; end concentration of 1 mg/mL) and 11x DNase I (#D4263, Sigma, Zwijndrecht, The Netherlands; end concentration of 2000 U/mL) for 20 minutes at 37°C and 5% CO_2. Single cell suspensions were filtered after digestion with a 100 µm sterile filter (#352360, BD Biosciences, Vianen, The Netherlands) before counting in complete RMPI (cRPMI = naRPMI supplemented with 10% heat-inactivated FCS [#S-FBS-EU-015, Serana, Pessin, Germany], 50 µM β-mercaptoethanol [#M6250, Sigma], 100 U/mL penicillin [#16128286, Eurecopharma, Ridderkerk, The Netherlands; purchased inside the LUMC] and 100 µg/mL streptomycin [#S9137, Sigma]). Spleens were subjected to red blood cell lysis (inhouse; 0.15 M NH4Cl, 1 mM KHCO3, 0.1 mM EDTA [#15575-038, Thermo, Waltham, Massachusetts, United States] in ddH_20) for 2 minutes at room temperature before counting.

Generation of bone marrow-derived GMDCs

BM cells were flushed from mouse femurs and tibia and plated in 'Nunc™ Cell-Culture Treated 6-well plate' wells (#140675, Thermo; approximate growth area of 9.5 cm^2) at a seeding density of 2x10^6 cells in a volume of 3 mL of complete RPMI for BM cells (cRPMI-BM = RPMI-1640 supplemented with GlutaMAX™ and also 5% FCS, 50 μM β-mercaptoethanol, 100 U/mL penicillin and 100 μg/mL streptomycin was put in) to which 20 ng/mL of recombinant GM-CSF (#315-03, PeproTech, Hamburg, Germany) was added. Media was refreshed on day 3-4 by adding 3 mL cRPMI-BM with 40 ng/mL GM-CSF and on day 7 by first removing 3 mL of supernatant and then adding 3 mL cRPMI-BM with 40 ng/mL GM-CSF. Semi-adherent cells were harvested for various assays on day 8. Alternatively, semi-adherent cells were collected on day 7 and seeded in a flat bottom 96-well plate (Nunc™; #167008, Thermo) at 1x10^5 cells in a volume of 200 μL of fresh cRPMI-BM with 20 ng/mL GM-CSF and rested overnight. Minimum rest time after transfer of GMDCs was 2-3 hours.

Flow cytometry

In general, single cell suspensions underwent viability staining for 20 minutes at room temperature using the LIVE/DEAD™ Fixable Aqua Dead Cell Stain Kit (#L34957, Thermo; 1:400 in PBS [from LUMC pharmacy; Braun, Zeist, The Netherlands) and fixation for 15 minutes at room temperature using 1.85% formaldehyde (F1635, Sigma) in PBS solution before surface staining with antibodies in an in-house cell separation buffer (= PBS supplemented with 0.5% BSA [fraction V, #10735086001, Roche, Woerden, The Netherlands] and 2 mM EDTA) for 30 minutes at 4 degrees Celsius. For detection of phosphorylated S6 on Ser235/236, single cell suspensions in cRPMI were returned to a cell incubator (37°C & 5% CO_2) for 1 hour after which 16% ultra-pure formaldehyde (#18814-20, Polysciences, Hirschberg an der Bergstraße, Germany) was added until the concentration reached 4% and the cells were left for 10 more minutes in the incubator to fix. For example, 67 μL of 16% ultra-pure formaldehyde was added to 200 μL of cell solution. Viability staining was not done before fixation to minimise changes in phosphorylation status. Single cell suspensions were first stained with anti-phosphorylated S6 in 1x Permeabilization Buffer (#00-8333-56, Thermo) for 1 hour at room before staining with other antibodies in the in-house cell separation buffer for 30 minutes at 4°C. For detection of mitochondrial mass and mitochondrial membrane potential, single cell suspensions were incubated with respectively 200 nM MitoTracker Green (#M7514, Invitrogen) or 200 nM TMRM (#T668, Thermo) in cRPMI for 30 minutes in a cell incubator. Subsequent viability and surface staining were done for 30 minutes on ice. No fixation occurred before running the samples. Uptake of 2-NBDG (N13195, Invitrogen) was done in a similar fashion but with 15 minutes of incubation. CD8+ T cells bearing antigen-specific T cell receptors were quantified using in-house produced tetramers of MHCI:peptide complexes with SIINFEKL (K^bOVA-tetramer) or RAHYNIVTF (D^bE7-tetramer) as their respective epitopes. For detection of antigen-specific cytokine production by T cells, single cell suspensions in cRPMI were restimulated with either 1 µg/mL of SIINFEKL (in-house) or 1 µg/mL of RAHYNIVTF (in-house) in the presence of 10 µg/mL of Brefeldin A (#B7651, Sigma) for 4 hours in a cell incubator. For polyclonal restimulation, single cell suspensions were stimulated with both 0.1 µg/mL of PMA (#P-8139, Sigma) and 1 µg/mL of ionomycin (#I-0634, Sigma) in the presence of Brefeldin A. These single cell suspensions underwent intracellular cytokine staining (ICS) with antibodies in the 1x Permeabilization Buffer. For detection of IL-12 by DCs, single cell suspensions were stimulated with either 100 ng/mL of LPS, 10 µg/mL of PolyIC or 5 µg/mL of CpG-B (#TLRL-PELPS, #tlrl-1826-1 and #TLRL-PIC, respectively and all InvivoGen, Toulouse, France) and all in the presence of Brefeldin A for 5 hours in a cell incubator. Cross presentation was quantified by surface staining with an anti-Kb-SIINFEKL antibody after 3 hours of stimulation with OVA SLP (in house; 50 µg/mL for skin draining lymph node cells) in the presence of 10 µg/mL PolyIC. SIINFEKL (1 µg/mL) was used as positive MHCI loading control. All samples were run on a BD LSR II or FACSCanto II and analysed using FACS Diva 8 (all BD Biosciences) and FlowJo (Version 10, TreeStar, Meerhout, Belgium).

Antibodies

The antibodies used in this study can be found in supplementary table 1.

Western blotting

A million GMDCs were washed twice with PBS before being lysed in 150 µL of EBSB buffer (8% [w/v] glycerol, 3% [w/v] SDS and 100 mM Tris–HCl [pH 6.8]). Lysates were immediately boiled for 5 min and their protein content was determined using a BCA kit. Ten µg of protein per lain was separated by SDS-PAGE followed by transfer to a PVDF membrane. Membranes were blocked for 1 h at room temperature in TTBS buffer (20 mM Tris–HCl [pH 7.6], 137 mM NaCl, and 0.25% [v/v] Tween 20) containing 5% (w/v) fat free milk and incubated overnight with primary antibodies. The primary antibodies used were raptor (A300-506A clone; 1:1000; Bethyl Laboratories, Montgomery, Texas, United States) and beta-actin (AC-15 clone; 1:2000; Sigma). The membranes were then washed in TTBS buffer and incubated with horseradish peroxidase-conjugated secondary antibodies for 2 h at room temperature. After washing, blots were developed using an in-house enhanced chemiluminescence solution (10 mL of substrate [16.67 mL 3M Tris-HCl <pH 8.8>, 125 mg sodium luminol <#A4685, Sigma>, 155 µL H2O2 <#7047, Baker> and mQ up to 500 mL] with 10 µL of enhancer [11 mg coumaric acid <#C9008> in 10 mL of DMSO]).

Preparation of Listeria monocytogenes bacteria

Listeria monocytogenes bacteria were scraped from a glycerol stock and transferred to a 15 mL round bottom polysterene tube (#352051, Corning, Amsterdam, The Netherlands) with 3 mL of 'Brain Heart Infusion (BHI) Broth' (#37500, BD Biosciences) and incubated overnight at 37 degrees with the cap loose and the tube rotating at 200 rpm. The next day, 20 and 50 µL of bacteria solution was transferred to new tubes with broth and cultured for another 3 hours. The optical density (OD) was measured at 600 nm (OD600) using a spectrophotometer (#Ultrospec 100 pro, GE Healthcare, Hoevelaken, The Netherlands after takeover of Amersham Biosciences by GE Healthcare) and the concentration of bacteria solution was corrected until the OD600 value corresponded approximately to 1.2x10^8 colony forming units (CFU) per mL of broth, which was previously determined by titration. To make new glycerol stocks, 1 mL of the overnight cultured bacterial solution and 500 µL of pure glycerol were mixed well and stored at -80 degrees.

Listeria monocytogenes infection and challenge

Mice were infected with a live attenuated OVA-expressing *L. monocytogenes* strain deficient in actin assembly-inducing protein (Lm-dActA-OVA), which is required for escape from phagosomes and cell-to-cell spreading [53]. Bacteria were centrifuged at 2000 rpm for 10 minutes at 4 degrees and brought to 2.5x107 CFU per mL of PBS. Mice were sedated with isoflurane and infected by retro-orbital intravenous (i.v.) injection with 200 µL of bacteria in PBS (=5x106 CFU). The remaining bacteria were brought to 103 CFU per mL of PBS and 50 µL of this bacteria solution (=50 CFU) was plated on a 'BHI Agar Plate' (#255003, BD Biosciences) and incubated overnight at 37 degrees for control counting of colonies next day. Mice were culled 7 days later, and organs were processed as described above. Alternatively, 21 days after infection, mice were challenged with 5x104 OVA-expressing wild type bacteria (Lm-OVA) in 200 µL of PBS by retro-orbital i.v. injection and at day 24, mice were culled, and organs were processed as described above. Bacterial load in the organs was determined by taking 100 µL of a 5 mL single cell suspension in PBS and lysing this in 900 µL 0.1% Triton-X-100 (T8532, Sigma) in mQ (1:10 single cell suspension:0.1% Triton) and making further dilutions of 1:100 and 1:1000 before plating on a agar plate and overnight incubation at 37 degrees for control counting of colonies the next day.

In vivo cDC expansion, isolation, sorting and transfer

The *in vivo* expansion of cDCs using Flt3L-secreting B16 melanoma cells and their subsequent sorting, *ex vivo* conditioning and transfer into recipient mice to induce DC-specific T cell responses was done as described previously [54]. cDC1s were stimulated with 100 µg/mL of ovalbumin (OVA; #vac-pova-100, InvivoGen) and 10 µg/mL of PolyIC. 300.000 cells were transferred.

Preparation of Schistosoma mansoni soluble egg antigens

S. mansoni eggs were isolated and processed into a SEA preparation as described previously [55]. Protein concentration was determined using a bicinchoninic acid (BCA) protein assay kit (Pierce, #PIER23225). Endotoxin contamination was determined by a direct comparison of SEA batches to LPS in a TLR4-transfected Human Embryonic Kidney 293 (HEK) reporter cell line, in which IL-8 secretion by 5x108 HEK cells after stimulation with 10 µg of SEA is expected to be similar or less than after stimulation with 1-3 ng/mL of LPS.

Schistosoma mansoni acute infection

Mice were infected with *S. mansoni* (Puerto Rican strain; Naval Medical Research Institute) by 30 minutes of percutaneous exposure to 60 cercariae (or up to 100 cercariae) on shaved abdomen. Mice were culled 8 weeks later. Cercariae were kept at 30 cercariae per mL of store bought Barleduc water, which was kept very carefully at 31 degrees Celsius. Female mice were anesthetized by intraperitoneal (i.p) injection with 300 µL of 50 mg/kg bodyweight ketamine + 0.5 mg/kg bodyweight dexdomitor, while male mice were anesthetized with 50 mg/kg bodyweight ketamine + 10 mg/kg bodyweight xylazine. Female mice were assisted in waking up by i.p. injection with 150 µL of 0.4 mg/kg bodyweight antisedan. All injections were done using PBS and a 25G needle. All anaesthetics were bought at the LUMC pharmacy. Livers were processed like spleens except that single cell suspensions were centrifuged twice at 20 g for 10 minutes in PBS to remove hepatocytes before red blood cell lysis.

In vivo T cell priming and DC activation following immunization

For evaluation of T cell priming, mice were injected s.c. either with a) 5 µg of LPS together with 25 µg of OVA and emulsified in 40 µL of incomplete Freunds' adjuvant (IFA; #vac-ifa-10, InvivoGen) in the hind footpad, or b) 10-25 µg of CpG-B with OVA and in IFA in the footpad, or c) 25 µg of PolyIC with 100 µg of E7-SLP in 50 µL of PBS in the tailbase, or d) 25 µg of CpG-B with E7-SLP in PBS in the tailbase. Mice were culled 7 days later and draining popLNs were collected after footpad injection and draining ingLNs were collected after tailbase injection. For evaluation of DC activation, OVA- and E7-SLP were omitted and draining LNs were collected after 24 hours instead of 7 days.

Cytometric bead array

Cell culture supernatants were analysed for IFNγ, IL-4, IL-5, IL-10 and IL-13 secretion using a cytokine bead array (#I558296, #558298, #558302, #558300 and #558349 respectively and all BD Biosciences) on a flow cytometer as recommended by the manufacturer, but with both the beads and antibodies diluted 1:10 relative to the original recommendation.

FITC painting

Mice were painted with 20 µL of inflammatory FITC paint (5 mg/ml fluorescein isothiocyanate [#F3651, Sigma] in a 1:1 mix of dibutylphalate [#524980, Sigma] and acetone [#100014, Merck, Amsterdam, The Netherlands]) on shaved flanks and draining ingLNs were collected either 1 or 3 days later.

Quantification and statistical analysis

Statistical analysis as specified in figure legends were performed with Prism 9 (GraphPad software Inc., San Diego, California, United States). Graphs with 2 bars were analysed with the non-paired Student's t test, while graphs with more than 2 bars were analysed with the two-way unpaired analysis of variance (ANOVA) corrected for multiple comparisons using Sidak's multiple comparison test. Graphs with multiple time points were analysed with a simple linear regression. A p value < 0.05 was considered significant (*/# for p < 0.05, **/## for p < 0.01 and ***/### for p < 0.001).

Acknowledgements

This work was supported by an LUMC fellowship awarded to BE.

Author contributions

LP, TP, FO, LN, AO, AvdH, HvdZ and BE performed experiments. LP and BE analysed experiments. LP, RA and BE designed experiments. BE conceived and supervised the study and wrote the manuscript together with LP.

Conflict of interest

The authors declare that no competing financial interests exist in relation to the work described.

Supplemental figures

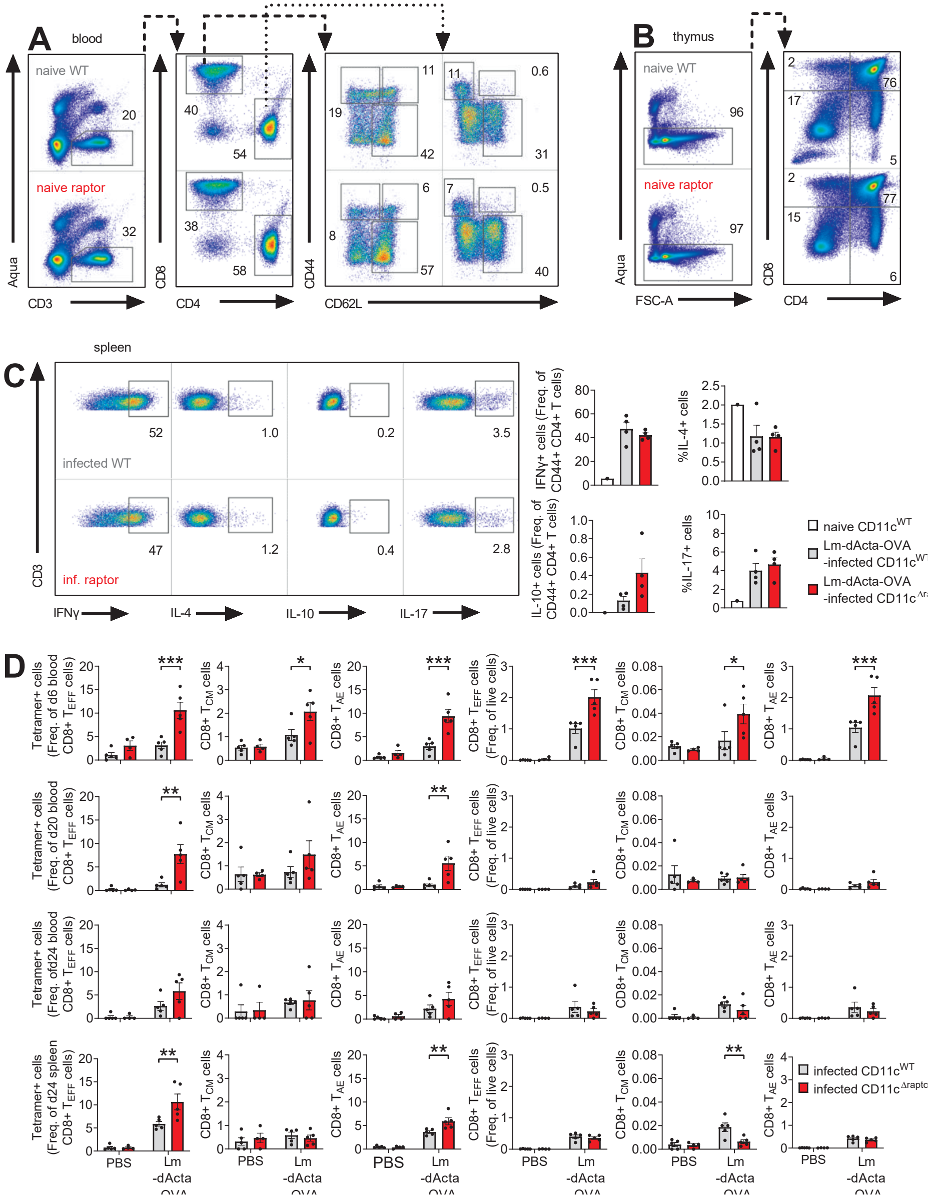

Figure S1.

(A) Gating strategy for T cell subsets in blood by sequential gating of intact cells (forward scatter area [FSC-A] versus side scatter area [SSC-A], not shown), singlets (FSC-A versus forward scatter height [FSC-H], not shown), live cells (Aqua- cells in panel 1), live T cells (CD3+ versus Aqua- cells in panel 1), total CD4 T cells (CD4+ versus CD8+ in panel 2) and total CD8+ T cells (CD4- versus CD8+ in panel 2), naïve CD8+ T cells (CD8+ TN; CD62L+ versus CD44- in panel 3) and effector CD8+ T cells (CD8+ TEFF; CD62L- versus CD44+ in panel 3) and central memory CD8+ T cells (CD8+ TCM; CD62L+ versus CD44+ in panel 3), and naïve CD4 T cells (CD4+ TN; CD62L+ versus CD44- in panel 4) and effector CD4 T cells (CD4+ TEFF; CD62L- versus CD44+ in panel 4) and central memory CD4+ T cells (CD4+ TCM; CD62L+ versus CD44+ in panel 4). Antigen-experienced T cells (TAE) are the sum of TEFF and TCM subsets. (B) Representative histograms of developing T cells in the thymus of naïve CD11c^{WT} and CD11c$^{\Delta raptor}$ mice. (C) Splenocytes were stimulated with PMA/ionomycin the presence of Brefeldin A and analysed for production of indicated cytokines by CD4+ TAE cells using flow cytometry. (D) Mice were infected with 5x10^6 Lm-dActa-OVA by i.v. injection and challenged 21 days later with 5x10^4 Lm-OVA. Blood was drawn on day 6,20 and 24 and mice were culled on day 24 to take spleen. OVA-specific CD8+ T cells based on K^{b}OVA-tetramer staining as analysed by flow cytometry. Frequencies of OVA-specific T cell subsets as gated in S2A are enumerated. Data is from 1 experiment out 3 (which together are the same mice as Figure 2B-D) using 1-4 mice per group (C) or from 1 out of 2 representative experiments (same mice as Figure 2E) using 4-5 mice per group (D) and shown as mean ± SEM; *$p < 0.05$, **$p < 0.05$, ***$p < 0.001$ when comparing samples between CD11c^{WT} and CD11c$^{\Delta raptor}$ mice.

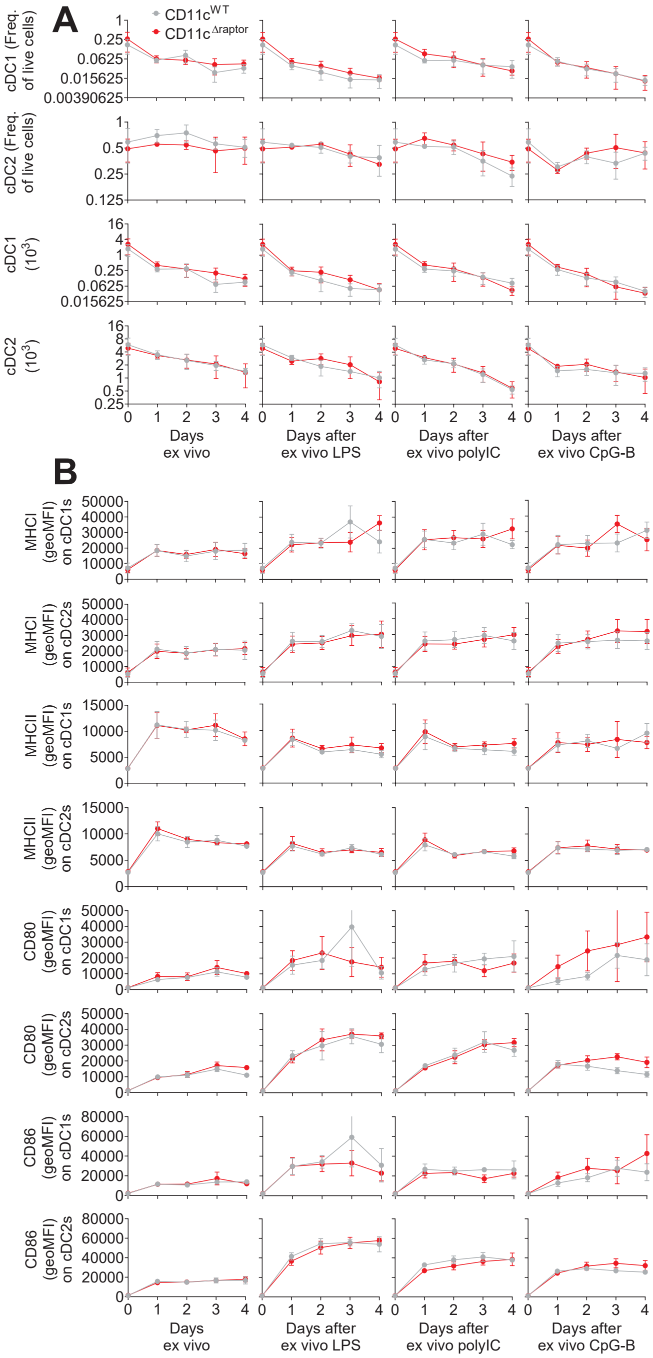
A
CD11c^WT
CD11c^Δraptor
cDC1 (Freq. of live cells)
1
0.25
0.0625
0.015625
0.00390625
cDC2 (Freq. of live cells)
1
0.5
0.25
0.125
cDC1 (10^3)
16
4
1
0.25
0.0625
0.015625
cDC2 (10^3)
16
8
4
2
1
0.5
0.25
0 1 2 3 4
Days ex vivo
Days after ex vivo LPS
Days after ex vivo polyIC
Days after ex vivo CpG-B
B
MHCI (geoMFI) on cDC1s
MHCI (geoMFI) on cDC2s
50000
40000
30000
20000
10000
0
MHCII (geoMFI) on cDC1s
MHCII (geoMFI) on cDC2s
15000
10000
5000
0
CD80 (geoMFI) on cDC1s
CD80 (geoMFI) on cDC2s
50000
40000
30000
20000
10000
0
CD86 (geoMFI) on cDC1s
CD86 (geoMFI) on cDC2s
80000
60000
40000
20000
0
0 1 2 3 4
Days ex vivo
Days after ex vivo LPS
Days after ex vivo polyIC
Days after ex vivo CpG-B

Figure S2.

Splenocytes from naïve CD11c^{WT} and CD11c$^{\Delta raptor}$ mice were stimulated with either 100 ng/mL LPS, 10 µg/mL PolyIC or 5 µg/mL CpG-B and cultured for the indicated time before manual counting and analysis by flow cytometry. (A) Frequencies and numbers of splenic cDCs are enumerated. (B) Splenic cDCs surface protein expression of indicated surface markers. (A-B) Data are from 1 experiment using 4 mice per group (A-B) and shown as mean ± SEM.

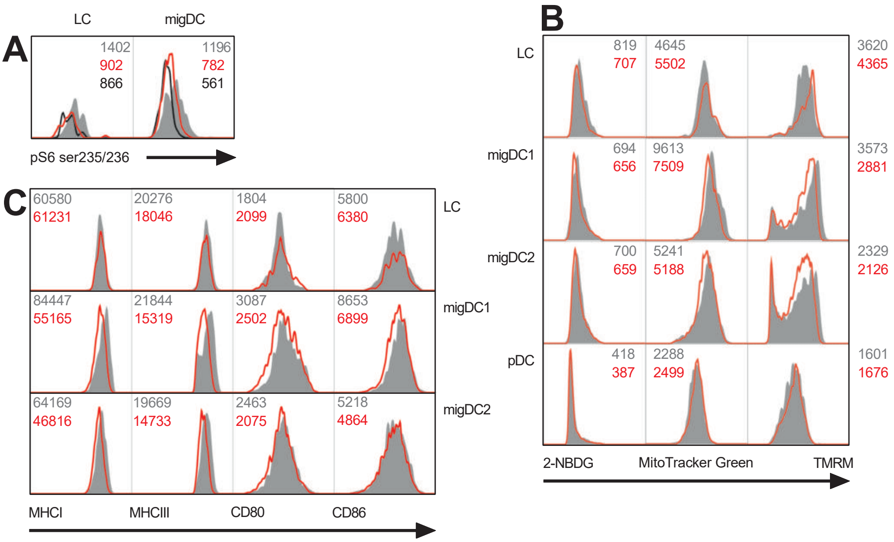

Figure S3.

(A) Representative histograms of S6 phosphorylation in sdLN total migDCs as described in Figure 4B and LCs as described in Figure S6A. (B) Representative histograms of 2-NBDG uptake by sdLN DC subsets and their mitochondrial mass and mitochondrial membrane potential as described in Figure 4D-E, while LCs are described in Figure S6D-E. (C) Representative histograms of indicated surface markers on sdLN migDCs as described in Figure 4F.

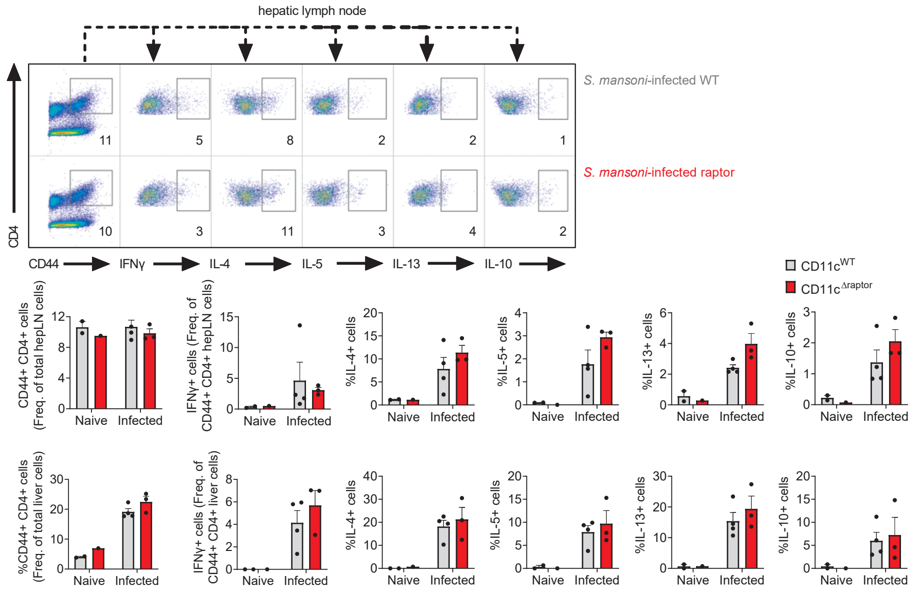

Figure S4.

Mice were infected with *S. mansoni* by percutaneous exposure to cercariae and CD44+CD4+ cell responses were evaluated in livers and draining hepatic lymph nodes eight weeks later. Single cell suspensions were stimulated with PMA/Ionomycin in the presence of Brefeldin A and analysed for production of indicated cytokines. Data are from 1 experiment using 1-4 mice per group and shown as mean ± SEM; *p < 0.05 when comparing samples between CD11c^{WT} and CD11c$^{\Delta raptor}$ mice.

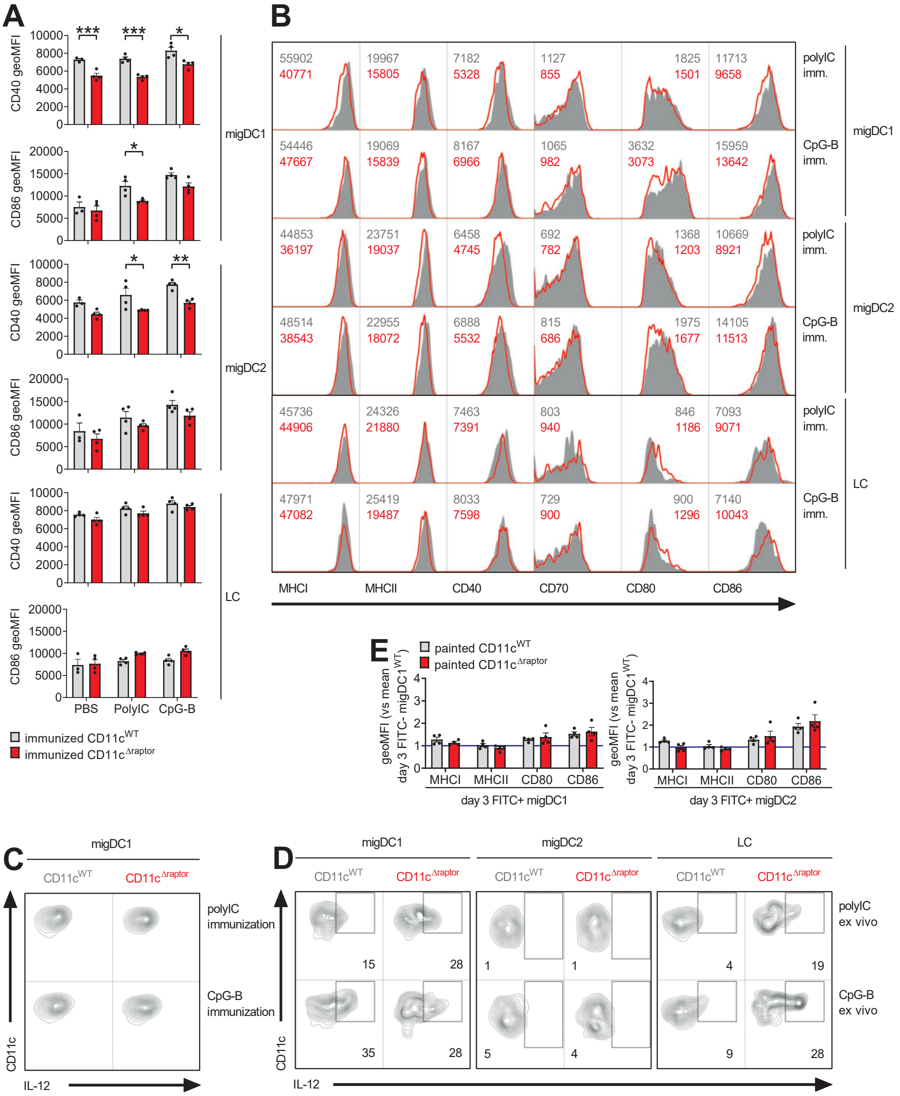
A
CD40 geoMFI
CD86 geoMFI
10000
8000
6000
4000
2000
0
20000
15000
10000
5000
***
*
**
migDC1
migDC2
LC
PBS
PolyIC
CpG-B
immunized CD11c^{WT}
immunized CD11c$^{\Delta raptor}$
B
55902 40771
19967 15805
7182 5328
1127 855
1825 1501
11713 9658
54446 47667
19069 15839
8167 6966
1065 982
3632 3073
15959 13642
44853 36197
23751 19037
6458 4745
692 782
1368 1203
10669 8921
48514 38543
22955 18072
6888 5532
815 686
1975 1677
14105 11513
45736 44906
24326 21880
7463 7391
803 940
846 1186
7093 9071
47971 47082
25419 19487
8033 7598
729 900
900 1296
7140 10043
polyIC imm.
CpG-B imm.
MHCI
MHCII
CD40
CD70
CD80
CD86
E
painted CD11c^{WT}
painted CD11c$^{\Delta raptor}$
geoMFI (vs mean day 3 FITC- migDC1^{WT})
4
3
2
1
0
day 3 FITC+ migDC1
day 3 FITC+ migDC2
C
migDC1
CD11c^{WT}
CD11c$^{\Delta raptor}$
polyIC immunization
CpG-B immunization
CD11c
IL-12
D
migDC1
migDC2
LC
15
28
1
1
4
19
35
28
5
4
9
28
polyIC ex vivo
CpG-B ex vivo

Figure S5.

(A) Same mice as Figure 6A. CD11c^{WT} and CD11c$^{\Delta raptor}$ mice were immunized with either 25 µg of CpG-B or 25 µg of PolyIC by s.c. tailbase injection and migAPC maturation in draining inguinal lymph nodes (ingLNs) was analysed 24 hours later by flow cytometry. (B) Representative histograms of indicated surface markers on sdLN migAPCs as described in Figure 6A,E and S5A. (C) Same mice as Figure 6A. Inguinal LNs were processed and incubated in the presence of Brefeldin A, before analysis of IL-12p40/p70 production by migAPCs, of which only migDC1s is shown, by flow cytometry. (D) Representative histograms of IL-12p40/p70 production by sdLN migAPCs as described in Figure 6B-G. Data is shown as a representative image from one CD11c^{WT} and one CD11c$^{\Delta raptor}$ mouse (same mice as Figure 6A-B, I). (E) Same mice as Figure 6C-D. Mice were painted on their flank with inflammatory FITC paint and FITC+ migDC maturation was analysed on the indicated days by flow cytometry.

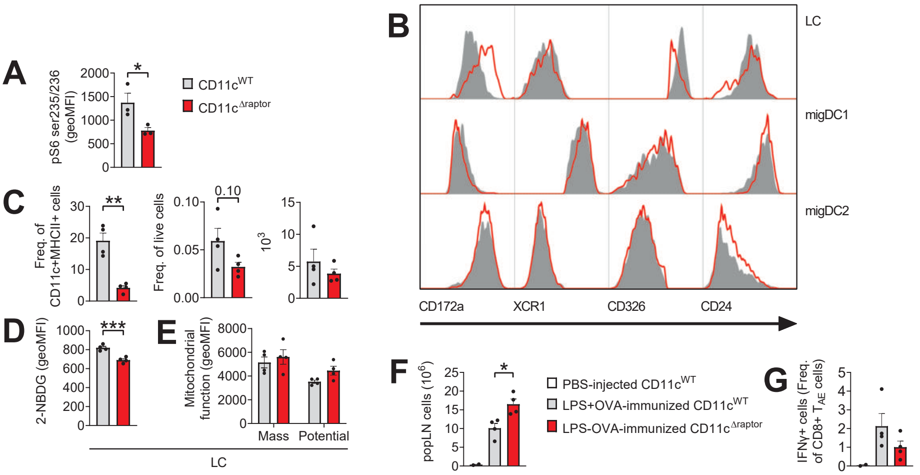

Figure S6.

(A) Flow cytometry-based analysis of S6 phosphorylation on serine 235/236 in LCs from skin draining lymph nodes (sdLNs) out of CD11c^{WT} mice in grey, CD11c$^{\Delta raptor}$ mice in red and a Fluroscence Minus One (FMO control in black). Representative histograms are in Figure S6A. sdLNs were a pool of brachial, axillary and inguinal LNs. (B) Representative histograms of indicated surface markers on sdLN migAPCs as described in Figure 4A with the addition of CD24. (C) Frequencies and numbers of LCs in sdLNs as gated in Figure 4A are enumerated. (D) Flow cytometry-based analysis of glucose uptake by sdLN LCs using the fluorescent glucose analogue 2-NBDG. (E) Flow cytometry-based analysis of mitochondrial mass and mitochondrial membrane potential in sdLN LCs using MitoTracker Green and TMRM, respectively. (F-G) CD11c^{WT} and CD11c$^{\Delta raptor}$ mice were immunized with OVA and 5 µg of LPS by s.c. footpad injection and T cell response in draining popliteal lymph nodes (popLNs) were analysed 7 days later by flow cytometry. (F) Cell counts of popLNs. (G) popLN cells were stimulated with SIINFEKL in the presence of Brefeldin A and analysed for OVA-specific IFNγ production by antigen-experienced CD44+ CD8+ T cells (CD8+ TAE) using flow cytometry. Data are from 1 out of 2 representative experiments (same mice as Figure 4) using 4 mice per group (A, C-E) or from 1 experiment using 2-4 mice per group (F-G) and shown as mean ± SEM; *$p < 0.05$, **$p < 0.01$, ***$p < 0.001$ when comparing samples between CD11c^{WT} and CD11c$^{\Delta raptor}$ mice.

Supplementary tables

Table 1. Antibodies used in study.

Target	Clone	Conjugate	Source	Identifier
CD11b	M1/70	PE-Cy7	Invitrogen/eBioscience	25-0112-82
CD11c	N418	BV421	BioLegend	117330
CD11c	N418	PE-Cy7	Invitrogen/eBioscience	25-0114-82
CD172a	P84	Biotin	BioLegend	144026
CD172a	P84	PE	BioLegend	144011
CD24	M1/69	APC-eF780	BioLegend	101839
CD3	17A2	FITC	Invitrogen/eBioscience	11-0032-82
CD3	17A2	eF450	Invitrogen/eBioscience	48-0032-82
CD3	17A2	BV605	BioLegend	100237
CD326	G8.8	BV605	BioLegend	118227
CD326	G8.8	APC-Fire	BioLegend	118229
CD4	GK1.5	PE-Cy7	Invitrogen/eBioscience	25-0041-81
CD4	GK1.5	PerCP-eF710	Invitrogen/eBioscience	46-0041-82
CD4	GK1.5	BV650	BD Biosciences	563232
CD40	HM40-3	FITC	Invitrogen/eBioscience	11-0402-82
CD44	IM7	eF450	Invitrogen/eBioscience	48-0441-82
CD44	IM7	PE-Cy7	Invitrogen/eBioscience	25-0441-81
CD62L	MEL-14	APC-eF780	Invitrogen/eBioscience	47-0621-82
CD70	FR70	biotin	BioLegend	104603
CD8a	53-6.7	BV711	BioLegend	100747
CD80	16-10A1	PE	Invitrogen/eBioscience	553769
CD86	GL-1	PerCp-Cy5.5	BioLegend	105028
CD8a	53-6.7	APC	Tonbo Biosciences	20-0081-U025
CD8a	53-6.7	APC-Cy7	BioLegend	100714
Goat anti-rabbit	-	AF647	Invitrogen	A27040
HPV tetramer	-	APC	in house	-
LC3A/B	-	Rabbit	Cell Signaling	4108
IFNγ	XMG1.2	PE-Cy7	Invitrogen/eBioscience	25-7311-82
IFNγ	XMG1.2	APC-Cy7	BD Biosciences	561479
IL-10	JES5-16E3	AF488	Invitrogen/eBioscience	53-7101-82

Table 1. Continued

Target	Clone	Conjugate	Source	Identifier
IL-12p40/ p70	C15.6	APC	Invitrogen/eBioscience	554480
IL-17A	eBio17B7	APC	Invitrogen/eBioscience	17-7177-81
IL-4	BVD4-1D11	PE	Invitrogen/eBioscience	554389
Kb-SIINFEKL	25-D1-16	PE	BioLegend	141604
MHCI	AF6-88.5	AF647	BioLegend	116511
MHCII	M5/114.15.2	AF700	Invitrogen/eBioscience	56-5321-80
MHCII	M5/114.15.2	APC-eF780	Invitrogen/eBioscience	47-5321-82
OVA tetramer	-	PE	in house	-
pS6 (ser240)	N4-41	PE	Invitrogen/eBioscience	560430
Siglec-H	511	APC	BioLegend	129611
Streptavidin	-	PerCP-Cy5.5	BioLegend	405214
Streptavidin	-	BV605	BioLegend	405229
Streptavidin	-	BV785	BioLegend	405249
XCR1	ZET	BV650	BioLegend	148220
XCR1	ZET	BV421	BioLegend	148216

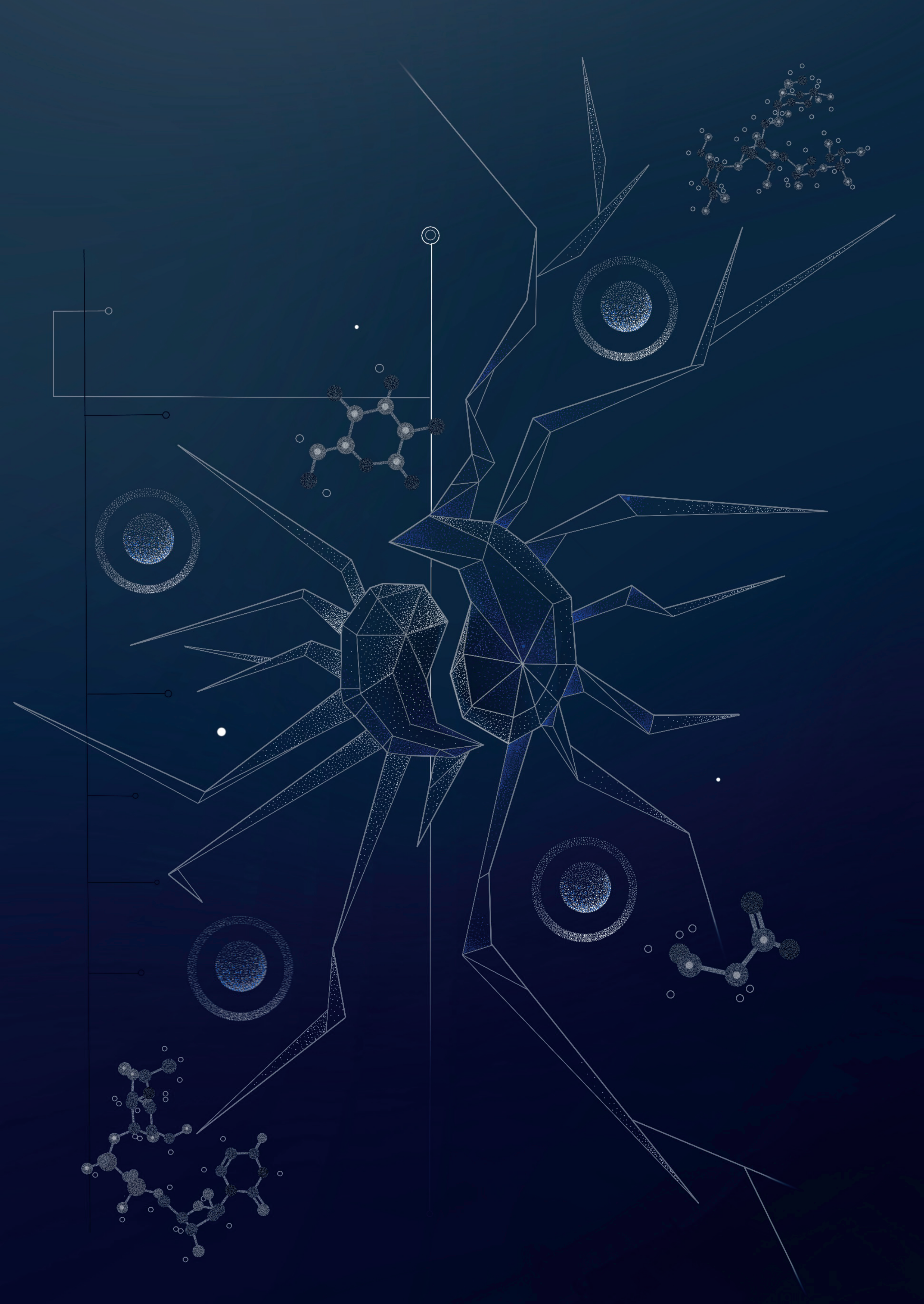

10

General discussion

Introduction

The establishment of a successful immune response depends on the timely coordination of multiple innate and adaptive immune cells; with divergent infectious agents in different locations leading to distinct combinations of immune cells [1-5]. Dendritic cells (DCs) are the quintessential antigen presenting cell type that integrates and relays danger signals from the peripheral tissues to activate and inform naïve T cells in secondary lymphoid tissues (reviewed in [6]). DCs (reviewed in **Chapter 2**) and other immune cells (reviewed in **Chapter 6**) update their metabolism to match the functional output that is required by a specific situation (reviewed in [7]) and understanding these changes to reveal new therapeutic opportunities can be considered the goal of 'immunometabolism'.

Cell culture systems have been indispensable for the development of key concepts in the field of immunometabolism. However, even if we would put the appropriately interacting immune cells in a dish, at exactly the right ratio of cells, with a carefully chosen media, this would still not recapitulate the metabolic gradients and zones that we can expect in tissues and organs (discussed in [8]). The liver is probably the best studied example of metabolic zonation [9, 10], but also secondary lymphoid organs - although more irregular in organization - have been described to show zones of respective pH [11] and oxygen [12, 13] and gradients of respective antigens [14] and cytokines [15]. All which can modify the metabolism of an immune cell (reviewed in [16]). In line with this, immune cells adapt their metabolism to the tissue they take residence in (reviewed in [17]) and can display further metabolic heterogeneity depending on their microanatomical position within the tissue. This has been shown most clearly in the context of tumours [18, 19]. A final layer of complexity is provided by the ability of immune cells to compete for nutrients (reviewed in [20]). The capacity of activated CD8 T cells to deprive adjacent DCs of glucose during their interaction [21] is an example of this that is most relevant to the establishment of successful DC mediated anti-viral and anti-tumour CD8 T cell responses (reviewed in [22]). This last point raises the question: if immune cell function is integrally linked to immune cell metabolism, but the nutrients that fuel these pathways are limited in the microenvironment, how do interacting immune cells coordinate their competing metabolisms in space and over time?

I will here discuss the findings presented in this thesis, what we have learned from it and where I envision the field of DC metabolism is heading. To do so, I will provide an in-depth summary of recent models of immune cell coordination during the generation of adaptive T cell responses. Particularly those that are driven by conventional DCs (cDCs) in secondary lymphoid organs. I will then give an update on the often-overlooked metabolism of plasmacytoid DCs (pDCs) and then try to combine these findings and a decade of other immunometabolic knowledge with the previously discussed models of immune cell coordination. Moreover, I will look at what is known about the understudied metabolome of lymph fluid that bathes immune cells in the lymph node. Finally, I will present my view on which tools are needed to better understand the topics considered here and can potentially further mature the field DC metabolism.

CD4 T cell help and innate immune cell assistance during DC mediated T cell priming

CD4 T cell help to CD8 T cells is critical for the generation of maximal CD8 T cell responses in many settings of DC driven immune responses (reviewed in [23]). This by itself implies that a co-culture of antigen loaded DCs and CD8 T cells is limited in its explanatory value. Another layer of complexity arises from the fact that DCs need to move across multiple different environments before they find their antigen specific naïve T cell partner. They can therefore potentially interact with numerous cells along the way. Prime examples for this have recently come from studies that investigated the role of type I cDCs (cDC1s) in the establishment of anti-viral CD8 T cell responses [1-3, 5]. All these interactions might modulate the metabolism of a DC, which traditionally has been investigated using homogenous cell preparations in extracellular flux (XF) analysers (described in **Chapter 3**). However, before we can discuss what to expect in terms of DC metabolism in vivo, we first must introduce which immune cells are likely to interact with antigen loaded DCs and at what step of the immune response.

Professional antigen presenting DCs can broadly be divided into cDC1s and cDC2s. The former is best known for its superior ability to cross present exogenous antigens on major histocompatibility complex I (MHCI) to CD8 T cells and the latter for its interaction with CD4 T cells in the context of MHCII (reviewed in [6]). The expression of X C motif chemokine receptor 1 (XCR1) - a chemokine receptor that upon triggering causes migration towards high concentrations of its ligands XCL1 and XCL2 – is restricted to cDC1s and can therefore be used as a surface marker to distinguish cDC1s from other cells. This has also led to generation of mice with fluorescently labelled XCR1 and mice with XCR1 specific conditional deletion systems [24] that have drastically improved our ability to study cDC1 biology in vivo. cDC2s can be distinguished from cDC1s based on surface markers such as SIRPα and transcription factors such as IRF4 [25], but no cDC2 exclusive protein is known currently. The interaction between DCs, T cells and other immune cells during DC driven immune responses is therefore best understood from the perspective of cDC1s and the anti-viral CD8 T cells they expertly instruct (reviewed in [22])

Naïve T cells continuously enter lymph nodes at the level of the paracortex through high endothelial venules (HEVs) that connect the lymph nodes to the blood circulation. In contrast, in response to local infection, antigen loaded migratory cDCs (migDCs) enter draining lymph nodes via the afferent lymphatics and pass the lymph node capsule, subcapsular sinus (SCS), cortical sinus and intrafollicular area (IFA) before finally moving into the deeper paracortex. The paracortex is especially rich in T cells and is therefore also known as the T cell zone. The cortical sinuses and IFAs together with the B cell follicles they separate are known as the cortex. Alternatively, during systemic infection, lymph borne pathogens and their antigens flow into the lymph node and are captured by SCS resident macrophages and DCs. Under the guidance of inflammatory cues DCs and T cells will then meet at some of these locations and interact. Most activated T cells leave the lymph node via the medullary sinus, lymph node medulla and efferent lymphatics. A minority of activated T cells differentiate into follicular B helper T cells (Tfh cells) and remain in the lymph node to interact with B cells in their follicles. Blood borne pathogens and their antigens are filtered from the circulation by the spleen. They are captured by macrophages and DCs residing in the marginal zones of splenic white pulp, which are isolated areas filled with white immune cells and that are distributed throughout the far more abundant red pulp. Importantly, like DCs in peripheral tissues, DCs in spleen marginal zones need to migrate to T cell areas. These are also located in splenic white pulp and are called the periarteriolar lymphoid sheath (reviewed in [6, 26]).

Studies with the model pathogen vaccinia virus (VV) have shown that after infection with VV by subcutaneous (s.c.) injection into the footpad, both virus infected type 1 migDCs (migDC1s) and migDC2s were found in the SCS of the lymph node, where they clustered with CD8 T cells in the absence of CD4 T cells, within the first 8-12 hours after infection [2]. Importantly, both DC subsets were able to activate CD8 T cells ex vivo at this point. During later stages of infection (38-40 hours), these activated CD8 T cells were found in the paracortex, where they clustered with different DC and CD4 T cells. This third subset of DCs were elucidated to be XCR1+ resident cDC1s (resDC1s) and without them, CD8 T cells did not form clusters with CD4 T cells and the number of activated CD8 T cells dropped. Mice that lacked resDC1 also failed to mount a robust memory recall response against *Listeria monocytes*, another intracellular pathogen. These findings together led to the notion that CD8 and CD4 T cells are initially activated separately in different intranodal locations on distinct DCs, but that they later interact with each other on resDC1s. Resident cDC1s therefore serve as a ‘critical platform’ for CD4 T cell help to CD8 T cells [2], which is important for the optimal induction of CD8 T cell responses in multiple settings (reviewed in [23]).

This concept was expanded by showing that pDCs translocate to these initial migDC-CD8 T cell clusters (10 hours) in a C C motif chemokine receptor type 5 (CCR5) dependent manner and failure to do so impaired later CD8 T cell responses [1]. Mechanistically, expression of the type I IFN receptor was required on resDC1s, but not on migDCs, for the maturation of resDC1s and their enhanced capacity to induce CD8 T cell responses [1]. This indicates that pDCs -through their canonical production of type I IFNs - activate the resDC1 platform and prepare it for optimal interaction with CD8 T cells and potentially also for interaction with CD4 T cells. It was also shown that CD8 T cells are likely to organize both clusters of migDCs-CD8 T cells-pDCs in the SCS [1] and CD8 T cell-resDC1s-CD4 T cells in the paracortex [2], or potentially a super cluster of CD8 T cell-resDC1s-pDC-CD4 T cells. This is because they produced robust amounts of CCL3 - a CCR5 ligand - in vitro and their production of XCL1 was needed for the formation of CD8 T cell-CD4 T cell clusters in vivo [1]. These findings together indicate that the optimal induction of CD8 T cell responses requires assistance of innate immune cells other than antigen loaded DCs and platform resDC1s.

Infection with herpes simplex virus (HSV) seems to share some features of this intranodal immune cell coordination during VV infection. Like VV infection, during later stages of HSV infection (42 hours), CD8 T cells were found to cluster in the paracortex around an activated non-migratory DC that expressed XCR1 [5]. In addition, these CD8 T cells were found to be frequently visited by CD4 T cells. However, unlike VV infection, CD4 T cells rather than CD8 T cells were the first to reduce velocity, cluster around migDCs and become activated. Furthermore, these cells were the first to leave the lymph node and to arrive in the spleen [5]. It should be noted that this model of infection was performed by scarification of epidermal flank skin and therefore local. Upon switching to s.c. injection - as was done in the VV model - initial CD8 T cells and CD4 T cell activation was synchronous as well rather than staggered. This opens the possibility that the reported differences between VV and HSV infection are the result of divergent infection strategies rather than the actions of distinct virus families. The transfer of antigen from CD103+ migDC1s to CD8+ resDC1s is necessary for the induction of anti-HSV immune responses [27, 28] and both these DC subsets express XCR1. The importance of resDC1s as a critical platform for CD4 T cell help to CD8 T cells during HSV infection [5] could therefore not be formally tested by conditional deletion of XCR1+ cells as was done in the VV model [2]. Still, CD4 T cells interact with CD8 T cells on resDC1s during HSV infection [5], CD4 T cells are needed for the production of CTL priming IL-15 by CD8+ DCs [29] and CD8+ DCs are required for the establishment of a successful immune response to HSV [30]. These findings together indicate that resDC1s are also a critical platform for CD4 T cell help to CD8 T cells during HSV infection. The production of IL-15 by CD8+ DCs needed both CD4 T cells and stimulation with type I IFNs [29], but pDCs were not required for protective immunity [31]. This suggests that perhaps another innate immune cell - through its production of type I IFNs - assists the activation of the resDC1 platform during HSV infection. For example, host protection against lymph borne vesicular stomatitis virus (VSV) depends on the early production of type I IFNs by SCS macrophages and not pDCs [32].

In response to mouse cytomegalovirus (MCMV) infection, natural killer cell (NK cell) distribution in the spleen changes from a homogenous spread throughout the red pulp to a more concentrated localization around the marginal zone of the white pulp [3]. Here cDC1s were found to cluster with these NK cells (40 hours) before they moved into deeper white pulp structures, such as the bridging channels (44 hours) and T cell areas (48 hours). Whole body deletion of XCR1 decreased the number of NK cell-cDC1 clusters at the marginal zone and the migration of cDC1s into the T cell zone. This was associated with a failure of cDC1s to upregulate their expression of the chemokine receptors GPR183 and CCR7. This was additionally associated with a strong decrease in IL-12 production by DCs and type II IFN (i.e. IFNγ) production by NK cells. The expression of costimulatory molecules on cDC1s was not affected. Reciprocal interaction between cDC1s and NK cells was revealed as XCR1 specific deletion of IL-15 significantly reduced the number of NK cells (4 days) and splenic NK cells isolated from MCMV infected mice induced the upregulation of CCR7 expression on immature type 1 Flt3L differentiated in vitro DCs (FLDC1s). The latter was dependent on stimulation of FLDC1s with granulocyte-macrophage colony-stimulating factor (GM-CSF), which NK cells were the major producers of during MCMV infection (40 hours). In turn, NK cells isolated from naïve mice produced GM-CSF after ex vivo stimulation with recombinant IL-12, of which cDC1s were the dominant source in vivo (40 hours; [3]). CCR7 [33] and GPR183 [34-36] are involved in the intrasplenic homing of cDC2s from the marginal zone into T cell areas. The authors proposed that during MCMV infection, splenic NK cells licence splenic cDC1s for migration towards T cell zones deeper in the white pulp. While NK cells were by far the major producers of XCL1 during both steady state conditions and in response to MCMV infection, NK cell specific deletion of XCL1 did not affect their clustering with cDC1s [3], suggesting that NK cells were are attracted to the cDC1s and not vice versa

Natural killer cells also seem to play a role in the induction of CD4+ Th1 responses to intradermally injected (i.d) *Mycobacterium smegmatis* [4], a facultative intracellular bacterium. In response to infection with *M smegmatis*, antigen loaded migDC2s (investigated on day 2) and large numbers of IL-12 producing monocyte derived inflammatory DCs (infDCs; day 2-3) appeared in the draining lymph node, together with IFNγ producing NK cells (day 1-2) and IFNγ producing Th1 cells (day 5). These infDCs surpassed migDC2s in their production of IL-12, which in combination with IL-18 was entirely responsible for the appearance of IFNγ producing NK cells in the lymph node. The production of IFNγ was conversely required for the recruitment of monocytes into the lymph node and their differentiation into infDCs. The recruitment of monocytes was in turn necessary for optimal induction of Th1 responses. Together, although the exact kinetics of this immune response was not assessed, the authors suggested that - based on other published literature - a cooperation between migDC2s and infDCs is likely, in which migDCs provide antigen and co-stimulation for T cell activation and infDCs provide high levels of IL-12 for T cell differentiation into Th1 cells [4].

In **Chapter 9** we showed how long-term loss of mTORC1 signalling in cDCs in vivo by deletion of raptor in CD11c expressing cells (CD11cΔraptor mice) leads to a pronounced reduction in MHC complexes and costimulatory molecules on cDCs. Of these, MHCI was most strikingly affected. Nevertheless, CD8 T cell responses to primary infection with *L. monocytogenes* were intact in these mice and so were CD8 T cell memory responses and host protection. A comparison of several s.c. injection strategies with antigenic peptides and TLR adjuvants revealed that the frequencies of antigen specific CD8 T cells within the CD8 T cell pool could even be increased in these mice following immunization. No matter the combination of ovalbumin, human papillomavirus (HPV) E7 protein, TLR3 ligand PolyIC and TLR9 ligand CpG-B. The exact mechanism for this was not elucidated, but we did report a doubling of IL-12 producing CD11c+ skin migratory Langerhans cells (LCs) in draining lymph nodes. Our current understanding of murine LCs is that they have a relatively poor cross priming capacity [37]. However, they might have taken up the role of high IL-12 production assisting innate immune cells in CD11cΔraptor mice, thereby explaining the intact or even enhanced immune responses in mice with impaired cDCs.

Taken together, these publications provide evidence for the existence of a resDC1 platform on which CD8 T cells and CD4 T cells organize themselves for the optimal induction of immunity in response to viral infection. In some settings, pDCs provide type IFNs that assist in the activation and preparation of the resDC1 platform, while in other settings pDCs are not are not required, but the ability of cDCs to react to type I IFNs is still crucial for their activation. Natural killer cells are likely to assist cDCs in their migration towards the deeper T cell zones in secondary lymphoid organs and NK cells can also interact in a reciprocal manner with IL-12 and IL-15 producing cells. These are cDC1s in some settings and in other settings infDCs, which are likely to assist antigen presenting cDCs in their interaction with T cells by providing additional IL-12. All of this suggests that complex clusters of several different immune cells interacting arise at multiple points along a spatiotemporal description of DC mediated T cell priming, in which these immune cells will need to coordinate their interplay for the optimal induction of immune responses and the establishment of protective immunity.

Nutrient competition between DCs and T cells

The concept of nutrient competition between immune cells is not new (reviewed in [20]) and especially the competition for tryptophan between DCs and T cells is well established (reviewed in [38]). However, the recent finding that DCs differentiated in vitro using GM-CSF (GMDCs) and were starved of glucose - which can occur during their interaction with glucose hungry activated CD8 T cells - perform better in T cell activation assays than their glucose satiated counterparts [21] is striking. This is because the metabolism of pro-inflammatory DCs has traditionally been associated with anaerobic glycolysis (reviewed in [39]. This competition for glucose between DCs and activated CD8 T cells occurred both in vitro and in vivo and mechanistically involved an immediate enhancement of costimulatory molecule expression and IL-12 transcription, but also the prolonged maintenance of this activated state. Low glucose availability inhibited mTORC1 activity in GMDCs and inhibited the establishment of a feed forward loop with mTORC1 mediated activation of hypoxia inducible factor 1 alpha (HIF1α). HIF1α mediates the synthesis of nitric oxide (NO) by inducing transcription of inducible NO synthase (iNOS). NO stabilizes HIF1α protein, thereby completing the loop [21]. Inhibition of mTORC1 activity in GMDCs had previously been shown to enhance GMDC immunogenicity after transfer in vivo [40-42], which was associated with increased autophagy [42] and improved survival [40] through prevention of mitochondria poisoning by NO [43]. This paper built upon those findings by showing the existence of a mTORC1-HIF1α-iNOS-NO-HIF1α feed forward loop that could also be initiated by exogenous NO. Most importantly in the context of immunometabolism, this paper visualized and pointed out that two DCs can be adjacent to each other and still display strikingly distinct nutrient sensing states. Dendritic cells that cluster with large numbers of T cells were found to be in a nutrient depleted “mTORC off” state, whereas DCs that were by themselves displayed active mTORC1 signalling. This highlights the need for tools that can “spatially resolve the metabolic configurations of single cells within their tissue microenvironment”, as was strongly argued for in an excellent recent review [44].

Although the glucose starvation of GMDCs by glucose greedy CTLs is the first example of nutrient competition that potentiates rather than limits DCs in their T cell priming capacity, it is possible that other combinations of DC and T cell subsets use similar mechanisms. For example, blocking glycolysis in human moDCs using 2-DG enhances their transcription of the Th17 associated cytokine IL-23, if it is part of an overarching program that induces the unfolding protein response (UPR; [45]). In T cells, the UPR can be induced by simultaneous inhibition of glucose and glutamine uptake [46] and just recently, it was shown that skin migDCs become metabolically reprogrammed during obesity to increase IL-23 and IL-6 production in an UPR dependent manner [47]. This was reproduced in GMDCs by either glutamine deprivation or 2-DG exposure. Interestingly, deletion of phosphofructokinase, an enzyme lower in the glycolysis pathway than the one inhibited by 2-DG, had no effect on IL-23 transcription [47]. This hints at a possible involvement of the hexosamine biosynthesis pathway (HBP), which requires both glutamine and the upper glycolysis metabolic intermediate fructose-6-phosphate for pathway activity. Together, it is therefore imaginable that the differentiation of T cells towards a CTL or Th1 cell is reinforced by starving DCs of glucose and thereby boosts the secretion of IL-12, while the differentiation towards a Th17 cell is reinforced by starving DCs of both glucose and glutamine and thereby boosts the secretion of IL-23 and IL-6. Studies have shown that the in vitro differentiation of murine Th1 and Th17 cells are both dependent on the glutamine transporter SLC1A5, in contrast to Th2 cells and Tregs [48, 49]. However, one of these studies also showed that the transfer of glutamine transporter deficient T cells into a mouse with experimental allergic encephalomyelitis resulted in less Th17 cells recovered as expected, but surprisingly more Th1 cells [49]. This suggests that primary Th17 cells are in fact more dependent on glutamine than their Th1 cell counterparts and makes it imaginable that physiologically differentiated Th17 cells are more competitive for glutamine.

Our own work shows that the intracellular glutamine pool of moDCs conditioned with the Th2 associated antigen omega-1 is larger than that of immature moDCs (**Chapter 7**) and it is also larger in moDCs conditioned with a combination of the Th1 associated antigens LPS and Poly (I:C). In contrast, moDCs conditioned with the Th17 associated antigen zymosan have unchanged quantities of glutamine (Pelgrom, *unpublished*). Metabolite abundance does not distinguish between altered extracellular uptake and altered pathway flux, but it is tempting to speculate that Th17 priming DCs have adapted their metabolic machinery to match that of Th17 cells. For example, by limiting their intracellular glutamine pool they might make themselves susceptible to glutamine starvation and by the same token render them poised to produce Th17 priming cytokines, which may involve a decreased engagement of the HBP. This would position Th17 priming DCs differently from the Th2 and Th1 priming DCs we investigated, as the latter two were found to depend on O-GlcNAcylation and N-glycosylation respectively for their T cell priming capacity (**Chapter 7**), which are both reactions that use the HBP end product uridine diphosphate N-acetylglucosamine (UDP-GlcNAc).

Taken together, in the microenvironment of DC-T cell interaction, T cells can starve DCs for nutrients, even when surrounded by culture media with supraphysiological concentrations of nutrients. Restriction of glucose can lead to CTL/Th1 priming IL-12 production associated with decreased mTORC1 activity, while restriction of glucose and glutamine flux through the HBP may lead to production of Th17 priming cytokines IL-23 and IL-6.

Instruction of DC metabolism through paracrine cytokines and metabolites

In the previous section we pointed out the importance of DC metabolism in the establishment of T cell responses. We additionally provided examples of how pDCs activate the lymph node resDC1 critical platform through their production of type I IFNs and how NK cells assist in migration of cDCs to T cell areas through their production of GM-CSF and potentially IFNγ. So, what do we know about the relationship between these cytokines and immune cell metabolism?

Type I IFNs stimulation was necessary but not enough for the activation of splenic cDCs and the acquisition of their T cell priming capacity after injection of Poly (I:C) in vivo [50]. This was associated with a switch from OXPHOS towards anaerobic glycolysis that involved HIF1α [50] in a manner that was disconnected from NO, as cDCs do not produce NO like GMDCs (reviewed in [51]). Lymph node resDC1s share many similarities with splenic cDC1s including their expression of CD8 (reviewed in [6]) and it is therefore imaginable that the lymph node resDC1s critical platform switches towards anaerobic glycolysis upon exposure to type I IFNs [1] like splenic cDCs and moreover, that this metabolic transition is required for their activation and platform function.

It has been shown that GM-CSF stimulation enhances glycolysis in macrophages [52, 53]. As glycolysis is necessary for the oligomerization of CCR7 in DCs [54] and splenic NK cell derived GM-CSF is thought to assists in the migration of splenic DCs [3], there will potentially be DCs in spleen marginal zones that are adjacent to each other but display strikingly distinct glycolytic pathway “on and off” states as a consequence of being in a cluster with GM-CSF producing NK cells (glycolysis on) or being by themselves (glycolysis off).

Although a clear role for NK cells in the intranodal priming of CD8 T cells during VV infection was excluded [2], GM-CSF induced glycolysis may still facilitate the migration of antigen loaded migDCs from the SCS to the T cell areas, as pDCs can also produce GM-CSF [55]. Alternatively, when SCS macrophages are delivered VV antigen and transfer this antigen to lymph node resDC1s [56], NK cells may play the same role as facilitators of intra-organ DC migration as they did during splenic MCMV infection [3].

For an in depth description of NK cell metabolism we like to refer you to another review [57], but briefly, short-term stimulation of NK cells with cytokines such as IL-12 and IL-15 does not result in increased rates of glycolysis and OXPHOS [58], while overnight stimulation results in a substantial enhancement of overall cellular metabolism [59]. Moreover, while NK cells do not seem to require FAO [58] and glutaminolysis [58, 60] for their functions, they are highly depend on glycolysis [61] and are likely to import glutamine from the extracellular environment to stimulate vital mTORC1 signalling (reviewed in [57]). This would make them poor company for glucose and glutamine hungry activated T cells (reviewed in [20]) in T cell areas of the spleen and might explain why they did not take part in the late stage formation of DC-T cell clusters during VV infection [2].

IFNγ is produced by NK cells upon viral infection [3] but also by activated CD8 T cells [2]. It was shown recently that intertumoral production of IFNγ by CD8 T cells promoted the classical activation of tumour associated macrophages by stimulating AMPK activity. This in turn down regulated SREBP1 and lipid metabolism in these macrophages that would otherwise sustain their alternative activation [62]. We have discussed in the previous section how inhibition of mTORC1 in DCs after their initial activation can enhance their CD8 T cell priming capacity. AMPK is a well-known negative controller of mTORC1 (reviewed in [63]). It is therefore possible to imagine that highly immunogenic DCs with low mTORC1 activity are kept in this state through the paracrine action of IFNγ produced by activated CD8 T cells they interact with.

In **Chapter 8** we showed how absence of AMPK signalling in cDCs in vivo by deletion of its upstream kinase liver kinase B1 (LKB1) in CD11c expressing cells (CD11cΔLKB1 mice) leads to increased maturation, migration and T cell priming capacity of peripheral cDCs. That the loss of AMPK signalling in DCs (**Chapter 8**) and stimulation of AMPK activity in myeloid cells [62] both result in enhanced immunogenicity seems incongruent. However, this inconsistency is also seen with mTORC1. Deletion of raptor led to decreased maturation of cDCs (**Chapter 9**), while acute inhibition of mTORC1 increased the CD8 T cell priming capacity of GMDCs [21]. This suggests that DCs need to be able to switch back and forth between AMPK high/mTORC1 low and AMPK low/mTORC1 high states, for optimal functioning from their initial activation in the periphery to their final interaction with T cells in the T cell area. In addition to timing, location also influences the immunological outcome of AMPK/mTORC1 manipulation in DCs. In **Chapter 8** we showed that LKB1 deficient cDC2s in the thymus have a potientiated ability to differentiate thymocytes into natural Tregs, while others provided further evidence that LKB1 deficient DCs in the periphery tend to promote the polarization of mature naïve T cells into Th17 cells [64]. The former relied on gain of phospholipase C β1 activity and intracellular calcium release, while the latter depended mostly on loss of AMPK mediated negative control on mTORC1. Together, these publications highlight the complexity of metabolic signalling in immune cells in situ and the value of more controllable deletion systems such as diphtheria toxin receptor mediated systems.

Tumour necrosis factor (TNF) is another cytokine that is produced by activated CD8 T cells and it can also promote the classical activation of macrophages, although in this setting by stimulation of SREBP2 [65] instead of inhibition of SREBP1 [62]. This in turn leads to the transcription of genes involved in sterol metabolism and in addition the transcription of pro-inflammatory genes in a manner that was independent of cholesterol synthesis [65]. Stimulation with the TLR3 and 4 ligands Poly (I:C) and LPS and also IFNα, IFNβ and IFNγ can induce the transcription of genes involved in cholesterol synthesis in GMDCs [66] and cholesterol accumulation induces inflammasome activation and production of pro-inflammatory cytokines in splenic cDC2s [67]. Conversely, acute inhibition of the mevalonate pathway involved in cholesterol synthesis using statins inhibits the production of type I IFNs by murine and human pDCs [68]. Together, this makes it imaginable that the stimulation of de novo cholesterol synthesis in DCs after exposure to CD8 T cell derived TNF supports the further development of DC mediated T cell responses in secondary lymphoid organs. This contrasts with de novo FA synthesis which seems to be dispensable for cDC function [69].

In this section we have described pro-inflammatory paracrine signals, but it is also important to have brakes in place that can prevent excessive inflammation which can lead to collateral host tissue damage. In this context, we have already referred to papers that showed how preventing autocrine production of NO by GMDCs could enhance their immunogenicity [21, 43], but importantly, NO produced by neighbouring cells can also institute a HIF1α-iNOS-NO-HIF1α feed forward loop that conversely supresses immunogenicity of DCs, even in iNOS deficient DCs [21]. It is noteworthy that NO serves as donor for the post-translational modification of proteins through nitrosylation and that in addition to prolyl hydroxylase (PHD), the enzyme that breaks down HIF1α, and nitrosylation of HIF1α itself, many other immunomodulatory transcription factors can be nitrosylated (reviewed in [70]). Moreover, a recent study showed that after high NO production, which was induced by acute kidney injury, the top nitrosylated proteins in kidney extracts were almost all metabolic enzymes [71]. This suggests that the effects of paracrine NO production extend well beyond that of on DCs and beyond that of HIF1α [21] and poisoning of mitochondria [72].

Classically activated macrophages are an obvious candidate for paracrine NO production because they are in part characterized by their production of NO (reviewed in [16]). However, SCS macrophages were not important for early-stage formation of DC-T cell clusters during VV infection [2] and in line with this, the contribution of SCS macrophages to host protection against VV infection seems limited [73]. Nevertheless, SCS macrophages are known to have important functions during other examples of viral infection [32, 74]. It is also noteworthy that in addition to production of arginine derived NO by classically activated macrophages, alternatively activated macrophages can secrete arginine derived polyamines, which can induce a tolerogenic program in neighbouring DCs [75]. In which in vivo settings this interaction occurs is currently unknown, although the tumour environment and its myeloid derived tumour suppressor cells seems a plausible scenario.

Monocytes are also recruited to the lymph node during viral infections in a type I IFN and CCL2 dependent manner (reviewed in [76]). These monocytes can be helpful in some situations (e.g. VSV infection [77]) and destructive in other circumstances (e.g. LCMV infection [77] & chikungunya virus [CHIKV; [78]). In the latter situations, protective immune responses could be restored by inhibition of NO production [77, 78]. This suggests that these pathogens recruit NO producing inflammatory monocytes to hijack a normally healthy form of negative feedback, in which IFNγ and TNF production by activated T cells stimulates lymph node reticular fibroblasts to produce NO, that in turn tempers further T cell proliferation [79]. Reticular fibroblasts are also known to alter the metabolism of T cells through production of cytokines such as IL-6 [80], while T cells in turn can alter the metabolism of reticular fibroblasts through production of IL-17 [81]. However, if these fibroblasts influence the activity and metabolism other immune cells such as DCs are yet to be elucidated. Moreover, although some lymph node reticular fibroblasts have the capacity to produce retinoic acid [82], if metabolites other than NO play a role in these processes remains unclear.

The anti-inflammatory cytokine IL-10 is known to control and resolve inflammation in part by controlling the cellular metabolism of macrophages [83], while the anti-inflammatory cytokine TFGβ can inhibit the activation and function of NK cells through mTORC1 dependent [84] and independent means [85]. However, while both cell types have been discussed above in the context of viral infections, if and how these cytokines play a role in the fine tuning of immune cell interactions during the establishment of an anti-viral immune response remains elusive for the moment.

Taken together, at every step of the DC-mediated immune responses discussed, be it the NK cell-DC cluster, the migDC-CD8 T cell-pDC cluster or the CD8 T cell-resDC1-CD4 T cell cluster, cytokines are being produced by non-DC cells that are very likely to alter the metabolism of the interacting DC. However, as there are no studies yet that have investigated the metabolism of DCs during the establishment of DC mediated immune responses in a spatiotemporal manner, the actual metabolic state of DCs at these junctions remains speculation.

Stocking up on nutrients before the long haul to the draining lymph node or inflamed tissue

In **chapter 4** we demonstrated that GMDCs have glycogen stores that are utilized in the production of citrate during the early stages of LPS induced metabolic reprogramming, when glucose transporters are not yet upregulated on the surface. This investigation was sparked by an older study showing that murine lymphoid cDCs and human adipose tissue cDCs also have glycogen stores and, in addition to that, also neutral lipid stores [86]. The conditioning of GMDCs with IL-4 resulted in the increased storage of glycogen and lipids, while the effects of LPS were not fully elucidated at the time. It was reported however that conditioning with LPS resulted in the increased storage of lipids [86] and we now know that stimulation with LPS conversely decreases glycogen stores (**Chapter 4**). Whether cDCs respond in a similar manner to these compounds as GMDCs remains to be seen. However, if this is the case, one might wonder if in response to these and other danger associated molecular patterns (DAMPs), DCs prepare themselves for different scenarios by outfitting themselves with distinct metabolic apparatus. Maybe the main function of the cDC that has recognized LPS is to travel to the draining lymph node, where it presents bacterial peptides to the T cells there and in line with the benefits of low mTORC1 activity in DCs during DC-T cell interaction [21] discussed in the previous section, has equipped itself with a metabolic machinery that avoids the consumption of mTORC1 activating glucose and glutamine and instead burn lipids. In contrast, the presence of IL-4 may indicate that an adaptive immune response has already been initiated and that the inflammatory moDCs must infiltrate an area of persistent infection and minimal nutrient availability, where low glucose levels can interfere with the oligomerization of the chemokine receptor CCR7 [54], something which might be overcome with the flux of glycogen derived carbons into glycolysis.

Stocking up on appropriate lipid species seems to be beneficial for DC immunogenicity in general (reviewed in [87]). Mouse and human liver DCs with a high lipid content produced more pro-inflammatory IL-6 and TNF at steady state conditions and after TLR triggering. These cells were shown to be nearly 10 times as efficient at cross presentation than their low lipid content counterparts. This improved the interaction of high lipid content mouse liver DCs with CD8 T cells, CD4 T cells and NK cells both in vitro and in vivo in a manner that could be diminished by administration of the ACC inhibitor TOFA. Interestingly, the authors noted that these DCs were as good as splenic DCs regarding their T cell priming capacity but even better at activating NK cells [88]. Regarding splenic DCs, CD8+ cDC1s in the spleen had almost 40% more lipid droplets than their CD8- cDC2 counterparts. Deletion of Irgm3, a family member of the immunity related 47kDa GTPases (p47 GTPases) that localizes to endoplasmic reticulum (ER) and lipid bodies, diminished the accumulation of lipid bodies in spleen DCs and their capacity for cross presentation independent of co-stimulatory molecules expression and cytokine production. Moreover, these effects could be recapitulated using the diglyceride acyltransferase (DGAT) inhibitor xanthohumol [89]. Finally, these studies combined show that abundance of lipid stores can be increased in GMDCs in vitro using LPS [86] and IFNγ [89], while LPS and PolyIC injection can increase the abundance of lipid stores in liver DCs and splenic DCs in vivo [88, 89], with splenic cDC1s being more responsive than splenic cDC2s [89].

In **Chapter 9** we showed how long-term loss of mTORC1 signalling in cDCs leads to a pronounced reduction in MHCI surface expression on cDC1s, which was associated with a reduced uptake of the glucose analogue 2-NBDG by the same DCs. It was previously shown that glucose is used for de novo synthesis of fatty acids and subsequent lipid droplet formation in TLR-stimulated in vitro DCs [90]. As glycolysis and fatty acid synthesis are dependent on mTORC1 [91], it is tantalizing to speculate that reduced glycolysis and MHCI expression are linked by changes in the lipid content of raptor deficient cDC1s.

The type of lipid species that build up intracellularly seems important as the accumulation of peroxidised lipid bodies in DCs prevents the translocation of MHCI:peptide complexes to the cell surface [92, 93]. In line with this, inhibition of the cystine/glutamate antiporter (system xc-), which is involved in positively regulating levels of the antioxidant glutathione (GSH) and therefore the cells redox state, lowered the cellular ratio of GSH and its oxidized disulphide form (i.e. GSSG) in moDCs and lowered surface expression of MHCI independent of antigen uptake and co-stimulatory molecules expression. This resulted in a blockade of antigen presentation to CD8 T cells and to a lesser degree to CD4 T cells, which was recapitulated in murine splenic DCs [94]. It is also the only or one of the few demonstrations of how amino acid metabolism in DCs affects their canonical function of T cell priming, separately from the effects of amino acid deprivation during in vitro differentiation or prolonged ex vivo culture [95-97].

Taken together, DCs have intracellular stores of nutrients that in some instances helps them with the acute demands of activation and in other cases might prepare them for the needs of T cell interaction. Intracellular lipid bodies seem to be particularly important for cDC1s because they have more of them, generate more of them in response to DAMPs, and lipid quantity and quality is associated with antigen presentation in the context of MHCI. Whether the use of intracellular glycogen stores by DCs extends beyond that of T cell activating capacity and the production of the Th1/CTL associated cytokine IL-12, remains unknown. Moreover, it is currently unclear if specific classes of lipids (e.g. fatty acyls, sphingolipids and sterols) are important for different effector functions of DCs or whether the balance of normal versus oxidized lipids is more important. Finally, mouse models of inflammation with distinct local and lymph node functions for respectively infDCs and cDCs, such as during HSV infection [98], or where titration of antigen can change how a DC participates in the immune response, such as during house dust mite allergy [99], might provide another layer of complexity that can help to elucidate the contribution of intracellular nutrient stores in different situations.

Lymph fluid metabolome

In comparison to the presence of metabolites in whole blood, serum and plasma, little is known about the metabolome of lymph fluid. In this context, the content of lipid-transporting lipoproteins in mesenteric lymph fluid (MLF) has been studied best, because of the essential role for lipoproteins in the absorption of dietary fats and fat-soluble vitamins (reviewed in [100]). In line with the abundance of lipoproteins in MLF, lipids were the predominant class of metabolites found to change in MLF during the transition from a fasted to fed state. However, changes in glucose and essential amino acids such as tryptophan were also apparent [101].

One of the lipids that was clearly increased after eating is the short chain fatty acid butyric acid (also known as butyrate). In **Chapter 5** we showed how exposure of moDCs to butyrate conditions them for Treg priming, which was associated with suppression of LPS induced anaerobic glycolytic remodelling and in addition to a concomitant suppression of oxidative metabolism. Such a profile of overall suppressed metabolism also occurs after exposure to the tolerogenic compound dexamethasone (Pelgrom, *unpublished*), although others have reported that exposure of monocytes to vitamin D or retinoic acid while they are differentiating into moDCs leads to a more a anaerobic glycolytic moDC phenotype [102-104]. Butyrate is produced by gut microbiota and is consumed locally by colonocytes [105], although some will be transported from the gut into the blood circulation (reviewed in [106]) and lymphatics [101]. The observed fluctuations of butyrate levels [101] suggests that a one-time exposure to butyrate as was done in **Chapter 5** of this thesis, is more in line with physiological exposure to butyrate, although the absolute concentrations of butyrate cannot be inferred from that study, as absolute concentrations of nutrients in MLF are rarely reported. However, concentrations of glucose and amino acids might be inferred from blood, as absolute levels of glucose and amino acids are comparable between lymph fluids and blood in certain steady state conditions [107, 108]. The metabolome of lymph fluid during inflammation remains elusive, as to our knowledge, only 2 studies investigated the change in the metabolome of lymph fluid during inflammation.

The first study focused on the lipid content of purified triglyceride-rich lipoproteins in MLF and found that puncture of the intestine and the subsequent release of faecal matter into the abdomen, resulted in the acute loss of lipid species in IMF lipoproteins. In contrast, reduced blood flow (i.e. ischaemia) induced by ligation of the mesenteric artery had no effect on lipid species [109]. It is tempting to speculate on the possibility of a preference for lipid consumption in response to the exposure to (commensal) bacteria versus the preferred consumption of non-lipid fuels as can be expected during hypoxia, which induces the transcription of glycolytic genes through the transcription factor HIF1α (reviewed in [110]). However, it should be noted that the duration of the first intervention was significantly longer and might have affected the absorption of dietary fats in the intestine through disruption of organ structural integrity [109].

The second study found that glutamine is one of three significantly modulated metabolites in brain lymph fluid (BLF) of rats after infection of the forelimb with a rabies pseudo virus [111]. Activated T cells consume large amounts of glutamine [20], so one might expect the concentration of glutamine to decrease during the initiation of anti-viral immune responses. However, instead, levels of glutamine were found to be increased in BLF after rabies pseudo virus infection [111]. The significance of improved glutamine availability was not investigated, but it is tempting to speculate on an intentional reorganization of glutamine metabolism to support the generation of glutamine-dependent anti-viral NK cells (reviewed in [57]) and anti-viral CD8+ cytotoxic T lymphocytes (CTLs; reviewed in [112]). Such a system has been described in the context of muscle repair, where intramuscular macrophages, endowed by high glutamine synthetase activity and low glutamate dehydrogenase activity, have the capacity to secrete glutamine and support the glutamine-dependent proliferation of muscle cells [113]. With respect to the brain, astroyctes are well known for their capacity to secrete glutamine to support the synthesis of glutamine-derived neurotransmitters by neurons (reviewed in [114]) and our brain releases measurable amounts of glutamine [115]. However, whether astrocytes use this capacity to support anti-viral immune responses remains to be elucidated.

The two other metabolites that were significantly modulated: dimethylglycine (DMG) - a product of choline metabolism - and dimethylamine were both decreased. Little is known about the interaction between DMG and immune cells, but a recent study suggested a potential mechanistic role for increased serum levels of DMG in the robust induction of IFNγ producing CD8 T cells in the intestine, which was dependent on intestinal CD103+ cDC1s and major histocompatibility class I (MHCI) expression, Moreover, this was associated with enhanced host resistance to infection with the intracellular bacterium *L. monocytegenes* [116]. However, this is the first publication linking DMG with immune cells, so, whether DMG can directly stimulate immune cells and if so, which immune cells, remains to be determined. Nevertheless, the intestine seems a relevant location for interaction between immune cells and DMG, as the abundance of its precursor choline is increased in IMF after feeding [101]. In addition, the consumption of DMG after rabies pseudo virus seems relevant, as CD103+ cDC1s are the subset best known for its capacity to cross-present antigens to CD8+ CTLS (reviewed in [117]).

Taken together, very little is known about changes in specific metabolites during lymph node inflammation except for glutamine and DMG in response to rabies pseudo virus.

The road ahead: development of new tools and platforms to study systems immunometabolism

As discussed in one of the previous sections, it takes time for a DC to migrate from a peripheral tissue to a draining lymph node and again more time to migrate from the outer SCS to the T cell area. Similarly, in the spleen, although the distances are considerably smaller, DCs still need to migrate from the marginal zone to the T cell area. This temporal aspect of DC function seems to be built into their biology. For example, blocking glycolysis was found to impair initial DC activation [54], which in vivo would most likely take place in the periphery, while blocking glycolysis was found to enhance later T cell priming capacity [21], that in vivo would most likely take place in T cell areas. Moreover, that there is also a spatial aspect to DC function is demonstrated in the most extreme manner by the evidence that two adjacent DCs can have completely opposite on and off states of the nutrient sensing kinase mTORC1 [21].

There is a clear need for new tools that can resolve these spatiotemporal aspects of DC metabolism and of immune cell metabolism in general [44]. However, the integration of single cell cytometry data with single cell RNA sequencing data might be sufficient to move the field of immunometabolism into the new era, while spatial mass spectrometry (MS) are still in their infancy [44].

One of the advantages of conventional fluorochrome based flow cytometry over mass cytometry by time of flight (CyTOF), is that it allows for the addition of other fluorescent tools such fluorescent nutrient analogues in addition to fluorescent antibodies [44]. The example given was the use of the fluorescent glucose analogue 2-NBDG [118], of which the uptake was said to be directly related to expression of the glucose transporter 1 [44]. However, another paper, that was published around the same time, has cast doubts on the reliability of 2-NBDG as a tool for the assessment of cellular glucose transporter capacity [119]. Herein, 2-NBDG was compared to the golden standard of stable isotope labelling (SIL) and it was found that in murine T cells, 2-NBDG uptake was not blocked by competitive substrates or inhibition of glucose transporters, while conversely, 2-NBDG could not competitively block the uptake of glucose [119]. Although the exact mechanism for the large discordance between 2-NBDG labelling and glucose transporter capacity was not investigated, the author has suggested that the attachment of such a bulky fluorophore [i.e. N-(7-Nitrobenz-2-oxa-1,3-diazol-4-yl)Amino] to 2-deoxyglucose probably interferes with the interaction between 2-deoxyglucose and its native transporters (personal communication with Linda Sinclair).

One possible solution to this problem is to simply stick to antibodies that recognize the nutrient transporter of interest and use the labelling intensity as a correlate for nutrient flux in or out of the cell. However, while this will probably be appropriate for most cases, there are instances where a reconfiguration of transporter localization is responsible for changes in nutrient flux before changes in transporter expression and therefore the labelling intensity that can be picked up. For example, flux through the glutamine transporter SLC1A5 (also known as ASCT2) is fully responsible for the acute increase in glutamine uptake that occurs 30 minutes after engagement of CD3 and CD28 on T cells in vitro, which manifests together with a rapid aggregation and colocalization of ASCT2 with the T cell receptor complex in the absence of altered glutamine transporter expression [49]. Moreover, the chances of an amino acid to be imported depends on the extracellular and intracellular abundance of that amino acid relative to other amino acids present (reviewed in [120]).

Taken together, the field of immunometabolism is quickly becoming a systems level science benefitting from technological improvements in single cell transcriptomics, proteomics and cytometry, which are simultaneously accompanied by a continuing refinement in antibody selection and computational approaches. Immunometabolism may also benefit from the development of more minimally modified nutrient analogues that are suitable for single cell cytometry and spatial microscopy.

Summary & conclusion

DCs are the canonical antigen presenting cell and therefore play a pivotal role in the establishment of successful antigen specific T cell responses. To facilitate their interaction with T cells, their biology undergoes drastic changes while migrating from peripheral tissues or spleen marginal zones all the way deep into the T cell areas of secondary lymphoid organs. These changes include necessary alterations in their metabolism as is illustrated in this thesis. In summary, the key novel findings presented in this thesis are:

- DCs can store glycogen to support early stages of their activation, which is especially important in environments with low levels of glucose (**Chapter 4**).
- Glycogen-derived carbons are preferentially used by DCs to support citrate metabolism (**Chapter 4**).
- Human DCs are conditioned by the short-chain fatty acid butyrate for Treg priming through production of retinoic acid (**Chapter 5**).
- Butyrate, propionate, and acetate – the three most common short-chain fatty acids - all suppress aerobic glycolysis and oxidative phosphorylation in human DCs (**Chapter 5**).
- DCs exposed to parasites or allergens are uniquely dependent on O-GlcNAcylation for Th2 priming, which is a post-translational modification of proteins with the metabolite N-acetylglucosamine (**Chapter 7**).
- Type 2 cDCs but not type 1 cDCs or pDCs in the blood of volunteers infected with hookworm show increased levels of protein O-GlcNAcylation (**Chapter 7**).
- The LKB1-AMPK signalling pathway – a master regulator of catabolic metabolism - limits DC immunogenicity in vivo **(Chapter 8**).
- Mice with LKB1-deficient DCs show enhanced output of thymic regulatory T cells that dominate the immunological phenotype of these mice (**Chapter 8**).
- The mTORC1 signalling pathway – a master regulator of anabolic metabolism – promotes DC immunogenicity in vivo (**Chapter 9**), in contrast to what was reported by in vitro bone marrow-derived DC models.
- Skin DCs are more severely affected by mTORC1 loss than splenic DCs (**Chapter 9**).
- mTORC1 limits skin Langerhans cells immunogenicity in vivo (**Chapter 9**).

Despite these novel insights, we are only beginning to delineate how temporal and qualitative changes in nutrient exposure control DC metabolism and biology in situ. Recently, elegant models that have allowed the study of type 1 conventional DCs have elucidated the presence of DC-immune cell clusters along this timeline of DC-mediated T cell priming, which include at least a NK cell-DC cluster, a migratory DC-CD8 T cell-plasmacytoid DC cluster and a CD8 T cell-resident type 1 conventional DC-CD4 T cell cluster. It is likely that the metabolism of DCs keep adapting to these microenvironments that are transitioned between, but we at minimum know that DCs can display distinct high glycolysis and glucose starved/mTORC1 signalling off states that are required for their initial activation versus their prolonged activation respectively. Moreover, adjacent DCs can also display distinct glucose starved/mTORC1 signalling off and glucose satiated/mTORC1 signalling on states in relation to the cells they are interacting with while being in proximity of each other. Although direct evidence for DC metabolism adaptations to their described immune cell partners in vivo is absent, many studies provide suggestions for how these adaptations might be regulated. CD8 T cells can enforce a glucose starved/mTORC1 signalling off state in DCs that enhances and prolongs their capacity for T cell priming. Moreover, the cytokines that were reported necessary for the formation of the described immune cell clusters, including prototypical cytokines such as IFNα and IFNγ, have well described metabolism altering properties in other contexts. Little is known how DCs prepare their metabolic machineries to match those of their described immune cells partners, but some evidence exists for cross priming cDC1s relying heavily on lipids for their cross presentation, which would make sense in relation to the high glucose demands of NK cells and T cells, at least what is known from in vitro studies. Finally, even less is known about changes in the metabolome of lymph fluid during inflammation, although glutamine levels have been described to shift in response to rabies virus infection. The development of metabolic probes that are more minimally modified than the currently often used fluorescent nutrient analogues such as 2-NBDG, would facilitate in delineating these described spatiotemporal aspects of DC metabolism and of immune metabolisms in general.

References

1. Brewitz, A., et al., *CD8(+) T Cells Orchestrate pDC-XCR1(+) Dendritic Cell Spatial and Functional Cooperativity to Optimize Priming*. Immunity, 2017. **46**(2): p. 205-219.
2. Eickhoff, S., et al., *Robust Anti-viral Immunity Requires Multiple Distinct T Cell-Dendritic Cell Interactions*. Cell, 2015. **162**(6): p. 1322-37.
3. Ghilas, S., et al., *NK cells orchestrate splenic cDC1 migration to potentiate antiviral protective CD8+ T cell responses*. bioRxiv, 2020.
4. Hilligan, K.L., et al., *Dermal IRF4+ dendritic cells and monocytes license CD4+ T helper cells to distinct cytokine profiles*. Nat Commun, 2020. **11**(1): p. 5637.
5. Hor, J.L., et al., *Spatiotemporally Distinct Interactions with Dendritic Cell Subsets Facilitates CD4+ and CD8+ T Cell Activation to Localized Viral Infection*. Immunity, 2015. **43**(3): p. 554-65.
6. Eisenbarth, S.C., *Dendritic cell subsets in T cell programming: location dictates function*. Nat Rev Immunol, 2019. **19**(2): p. 89-103.
7. Ayres, J.S., *Immunometabolism of infections*. Nat Rev Immunol, 2020. **20**(2): p. 79-80.
8. Lercher, A., H. Baazim, and A. Bergthaler, *Systemic Immunometabolism: Challenges and Opportunities*. Immunity, 2020. **53**(3): p. 496-509.
9. Ben-Moshe, S., et al., *Spatial sorting enables comprehensive characterization of liver zonation*. Nat Metab, 2019. **1**(9): p. 899-911.
10. Halpern, K.B., et al., *Single-cell spatial reconstruction reveals global division of labour in the mammalian liver*. Nature, 2017. **542**(7641): p. 352-356.
11. Wu, H., et al., *T-cells produce acidic niches in lymph nodes to suppress their own effector functions*. Nat Commun, 2020. **11**(1): p. 4113.
12. Abbott, R.K., et al., *Germinal Center Hypoxia Potentiates Immunoglobulin Class Switch Recombination*. J Immunol, 2016. **197**(10): p. 4014-4020.
13. Cho, S.H., et al., *Germinal centre hypoxia and regulation of antibody qualities by a hypoxia response system*. Nature, 2016. **537**(7619): p. 234-238.
14. Gerner, M.Y., et al., *Dendritic cell and antigen dispersal landscapes regulate T cell immunity*. J Exp Med, 2017. **214**(10): p. 3105-3122.
15. Oyler-Yaniv, A., et al., *A Tunable Diffusion-Consumption Mechanism of Cytokine Propagation Enables Plasticity in Cell-to-Cell Communication in the Immune System*. Immunity, 2017. **46**(4): p. 609-620.
16. O'Neill, L.A., R.J. Kishton, and J. Rathmell, *A guide to immunometabolism for immunologists*. Nat Rev Immunol, 2016. **16**(9): p. 553-65.
17. Caputa, G., A. Castoldi, and E.J. Pearce, *Metabolic adaptations of tissue-resident immune cells*. Nat Immunol, 2019. **20**(7): p. 793-801.
18. Argüello, R.J., et al., *ZENITH: A flow cytometry based method for functional profiling energy metabolism with single cell resolution*. bioRxiv, 2020.
19. Hartmann, F.J., et al., *Single-cell metabolic profiling of human cytotoxic T cells*. Nat Biotechnol, 2020.
20. Kedia-Mehta, N. and D.K. Finlay, *Competition for nutrients and its role in controlling immune responses*. Nat Commun, 2019. **10**(1): p. 2123.
21. Lawless, S.J., et al., *Glucose represses dendritic cell-induced T cell responses*. Nat Commun, 2017. **8**: p. 15620.

22. Theisen, D. and K. Murphy, *The role of cDC1s in vivo: CD8 T cell priming through cross-presentation*. F1000Res, 2017. **6**: p. 98.
23. Bedoui, S., W.R. Heath, and S.N. Mueller, *CD4(+) T-cell help amplifies innate signals for primary CD8(+) T-cell immunity.* Immunol Rev, 2016. **272**(1): p. 52-64.
24. Yamazaki, C., et al., *Critical roles of a dendritic cell subset expressing a chemokine receptor, XCR1.* J Immunol, 2013. **190**(12): p. 6071-82.
25. Guilliams, M., et al., *Unsupervised High-Dimensional Analysis Aligns Dendritic Cells across Tissues and Species.* Immunity, 2016. **45**(3): p. 669-684.
26. Qi, H., W. Kastenmuller, and R.N. Germain, *Spatiotemporal basis of innate and adaptive immunity in secondary lymphoid tissue.* Annu Rev Cell Dev Biol, 2014. **30**: p. 141-67.
27. Allan, R.S., et al., *Migratory dendritic cells transfer antigen to a lymph node-resident dendritic cell population for efficient CTL priming*. Immunity, 2006. **25**(1): p. 153-62.
28. Bedoui, S., et al., *Cross-presentation of viral and self antigens by skin-derived CD103+ dendritic cells.* Nat Immunol, 2009. **10**(5): p. 488-95.
29. Greyer, M., et al., *T Cell Help Amplifies Innate Signals in CD8(+) DCs for Optimal CD8(+) T Cell Priming.* Cell Rep, 2016. **14**(3): p. 586-597.
30. Allan, R.S., et al., *Epidermal viral immunity induced by CD8alpha+ dendritic cells but not by Langerhans cells.* Science, 2003. **301**(5641): p. 1925-8.
31. Swiecki, M., et al., *Plasmacytoid dendritic cells contribute to systemic but not local antiviral responses to HSV infections*. PLoS Pathog, 2013. **9**(10): p. e1003728.
32. Iannacone, M., et al., *Subcapsular sinus macrophages prevent CNS invasion on peripheral infection with a neurotropic virus*. Nature, 2010. **465**(7301): p. 1079-83.
33. Calabro, S., et al., *Differential Intrasplenic Migration of Dendritic Cell Subsets Tailors Adaptive Immunity.* Cell Rep, 2016. **16**(9): p. 2472-85.
34. Gatto, D., et al., *The chemotactic receptor EBI2 regulates the homeostasis, localization and immunological function of splenic dendritic cells.* Nat Immunol, 2013. **14**(5): p. 446-53.
35. Lu, E., et al., *Distinct oxysterol requirements for positioning naïve and activated dendritic cells in the spleen.* Sci Immunol, 2017. **2**(10).
36. Yi, T. and J.G. Cyster, *EBI2-mediated bridging channel positioning supports splenic dendritic cell homeostasis and particulate antigen capture*. Elife, 2013. **2**: p. e00757.
37. Kaplan, D.H., *Ontogeny and function of murine epidermal Langerhans cells.* Nat Immunol, 2017. **18**(10): p. 1068-1075.
38. Mondanelli, G., et al., *The immune regulation in cancer by the amino acid metabolizing enzymes ARG and IDO.* Curr Opin Pharmacol, 2017. **35**: p. 30-39.
39. Pearce, E.J. and B. Everts, *Dendritic cell metabolism.* Nat Rev Immunol, 2015. **15**(1): p. 18-29.
40. Amiel, E., et al., *Inhibition of mechanistic target of rapamycin promotes dendritic cell activation and enhances therapeutic autologous vaccination in mice*. J Immunol, 2012. **189**(5): p. 2151-8.
41. Jagannath, C. and P. Bakhru, *Rapamycin-induced enhancement of vaccine efficacy in mice.* Methods Mol Biol, 2012. **821**: p. 295-303.
42. Jagannath, C., et al., *Autophagy enhances the efficacy of BCG vaccine by increasing peptide presentation in mouse dendritic cells*. Nat Med, 2009. **15**(3): p. 267-76.

43. Amiel, E., et al., *Mechanistic target of rapamycin inhibition extends cellular lifespan in dendritic cells by preserving mitochondrial function.* J Immunol, 2014. **193**(6): p. 2821-30.
44. Artyomov, M.N. and J. Van den Bossche, *Immunometabolism in the Single-Cell Era.* Cell Metab, 2020.
45. Marquez, S., et al., *Endoplasmic Reticulum Stress Sensor IRE1alpha Enhances IL-23 Expression by Human Dendritic Cells.* Front Immunol, 2017. **8**: p. 639.
46. Song, M., et al., *IRE1alpha-XBP1 controls T cell function in ovarian cancer by regulating mitochondrial activity.* Nature, 2018. **562**(7727): p. 423-428.
47. Mogilenko, D.A., et al., *Metabolic and Innate Immune Cues Merge into a Specific Inflammatory Response via the UPR.* Cell, 2019. **177**(5): p. 1201-1216.e19.
48. Johnson, M.O., et al., *Distinct Regulation of Th17 and Th1 Cell Differentiation by Glutaminase-Dependent Metabolism.* Cell, 2018. **175**(7): p. 1780-1795.e19.
49. Nakaya, M., et al., *Inflammatory T cell responses rely on amino acid transporter ASCT2 facilitation of glutamine uptake and mTORC1 kinase activation.* Immunity, 2014. **40**(5): p. 692-705.
50. Pantel, A., et al., *Direct type I IFN but not MDA5/TLR3 activation of dendritic cells is required for maturation and metabolic shift to glycolysis after poly IC stimulation.* PLoS Biol, 2014. **12**(1): p. e1001759.
51. Thwe, P.M. and E. Amiel, *The role of nitric oxide in metabolic regulation of Dendritic cell immune function.* Cancer Lett, 2018. **412**: p. 236-242.
52. Na, Y.R., et al., *GM-CSF Induces Inflammatory Macrophages by Regulating Glycolysis and Lipid Metabolism.* J Immunol, 2016. **197**(10): p. 4101-4109.
53. Singh, P., et al., *GM-CSF Enhances Macrophage Glycolytic Activity In Vitro and Improves Detection of Inflammation In Vivo.* J Nucl Med, 2016. **57**(9): p. 1428-35.
54. Guak, H., et al., *Glycolytic metabolism is essential for CCR7 oligomerization and dendritic cell migration.* Nat Commun, 2018. **9**(1): p. 2463.
55. Bauer, M., et al., *Bacterial CpG-DNA triggers activation and maturation of human CD11c-, CD123+ dendritic cells.* J Immunol, 2001. **166**(8): p. 5000-7.
56. van Dinther, D., et al., *Functional CD169 on Macrophages Mediates Interaction with Dendritic Cells for CD8(+) T Cell Cross-Priming.* Cell Rep, 2018. **22**(6): p. 1484-1495.
57. O'Brien, K.L. and D.K. Finlay, *Immunometabolism and natural killer cell responses.* Nat Rev Immunol, 2019. **19**(5): p. 282-290.
58. Keppel, M.P., et al., *Activation-specific metabolic requirements for NK Cell IFN-γ production.* J Immunol, 2015. **194**(4): p. 1954-62.
59. Marçais, A., et al., *The metabolic checkpoint kinase mTOR is essential for IL-15 signaling during the development and activation of NK cells.* Nat Immunol, 2014. **15**(8): p. 749-757.
60. Loftus, R.M., et al., *Amino acid-dependent cMyc expression is essential for NK cell metabolic and functional responses in mice.* Nat Commun, 2018. **9**(1): p. 2341.
61. Mah, A.Y., et al., *Glycolytic requirement for NK cell cytotoxicity and cytomegalovirus control.* JCI Insight, 2017. **2**(23).
62. Liu, C., et al., *Treg Cells Promote the SREBP1-Dependent Metabolic Fitness of Tumor-Promoting Macrophages via Repression of CD8(+) T Cell-Derived Interferon-gamma.* Immunity, 2019.

63. Saxton, R.A. and D.M. Sabatini, *mTOR Signaling in Growth, Metabolism, and Disease*. Cell, 2017. **168**(6): p. 960-976.
64. Wu, D., et al., *Lkb1 maintains Treg cell lineage identity*. Nat Commun, 2017. **8**: p. 15876.
65. Kusnadi, A., et al., *The Cytokine TNF Promotes Transcription Factor SREBP Activity and Binding to Inflammatory Genes to Activate Macrophages and Limit Tissue Repair*. Immunity, 2019.
66. Park, K. and A.L. Scott, *Cholesterol 25-hydroxylase production by dendritic cells and macrophages is regulated by type I interferons*. J Leukoc Biol, 2010. **88**(6): p. 1081-7.
67. Westerterp, M., et al., *Cholesterol Accumulation in Dendritic Cells Links the Inflammasome to Acquired Immunity*. Cell Metab, 2017.
68. Amuro, H., et al., *Statins, inhibitors of 3-hydroxy-3-methylglutaryl-coenzyme A reductase, function as inhibitors of cellular and molecular components involved in type I interferon production*. Arthritis Rheum, 2010. **62**(7): p. 2073-85.
69. Stuve, P., et al., *De Novo Fatty Acid Synthesis During Mycobacterial Infection Is a Prerequisite for the Function of Highly Proliferative T Cells, But Not for Dendritic Cells or Macrophages*. Front Immunol, 2018. **9**: p. 495.
70. Sha, Y. and H.E. Marshall, *S-nitrosylation in the regulation of gene transcription*. Biochim Biophys Acta, 2012. **1820**(6): p. 701-11.
71. Zhou, H.L., et al., *Metabolic reprogramming by the S-nitroso-CoA reductase system protects against kidney injury*. Nature, 2019. **565**(7737): p. 96-100.
72. Everts, B., et al., *Commitment to glycolysis sustains survival of NO-producing inflammatory dendritic cells*. Blood, 2012. **120**(7): p. 1422-31.
73. Davies, M.L., et al., *A systemic macrophage response is required to contain a peripheral poxvirus infection*. PLoS Pathog, 2017. **13**(6): p. e1006435.
74. Junt, T., et al., *Subcapsular sinus macrophages in lymph nodes clear lymph-borne viruses and present them to antiviral B cells*. Nature, 2007. **450**(7166): p. 110-4.
75. Mondanelli, G., et al., *A Relay Pathway between Arginine and Tryptophan Metabolism Confers Immunosuppressive Properties on Dendritic Cells*. Immunity, 2017. **46**(2): p. 233-244.
76. Kuka, M. and M. Iannacone, *Viral subversion of B cell responses within secondary lymphoid organs*. Nat Rev Immunol, 2018. **18**(4): p. 255-265.
77. Sammicheli, S., et al., *Inflammatory monocytes hinder antiviral B cell responses*. Sci Immunol, 2016. **1**(4).
78. McCarthy, M.K., et al., *MyD88-dependent influx of monocytes and neutrophils impairs lymph node B cell responses to chikungunya virus infection via Irf5, Nos2 and Nox2*. PLoS Pathog, 2020. **16**(1): p. e1008292.
79. Lukacs-Kornek, V., et al., *Regulated release of nitric oxide by nonhematopoietic stroma controls expansion of the activated T cell pool in lymph nodes*. Nat Immunol, 2011. **12**(11): p. 1096-104.
80. Brown, F.D., et al., *Fibroblastic reticular cells enhance T cell metabolism and survival via epigenetic remodeling*. Nat Immunol, 2019. **20**(12): p. 1668-1680.
81. Majumder, S., et al., *IL-17 metabolically reprograms activated fibroblastic reticular cells for proliferation and survival*. Nat Immunol, 2019. **20**(5): p. 534-545.
82. Valencia, J., et al., *Characterization of human fibroblastic reticular cells as potential immunotherapeutic tools*. Cytotherapy, 2017. **19**(5): p. 640-653.

83. Ip, W.K.E., et al., *Anti-inflammatory effect of IL-10 mediated by metabolic reprogramming of macrophages*. Science, 2017. **356**(6337): p. 513-519.
84. Viel, S., et al., *TGF-beta inhibits the activation and functions of NK cells by repressing the mTOR pathway*. Sci Signal, 2016. **9**(415): p. ra19.
85. Zaiatz-Bittencourt, V., D.K. Finlay, and C.M. Gardiner, *Canonical TGF-beta Signaling Pathway Represses Human NK Cell Metabolism*. J Immunol, 2018. **200**(12): p. 3934-3941.
86. Maroof, A., et al., *Developing dendritic cells become 'lacy' cells packed with fat and glycogen*. Immunology, 2005. **115**(4): p. 473-83.
87. Brombacher, E.C. and B. Everts, *Shaping of Dendritic Cell Function by the Metabolic Micro-Environment*. Front Endocrinol (Lausanne), 2020. **11**: p. 555.
88. Ibrahim, J., et al., *Dendritic cell populations with different concentrations of lipid regulate tolerance and immunity in mouse and human liver*. Gastroenterology, 2012. **143**(4): p. 1061-72.
89. Bougnères, L., et al., *A role for lipid bodies in the cross-presentation of phagocytosed antigens by MHC class I in dendritic cells*. Immunity, 2009. **31**(2): p. 232-44.
90. Everts, B., et al., *TLR-driven early glycolytic reprogramming via the kinases TBK1-IKKvarepsilon supports the anabolic demands of dendritic cell activation*. Nat Immunol, 2014. **15**(4): p. 323-32.
91. Weichhart, T., M. Hengstschlager, and M. Linke, *Regulation of innate immune cell function by mTOR*. Nat Rev Immunol, 2015. **15**(10): p. 599-614.
92. Cubillos-Ruiz, J.R., et al., *ER Stress Sensor XBP1 Controls Anti-tumor Immunity by Disrupting Dendritic Cell Homeostasis*. Cell, 2015. **161**(7): p. 1527-38.
93. Veglia, F., et al., *Lipid bodies containing oxidatively truncated lipids block antigen cross-presentation by dendritic cells in cancer*. Nat Commun, 2017. **8**(1): p. 2122.
94. D'Angelo, J.A., et al., *The cystine/glutamate antiporter regulates dendritic cell differentiation and antigen presentation*. J Immunol, 2010. **185**(6): p. 3217-26.
95. Kakazu, E., et al., *Branched chain amino acids enhance the maturation and function of myeloid dendritic cells ex vivo in patients with advanced cirrhosis*. Hepatology, 2009. **50**(6): p. 1936-45.
96. Kakazu, E., et al., *Plasma amino acids imbalance in cirrhotic patients disturbs the tricarboxylic acid cycle of dendritic cell*. Sci Rep, 2013. **3**: p. 3459.
97. Kakazu, E., et al., *Extracellular branched-chain amino acids, especially valine, regulate maturation and function of monocyte-derived dendritic cells*. J Immunol, 2007. **179**(10): p. 7137-46.
98. Wakim, L.M., et al., *Dendritic cell-induced memory T cell activation in nonlymphoid tissues*. Science, 2008. **319**(5860): p. 198-202.
99. Plantinga, M., et al., *Conventional and monocyte-derived CD11b(+) dendritic cells initiate and maintain T helper 2 cell-mediated immunity to house dust mite allergen*. Immunity, 2013. **38**(2): p. 322-35.
100. Giammanco, A., et al., *The pathophysiology of intestinal lipoprotein production*. Front Physiol, 2015. **6**: p. 61.
101. Kaplan, K., et al., *Monitoring dynamic changes in lymph metabolome of fasting and fed rats by electrospray ionization-ion mobility mass spectrometry (ESI-IMMS)*. Anal Chem, 2009. **81**(19): p. 7944-53.

102. Ferreira, G.B., et al., *Vitamin D3 Induces Tolerance in Human Dendritic Cells by Activation of Intracellular Metabolic Pathways.* Cell Rep, 2015. **10**(5): p. 711-725.

103. Hansen, I.S., et al., *FcαRI co-stimulation converts human intestinal CD103(+) dendritic cells into pro-inflammatory cells through glycolytic reprogramming.* Nat Commun, 2018. **9**(1): p. 863.

104. Malinarich, F., et al., *High mitochondrial respiration and glycolytic capacity represent a metabolic phenotype of human tolerogenic dendritic cells.* J Immunol, 2015. **194**(11): p. 5174-86.

105. Cummings, J.H., et al., *Short chain fatty acids in human large intestine, portal, hepatic and venous blood.* Gut, 1987. **28**(10): p. 1221-7.

106. Koh, A., et al., *From Dietary Fiber to Host Physiology: Short-Chain Fatty Acids as Key Bacterial Metabolites.* Cell, 2016. **165**(6): p. 1332-1345.

107. Braun, P., et al., *Free amino-acid content of the lymph.* Nature, 1956. **177**(4520): p. 1133-4.

108. Broussard, J.L., et al., *Insulin access to skeletal muscle is impaired during the early stages of diet-induced obesity.* Obesity (Silver Spring), 2016. **24**(9): p. 1922-8.

109. Hong, J., et al., *Altered Metabolic Profile of Triglyceride-Rich Lipoproteins in Gut-Lymph of Rodent Models of Sepsis and Gut Ischemia-Reperfusion Injury.* Dig Dis Sci, 2018. **63**(12): p. 3317-3328.

110. McGettrick, A.F. and L.A.J. O'Neill, *The Role of HIF in Immunity and Inflammation.* Cell Metab, 2020. **32**(4): p. 524-536.

111. He, W., et al., *The anatomy and metabolome of the lymphatic system in the brain in health and disease.* Brain Pathol, 2019.

112. Kelly, B. and E.L. Pearce, *Amino Assets: How Amino Acids Support Immunity.* Cell Metab, 2020. **32**(2): p. 154-175.

113. Shang, M., et al., *Macrophage-derived glutamine boosts satellite cells and muscle regeneration.* Nature, 2020.

114. Bak, L.K., A. Schousboe, and H.S. Waagepetersen, *The glutamate/GABA-glutamine cycle: aspects of transport, neurotransmitter homeostasis and ammonia transfer.* J Neurochem, 2006. **98**(3): p. 641-53.

115. Berg, A., et al., *The pattern of amino acid exchange across the brain is unaffected by intravenous glutamine supplementation in head trauma patients.* Clin Nutr, 2008. **27**(6): p. 816-21.

116. Tanoue, T., et al., *A defined commensal consortium elicits CD8 T cells and anti-cancer immunity.* Nature, 2019. **565**(7741): p. 600-605.

117. Durai, V. and K.M. Murphy, *Functions of Murine Dendritic Cells.* Immunity, 2016. **45**(4): p. 719-736.

118. Scharping, N.E., et al., *The Tumor Microenvironment Represses T Cell Mitochondrial Biogenesis to Drive Intratumoral T Cell Metabolic Insufficiency and Dysfunction.* Immunity, 2016. **45**(2): p. 374-88.

119. Sinclair, L.V., C. Barthelemy, and D.A. Cantrell, *Single Cell Glucose Uptake Assays: A Cautionary Tale.* Immunometabolism, 2020. **2**(4): p. e200029.

120. Bröer, S. and A. Bröer, *Amino acid homeostasis and signalling in mammalian cells and organisms.* Biochem J, 2017. **474**(12): p. 1935-1963.

Nederlandse samenvatting

Het afweersysteem en dendritische cellen

Het wemelt van de micro-organismen om ons heen. Bacteriën, virussen, schimmels en parasieten. Ze zitten in de lucht om ons heen, op onze huid, en zelfs in ons lichaam. Toch worden we zelden ziek. Dit komt omdat we een afweersysteem hebben dat ons beschermt. Tegen ziektemakers van buitenaf en kankercellen van binnenuit. We hebben onder andere een praktisch ondoordringbare huid, slijm dat ziektemakers afvoert, antistoffen in dit slijm en andere vloeistoffen, en afweercellen –die ziektemakers kunnen opeten. De zogenaamde aangeboren tak van ons afweersysteem.

Maar soms zijn er simpelweg te veel ziektemakers of hebben ze trucjes waarmee ze ons afweersysteem te slim af zijn. In dat geval moet een tweede verdedigingslinie geactiveerd worden. De zogenaamde verworven tak van ons afweersysteem. Deze bestaat onder andere uit afweercellen die T cellen worden genoemd. Deze kunnen zich snel vermenigvuldigen en eigenschappen aanmeten die specifiek zijn voor, en passen bij, de te elimineren ziekteverwekkers. Dit snelle vermenigvuldigen kunnen we soms ook opmerken. Zo kunnen er knobbels in de hals ontstaan tijdens een keelontsteking. Dat zijn dan de snel delende cellen van ons afweersysteem wat hard aan het werk is.

T cellen moeten wel verteld worden wie aan te vallen en wanneer dit gepast is. Speciaal opgeleid voor het doorgeven van dergelijke informatie aan T cellen zijn zogenaamde dendritische cellen. Als we kunnen beïnvloeden hoe dendritische cellen informatie doorgeven, dan kunnen we misschien bepalen of er überhaupt een afweerreactie tot stand komt, welke vorm deze aanneemt en hoe sterk deze is. Dit kan relevant zijn voor bijvoorbeeld het verbeteren van preventieve vaccinaties en bepaalde vormen van kankerbehandeling.

De link tussen stofwisseling en de afweerrespons

Stofwisseling is het geheel aan chemische reacties in cellen waarbij de ene organische stof in een andere stof wordt omgezet. Stofwisseling kan grofweg worden onderverdeeld in anabole/opbouwende stofwisseling en katabole/afbrekende stofwisseling. In het eerste geval worden kleine/simpele stoffen omgezet in grotere/meer complexe stoffen, een proces waarbij energie wordt opgeslagen. In het tweede geval worden grote/complexe stoffen omgezet in kleinere/meer simpele stoffen, een proces waarbij energie vrijkomt.

In de afgelopen jaren is duidelijk geworden dat de manier waarop dendritische cellen voedingstoffen opnemen, verwerken en verteren verandert nadat ze met ziektemakers in aanraking komen. Voorbeelden van voedingstoffen zijn suikers, vetten en aminozuren. Bovendien is duidelijk geworden dat deze verandering in stofwisseling bepaalt wat voor signalen dendritische cellen doorgeven aan T cellen. Als wat en hoe de dendritische cel eet direct gevolgen heeft voor hoe de dendritische cel informatie doorgeeft aan T cellen, dan is het beïnvloeden van dendritische celstofwisseling wellicht een manier om afweerreacties in de gewenste richting te sturen. Dit kan relevant zijn voor het ontwikkelen van nieuwe immuuntherapieën of het verbeteren van bestaande therapieën.

In dit proefschrift heb ik onderzocht hoe de stofwisseling van dendritische cellen verandert nadat ze blootgesteld zijn aan verschillende ziektemakers, maar ook aan stoffen die zorgen voor een ontstekingsremmende/tolerogene functie van dendritische cellen. Vervolgens heb ik onderzocht of er ook unieke stofwisselingsprofielen zijn waarmee deze dendritische cellen van elkaar onderscheiden kunnen worden en of deze unieke profielen gemanipuleerd kunnen worden om op een gerichte manier ontstekingsbevorderende antibacteriële, antischimmel, anti-parasitaire en ontstekingsremmende/regulatoire T cellen te genereren. Al laatste heb ik onderzocht of dit ook bereikt kan worden door in dendritische cellen aanpassingen te maken in eiwitten die respectievelijk een anabole en katabole stofwisseling aansturen.

Hoofdstukken

In **hoofdstuk 2** geven we een ge-update overzicht van wat bekend is over dendritische cellen en hun stofwisseling. Het lijkt erop dat dendritische cellen die beschermen tegen bacteriën, virussen en schimmels vaker gebruik maken van een opbouwende stofwisseling, gedreven door de verbranding van glucose zonder zuurstof. Een belangrijke rol is weggelegd voor het eiwitcomplex ‘mechanistic target of rapamycin (mTOR)’ wat meet of er voldoende voedingstoffen aanwezig zijn en een signaal afgeeft voor meer anabole stofwisseling. Daar en tegen lijkt het erop dat dendritische cellen die beschermen tegen parasieten en auto-immuunziekten vaker gebruik maken van een afbrekende stofwisseling, gedreven door de verbranding van vetzuren met behulp van zuurstof. Een belangrijke rol lijkt hier weggelegd voor het eiwit ‘adenosine monophosphate-activated protein kinas (AMPK)’ wat meet of er weinig energie is en een signaal afgeeft voor meer katabole stofwisseling. Dit laatste om zo meer energie te genereren.

In **hoofdstuk 3** leggen we uit hoe de techniek ‘extracellular flux (XF)’ analyse werkt en hoe deze op dendritische cellen toegepast kan worden. Door te meten hoeveel verzuring er plaats vindt en hoeveel zuurstof er wordt opgenomen kan een indruk worden gekregen van in hoeverre een cel gebruik maakt van een verbranding van glucose zonder zuurstof versus de verbranding van voedingstoffen met zuurstof. Bij de verbranding van glucose zonder zuurstof wordt namelijk melkzuur (lactaat) gevormd.

In **hoofdstuk 4** laten we zien dat dendritische cellen in staat zijn om glucose op te slaan in de vorm van glycogeen. Dit blijkt cruciaal te zijn om de dendritische cellen voor te bereiden op situaties waar er weinig suiker voor handen is, maar er toch gereageerd moet worden op bacteriën. Blokker je de afbraak van glycogeen in glucose, dan kan de dendritische cel nog maar beperkt informatie doorgeven aan T cellen. Deze informatie zou gebruikt kunnen worden om dendritische cellen beter voor te bereiden op het doen van hun werk in omgevingen met weinig glucose, zoals tijdens infecties en in tumoren.

Sommige bacteriën zijn goed voor ons doordat zij in onze darmen voedingstoffen omzetten in boterzuur (butyraat), een korte vettige stof. Butyraat kan dendritische cellen stimuleren om meer ontstekingsremmende T cellen te activeren, maar de manier waarop was nog niet duidelijk. In **hoofdstuk 5** laten wij zien dat butyraat dendritische cellen niet meer energie geeft, maar hun energieproductie juist verlaagt. Wel stimuleert butyraat dendritische cellen om retinoïnezuur aan te maken en uit te scheiden. Deze uit vitamine A verkregen stof was uiteindelijk verantwoordelijk voor de vorming van regulatoire T cellen door butyraat-gestimuleerde dendritische cellen. Deze studie bevestigt de positieve werking van sommige korte vetzuren op ons afweersysteem, maar laat ook zien welke eiwitten op en in dendritische cellen reageren op butyraat. Dit laatste kan nieuwe aangrijpingspunten voor de ontwikkeling van medicijnen opleveren.

In **hoofdstuk 6** benadrukken we nog eens hoe weinig er bekend is over de stofwisseling van dendritische cellen die anti-parasitaire T helper 2 cellen activeren. Daarom onderzoeken we in **hoofdstuk 7** wat er gebeurt met de stofwisseling van dendritische cellen wanneer zij worden blootgesteld aan de producten van parasitaire wormen. We laten zien dat deze dendritische cellen juist minder glucose gaan verbranden. De verbranding van glucose blokkeren in dendritische cellen an sich is zelfs voldoende om ze T helper 2 cellen te laten activeren. Anti-parasiet dendritische cellen maken wel meer uridinedifosfaat N-acetylglucosamine aan, een nucleotide suiker dat gebruikt kan worden om eiwitten aan of uit te zetten. Deze bijzondere manier van eiwit regulatie bleek cruciaal te zijn voor T helper 2 activatie door aan parasiet producten blootgestelde dendritische cellen. Dit geldt ook voor dendritische cellen die T helper 2 responsen activeren in reactie op allergenen. Hiermee is een stofwisselingsroute in dendritische cellen gevonden die wellicht gemanipuleerd kan worden om specifiek T helper 2 responsen te stimuleren of te remmen.

In **hoofdstuk 8** laten we zien dat het eiwit ‘liver kinase B 1 (LKB1)’ - dat nodig is voor de activering van AMPK – een belangrijk rol speelt in het bevorderen van katabole stofwisseling in dendritische cellen en het beperken van hun T cel activerende capaciteit. Waar we verwacht hadden dat muizen waarin LKB1 genetisch was verwijderd in dendritische cellen gekenmerkt zouden worden door een ophoping van ontstekingsbevorderende T cellen, was het tegenovergestelde het geval. We vonden een ophoping van ontstekingsremmende T cellen in deze muizen. Deze T cellen bleken afkomstig uit de zwezerik (thymus). We zagen dat er meer type 2 dendritische cellen in de zwezerik waren en dat ze ook meer geactiveerd waren. Het waren deze thymus type 2 dendritische cellen die beter in staat waren om regulatoire T cellen voort te brengen na verlies van LKB1. Op dit moment zijn er echter nog geen medicijnen die specifiek ingrijpen op LKB1. Maar dit onderzoek – vooral in combinatie met het tegelijkertijd gepubliceerde werk van collega's in Amerika – laat wel zien zien dat afhankelijk van waar de dendritische cellen zich bevinden een verandering in de katabole stofwisseling van dendritische cellen kan leiden tot zowel immunologische tolerantie of ontsteking.

In **hoofdstuk 9** laten we zien dat het eiwitcomplex ‘mTOR complex 1 (mTORC1)’ in conventionele dendritische cellen nodig is voor hun aanmaak van eiwitten waarmee ze ontstekingsbevorderende T cellen kunnen activeren. Dit in tegenstelling tot eerdere onderzoeken waarin dendritische cellen in kweekschalen in het lab blootgesteld waren aan het mTORC1 remmende medicijn rapamycin (ook bekend als Sirolimus) en juist minder van deze eiwitten aanmaakten. Waar het blokkeren van mTORC1 in dendritische cellen door het genetisch weghalen van het eiwit ‘raptor’ geen effect had op afweer responsen tegen systemische infecties met bacteriën en parasitaire wormen, zagen we dat afweerreacties na immunisaties in de huid sterker waren. We merkten op dat Langerhans cellen in de huid, een aan dendritische cellen verwante cel soort, na verlies van raptor juist meer ontstekingsbevorderende eiwitten aanmaakten. Het is nu nog onduidelijk of het inderdaad de Langerhans cellen zijn die zorgen voor een sterkere afweerreactie in de huid na verlies van raptor. Het is het wel duidelijk dat het blokkeren van mTORC1 – wat een veel toegepaste behandeling is in de geneeskunde – uiteenlopende effecten kan hebben op cellen, afhankelijk van de locatie en het type cellen die eraan blootgesteld worden.

In **hoofdstuk 10** wordt geprobeerd de bevindingen in dit proefschrift, meestal gedaan met dendritische cellen in kweekschalen in het lab, te plaatsen in situaties van natuurlijke infectie. Gedurende het verloop van een infectie komen dendritische cellen op veel verschillende plekken, waar ze worden blootgesteld aan verschillende soorten voedingstoffen en verschillende samenstellingen van cellen. Een kweekschaal kan nooit deze diversiteit nabootsen. Maar de beschikbaarheid van technieken om de stofwisseling van individuele cellen in een groep cellen te bestuderen zijn nog beperkt. Daarom is innovatie in de detectie van celstofwisseling in een complexe omgeving gewenst om zo snel mogelijk tot therapieën te komen die relevant zijn voor de patiënt.

Conclusie

De studies in dit proefschrift laten zien dat eiwitten die ofwel een afbrekende ofwel een opbouwende stofwisseling bevorderen in dendritische cellen een belangrijke rol spelen in hun T cel activerende eigenschappen. LKB1 verlaagt de ontstekingskracht van dendritische cellen (**hoofdstuk 8**), terwijl mTORC1 de ontstekingskracht van dendritische cellen verhoogt (**hoofdstuk 9**). Maar afhankelijk van het type cel en de locatie kan de tot stand gekomen afweerreactie verschillen (**hoofdstuk 8 en 9**). Aan de ene kant verbranden dendritische cellen die anti-bacterie en antischimmel T cellen tot stand brengen verbranden veel suiker zonder zuurstof (**hoofdstuk 4 en 7**). Aan de andere kant hebben dendritische cellen die ontstekingsremmende T cellen (**hoofdstuk 5**) en anti-parasiet/allergische T helper 2 cellen activeren (**hoofdstuk 7**) relatief een lage stofwisseling, maar wel met unieke eigenschappen. Deze dendritische cellen maken respectievelijk retinoïnezuur en de nucleotide suiker uridinedifosfaat N-acetylglucosamine aan om T cellen de juiste instructie te geven. Bovendien slaan dendritische cellen glucose op in de vorm van glycogeen om een buffer te hebben tegen omstandigheden van weinig suiker (**hoofdstuk 4**). Deze verkregen inzichten over hoe de functie van dendritische cellen door hun stofwisseling wordt gestuurd, bieden nieuwe aanknopingspunten om de functionaliteit van dendritische cellen te verbeteren voor therapeutisch gewin. Een voorbeeld van een klinische setting waarbij dit goed kan worden toegepast is dendritische celtherapie. Hierbij worden dendritische cellen uit het lichaam van de patiënt gehaald, veranderd, en vaak ook vermenigvuldigd, voordat ze terug worden gebracht. Wel zou het helpen als we een beter beeld krijgen over de stofwisseling van dendritische cellen in situaties van natuurlijke infectie, om zo beter te kunnen inspelen op de obstakels die dendritische cellen tegenkomen, wanneer ze ons proberen te beschermen tegen micro-organismen en kankercellen.

Curriculum vitae

Leonard Reinier Pelgrom was born in Haarlem, the Netherlands on May 27th 1988. He graduated from the Ichtus College (Driehuis, The Netherlands) in 2006 and started the bachelor Biomedical Sciences at Leiden University Medical Center in the same year. During his bachelor he took a one-year sabbatical to work as a board member of a student rowing club (Asopos de Vliet, Leiderdorp, The Netherlands) before obtaining his bachelor diploma in 2012. He obtained his master diploma in with distinction at the same university in 2015.

During his master he used molecular biology techniques to help study how blockade of the endocannabinoid system can activate brown fat tissue and diminish obesity at the laboratory of Prof. Rensen (LUMC, department of Endocrinology). For his contribution to this research, he was awarded the LUMC Student Research Award Biomedical Sciences in 2014. During his next internship, at the group of Dr. Guigas (LUMC, department of Molecular Cell Biology & department of Parasitology), he used flow cytometry techniques to help investigate how the generation of white fat cells can be influenced by immunogenic parasite-derived molecules. A growing fascination for this interplay between metabolic and immunological systems led him to pursue a PhD at the LUMC department of Parasitology, under the supervision of Dr. Everts. Here he researched how specific metabolic states of dendritic cells are linked to their ability to prime diverse antigen-specific T cell responses.

He gave presentations at the Keystone Symposia Conferences in 2016 and 2017, for which he was awarded a Seahorse Travel Award and a Keystone Symposium Scholarship respectively. He also gave oral presentations at the Dutch Society of Immunology (NNVI) in 2015 and 2017, the Dutch Society of Parasitology (NVP) in 2016, the European Macrophage and Dendritic Cell Society (EMDS) in 2016, the International Symposium on Dendritic Cells in 2018 and the European Congress of Immunology in 2018. He won the presentation prize at the EMDS.

From 2019-2021 he worked at the group of Dr. Finlay (Trinity Biomedical Sciences Institute, Trinity College Dublin, Dublin, Ireland), where he took his interests in a new direction by researching the potential of bioorthogonal click chemistry to interrogate metabolic states of cells.

Currently he is working at the group of Dr. van Kasteren (Leiden Institute of Chemistry, Leiden University), with whom he wrote a Leiden University Fund (LUF) Impulse Grant - in collaboration with Dr. Kooijman (LUMC, department of Endocrinology) - to investigate the initiation events in atherosclerosis with clickable lipids, a grant which has been accepted in October 2021.

List of publications

1. van der Zande, H.J.P., M.A. Gonzalez, K. de Ruiter, R.H.P. Wilbers, N. García-Tardón, M. van Huizen, K. van Noort, **L.R. Pelgrom**, J.M. Lambooij, A. Zawistowska-Deniziak, F. Otto, A. Ozir-Fazalalikhan, D. van Willigen, M. Welling, J. Poles, F. van Leeuwen, C.H. Hokke, A. Schots, M. Yazdanbakhsh, P. Loke, and B. Guigas, *The helminth glycoprotein omega-1 improves metabolic homeostasis in obese mice through type 2 immunity-independent inhibition of food intake.* Faseb j, 2021. **35**(2): p. e21331.

2. Embgenbroich, M., H.J.P. van der Zande, L. Hussaarts, J. Schulte-Schrepping, **L.R. Pelgrom**, N. García-Tardón, L. Schlautmann, I. Stoetzel, K. Händler, J.M. Lambooij, A. Zawistowska-Deniziak, L. Hoving, K. de Ruiter, M. Wijngaarden, H. Pijl, K. Willems van Dijk, B. Everts, V. van Harmelen, M. Yazdanbakhsh, J.L. Schultze, B. Guigas, and S. Burgdorf, *Soluble mannose receptor induces proinflammatory macrophage activation and metaflammation.* Proc Natl Acad Sci U S A, 2021. **118**(31).

3. Winkel, B.M.F., **L.R. Pelgrom**, R. van Schuijlenburg, E. Baalbergen, M.S. Ganesh, H. Gerritsma, C.M. de Korne, N. Duszenko, M.C.C. Langenberg, S.C. Chevalley-Maurel, H.H. Smits, E.C. de Jong, B. Everts, B. Franke-Fayard, and M. Roestenberg, *Plasmodium sporozoites induce regulatory macrophages.* PLoS Pathog, 2020. **16**(9): p. e1008799.

4. **Pelgrom, L.R.**, T.A. Patente, A. Sergushichev, E. Esaulova, F. Otto, A. Ozir-Fazalalikhan, H.J.P. van der Zande, A.J. van der Ham, S. van der Stel, M.N. Artyomov, and B. Everts, *LKB1 expressed in dendritic cells governs the development and expansion of thymus-derived regulatory T cells.* Cell Res, 2019. **29**(5): p. 406-419.

5. Patente, T.A., **L.R. Pelgrom**, and B. Everts, *Dendritic cells are what they eat: how their metabolism shapes T helper cell polarization.* Curr Opin Immunol, 2019. **58**: p. 16-23.

6. Winkel, B.M.F., M.R. Dalenberg, C.M. de Korne, C. Feijt, M.C.C. Langenberg, **L. Pelgrom**, M.S. Ganesh, M. Yazdanbakhsh, H.H. Smits, E.C. de Jong, B. Everts, F.W.B. van Leeuwen, C.H. Hokke, and M. Roestenberg, *Early Induction of Human Regulatory Dermal Antigen Presenting Cells by Skin-Penetrating Schistosoma Mansoni Cercariae.* Front Immunol, 2018. **9**: p. 2510.

7. Kaisar, M.M.M., M. Ritter, C. Del Fresno, H.S. Jónasdóttir, A.J. van der Ham, **L.R. Pelgrom**, G. Schramm, L.E. Layland, D. Sancho, C. Prazeres da Costa, M. Giera, M. Yazdanbakhsh, and B. Everts, *Dectin-1/2-induced autocrine PGE2 signaling licenses dendritic cells to prime Th2 responses.* PLoS Biol, 2018. **16**(4): p. e2005504.

8. Thwe, P.M., **L.R. Pelgrom**, R. Cooper, S. Beauchamp, J.A. Reisz, A. D'Alessandro, B. Everts, and E. Amiel, *Cell-Intrinsic Glycogen Metabolism Supports Early Glycolytic Reprogramming Required for Dendritic Cell Immune Responses.* Cell Metab, 2017. **26**(3): p. 558-567.e5.

9. **Pelgrom, L.R**. and B. Everts, *Metabolic control of type 2 immunity.* Eur J Immunol, 2017. **47**(8): p. 1266-1275.

10. Kaisar, M.M.M., **L.R. Pelgrom**, A.J. van der Ham, M. Yazdanbakhsh, and B. Everts, *Butyrate Conditions Human Dendritic Cells to Prime Type 1 Regulatory T Cells via both Histone Deacetylase Inhibition and G Protein-Coupled Receptor 109A Signaling.* Front Immunol, 2017. **8**: p. 1429.

11. **Pelgrom, L.R**., A.J. van der Ham, and B. Everts, *Analysis of TLR-Induced Metabolic Changes in Dendritic Cells Using the Seahorse XF(e)96 Extracellular Flux Analyzer.* Methods Mol Biol, 2016. **1390**: p. 273-85.

12. Boon, M.R., S. Kooijman, A.D. van Dam, **L.R. Pelgrom**, J.F. Berbée, C.A. Visseren, R.C. van Aggele, A.M. van den Hoek, H.C. Sips, M. Lombès, L.M. Havekes, J.T. Tamsma, B. Guigas, O.C. Meijer, J.W. Jukema, and P.C. Rensen, *Peripheral cannabinoid 1 receptor blockade activates brown adipose tissue and diminishes dyslipidemia and obesity.* Faseb j, 2014. **28**(12): p. 5361-75.

Acknowledgements

Thank you, **Bart Everts**, for giving me the opportunity to work with you and thereby allowing me to combine my interests in metabolism and immunology. I have learned a lot from you and I appreciate that your door is always open for discussion. However, I am most grateful for things that were not in the job description. Your invitation to join you and your friends on a cycling holiday - an invitation you extended to my friends as well - has had a profound impact on me. Cycling on Mont Ventoux has been one of the most joyous, even spiritual, moments of my live. Another such happening occurred on the top of Mount Grouse. An event which would not have happened without your invitation to accompany you to the Keystone Symposium in Banff. Thank you especially for allowing these experiences to happen.

Thank you, **Maria Yazdanbakhsh**, for bringing together such a special group of people we call the PARA. They play key roles in some of my fondest memories and their friendship has transformed me. Thank you, Ron, for it was your enthusiasm that got me hooked (pun intended) on the department of Parasitology when I was a master student. Thank you, Bruno, for supervising me during my master research project. Without that project I would not have met Bart and I would have missed out on these people that are so important to me today.

Thank you, Beatrice and Patrick vd Z, my paranymphs, and Thiago, my scientific brother from another mother. Crying, cursing, and laughing about mistakes that messed up experiments that took hours, days or even weeks to plan and perform. Followed by the high of finally getting a crucial experiment to work. This is what that first come to mind when I think back on my PhD.

Thank you, Alwin, Arifa and Frank, for teaching me the ways of the lab and providing much needed hands during experiments. Thank you, Beatrice, Michelle and Sanne, for joining me in the first PARA borrel committee. Thank you, Karin and Marijke, for bringing back the PARA lab outing committee with me and Beatrice. Thank you, Lisa, Lonneke en Stefan, for being my students and helping me with my research. Thank you, Abena, Alice, Amke, Angela, Astrid, Catherin, Chris, Clarize, Corrie, Dian, Dicky, Eddy, Eline, Erliyani, Eric, Eunice, Fabrizio, Fiona, Firdaus, Gerdien, Graham, Hans, Hermelijn, Jacqueline, Jai, Jan-Pieter, Jantien, Jeroen, Joost, Katja, Koen, Kyra, Laudine, Linh, Lisette, Łucja, Luis, Maria K, Marie-Astrid, Marije, Marion, Marjolein, Mathilde, Meta, Mikhael, Miriam, Mirjam, Moses, Nathalia, Nicole, Nikolas, Rike, Roos, Séverine, Shahid, Simone, Suzanne, Tom, Yoanne, Yolanda, Yvonne, Wouter and all other PARA colleagues that I have missed here. Science is a group effort, if not a team survival expedition.

Thank you, Eileen, Eline, Ingmar, Paul and Tessa, my Biomedical Sciences master buddies.

Thank you, Amke, Amy, Annemieke, Boudewijn, Brigitte, Guido, Iris, Jocelyn, Koen, Laura, Leonie, Marije, Michiel, Nikolas, Ruud, Thomas, Ward, Wouter d G, Wouter v I and Desiree. Some of you have been my closest friends for 15 years, while others have come into my life more recently. However, all of you have been instrumental - through small and large actions - in helping me navigate challenging times and coming out improved.

Thank you, Dave and Sander, for showing me patience and kindness when you did not have to. Without you this thesis would not have been completed. You are the kind of person I aspire to be.

Thank you, most importantly, mom and dad. You supported me through a master and long bachelor, where I was trying to find myself. You accepted my workaholic attitude during my master and PhD, where I was trying to prove myself. You gave me a home when the adventure in Dublin stopped and a workplace to finish my PhD during the Corona lockdown. Without you this thesis would not have been completed and your love has shaped me into the man I am today.